THE UNIVERSITY
of EDINBURGH

Protodeboronation

THE UNIVERSITY *of* EDINBURGH

Paul Cox

Doctor of Philosophy

University of Edinburgh

2016

Declaration

I declare that the work in this thesis was carried out by me under the supervision of Prof. Guy Lloyd-Jones FRS and is in accordance with the requirements of the University of Edinburgh. This work is original, except where indicated by special reference in the text, and no part of the dissertation has been previously submitted for any other academic award.

Signed …….

Date ……

Publications

The work presented in Chapters 2 and 3 have been communicated:

Cox, P. A.; Leach, A. G.; Campbell, A. D.; Lloyd-Jones, G. C. *J. Am. Chem. Soc.* **2016**, *138*, 9145-9157

Abstract

Boronic acids are key reagents in a host of chemical applications. In particular, they have been utilised in a range of metal-catalysed coupling reactions, involving the facile formation of carbon-carbon or carbon-heteroatom bonds under mild conditions that often boasts high yields and selectivity, thus becoming a vital tool in the design of complex molecules. Alongside the increased application of boronic acids, there has been a substantial increase in their commercial availability and now a wide range of elaborate boronic acids exist. However, many of these motifs are prone to undesired and troublesome side reactions, namely protodeboronation. Although many efforts have been made towards mitigating decomposition during coupling, the general mechanistic understanding of *in situ* protodeboronation is remarkably limited and outdated.

pH-rate profiles for the protodeboronation of many heterocyclic, vinyl and cyclopropyl boronic acids (1:1 H_2O/dioxane, pH 1-13, 70 °C) have been constructed using NMR spectroscopy. A general model was constructed to allow the simulation of pH-rate profiles and allow facile extrapolation of equilibrium and rate constants. With computational support, a range of novel protodeboronation mechanisms have been elucidated. Concentration-dependent processes (self-/auto-catalytic protodeboronation and disproportionation of boronic acid into borinic acid and boranes) are present when both boronic acid and boronate are present in high concentrations. Non-basic heterocyclic, vinyl and cyclopropyl boronic acids display common acid- and base-catalysed protodeboronation mechanisms, however basic heterocyclic boronic acids exhibit additional pathways. The formation and subsequent fragmentation of zwitterion water adducts (particularly for 2-pyridyl, 5-thiazolyl and 5-pyrazolyl boronic acids) leads to surprisingly rapid protodeboronation at neutral pH values, which can be attenuated (2-pyridyl) or accelerated (5-thiazolyl/5-pyrazolyl) with various Lewis acid additives.

Protodeboronation of a series of polyfluorophenyl boronic acids under alkaline conditions revealed an immense range of reactivity, spanning several orders of magnitude (phenyl boronic acid, $t_{½} \approx$ months; pentafluorophenyl boronic acid, $t_{½} \approx$ milliseconds). *Ortho*-fluorine substituents were found to heavily influence the reactivity of such substrates. Detailed KIE and computational studies indicate the presence of a unique mechanism involving rate-limiting fragmentation of aryl boronate to form an aryl anion intermediate. Strong correlations with LFER and computational parameters indicate this mechanism is predominant with extremely electron deficient or *ortho*-fluoro substituted substrates, and can be used as a predictive model for the reactivity of aryl and polyfluorophenyl boronic acids.

Lay Summary

Boronic acids are a versatile class of chemical compound found in many branches of chemical science. One key use is in chemical synthesis, whereby boronic acids are used as ‘building blocks’ to aid in the construction of novel and complex substrates. In addition, boronic acids are often regarded as being non-hazardous and easily handled, making these substrates particularly appealing to chemical researchers and industries. However, it has been reported that some boronic acids are difficult to use and undergo decomposition processes (side reactions), transforming the boronic acid into unwanted and unusable chemicals. Surprisingly, only a few limited studies have been carried out into understanding these problematic side reactions and thus predicting the stability (propensity to decomposition) of a given boronic acid is troublesome.

This thesis is centred on one of the most predominant side reactions that boronic acids endure, protodeboronation. A diverse range of notoriously, or at least anecdotally, unstable boronic acids were dissolved in water-based solutions and rates of protodeboronation measured at various pH values (acidic, neutral and basic solutions) using analytical techniques. This work not only aims to expand the understanding of this problematic side reaction, but can also be used to help predict the stability of a range of boronic acids and aid a more informed choice of conditions for their preparation, storage and application in key chemical processes.

Acknowledgements

My PhD has been filled with many challenging and enjoyable experiences, and I owe a debt of gratitude to the many people who have made it so fulfilling.

First and foremost, I would like to express my sincere gratitude to Prof. Guy Lloyd-Jones FRS for the huge amount of patience, advice and enthusiasm over the past four years. I am incredibly grateful for the numerous meetings which have developed my project into the research that I have been proud to present and publish.

Dr Andrew Campbell (AstraZeneca), Dr Andrew Leach (Liverpool John Moores University) and Dr Marc Reid (University of Edinburgh) have also helped to take this project into directions that originally would not have been possible. It has been a great honour to collaborate with you all. Special thanks go to the unsung heroes of both Bristol and Edinburgh departments, particularly for the NMR facilities, including Dr Craig Butts, Paul Lawrence, Rose Silvester, Juraj Bella and Dr Lorna Murray.

I would also like to acknowledge all members of the GLJ group who have provided support and some much needed entertainment during my studies, including: Dr Louise Evans, Dr Alistair Lennox, Dr Bertram Ong, Dr Liam Ball, Dr Tomas Racys, Dr Carl Poree, Dr Ruth Dooley, Dr Rob Cox, Dr Nicholas Taylor, Joe Tate, Jorge Gonzalez, Tom Corrie, Dr Alex Cresswell, Katherine Geogheghan, Matt Robinson, Dr Eric Keske, Dr Alba Collado, Ariana Jones, Eduardo Nieto and Magdalene Teh. Special thanks go to all members of Team Boron. The willingness to learn, discuss and debate ideas have provided a platform to design some of the most creative experiments during my research. I hope that Team Boron continues to flourish in the future, and that our t-shirts will be a reminder of our connection. Also particular thanks go to Rob and Nick for making the first couple of years in Edinburgh very enjoyable.

I would like to thank my family and friends for tolerating my absence over the past few years, while still providing unrelenting support and encouragement. And lastly, I would like to thank Emma Sackville, who has provided the greatest support of all. “Caring, considerate, calm and thoughtful” is not enough to describe the level of patience and unselfishness she has displayed throughout the entirety of my PhD, and therefore, it is her to whom I dedicate this thesis.

Contents

Abbreviations

Ac	acetyl
Ar	aryl
bipy	2,2-bipyridine
DFT	density functional theory
dtbpy	4,4’-di-*tert*-butyl-2,2’-dipyridyl
ESI	electrospray ionisation
HFIP	1,1,1,3,3,3-hexafluoro-2-propanol
HRMS	high-resolution mass spectrometry
LFER	linear free energy relationship
MIDA	*N*-methyliminodiacetic acid
NMR	nuclear magnetic resonance
MO	molecular orbital
pin	pinacol
PPA	propionic acid
RQF	rapid quench-flow
SF-IR	stopped-flow infrared
SSE	sum square error
TBAF	tetrabutylammonium fluoride
TFA	trifluoroacetic acid
THF	tetrahydrofuran
UV-vis	ultraviolet-visible
xs	excess

Chapter 1

Introduction

Synopsis of protodeboronation

Protodeboronation is a chemical reaction involving the protonolysis of a boronic acid (**X**) (or other organoborane compound) in which a C-B bond is broken and a C-H bond is formed. This results in the formation of the so called protodeboronated product ($\mathbf{X}_H$) and a boron-containing by-product, such as boric acid (Scheme 1.1).

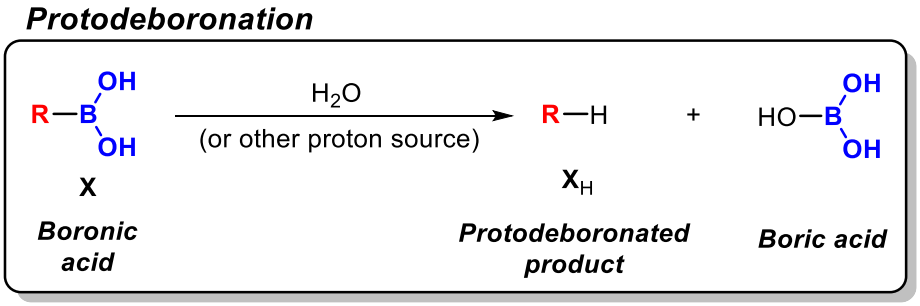

Scheme 1.1 General scheme for the protodeboronation of a boronic acid.

Some of the earliest reports of protodeboronation were made alongside the discovery of the hydroboration reactions; their combination allowing the conversion of olefins to the corresponding saturated analogues (Scheme 1.2).[1,2] Beyond this synthetic application, protodeboronation was rarely noted or valued in other chemical processes during the 1900s.

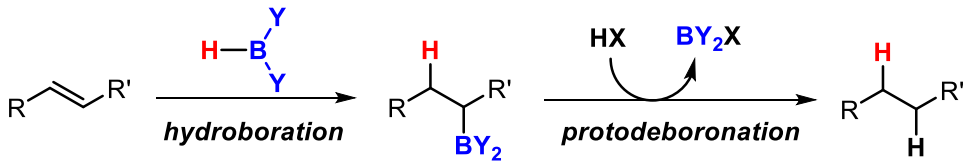

Scheme 1.2 Sequential hydroboronation-protodeboronation protocol for the conversion of olefins to saturated compounds. HX = variety of proton sources.[1,2]

In the past three decades, boronic acids have emerged as a key chemical reagent with ever-growing applications in synthetic, biomedical and medicinal chemistry. As a result, many boronic acids are now commercially available and the design of novel structures is a developing area of research. However, the recent upsurge in boronic acid usage has brought about an increase in the number of reported cases of protodeboronation. The greater part of these reports state protodeboronation to be an *undesired* reaction, which consumes the valuable and sometimes expensive boron-based reagents. A combination of anecdotal reports and limited mechanistic studies has ultimately led to much folklore regarding boronic acid (in)stability. The research in this thesis aims to address these issues with detailed studies into the stability of boronic acids, and thus to gain a deeper mechanistic understanding of protodeboronation.

1.1. Structure and properties of boronic acids

Boronic acids (**X**) belong in the family of organoboron compounds, which all contain at least one C-B bond. Boronic acids contain a tricoordinate boron atom, and possess a single organic substituent (i.e. one C-B bond) and two hydroxyl groups (Figure 1.1). Borinic acids ($\mathbf{X}_{borinic}$) and boranes ($\mathbf{X}_{borane}$) possess more organic substituents and less hydroxyl groups, whereas boric acid ($B(OH)_3$) has a fully oxygenated boron centre with three hydroxyl groups and no organic substituents. Boronic acids are trigonal planar in structure with a central sp^2 hybridised boron atom. With only six valence electrons and a resulting deficiency of two electrons, the tricoordinate boron atom possess a vacant p orbital, orthogonal to the substituent plane. This empty orbital renders these substrates as Lewis acids (electron-pair acceptors).[3]

In organic solvents, boronic acids are known to undergo condensation to form linear and cyclic oligomers, predominately to form boroxines ($\mathbf{X}_{boroxine}$) (Figure 1.1). The formation of these trimeric, 6-membered cycles is promoted during the removal of water (dehydration). Fortunately, many of the important reactions utilising boronic acids proceed regardless of the hydration state (i.e. boronic acid or boroxine). However, variable levels of dehydration can make analysis and characterisation of these substrates troublesome. This problem has been overcome in recent years with the development of various boronic acid derivatives that provide stable monomeric substrates that resist dehydration (*vide infra*, section 1.4.3.)

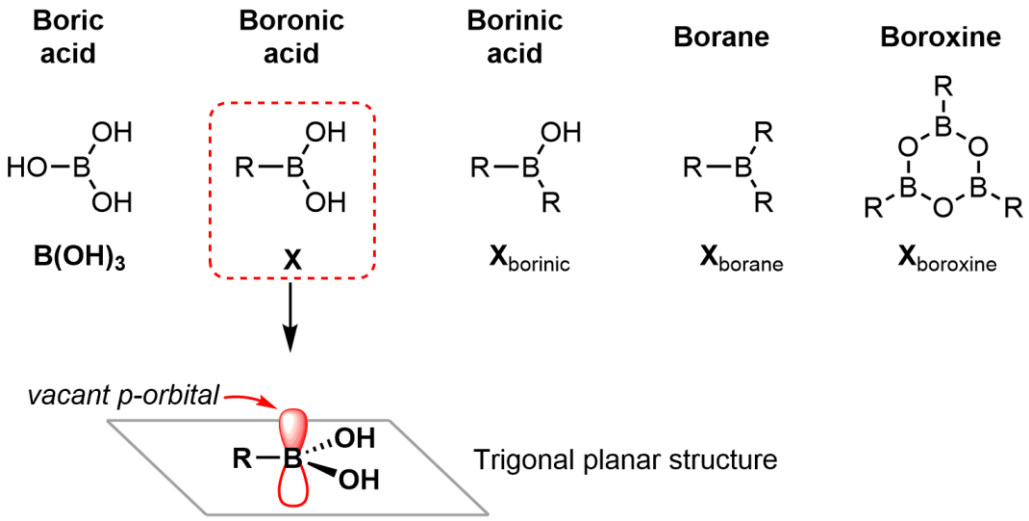

Figure 1.1 Organoboron compounds and the trigonal planar structure of boronic acids.

Boronic acids display acidic character when dissolved in aqueous media due to the affinity of water towards the vacant orbital. This establishes a dynamic equilibrium in which the boronic acid undergoes rehybridisation to form a tetrahedral, sp^3 hybridised, boronate ($\mathbf{X}_{OH}$)

with the concurrent release of a hydronium ion (H^+) (equilibrium defined as K_a, Equation 1.1, Figure 1.2).[4] It is important to note that this acidity differs from the usual Brønsted acidity of many commonly acidic compounds (carboxylic acids, phenols, ammonium salts etc.) and instead arises from the Lewis acidic nature of the electron-deficient boron atom. The most acidic boronic acids are those that possess strongly electron-withdrawing substituents, which can best stabilise the resulting boronate anion ($\mathbf{X}_{OH}$). Although dependent on the exact temperature and solvent, the pK_a of most boronic acids are between 7 and 9, and thus are relatively weak acids in comparison to carboxylic acids (pK_a ~4-5).[5]

Using the auto-ionisation constant of water (K_w, Equation 1.2, Figure 1.2), the aqueous association equilibrium (K_a) can be expressed as a hydroxide association to boronic acid (equilibrium defined as K_a/K_w, Equation 1.3, Figure 1.2). This can be particularly useful when considering the formation of boronate ($\mathbf{X}_{OH}$) relative to the concentration of hydroxide, rather than hydronium (or pH). The association equilibria are reversible and rapid, therefore, in aqueous solution the position of the boronic acid-boronate equilibrium can be modified by altering the proton or hydroxide concentration (i.e. the pH).[6]

.

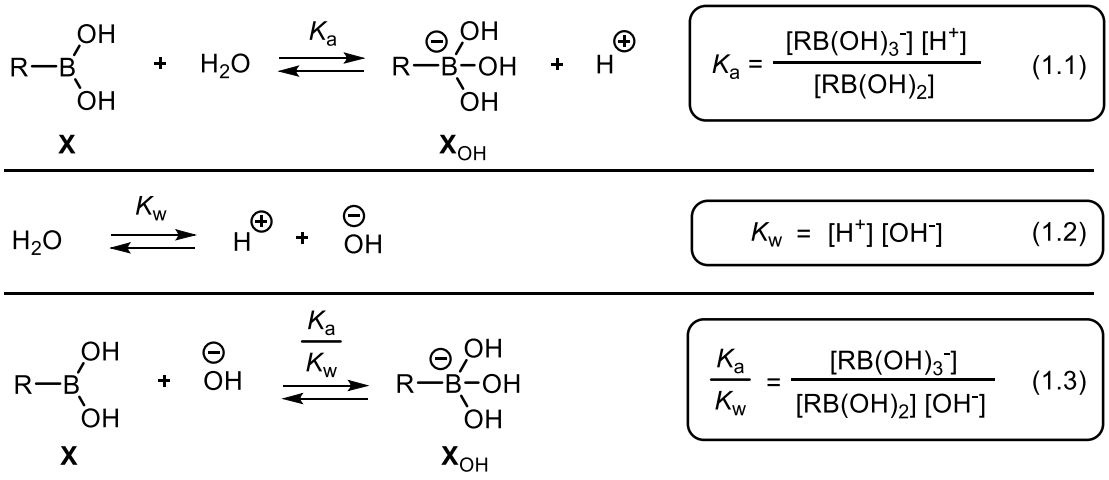

Figure 1.2 Aqueous association equilibrium of boronic acids (K_a) and conversion into hydroxide association (K_a/K_w).

1.2. Selected applications of boronic acids

1.2.1. Metal-catalysed cross-coupling

Unquestionably, boronic acids are key reagents in synthesis and one of their greatest applications is their use as nucleophilic coupling partners in a variety of metal-catalysed reactions (Scheme 1.3). The simplicity of connecting a variety of building blocks *via* carbon-carbon or carbon-heteroatom bonds renders these reactions superior to some of the more traditional methods, and provides a simple solution to difficult retrosyntheses. A wide range of couplings using boronic acids have been described, including Suzuki-Miyaura,[7] oxidative Heck,[8] Chan-Evans-Lam[9–11] and Liebeskind-Srogl couplings.[12] Additionally boronic acids have been widely applied in the 1,4-addition to enones,[13] and 1,2-addition to carbonyls and imines.[14,15] Each coupling employs a particular metal catalyst (Pd, Cu, Rh) and sometimes a base (K_2CO_3, pyridine, etc.) to complete the catalytic turnover. These transformations allow access to diverse range of functionality, including biaryls, aryl ethers, anilines, ketones and alcohols.

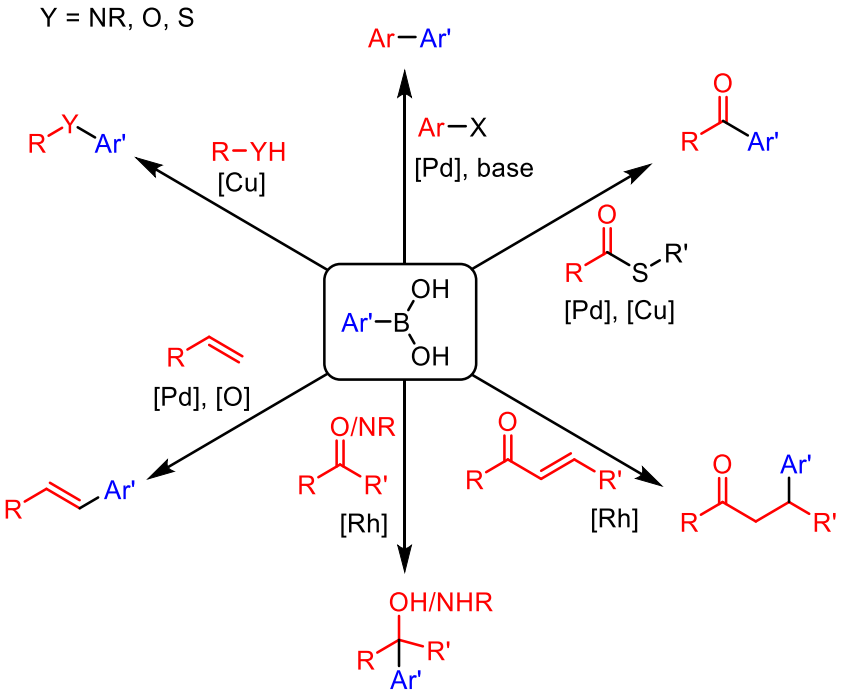

Scheme 1.3 Selected applications of boronic acid in metal-catalysed processes.

1.2.1.1. Suzuki-Miyaura cross-coupling

The Suzuki-Miyaura cross-coupling reaction, which makes use of a palladium catalyst, stands out from other metal-catalysed couplings due to a combination of advantageous features.[7] These include its relatively mild, non-toxic and cheap reaction conditions/reagents

and its exceptional functional group tolerance in comparison to other cross-coupling methods. This coupling protocol has therefore been comprehensively utilised for the construction of many biaryl motifs and has remained widespread in chemical synthesis since its discovery. In particular, its prevalence can be attributed to the wide range of developments over the past 30 years, which include optimising the reaction to tolerate challenging reagents,[16,17] perform at low temperatures[18,19] and with very low catalyst loadings.[20,21]

Many efforts have been made towards understanding the mechanism of the Suzuki-Miyaura cross-coupling reaction, and it has become an area of much controversy. Nonetheless, a simple model of the catalytic reaction is generally agreed upon and consists of 3 major steps within a catalytic cycle: oxidative addition, transmetalation, and reductive elimination (Scheme 1.4).

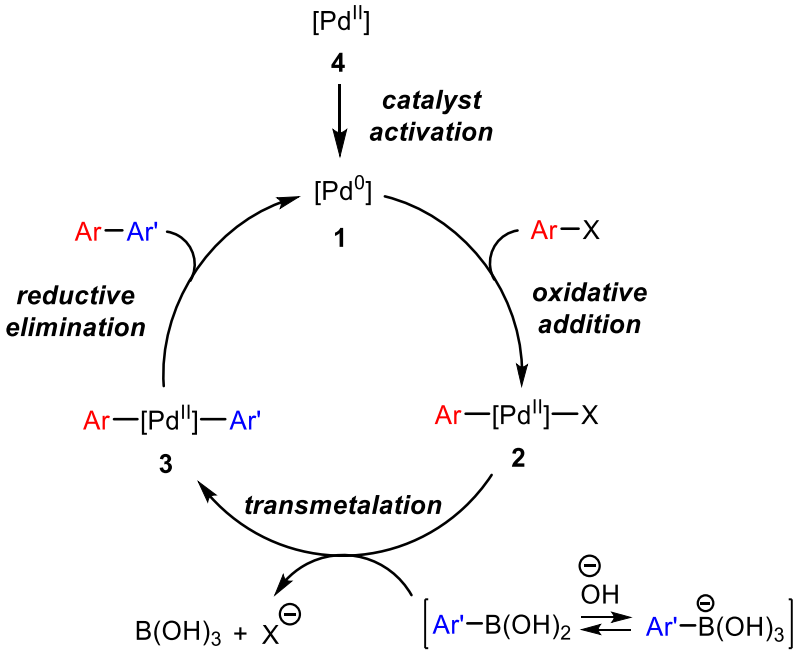

Scheme 1.4 General mechanism for the Suzuki-Miyaura cross-coupling reaction (ligands excluded).

The catalytic cycle begins with a Pd(0) source (**1**), which can undergo oxidative addition with an organohalide or pseudohalide to produce a Pd(II) intermediate (**2**). The ease of oxidative addition is proportional to the bond dissociation enthalpy of the aryl halide (I>OTf>Br>>Cl), and thus aryl iodides and triflates undergo facile oxidative addition, whereas aryl chlorides do not. Electron-withdrawing substituents on the aryl halide substrate promote oxidative addition by weakening the C-X bond. Additionally, oxidative addition can be promoted by employing electron-rich ligands, which in turn produce an electron-rich

Pd(0) source.[16] Since many Pd(0) sources are prone to decomposition upon storage, Pd(II) precatalysts (**4**) are often employed and require an *in situ* reduction to release the active catalyst.[22]

The following transmetalation step requires the transfer of the organic fragment of the boronic acid to the Pd(II) centre and produces a new Pd(II) intermediate (**3**). An understanding of this process is particularly important for the informative design and optimisation of the reaction conditions when transmetalation is turnover limiting. It is well known that base is required for the transmetalation of boronic acids, however, the exact role of base is unclear and has been of much debate.[23,24] Numerous mechanistic studies have been conducted to elucidate the possible pathways, and two key mechanisms have been proposed. One proposal states that hydroxide (generated from water and base) activates the boronic acid by forming a tetrahedral boronate (boronate pathway, Scheme 1.5), whereas the second proposal states that hydroxide activates the palladium catalyst to form an oxo-palladium species (**5**) (oxo-palladium pathway, Scheme 1.5).

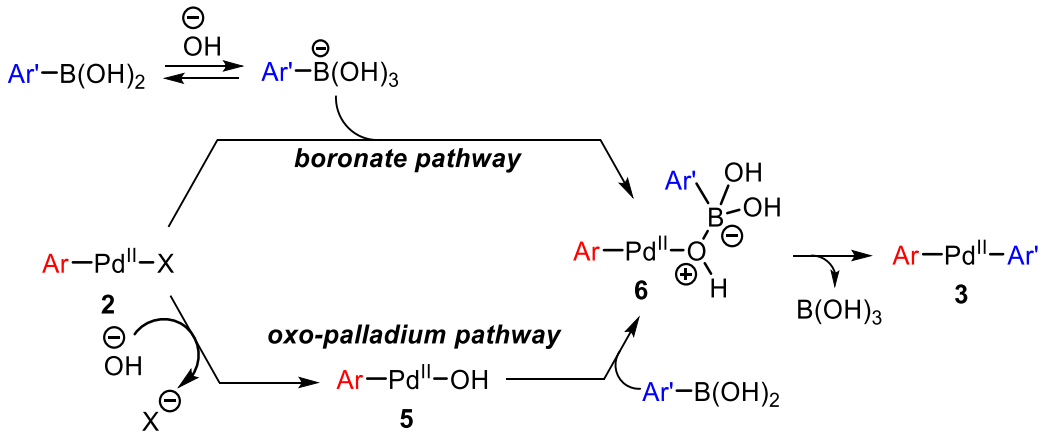

Scheme 1.5 Possible pathways of transmetalation.

It has been postulated that under the reaction conditions, hydroxide association to boronic acids proceeds to form the tetrahedral anion, although this does not confirm its reactivity in the subsequent transmetalation.[25] ESI experiments have identified the boronate pathway as the likely route,[26] yet kinetic studies conclude that either pathway could proceed.[27] Computational studies also suggest the boronate pathway was more favourable for a particular model reaction.[28] However, studies by Amatore and Hartwig have provided compelling evidence for the oxo-palladium pathway with representative Suzuki-Miyaura coupling conditions.[29,30] More recently, Denmark has successfully monitored the formation of the elusive pre-transmetalation intermediates using low-temperature rapid injection NMR.[31] Three distinct species containing a Pd-O-B linkage were identified, which all

productively react to form the cross-coupled product. These include both tricoordinate (boronic acid) and tetracoordinate (boronate) complexes, and thus indicates that both boronate and oxo-palladium pathways can exist.

Regardless of the pathway, both routes lead to the formation of a Pd(II) intermediate attached to two organic fragments (**3**). Various ligand dissociations and re-associations are required to isomerise the palladium complex into a *cis* configuration to allow the final reductive elimination step. It has also been suggested that base may assist the isomerisation through coordination of hydroxide to form a pentavalent palladium(II) intermediate, prior to reductive elimination.[29] This step is often considered to be rapid, especially when employing bulky ligands.

1.2.2. Boronic acid catalysis

In addition to their use as cross-coupling reagents, boronic acids have emerged as suitable catalysts for a variety of chemical transformations including amidations, cycloadditions and Friedel-Crafts alkylations. Such chemical transformations classically require metal catalysts that are often expensive, toxic and unsuitable for large scale processes. Thus, organocatalysts, such as boronic acids, are particularly appealing.

1.2.2.1. Amidations

Amide bonds are ubiquitous in nature, yet their formation from the retrosynthetic components, a carboxylic acid and amine, is not simple. Although thermodynamically downhill, the thermal condensation of a carboxylic acid and an amine exhibits a large activation energy. Traditional methods to overcome this matter involve the stoichiometric addition of amide-coupling reagents, such as carbodiimides or phosphonium salts.[32,33] These methods are far from ideal, as the stoichiometric coupling reagents are often toxic and also generate large amounts of by-products which complicates product isolation.

However, in 1996 Yamamoto and coworkers reported an efficient condensation between carboxylic acids and amines/ureas with a variety of electron-deficient aryl boronic acids.[34–37] High yields are obtained in refluxing toluene, with concurrent removal of water, whereas the catalytic activity is greatly reduced in polar solvents. The reaction mechanism is proposed to involve a monoacyl boronate intermediate, which activates the carboxylate group through an internal hydrogen-bonding interaction (Scheme 1.6).[38]

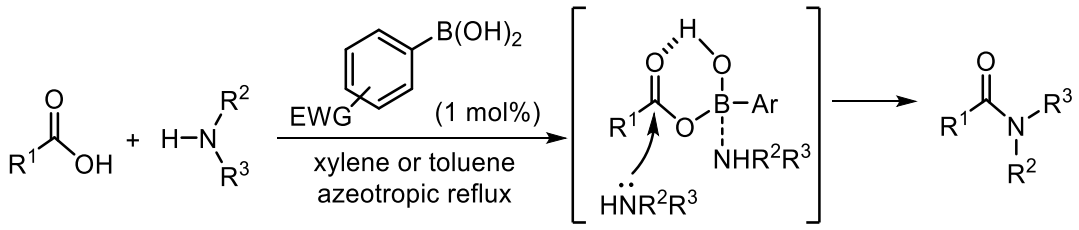

Scheme 1.6 Boronic acid catalysed amidiation, and the proposed transition state.

1.2.2.2. Cycloadditions

Hall and coworkers have demonstrated that a variety of electron-deficient aryl boronic acids can catalyse the Diels-Alder cycloaddition reaction between propiolic acid (**7**) and numerous dienes (Scheme 1.7).[39] Interestingly, *ortho*-substituted boronic acids were shown to display good activity, particularly *ortho*-bromophenyl boronic acid (**8**). Non-polar solvents (DCM, toluene etc.) afforded much higher yields than polar solvents (MeOH, MeCN etc.). It is thought that the boronic acid catalyses the cycloaddition through interaction with the carboxylic acid functionality, and thus lowers the LUMO of the dienophile. The methodology was extended to allow a sequential Nazarov cyclisation/Diels-Alder reaction of divinyl alcohols,[40] and also the [3+2] dipolar cycloaddition of azides and propioloic acid to form 1,2,3-triazenes.[41]

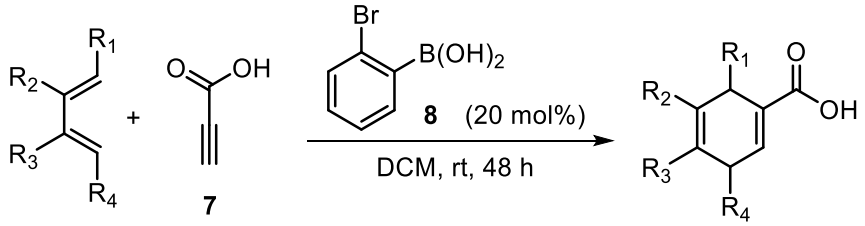

Scheme 1.7 Boronic acid catalysed Diels-Alder cycloaddition with propiolic acid (**7**).

1.2.2.3. Friedel-Crafts alkylations

Many catalysts have been developed and applied to Friedel-Crafts alkylations, including Brønsted acids,[42,43] conventional Lewis acids,[44,45] and transition metals.[46,47] However, many of these cases require toxic materials or strongly acidic conditions, and so a boronic acid-catalysed alternative would provide a milder, safer and more appealing route. McCubbin and Hall have both reported the ability of some heavily fluorinated polyfluorophenyl boronic acids to catalyse the Friedel-Crafts alkalyation of various (hetero)arenes with allylic alcohols.[48,49] *Ortho*-fluorine substituted aryl boronic acids were found to have good catalytic activity, but di*ortho*-fluorine analogues were less effective. A correlation between activity

and pK_a was not observed, and a destabilising steric interaction within the transition state was used to explain the high efficacy of *ortho*-fluorine derivatives (Scheme 1.8).

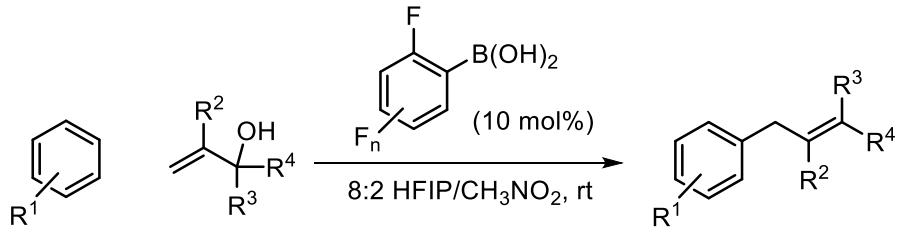

Scheme 1.8 Boronic acid catalysed Friedel-Crafts alkylation with allylic alcohols.

1.2.3. Biomedical applications

Outside of synthetic applications, boronic acids are also used in numerous biomedical protocols. Although boronic acids are not found in nature, their general lack of toxicity and their *in vivo* stability make them ideal functionalities for biological interactions. This has been advocated with approval of a boronic acid-based proteasome inhibitor, Bortezmoib (Velcade®), for the treatment of patients with multiple myeloma.[50,51]

1.2.3.1. Molecular sensing

Boronic acids have found utility in a wide range of biomedical applications due to their ability to reversibly form covalent complexes with 1,2- and 1,3-diols. Consequently, these reagents have been applied in physiological conditions as homogeneous sensors for carbohydrates, which contain a polyol functionality.[52] Interaction between an analyte and a boronic acid sensor results in a change in the physico-chemical properties of the system, which can be detected by a measurable output, commonly an optical (fluorescence),[53] or conductivity (pH) property.[54] Due to the prevalence of diabetes, much attention has been focused on creating a selective glucose molecular sensor that would allow a reliable and real-time method to monitor glucose levels in patients. Although not currently commercially available, molecular glucose-sensing would provide a variety of advantages over conventional methods, and thus developments with boronic acid-based glucose sensors are ongoing.[55]

1.2.3.2. Positron emission tomography

Positron emission tomography (PET) is an important tool in biomedicine, and is used to detect gamma ray emissions from positron-emitting radioactive isotopes. PET imaging allows cellular events to be tracked and, in turn, provides information at the molecular level in living systems.[56] The ^{18}F nucleus delivers ideal nuclear characteristics for PET imaging (97% positron emission, $t_{½}$ = 110 min), and a plethora of ^{18}F-radiolabelling pathways are

available.[57] Synthetically made biomolecules with boronic acid moieties have been used to incorporate [^{18}F]-radiolabels with the addition of [^{18}F]-KHF_2 to form [^{18}F]-trifluoroborate motifs in a convenient, single step protocol (Scheme 1.9).[58] ^{18}F-fluorinated aryl boronic acids have also been used directly in Suzuki-Miyaura couplings to connect radiolabels to a variety of biomolecules, albeit with low yields.[59] Nonetheless, developments in this field may result in further biomedical applications of boronic acids and their derivatives in the near future.

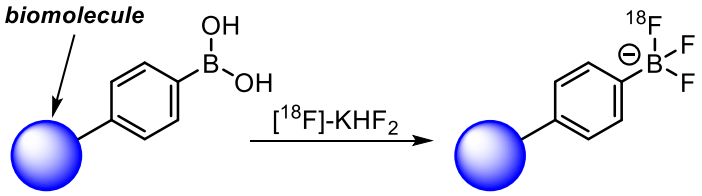

Scheme 1.9 Facile radiolabelling of boronic ester to [^{18}F]-trifluoroborate with [^{18}F]-KHF_2.

1.3. Boronic acid stability and associated side reactions

As described above, boronic acids have a wide range of applications. However these prevalent substrates sometimes present stability issues that can be detrimental to the efficiency of the process in question. A large range of structurally different boronic acids now exist (alkyl, aryl, heteroaryl etc.), but their stability is variable, and thus cannot be generalised. Instead, the stability must be assessed on an individual basis, considering both the inherent substrate structure and that of the reaction conditions in which they are employed. These stability issues result in side reactions such as protodeboronation, oxidation and homocoupling.

1.3.1. Protodeboronation

The propensity for boronic acids to undergo hydrolytic protodeboronation is evidently dependent on the conditions employed, as well as the type of boronic acid used (alkyl, aryl, heteroaryl etc). For example, benzene boronic acid required heating in water at 140 °C for 40 h to evoke significant protodeboronation,[60] and some substituted aromatic boronic acids were determined to be considerably stable in water at 90 °C ($t_{½}$ ≈ days).[61] However, protodeboronation of aromatic boronic acids can be accelerated in strong acid or base (*vide infra*, section 1.5.3.).[61,62]

This pH dependence presents a problem for some cross-coupling reactions previously described, such as the Suzuki-Miyaura coupling, which requires basic reaction conditions. For example, it was found that protodeboronation was responsible for 50% of boronic acid consumption during a Suzuki-Miyaura coupling reaction towards the synthesis of diflurisal.[63] Additionally, the yields of homologation protocols, achieved through cross-coupling of boronic acids with conjunctive haloaryl boronic acid derivatives, were also significantly affected by competitive protodeboronation.[64] For cyclopropyl boronic acid, an excess of boronic acid is often utilised as competitive protodeboronation is thought to lower the overall yields of some Suzuki-coupling reactions.[65–68]

The protodeboronation of heteroaromatic boronic acids has been claimed, often anecdotally, to be problematic in numerous publications.[69–74] Many of these reports refer specifically to 2-heteroaromatic boronic acids, which contain a heteroatom (typically N, O or S) adjacent to a boronic acid functional group. A good example of this was reported by Yang and coworkers, who observed significant protodeboronation of 2-thienyl boronic acid during a Suzuki-Miyaura cross-coupling, whereas identical reactions conditions employing 3-thienyl boronic acid did not.[73] The supposed instability of 2-heteroaromatic boronic acids is particularly

apparent for the 2-pyridyl boronic acid. This highly desired substrate is often considered as an ideal candidate for the installation of this valuable motif through metal-catalysed processes. Several reports have stated that the preparation of 2-pyridyl boronic acid is far from simple and decomposition is observed upon either isolation or storage, presumably through protodeboronation.[69,75,76] Interestingly, it has been reported that the corresponding boronate ($\mathbf{X}_{OH}$) is less susceptible to protodeboronation than the free boronic acid,[75] although independent studies suggest the boronate still decomposes upon storage.[76] Moreover, even boronic acid derivatives displayed decomposition upon storage (*vide infra*, section 1.4.3.).[77]

Lastly, some polyfluorophenyl boronic acids and derivatives have been studied under differing basic conditions, and protodeboronation kinetics have been reported (*vide infra*, section 1.5.3.).[78–82] Depending on the exact fluorine substitution patterns, some polyfluorophenyl boronic acids are known to protodeboronate in aqueous basic solution in seconds at room temperature. Perrin has reported the kinetics for several electron-deficient 2,6-disubstituted aryl boronic acids including other electronegative substituents (Cl, Br, CF_3 etc.) which also promote rapid protodeboronation.[82]

Many types of boronic acids, including the allegedly stable species, can be protodeboronated using metal-catalysed processes and are discussed in section 1.5.2. in full detail.

1.3.2. Oxidation and homocoupling

A comparison of bond energies show there is a significant thermodynamic driving force for the oxidation of the B-C bond to form a B-O bond.[83] Fortunately, the oxidation of boronic acids with water or atmospheric oxygen (O_2) requires a large activation energy, and thus many boronic acids are stable in air and in water over a wide pH range. It has been proposed that the coordination of water or hydroxide ions to boron may "protect" the boronic acid from the action of oxygen.[84,85] However, oxidation is facile with common oxidants, such as hydrogen peroxide or oxone®, which readily oxidises boronic acids to the corresponding alcohol (or phenol) under basic conditions.[86] Boronic acid oxidation has also been observed in ethereal solvents, particularly in unstabilised (radical inhibitor free) solvents, which are known to undergo photo- or metal-catalysed aerobic oxidation to form hydroperoxides.[5,87]

Boronic acid oxidation has also been noted to occur during Suzuki-Miyaura couplings reactions through palladium-catalysed pathways.[87] Investigations by Amatore and Jutand have revealed an oxidative homocoupling process that runs in competition with the desired cross-coupling (Scheme 1.10).[88] This process starts with the activation of atmospheric oxygen by Pd(0) (**1**) to generate a peroxo complex (**9**). Reaction with boronic acid affords a

new peroxo complex with the organic fragment bonded to palladium (**10**). Subsequent transmetalation to form **11**, and reductive elimination affords the homocoupled product. However, it is the released peroxide prior to transmetalation which is responsible for the oxidation of a molecule of boronic acid to the corresponding alcohol (or phenol).

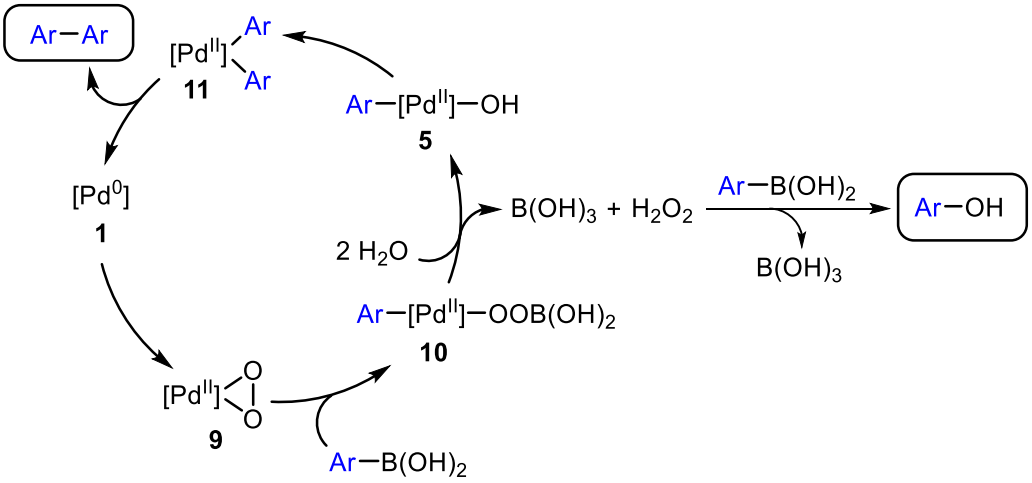

Scheme 1.10 Catalytic cycle for oxidative homocoupling of boronic acids.

1.4. Efforts to mitigate boronic acid side reactions

The associated side reactions of boronic acids have resulted in the development of a variety of strategies focused on their mitigation. Due to its prevalence in synthetic chemistry, many of these developments have been constructed specifically for the Suzuki-Miyaura cross-coupling reaction. Three important methods of side reaction mitigation exist: (i) the design of active catalysts, (ii) the addition of enhancing additives, and (iii) the use of boronic acid derivatives.

1.4.1. Catalyst optimisation

Catalyst design and optimisation has led the way for extremely efficient systems that can undergo rapid oxidative addition and thus increase the concentration of transmetalating metal species.[89] In turn, this increases the turnover frequency and subdues unwanted decomposition pathways. The most common method of catalyst tuning is through modification of auxiliary ligands (Figure 1.3). Buchwald has developed a range of dialkylbiaryl phosphine ligands, specifically designed for the coupling of troublesome heteroaromatic boronic acids (**12**, Figure 1.3).[90,91] These elaborate ligands have also been used to develop precatalysts that activate in remarkably mild conditions at room temperature, whereby decomposition pathways are reduced (**13**, Figure 1.3).[81] Similarly, Fu has demonstrated that electron-rich and bulky trialkyl phosphines successfully cross-couple some unactivated aryl halides to a range of heterocyclic boronic acids (**14**, Figure 1.3).[92] *N*-heterocyclic carbenes have also been demonstrated to be particularly effective for the coupling of pentafluorophenyl boronic acid derivatives (**15**, Figure 1.3).[93]

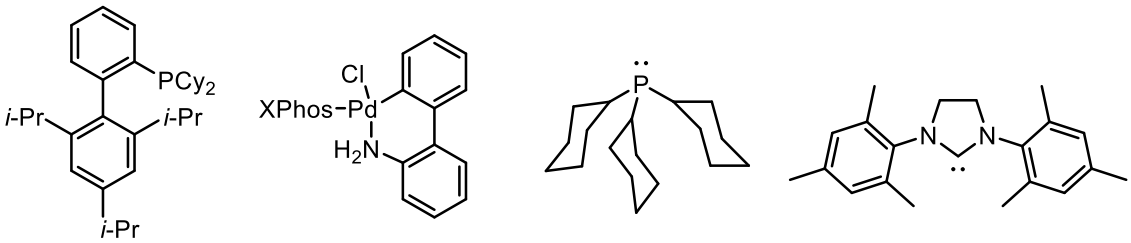

XPhos (**12**) **13** **14** **15**

Figure 1.3 Selected ligands (**12**, **14** and **15**) and precatalyst (**13**) utilised for troublesome Suzuki-Miyaura cross-coupling reactions of unstable boronic acids and derivatives.

1.4.2. Metal additives

An alternative approach to mitigating side reactions has been achieved through the activation of the boron reagents with various metal additives. Notably, stoichiometric amounts of silver oxide have been demonstrated to promote the cross-coupling of the notoriously reactive

polyfluorophenyl boronic acids with aryl halides in good yields.[94–97] The same methodology has also been productive in the coupling of some *n*-alkyl boronic acids.[98] In both cases, it has been suggested that silver promotes the transmetalation step by accelerating the B-to-Pd alkyl/aryl transfer, possibly through the exchange of Pd-Cl bond into Pd-OH. Copper salts have also been shown to have a productive outcome on the cross-coupling of some 2-heteroaromatic boronic acids.[99,100] Similar cooperative effects between palladium and copper have also been noted in borylation reactions.[101] Studies by Deng indicate that copper acts as a transmetalating stepping-stone in which an organocopper species is formed, followed by transfer to the palladium centre (Scheme 1.11).

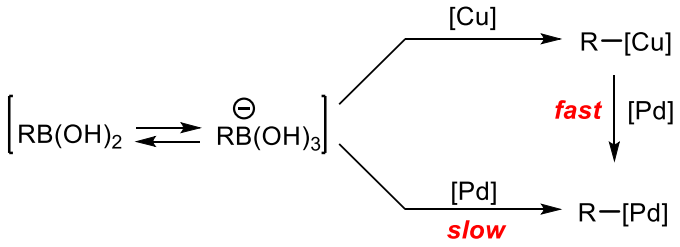

Scheme 1.11 Copper facilitated transmetalation.

1.4.3. Boronic acid derivatisation

To circumvent the numerous stability and purification issues, a variety of boronic acid derivatives have been developed, many of which have been highly beneficial in mitigating side reactions (Figure 1.4).[5,70] An important feature in all of these species is that the boron atom exits as either a tetrahedral centre, or its empty p-orbital is sterically or electronically blocked. As a result, most of these derivatives exist as discrete monomeric structures, and thus unlike boronic acids, do not condense to form boroxines (*vide supra*, section 1.1.1.).

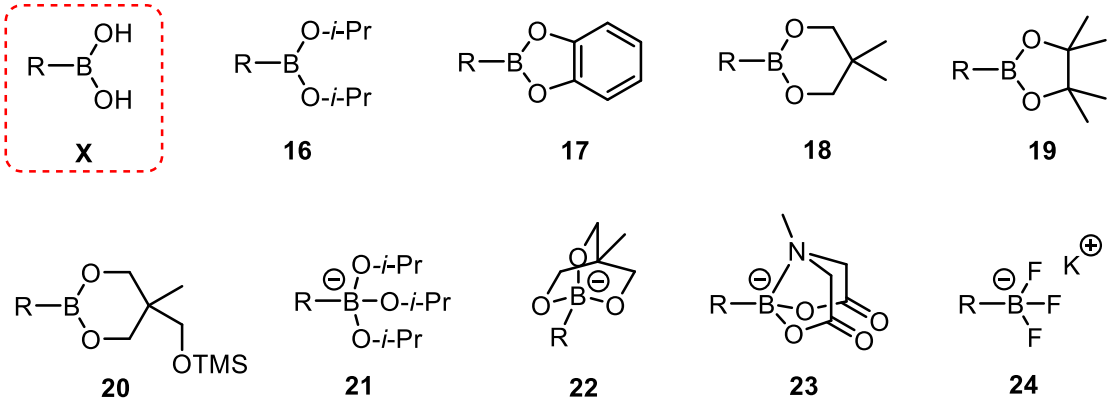

Figure 1.4 Common boronic acid derivatives.

1.4.3.1. Boronic and boronate esters

Some of the most commonly employed derivatives are boronic esters (**16** – **20**). Generally, the hydrolysis of these species back to the corresponding boronic acid is facile, and can occur *via* atmospheric moisture. However, the hydrolysis can be kinetically suppressed through the incorporation of sterically demanding substituents on the ester backbone (**18** – **20**).[102–104] The bulky and electron-rich ligands within boronic esters result in a reduced Lewis acidity at the boron centre.[105,106] It is thought that the reduced association at boron improves boronic ester stability, especially in basic conditions (*vide infra*, section 1.5.3.). In particular, pinacol esters (**19**) have become widespread in synthetic applications and are commercially available.[100,107] Many other variants now exist, which all display their individual benefits in different applications. For example, silyl-protected dioxaborinanes (**20**) perform exceptionally well in palladium-catalysed applications, although the exact reasoning why is unclear.[108]

Boronate esters are 4-coordinate and formally anionic at boron, and thus do not display Lewis acidic characteristics. Key examples include triisopropoxyboronate complexes (**21**) and cyclic triolboronates (**22**), which have been utilised in the coupling of troublesome heteroaromatic moieties.[109,110] It is important to note that it is not clear if a formal deprotection step is required during the metal-catalysed coupling reactions of boronic and boronate esters (i.e. to release the free boronic acid).

1.4.3.2. MIDA boronate esters and organotrifluoroborates

Inert boron derivatives have also been used to avoid problematic side reactions, which under certain conditions can give a controlled *in situ* release of reactive boronic acid. This "slow release" strategy has proved particularly useful in metal-catalysed coupling reactions by avoiding the accumulation of "free" boronic acid in solution, thereby mitigating the potential for side reactions.[87] A key concept with this protocol is having a release rate that complements the catalytic turnover rate. This ensures that reaction times are kept to a minimum, while also reducing the potential for decomposition pathways.

MIDA boronate esters (**23**) are one example of a slow release reagent, and have been employed in a variety of cross-couplings. They display a unique internal coordination between a nitrogen lone pair and the vacant p orbital, and thus are tetrahedral at boron. The structure has been demonstrated to be rigid, as conformation flipping is not detected by ^{1}H NMR.[111,112] The MIDA boronate functional group is remarkably stable to storage, chromatography and a wide range of reaction conditions including harsh oxidation and

various olefination reactions.[111,113] MIDA boronates have proven most useful in the coupling of classically unstable boronic acids, including heteroaromatic, vinyl and cyclopropyl moieties.[74,114] In particular, Burke and coworkers have demonstrated that the 2-pyridyl moiety can be successfully cross-coupled with some unactivated aryl chlorides.[113]

The slow hydrolysis of MIDA boronates is commonly performed with weak bases in aqueous/organic solution and a detailed understanding has recently been reported by Lloyd-Jones and coworkers.[115] While the solvent composition, stirring and reagent substitution all have an effect on the hydrolysis rate, the reaction pH is often the dominant factor in the speed of hydrolysis. Three mechanisms of MIDA hydrolysis were identified including acid-, base- and non-catalysed pathways, with the fastest rates of hydrolysis observed in strongly alkaline conditions. Hydrolysis is still observed in neutral conditions but is approximately 4 orders of magnitude slower (left, Figure 1.5). With this information, the reaction conditions can be fine-tuned to allow a controlled release of unstable boronic acid that suits the reaction at hand.

Organotrifluoroborate salts (RBF_3Ks, **24**) are another derivative used in the slow release of boronic acids. Structurally, RBF_3Ks consist of a 4-coordinate boron centre bonded to 3 fluorine atoms and one organic substituent. Many elaborate RBF_3Ks have been successfully synthesised that display significant stability and are often highly crystalline allowing for facile purifcation.[116] Their slow hydrolysis to release the free boronic acid has also been widely applied to coupling reactions, and has similarly displayed productive couplings for some unstable moieties, such as heteroaromatics, vinyl and cyclopropyl groups.[117–119]

Lloyd-Jones and coworkers have conducted detailed mechanistic studies to understand the hydrolysis of RBF_3Ks reagents and have determined that, unlike MIDA boronates, the rate of hydrolysis is heavily dependent on the substituent type.[120] Electron-deficient aryl trifluoroborates may require many days to hydrolyse whereas electron rich aryl substituents may require minutes (10:1 THF/H_2O, 55 °C). Additionally, the hybridisation of the carbon atom bonded to boron was reported to have large influence on the rate of hydrolysis, with alkynyl substituents displaying the slowest hydrolysis, and alkyl substituents the fastest. Two key mechanisms of hydrolysis were identified, including an acid-catalysed loss of KF from RBF_3K, or direct equilibrium dissociation of KF (right, Figure 1.5). Using DFT studies, a good correlation was found between the rate of hydrolysis and the B-F bond length in the suspected intermediate difluoroborane (RBF_2). Overall, given the very large span of hydrolysis rates observed, unique conditions are often required to ensure the release of "free" boronic acid is at an optimum level to mitigate side reactions.

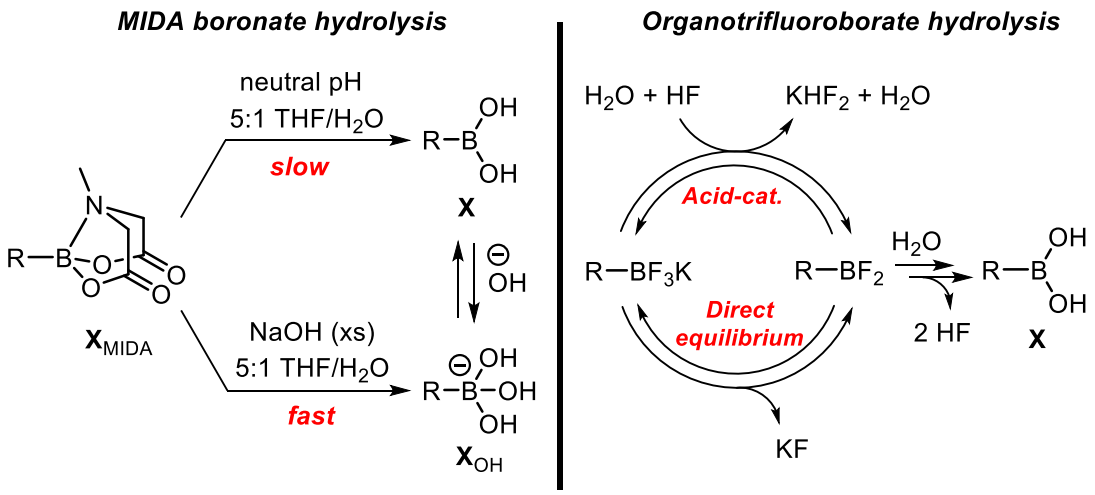

Figure 1.5. Hydrolysis pathways for MIDA boronate esters (left) and organotrifluoroborates (right).

Unquestionably, boronic acid derivitisation has proven to be a useful strategy in the mitigation of side reactions for some troublesome reagents. However, in some cases, the synthesis of these derivatives require *in situ* formation or isolation of the "free" boronic acid. Thus, the preparation of boronic acid derivatives is often more time consuming, and can also be troublesome when the boronic acid is unstable. For example, 2-pyridyl boronic esters are reported to be difficult to prepare and may decompose upon storage.[77] Also 2-heteroaromatic trifluoroboronates (namely 2-pyridyl and 2-furyl) were noted to be have an inadequate shelf life.[121] Consequently, there is a demand to gain a better understanding on the stability of boronic acids and their derivatives which, in turn, may allow for a more informative design of new and improved derivatives.

1.5. Applications and understanding of protodeboronation

1.5.1. Deliberate protodeboronation

Under some scenarios it can be beneficial to induce the deliberate protodeboronation of a boronic acid. Protodeboronation has been applied in a synthetic context as a directing or blocking group towards the synthesis of *ortho*- and *meta*-functionalised phenols.[122] Using 4-hydroxylphenyl boronic acid pinacol ester (**25**), the boronic ester moiety can be used as a temporary blocking group to force electrophilic aromatic substitutions reactions into the *ortho* position (**26**), subsequently followed by protodeboronation to afford *ortho*-substituted phenols (**27**) (top, Scheme 1.12). On the other hand, the boronic acid motif can be used as a directing group. Suginome has developed a pyrazole ligand (**29**) that can associate with 4-methoxyphenyl boronic acid (**28**) and subsequently direct a Ru-mediated silylation into the *meta* position to form **30**.[123] Further demethylation and protodeboronation then affords the *meta*-silylated phenol (**31**) (bottom, Scheme 1.12).

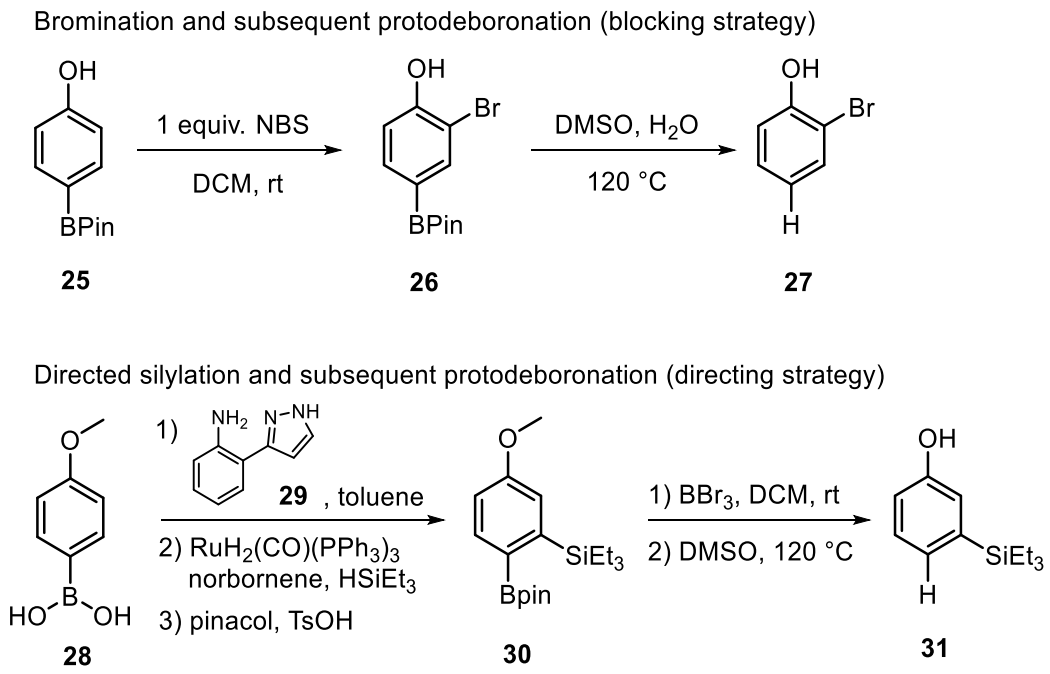

Scheme 1.12 *Ortho*- and *meta*-functionalisation of phenols using the boronic acid moiety as a blocking or directing group.

Aggarwal and coworkers have demonstrated that the sequential lithiation-borylation-protodeboronation methodology can be applied to synthesise various natural products.[124,125] A particularly interesting example is the synthesis of bifluranol (**37**), which utilises the methodology to form 1,2-stereogenic centres (Scheme 1.13).[126] The lithiation-borylation reaction provides a controlled strategy for the formation of a C-C bond between two existing

stereocentres, while the following protodeboronation of the boronic ester allows a stererocontrolled installation of a proton.

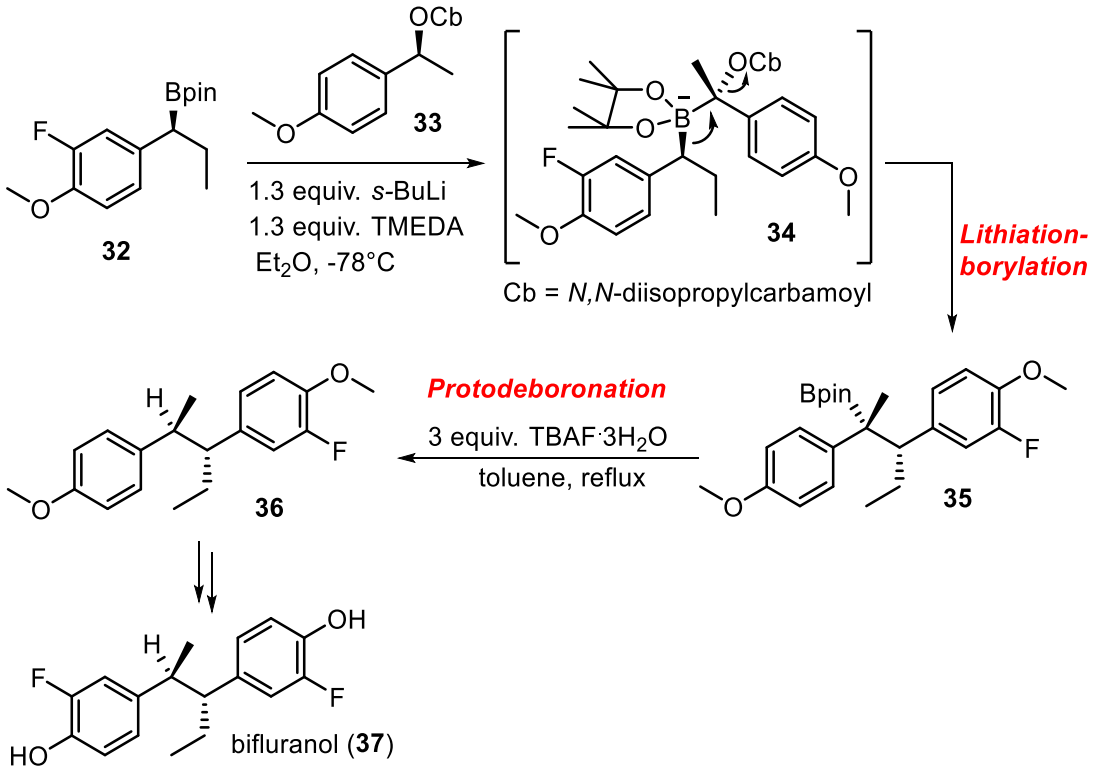

Scheme 1.13 Synthesis of bifluranol (**37**), utilising lithation-borylation-protodeboronation methodology.

Boronic acids are often referred to as having low toxicity,[127–129] most commonly when being compared to other cross-coupling partners such as organozinc or organotin reagents that exhibit serious toxicity concerns.[130] Nonetheless, in a recent study, many boronic acids were reassessed in an extensive Ames assay.[131] Several boronic acids and their precursors (such as HBpin and B_2pin_2) tested positive in the Ames assay, and thus boronic acid mutagenicity must be carefully assessed when being used. On the other hand, the product of protodeboronation, boric acid, does not display mutagenic activity. Therefore, the deliberate protodeboronation of boronic acids may provide a suitable method for the removal of genotoxic or mutagenic boronic acids from the product stream.

1.5.2. Metal-promoted protodeboronation

In 1964, Kuivila demonstrated protodeboronation could be catalysed with cadmium ions between pH ~4-6.[132] Various other metal ions were tested (Ni^{2+}, Mg^{2+}, Co^{2+}, Zn^{2+}, Pb^{2+}, Cu^{2+}), and the greatest acceleration was observed with copper ions. Mechanistic studies

support a mechanism approaching a bimolecular electrophilic substitution (S_E2) process (*vide infra*, section 1.5.3.).

Further studies in this area were not conducted until 2014, where Liu and coworkers developed an efficient and rapid copper-catalysed protodeboronation protocol for aryl boronic acids in basic aqueous/ethanol solvents.[133] Near quantitative yields were obtained for a range of electron-rich and electron-poor aryl boronic acids, including some heteroaromatic examples. Interestingly, the reactions were faster when performed under air rather than under inert atmospheric conditions, and thus a mechanism was proposed that involved a Cu(I)/Cu(II) catalytic cycle, fuelled by atmospheric oxygen. Liu and coworkers also established an analogous silver-catalysed protodeboronation procedure that required basic aqueous conditions.[134] Again, this process was highly efficient for a variety of substituted aryl boronic acids, and was also extended to the deprotection of bifunctional amines.

Shortly afterwards, Lee and coworkers developed a mild gold-catalysed protodeboronation protocol that operates effectively under neutral pH conditions, and thus tolerates a range of acid- and base-sensitive functional groups.[135] DFT studies support a mechanism in which C-B cleavage is rate-limiting and is followed by rapid porotonolysis of a Au-C bond.

Furthermore, iridium-catalysed di- or tri-borylations followed by sequential bismuth-catalysed protodeboronation has proved a valuable technique for producing a diverse range of borylated indoles.[136] This methodology provides a method for the selective borylation in the 4-position of indoles (Scheme 1.14).

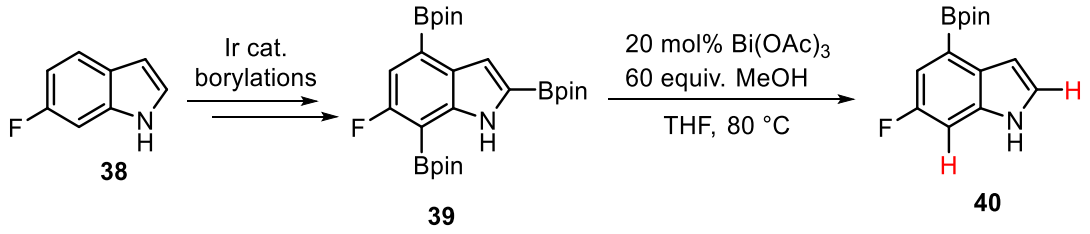

Scheme 1.14 Sequential protodeborylation of 2,4,7-triborylated indole **39**, to afford 4-monoborylated indole **40**.

Interestingly, the sequential protodeboronations occur in the same order in which the Bpin groups are installed *via* iridium-catalysed borylation. By tuning the reaction conditions the extent of protodeboronation can be controlled to selectively afford either mono- or di-borylated products from a tri-borylated starting material.

1.5.3. Literature mechanistic studies

1.5.3.1. Simple aromatic boronic acids

The first detailed mechanistic investigations into protodeboronation were conducted by Kuivila and co-workers in the 1960s, long before the discovery and optimisation of the popular Suzuki-Miyaura cross-coupling reaction.[7,137] A series of publications by Kuivila describe a range of mechanisms for the protodeboronation of some simple arylboronic acids in aqueous systems.[61,62,132,138,139] On the basis of reaction kinetics and using UV-vis spectroscopy, Kuivila was able to distinguish two key modes of protodeboronation including acid-catalysed (k_1) and base-catalysed (k_2) protodeboronation.[61,62] In particular, Kuivila displayed many of these results in the form of pH – log k_{obs} profiles, whereby the dependency of pH on the observed reaction rate constant (k_{obs}) is easily examined (Figure 1.6).

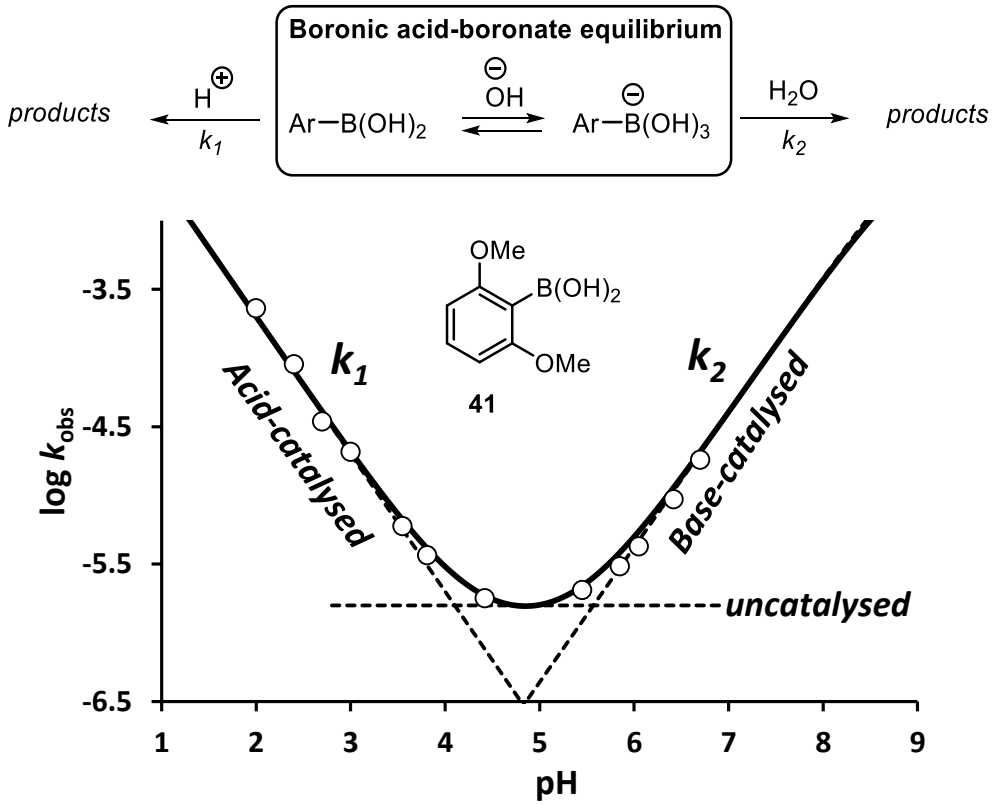

Figure 1.6 Reconstruction of pH – log k_{obs} data from acid- and base-catalysed protodeboronation of 2,6-dimethoxyphenylboronic acid (**41**) in aqueous malonate buffers at 90 °C. White circle = experimental data. Dashed black lines = individual simulations of k_1 and k_2 processes. Solid black line = simulated combination of k_1 and k_2 processes, plus an additional background process (k_{uncat} = 7.5 x 10^{-7} s^{-1}).

In-depth studies for acid-catalysed protodeboronation were carried out using 4-methoxyphenyl boronic acid (**28**), which was subjected to a range of concentrated acidic

solutions (formic, phosphoric, perchoric and sulfuric) and reaction rates correlated to the Hammett acidity function.[140] Reaction rates with formic acid plus sodium formate were dependent solely on the molecular formic acid concentration. Similarly, 2,6-dimethoxyphenyl boronic acid (**41**) was reacted in solutions containing phosphoric acid and dihydrogen phosphate which displayed a dependence on pH and molecular phosphoric acid concentration, suggestive of a general acid-catalysed process. Solvent isotope effects for both boronic acids in varying acidic solutions revealed rate limiting proton transfer. Kuivila noted that an aromatic unimolecular electrophilic substitution (A-S_E1, Scheme 1.15) mechanism does not fit with the evidence in hand, and thus an aromatic bimolecular electrophilic substitution mechanism was proposed (A-S_E2, Scheme 1.15).[62]

Additionally, Kuivila reported substituent effects for some simple aromatic boronic acids, and complex correlations with the acidity function were observed.[138] A noteworthy observation is that the activation parameters for some boronic acids reacted in 30% sulfuric acid indicate that alternative mechanisms may be present, particularly for substrates containing electron-withdrawing groups. New mechanisms were speculated involving the conjugate base, particularly bisulfate in sulfuric acid, which can coordinate at boron to form a 4-coordinate boronate. Kuivila speculated this step to be fast and reversible, followed by rate limiting internal proton transfer from the sulfate moiety to the aromatic ring (A-S_Ei, Scheme 1.15).

Analogous studies were carried out for a limited range of substituted aryl boronic acids at higher pH values using malonate buffers at 90 °C.[61] Studies were restricted to a narrow pH window due to suspected boronic acid oxidation above pH 6.7, that resulted in strong UV-dominating absorptions and prevented reaction monitoring. Indeed, the hydrolysis of methoxybenzenes and their oxidation in basic solution with O_2 has been documented in more recent years.[141,142] Although not strongly alkaline, Kuivila was able to detect the presence of a base-catalysed process due to an increase in reaction rate from pH 6.42 to pH 6.70. Changes in the malonate buffer concentration had no effect on the rate, indicating specific hydroxide ion catalysis whereby *an increase in base concentration results in an increase in rate **only** when it leads to an increase in the concentration of boronate anion*.[61] A two-step mechanism was proposed, involving pre-equilibrium formation of boronate anion (governed by pH) followed by rate-limiting proton transfer from water (A-2, Scheme 1.15).

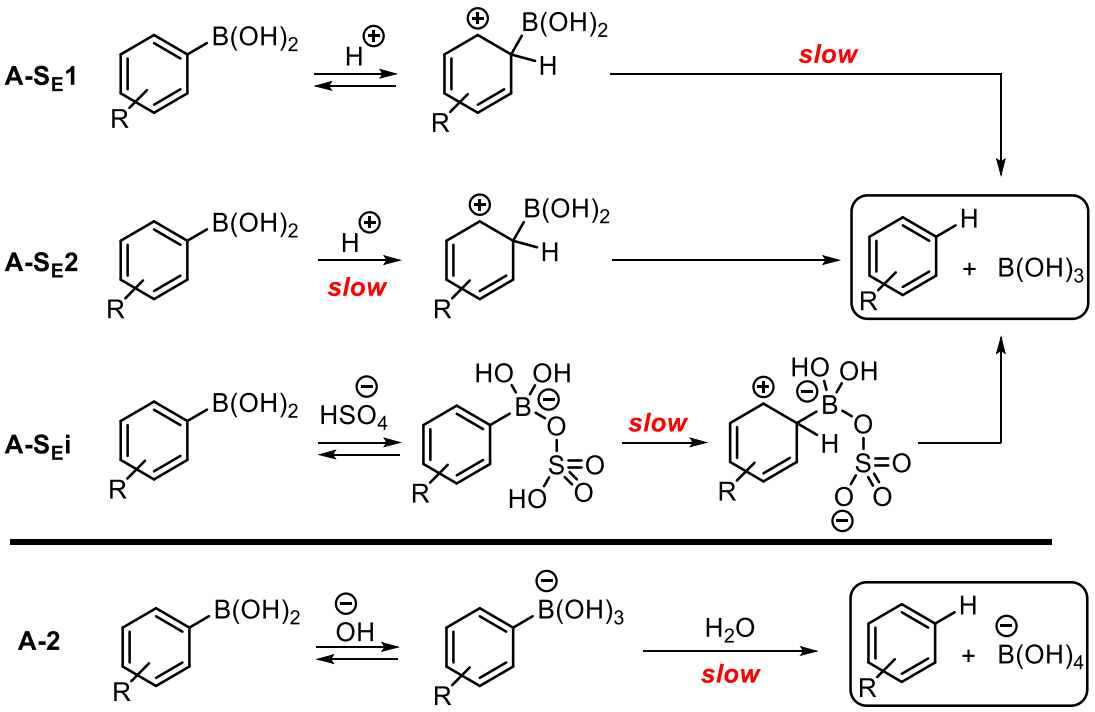

Scheme 1.15 Proposed mechanisms for acid-catalysed (A-S_E1, A-S_E2 and A-S_Ei) and base-catalysed (A-2) protodeboronation, indicating the rate determining step in each case.

Using 2,6-dimethoxyphenylboronic acid (**41**), a pH – log k_{obs} profile was constructed between pH 2.0 and 6.7 (Figure 1.6). A clear transition from an acid-catalysed process (k_1) to a base-catalysed process (k_2) was observed at approximately pH 4.85. Interestingly, experiments carried out in this pH region (where protodeboronation rates are at a minimum) displayed rate constants that are larger than the sum of the expected contributions from both acid- and base-catalysed mechanisms (dotted black lines, Figure 1.6). Kuivila concluded that a background pH-independent mechanism must exist which may involve attack on boronic acid by water, or a kinetically equivalent process such as attack on a boronate anion by a hydronium ion. It is important to note that Kuivila's pH measurements were made at room temperature, although reaction kinetics were performed at 90 °C. Consequently, the autoionisation differences in water are not accounted for and thus the temperature disparity may lead to incorrect absolute pH readings. Nonetheless, the pH readings can be used in a qualitative sense to exhibit the general shape of the pH – log *k* profile.

Substituent effects were also investigated at pH 6.42 and 6.70, whereby all substrates displayed a linear dependence with hydroxide concentration, fitting with a specific-catalysed process. Various LFER plots were attempted and the best correlation was obtained with normal Hammett σ values. The negative and mild magnitude of the slope (ρ = -2.3) was deemed unfitting for a standard electrophilic aromatic substitution mechanism when

compared to ρ values for the analogous protonolysis of silicon, germanium, tin and lead aromatics.[143–146] Nevertheless, it is noted that a small positive charge may be developed in the π-system during the transition state.

Lastly, Kuivila investigated the effect of cadmium ions on the pH – log k_{obs} profile of 2,6-dimethoxyphenylboronic acid and reported an acceleration of base-catalysed protodeboronation (k_2), but no effect on the acid catalysed mechanism (k_1). It was found that the dependence of the rate constant with cadmium ion concentration was linear at low metal concentrations, but appeared to plateau at higher concentrations. A range of other metal ions were found to enhance protodeboronation rates under acidic conditions (Ni^{2+}, Mg^{2+}, Co^{2+}, Zn^{2+}, Pb^{2+}, Cu^{2+}). It is noteworthy that cupric salts (Cu^{2+}) accelerated protodeboronation rates at pH 6.7 by over 300-fold at copper concentrations not dissimilar to those found in non-distilled water sources.[147] Thus, the water source purity may have a significant impact on boronic acid stability in solution.

1.5.3.2. Heteroaromatic boronic acids

The only remaining significant study on protodeboronation before the 21st century was reported by Brown and coworkers and focused on the protodeboronation of thienyl boronic acids.[148] Completing their studies with heterocyclic displacement reactions,[149] protodeboronation of phenyl, 2-thienyl and 3-thienyl boronic acids were carried out at various temperatures (25 – 90 °C) in concentrated acid. Perchloric acid was chosen in an attempt to reduce the presence of the various, but minor, sulfonation and phosphoration side reactions noted in sulfuric acid and phosphoric acid respectively.[62] Both the kinetics and activation parameters obtained were in agreement with Kuivila's studies with arylboronic acids, thus consistent with an A-S_E2 mechanism. Brown hypothesised an alternative, yet kinetically indistinguishable, mechanism involving a 4-membered transition state formed via protonation of a boron hydroxyl group (B-OH) followed by coordination of water to the *ipso*-carbon and boron in a concerted fashion (Scheme 1.16).

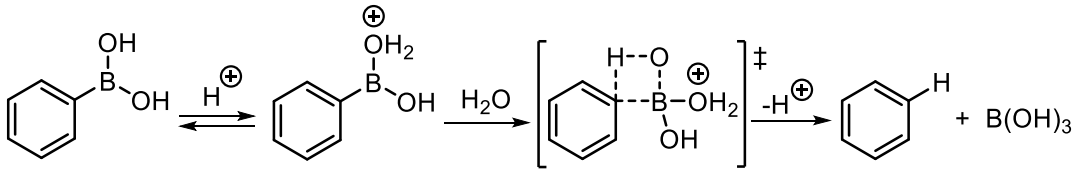

Scheme 1.16 Alternative proposal for concerted acid-catalysed protodeboronation.

In more recent years, Stevens has reported the troubles encountered towards the synthesis and cross-coupling of the infamous 2-pyridyl boronic acid (**44**) and its derivatives.[71]

Attempts to synthesise the 2-pyridyl boronic acid pinacol ester (**46**) through standard Miyaura borylation routes were plagued with high levels of homo-coupling and protodeboronation by-products upon work-up, isolation and analysis. The direct and facile protodeboronation of 2-pyridyl boronic acid (**44**) and its pinacol ester (**46**) were analogised to the decarboxylation of the 2-pyridyl carboxylic acid (**42**), in which its amphoteric nature can lead to the formation of zwitterionic intermediates (**43**, **45** or **47**), followed by expulsion of CO_2 to produce a pyridinium ylide ($\mathbf{44}_{YL}$) (Scheme 1.17).[150]

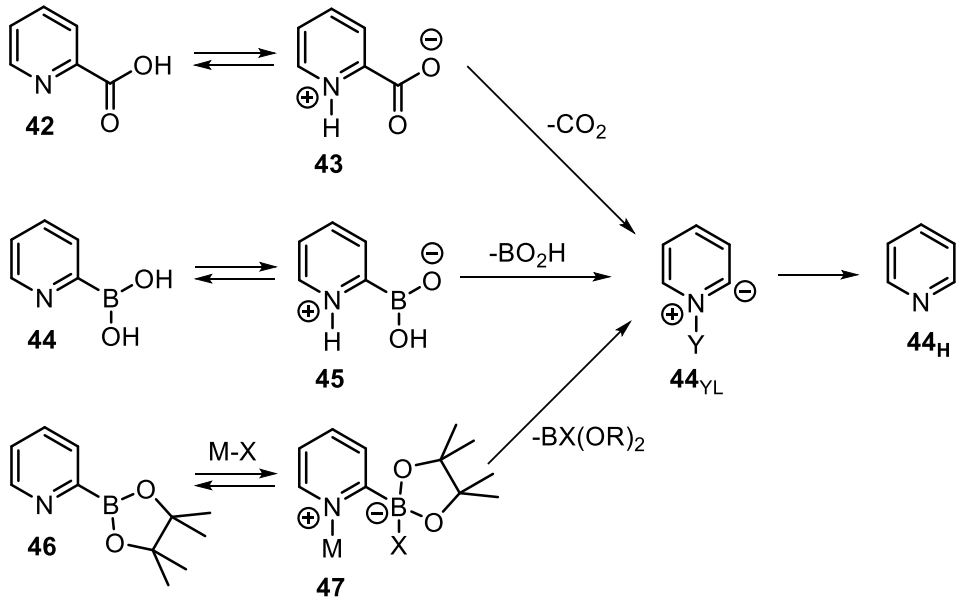

Scheme 1.17 Proposed similarities between 2-pyridyl decarboxylation and protodeboronation through a common pyridinium ylide intermediate.

1.5.3.3. Electron deficient 2- and 2,6-substituted arylboronic acids

The remaining noteworthy studies into protodeboronation all come from within this century and focus on a unique class of arylboronic acids containing *ortho*-substitution, particularly with electronegative functionalities (F, CF_3, OMe etc.). In 2003, Cammidge reported unanticipated levels of protodeboronation during the cross-coupling of 2,3-difluoro-4-heptyl-6-tolyl boronic acid (**48**) with an arylbromide (**49**) (Scheme 1.18).[78] Interestingly it was noted that palladium may have been responsible for catalytic protodeboronation. A control experiment run under dry conditions with caesium fluoride at 100 °C indicated that protodeboronation of ($\mathbf{48}_{H}$) was complete within 4 hours, whereas the same conditions with catalytic amounts of $PdCl_2$ displayed quantitative protodeboronation within minutes.

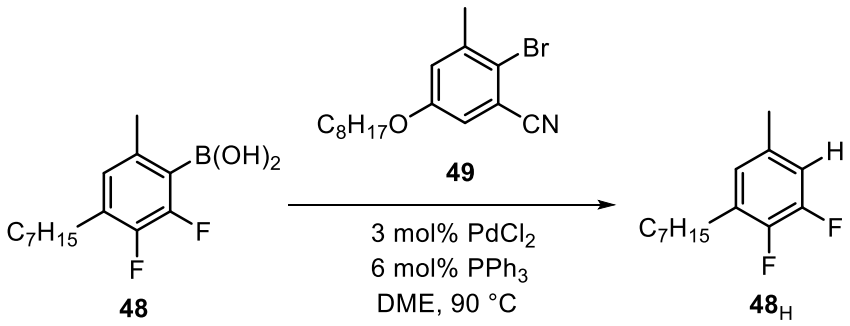

Scheme 1.18 Observed protodeboronation during the cross-coupling of **48** and **49**.

A larger range of polyfluorophenyl boronic acids were investigated by Frohn, who reported protodeboronation kinetics in aqueous pyridine, and in basic aqueous/methanol solvent blends between 25 and 100 °C.[79] The position of fluorine substitution was shown to have a profound impact on the rate of protodeboronation. Substrates containing *ortho*-fluoro or di*ortho*-fluoro substitution displayed the highest level of reactivity whereas substrates with no *ortho*-fluoro substitution displayed little or no reaction, even at high temperature. Similar conclusions with fluorine substitution patterns were made by Adonin, using potassium polyfluorophenyl trifluoroborate salts in alcoholic solvents.[80] It was deemed plausible that protodeboronation may proceed through a specific base-catalysed process as proposed by Kuivila.[61] Alternatively, it was hypothesised that significant fluorine substitution may facilitate deprotonation at the boron-hydroxyl moiety of a boronic acid to form an anion retaining a three-coordinate boron atom. Using ^{19}F NMR, Frohn noted that no significant differences were observed in the chemical shift of boronic acids in various basic solvent blends, and thus was unable to distinguish if aryl(hydroxy)oxylate anion (pathway **I**, Scheme 1.19), hydrogen-bridged species (pathway **II**, Scheme 1.19), or aryl boronate (pathway **III**, Scheme 1.19) were the reactive intermediates to protodeboronation.

In 2010, Buchwald used calorimetry to measure protodeboronation kinetics of a series of 2,6-difluorophenyl boronic acids in a biphasic basic-aqueous medium at room temperature, typically proceeding with half-lives in the order of minutes.[81] From the comparison of direct protodeboronation rates with apparent transmetalation rates, it was concluded that boronic acids that were more prone to protodeboronation were somewhat counterbalanced with an increase in the rate of transmetalation when utilising active precatalysts.[81]

Perrin extended the understanding of direct protodeboronation to include a range of other electronegative 2,6-disubstituents such as Cl, Br and CF_3.[82] Initial rates were measured at room temperature in aqueous-organic solvent blends and reported to be linearly proportional between 1 and 4 equiv. of hydroxide, implying the rate law is first order in both base and

arylboronate. Further supported by analysis of pH – log k_{obs} profiles, a new mechanism involving specific-base mediated protolysis of the arylboronate was proposed (k_3, pathway **IV**, Scheme 1.19). It was noted that while separation of electronic and steric effects of *ortho* substituents is difficult,[151–153] it is unlikely that protodeboronation rates are controlled solely by sterics as the substitution of the relatively bulky methoxy group in the *ortho* position does not exhibit such high levels of reactivity.

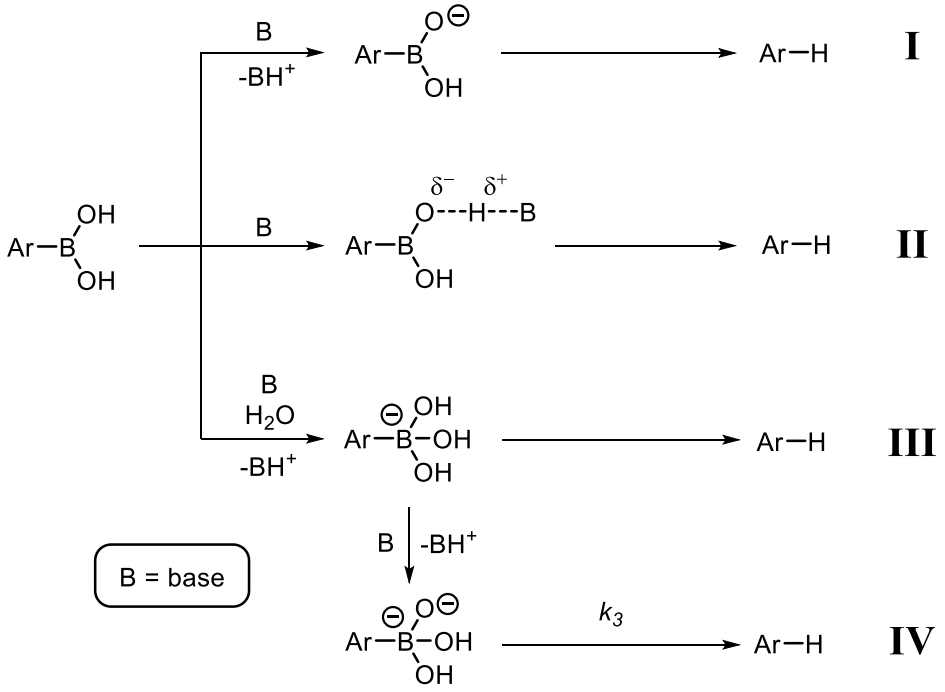

Scheme 1.19 Summary of proposed protodeboronation pathways for electron deficient 2- and 2,6-substituted aryl boronic acids.

1.6. Aims

Unquestionably, Kuivila and co-workers have laid the foundation for the mechanistic understanding of arylboronic acid protodeboronation, however at the time they could not have foreseen how this process would become a key side reaction in one of the most renowned cross-coupling reactions. Due to troublesome oxidative processes, Kuivila was unable to examine protodeboronation reactions at pH values higher than 6.7, and thus could not determine if this mechanism continues into strongly alkaline conditions, or if new mechanisms prevail. Such studies are crucial for determining the relevance of base-catalysed protodeboronation in the abundant applications of boronic acids in basic media, such as the Suzuki-Miyaura cross-coupling reaction. Hence, we sought to investigate the mechanism of protodeboronation by the construction of pH – log k_{obs} profiles across the entire pH range for some simple aromatic and heteroaromatic boronic acids. Additionally, we aimed to build mechanistic models to aid the simulation of experimental data and provide a means of simple extrapolation of kinetic parameters.

Chapter 2

Protodeboronation of Non-Basic Boronic Acids

2.1. Initial studies

2.1.1. pH – log k_{obs} profile for 4-methoxyphenyl boronic acid

Initial studies focused on replicating Kuivila's original results for the 4-methoxyphenylboronic acid (**28**) using identical reaction concentrations (3 – 5 mM) and conditions (H_2O, 90 °C). Control experiments confirmed that alkaline solutions of **28** became pale brown in colour with large increases observed in the UV-vis absorption spectra, as reported by Kuivila.[61] However, at increased reaction concentrations (10 – 200 mM) the NMR spectra of reaction samples displayed solely starting material and protodeboronated products; anisole and boric acid. ^{11}B NMR spectroscopy was deemed suitable for the analysis of reaction kinetics, which displayed distinct time-average signals for both boron compounds (**28** and $B(OH)_3$) at all pH values.

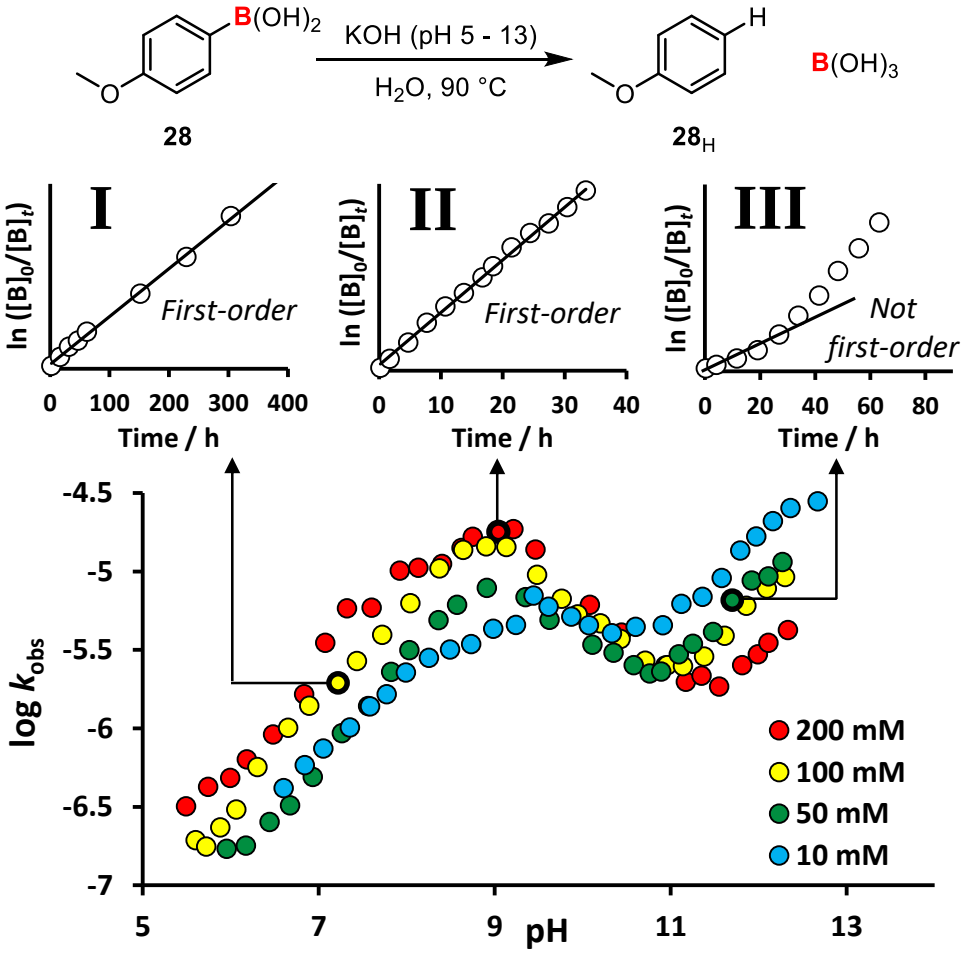

Figure 2.1 pH – log k_{obs} profiles for protodeboronation of 4-methoxyphenylboronic acid (**28**) in H_2O at 90 °C (10 – 200 mM). Reactions performed in borosilicate reaction vessels.

Protodeboronation kinetics were determined at reaction concentrations between 10 – 200 mM using KOH to modify the pH in the absence of buffers. KOH was chosen as a suitable

strong base to simplify equilibrium calculations and is preferred over NaOH due to the known sodium ion error effect with alkaline pH readings.[154] Rate constants were calculated by single-point kinetics between pH 5 – 13 assuming pseudo first-order decay of substrate (see Experimental 6.3.1.). Plotting a pH – log k_{obs} profile displayed unexpected and interesting features that could not be fully explained with Kuivila's proposed mechanisms of protodeboronation (Figure 2.1). In particular, reactions conducted at different initial boronic acid concentrations displayed unique profiles, consistent with a concentration-dependent process. At pH values below 10 an increase in reaction concentration resulted in an increase in log k_{obs}, and clean pseudo first-order kinetics were observed in this region regardless of the reaction concentration (inset graphs **I** and **II**, Figure 2.1). The opposite effect was observed above pH 10, where an apparent inhibition of log k_{obs} was observed with increasing reaction concentration. Furthermore, a distinct skew in the first-order log plots of this pH region indicated some abnormal effects were at play (inset graph **III**, Figure 2.1).

2.1.2. Salt effects and counterion effects

Aqueous reactions can be sensitive to the concentration of ions in solution (ionic strength) or the exact nature of the ions (counterion effects). Hence, it was speculated that the concentration-dependent effects observed in the pH – log k_{obs} profiles might be due to increases in ionic strength. For example, consider two reaction conditions with different initial concentrations of boronic acid. To obtain the same reaction pH in both scenarios, different amounts of strong base are required to obtain an identical boronic acid-boronate ratio, thus resulting in variable ion concentrations (or ionic strength). pH – log k_{obs} profiles were reproduced using a 50 mM initial boronic acid concentration with various KCl and KNO_3 concentrations (graphs **A** and **B**, Figure 2.2). The addition of KCl (0 - 400 mM) displayed no impact on the reaction kinetics between pH 5 – 13. However, the addition of KNO_3 (50 – 700 mM) resulted in accelerated protodeboronation at neutral pH values, yet left the alkaline region of the profile unchanged. It seemed unlikely that a specific nitrate ion effect would accelerate protodeboronation and was therefore suspected that impurities in the reagent may well be the cause for the accelerated reaction rates. Interestingly, a mix of KNO_3 and KCl (400 mM each) had no impact on the protodeboronation rate, even at low pH values. It seemed plausible that KCl may have an inhibitory effect on the potential impurities present in KNO_3, explaining the null effect with mixed KCl and KNO_3. Cation counterion effects were also investigated with the use of alternative hydroxide bases including LiOH, CsOH and NMe_4OH (graph **C**, Figure 2.2). In all cases, only minor deviations in the pH – log k_{obs} profile were observed when compared to KOH, predominantly below pH 7. Overall

it can be seen that the system is rather robust, and reproducible results can be obtained regardless of potential salt contamination – particularly above pH 7.

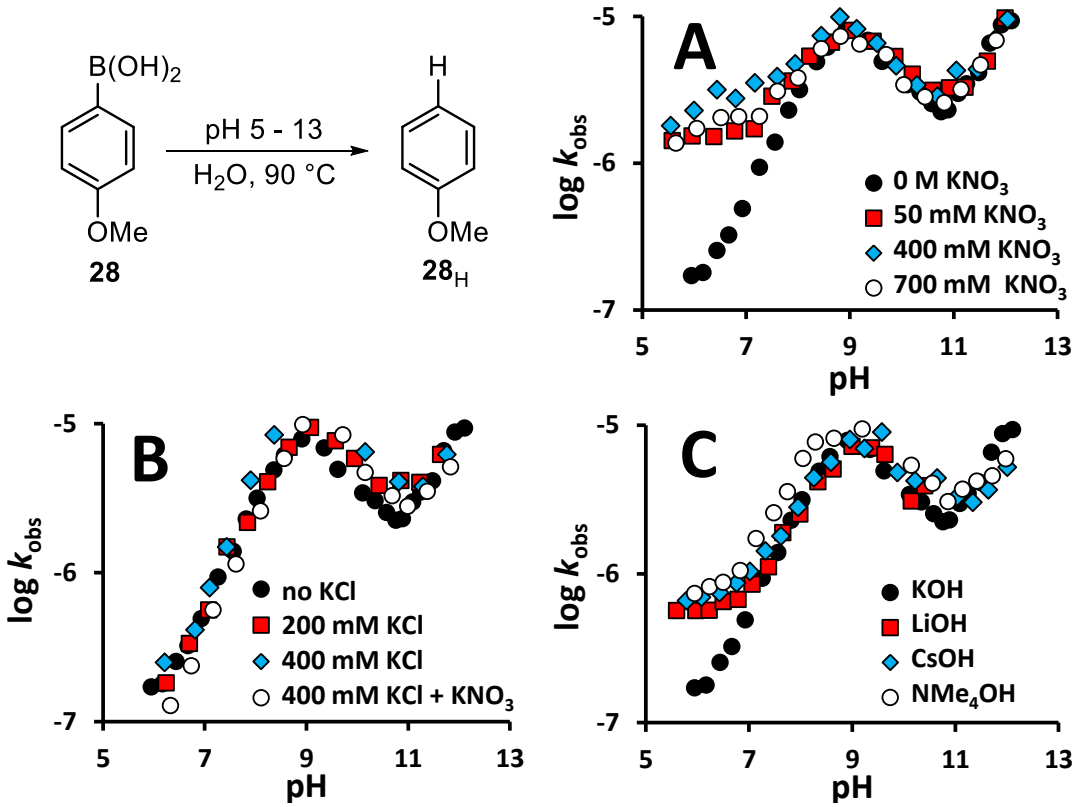

Figure 2.2 pH – log k_{obs} profiles for protodeboronation of 50 mM 4-methoxyphenylboronic acid (**28**) in H_2O at 90 °C with various salt additives (KCl and/or KNO_3), and with various hydroxide bases (KOH, LiOH, CsOH and NMe_4OH). Reactions performed in borosilicate reaction vessels.

2.1.3. Glass effects

Reaction kinetics for the protodeboronation of **28** at high pH values (pH > 10) displayed an increase in the overall ^{11}B NMR signal intensity over the course of the reaction, which was variable depending on the initial boronic acid concentration (refer to Figure 2.1). It was speculated that this peculiar effect could be caused by the leaching of boron compounds from the glass reaction vessels. This theory seemed plausible given the high boron content of borosilicate glassware (>10% boric oxide). The hypothesis was investigated by *in situ* monitoring of a 1 M KOH aqueous solution at 90 °C in a Norell® 5 mm S400 NMR sample tubes by ^{11}B NMR spectroscopy. Within 30 minutes, a sharp ^{11}B NMR signal developed at ~3 ppm, representative of the tetrahydroxyborate anion (Figure 2.3). The leaching of boric acid leads to an apparent increase in 'product concentration' when analysing reaction kinetics by ^{11}B NMR and explains the observed skew in first-order kinetics above pH 10 (inset graph **III**, Figure 2.1). This effect is more evident with reactions carried out at lower

boronic acid concentrations (compare $[RB(OH)_2]_0$ = 10 and 200 mM at pH ~13, Figure 2.1). Complications with boric acid leaching were removed by switching to natural-quartz glassware, which has a lower boron content (Norell® 5 mm Natural Quartz NMR sample tubes, S-5-200-QTZ-7 graded at < 0.1 ppm boron). Repeated reactions in quartz glassware afforded new pH – log k_{obs} plots that revealed a merging of log k_{obs} values for all reaction concentrations at high pH values (Figure 2.4). Nevertheless, a clear acceleration of protodeboronation was evident at pH ~9, presumably *via* a concentration-dependent mechanism. This effect was investigated in-depth in the following section.

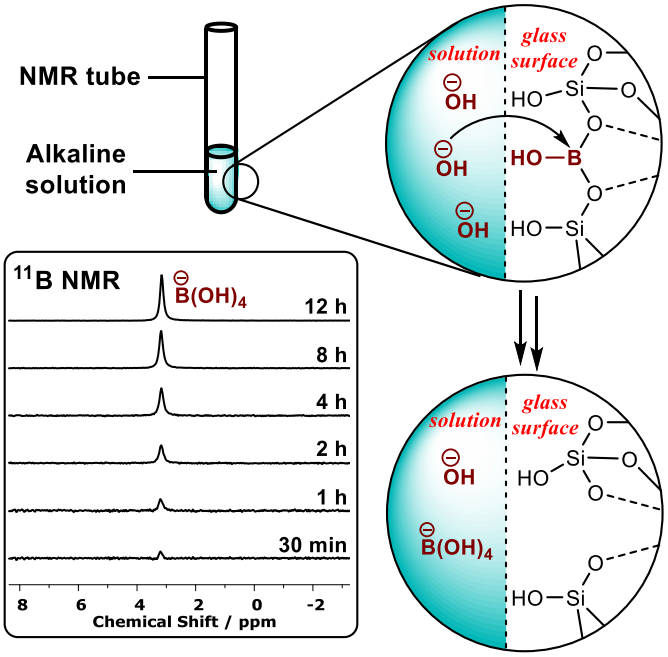

Figure 2.3 Representative illustration of boric acid leaching in alkaline solution. ^{11}B NMR spectra displaying the formation of $B(OH)_4^-$ in 1 M KOH aqueous solution at 90 °C.

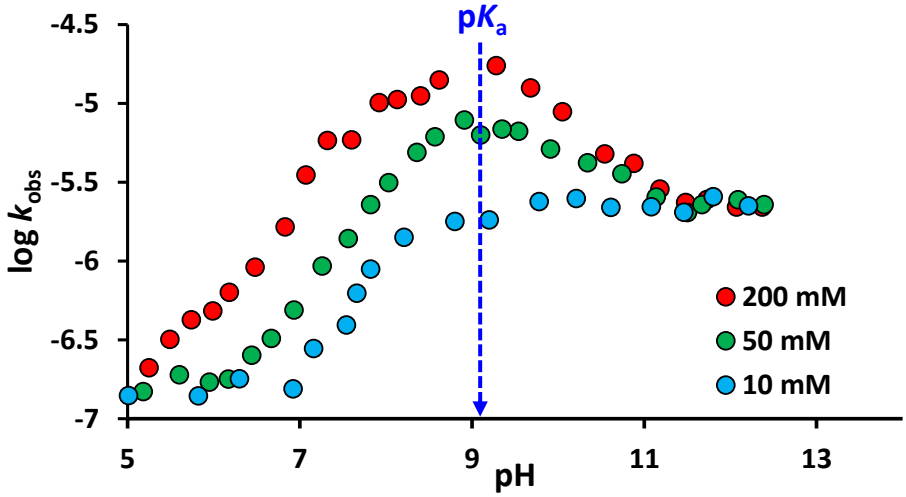

Figure 2.4 pH – log k_{obs} profiles for protodeboronation of 10 – 200 mM 4-methoxyphenyl boronic acid (**28**) in H_2O at 90 °C. Reaction performed in quartz glass reaction vessels.

2.2. Concentration-dependent mechanisms

2.2.1. Self- and auto-catalytic protodeboronation (k_2cat)

2.2.1.1. pH – log k_{obs} profile for 3-thienyl boronic acid

3-thienyl boronic acid (**50**) was selected for further studies into the concentration-dependent protodeboronation mechanism(s) on the basis of its increased reactivity and solubility in aqueous conditions. Pseudo first-order rate constants (k_{obs}) were measured using ^{11}B NMR spectroscopy using the same reaction conditions (H_2O, 90 °C) at a range of concentrations (50 – 800 mM) at various pH values (pH 0 – 13, modified with HCl or KOH).[a] With access to much higher concentrations than 4-methoxyphenylboronic acid (**28**), a clear acceleration in log k_{obs} was observed at higher substrate concentrations, with more than a 10-fold rate increase between 50 mM and 800 mM initial boronic acid concentrations at pH ~8.9. As observed previously, a merging of log k_{obs} occurs at high pH values (pH > 12) while no concentration effects were observed in the acidic pH region (pH < 4) (Figure 2.5).

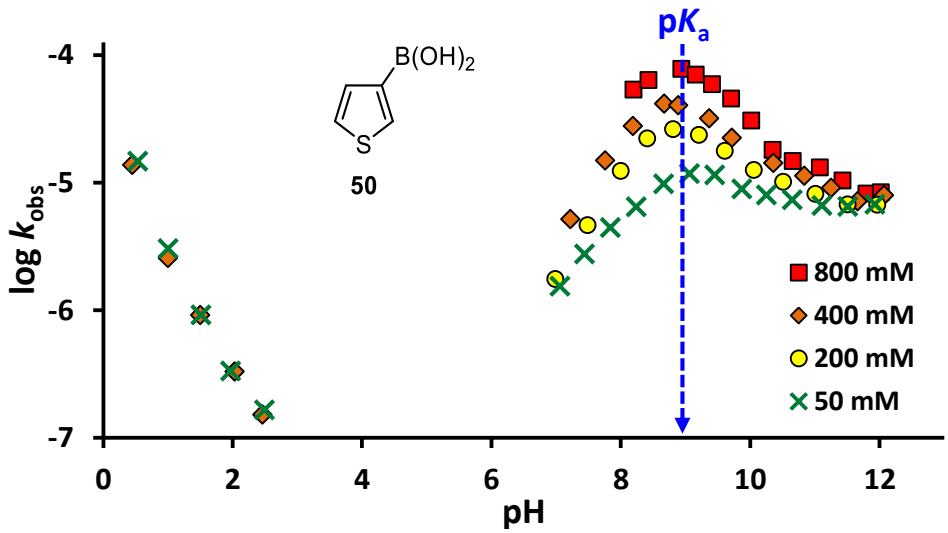

Figure 2.5 pH – log k_{obs} profiles for protodeboronation of 50 – 800 mM 3-thienyl boronic acid (**50**) in H_2O at 90 °C. Markers = experimental data at various initial boronic acid concentrations. Blue arrow indicates pK_a = 8.91 (determined by ^{11}B NMR pH titration at 90 °C).

At all initial boronic acid concentrations, the highest log k_{obs} values were obtained at approximately pH 8.9 (blue arrow, Figure 2.5), whereby the speciation of boronic acid and boronate are equal (i.e. pH = pK_a). Considering this in the form of a Job-plot,[155] a 'self-catalytic' mechanism ($k_2$cat) involving a bimolecular reaction between boronic acid and boronate would seem plausible, however, this would not explain the pseudo first-order

[a] From this point onwards, all reactions were performed in quartz glassware to remove boric acid leaching (refer to section 2.1.3.)

kinetics observed in this distinctive region (refer to inset graph **B**, Figure 2.1). To account for this, the product (boric acid, $B(OH)_3$) needs to be similarly effective as an autocatalyst. The effect of boric acid was tested by Kuivila, and was found to be negative. However these tests were conducted at very low reaction concentrations and therefore his conclusions cannot be extrapolated to reactions at much higher concentrations.[61] The presence of an autocatalytic mechanism was probed with the addition of product (boric acid, $B(OH)_3$) to reaction mixtures containing a low concentration of boronic acid at pH 8.9. Isotopically enriched 10-labelled boric acid ($^{10}B(OH)_3$) was specifically chosen to help simplify the ^{11}B NMR analysis. Protodeboronation of 50 mM 3-thienyl boronic acid (**50**) with 350 mM $^{10}B(OH)_3$ at pH 8.9 displayed a similar k_{obs} values as 400 mM 3-thienyl boronic acid (**50**) (Figure 2.6). Notably, the total boron concentration was 400 mM in both cases, implying that both boronic acid and boric acid are equally efficient at catalysing protodeboronation. At high initial concentrations of 3-thienyl boronic acid (**50**) (left, Figure 2.6), a small deviation in the pseudo first-order kinetics was observed due to the formation of a new boron species, borinic acid ($R_2B(OH)$), which formed and subsequently decayed to protodeboronated products (*vide infra*, section 2.2.2.)

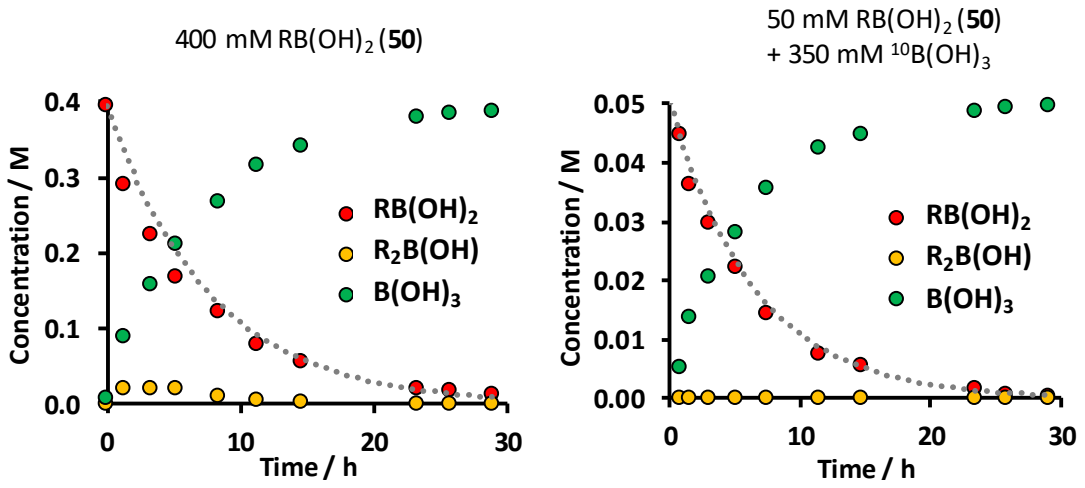

Figure 2.6 Temporal concentration graphs for the protodeboronation of 3-thienyl boronic acid (**50**) at pH 8.9 in H_2O at 90 °C. Circle markers = experimental data. Grey dotted line = simulated pseudo first-order fitting. Left: 400 mM 3-thienyl boronic acid (**50**) (k_{obs} = 3.6 x 10^{-5} s^{-1}). Right: 50 mM 3-thienyl boronic acid (**50**) + 350 mM $^{10}B(OH)_3$ (k_{obs} = 4.4 x 10^{-5} s^{-1}).

Computational studies (carried out by Andrew G. Leach (AGL), John Moores University) were used to help elucidate the finer mechanistic details of self/auto-catalysed protodeboronation. Rate limiting protonolysis was computationally identified in the reaction of 3-thienyl boronate ($\mathbf{50}_{OH}$) with three separate proton sources; water, boronic acid and boric acid. In all cases, the transition states displayed intricate hydrogen bonding between hydroxyl groups on boronic acid, boronate and water (Figure 2.7).

It was found that both boronic acid and boric acid can act as Brønsted acids, whereby a proton is transferred from the boron hydroxyl group to the *ipso*-carbon of the boronate in the rate-limiting event ($k_2$cat). Calculated free energies for both of these processes (self-catalysis 19.5 kcal mol^{-1}, autocatalysis 20.3 kcal mol^{-1}) were similar in energy, supporting the equal catalytic efficiencies of these mechanisms. Moreover, the energies of both concentration-dependent processes were lower than the computed energy for a standard base-catalysed mechanism between aryl boronate and water (k_2, 22.3 kcal mol^{-1}), which is in good agreement with the experimental data at high reaction concentrations.

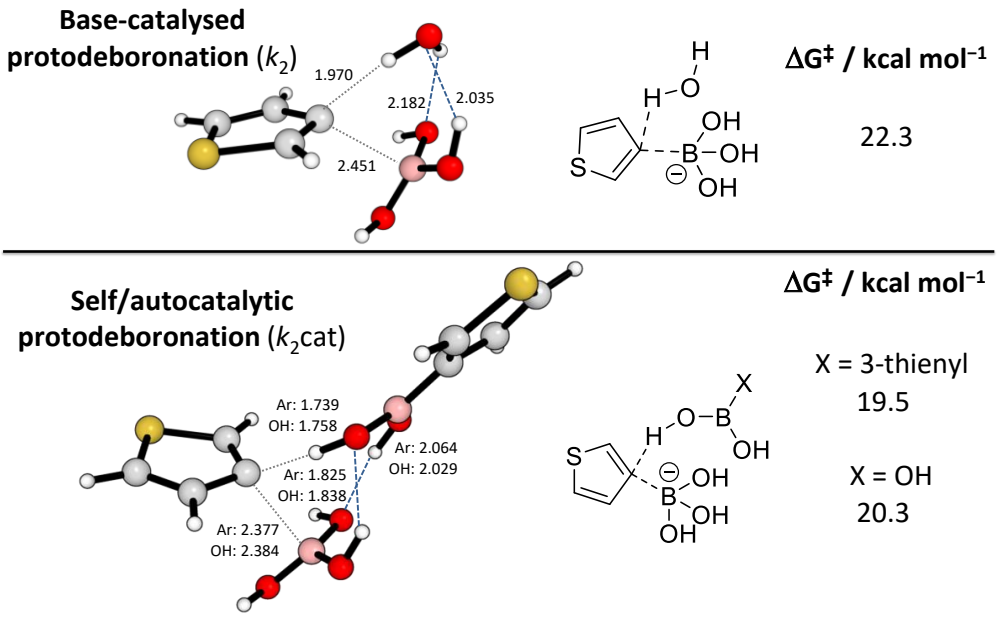

Figure 2.7 DFT (M06L/6-311++G**) transition state structures for protonolysis of 3-thienyl boronate (**50**$_{OH}$) by water (k_2, top) and by boronic acid ($k_2$cat, bottom)

It is important to note that the self- and autocatalytic processes involve a Brønsted-type protonation. Experimentally, measuring the Brønsted acidity of the boronic acid hydroxyl groups is a problematic task as the Lewis acidity (forming the boronate) is the predominant result when working under aqueous conditions. It appears that the unique network of intermolecular bonding between the two substrates facilitates this unusual process. Analogous self-catalytic protodeboronation has been previously observed in the solid state, whereby a large reduction in the entropy of activation aids facile protodeboronation.[156]

2.2.1.2. Model for the simulation of pH – log k_{obs} profiles

A simple mechanistic model was developed to allow analysis and simulation of pH – log k_{obs} profiles for non-basic boronic acids, and provide a simple method for the extraction of multiple rate and equilibrium constants simultaneously (Figure 2.8). The model was designed to contain one pH-dependent equilibrium (K_a) and three possible protodeboronation

pathways including (i) an acid-catalysed process (k_1); (ii) a base-catalysed process (k_2); (iii) a self- and autocatalytic process ($k_2$cat). An overall rate equation can be derived:

$let\ [\mathrm{RB(OH)_2}] = [\mathbf{X}];\ \ [\mathrm{RB(OH)_3}^-] = [\mathbf{X}_{\mathrm{OH}}];$

$$rate = k_1[\mathbf{X}][\mathrm{H^+}] + k_2[\mathbf{X}_{\mathrm{OH}}][\mathrm{H_2O}] + k_2cat[\mathbf{X}_{\mathrm{OH}}]([\mathbf{X}] + [\mathrm{B(OH)_3}]) \quad (2.1)$$

$$k'_2 = k_2[\mathrm{H_2O}] \quad (2.2)$$

$$rate = k_1[\mathbf{X}][\mathrm{H^+}] + k'_2[\mathbf{X}_{\mathrm{OH}}] + k_2cat[\mathbf{X}_{\mathrm{OH}}]([\mathbf{X}] + [\mathrm{B(OH)_3}]) \quad (2.3)$$

Note that the self- and autocatalytic processes are unique mechanisms but, for simplicity, were combined into a single pathway. The simplification can be taken further by assuming that at a given fixed pH value, the concentration of boronic acid plus the concentration of boric acid is constant.

$$[\mathbf{X}] + [\mathrm{B(OH)_3}] = constant\ concentration = [\mathrm{C}] \quad (2.4)$$

$$rate = k_1[\mathbf{X}][\mathrm{H^+}] + k'_2[\mathbf{X}_{\mathrm{OH}}] + k_2cat[\mathbf{X}_{\mathrm{OH}}][\mathrm{C}] \quad (2.5)$$

This simplification is particularly useful in condensing the overall rate equation into a pseudo first-order expression, and was deemed reasonable given the observed equal activities of each process both experimentally and computationally. However, this simplification also requires the boronic acid and boric acid to have similar pH-dependent equilibria (i.e. they require similar pK_a values). ^{11}B NMR titrations confirmed the pK_a values of 4-methoxyphenyl boronic acid (**28**, pK_a = 9.1) and 3-thienyl boronic acid (**50**, pK_a = 8.9) to be similar to that of boric acid (pK_a = 9.0) in H_2O at 90 °C (for pK_a titration data, see Appendix 8.2.). When $\Delta pK_a \leq 0.1$, the total concentration of boronic acid plus boric acid (i.e. [**X**] + [$B(OH)_3$]) varies less than 3% at all pH values, supporting the feasibility of this simplification.

With the input of initial boronic acid concentration ($[B]_{initial}$), water concentration ($[H_2O] \approx 54$ M), auto-ionisation constant of water (pK_W(90 °C) = 12.28)[157] and the aqueous association constant (K_a) the concentrations of boronic acid and boronate can be calculated at all pH values using the Henderson-Hasselbalch equation. In turn, with inputted rate constants (k_1, k_2, $k_2$cat), the initial rate of each pathway can be calculated and subsequently summed to calculate an overall rate, and lastly divided by the initial boronic acid concentration ($[B]_{initial}$) to give a calculated pseudo first-order rate constant. Plotting the pH against the calculated logarithmic rate constant produces a simulated pH – log k_{obs} profile that can be modified through variation of the individual rate constants (k_1, k_2, $k_2$cat) and ultimately optimised to

achieve the best fitting to an experimental data set through minimisation of the sum square error (SEE). Figure 2.8 displays representative individual pH – log k_{obs} profiles for each mechanism (k_1, k_2 and $k_2$cat), and their combination into an overall pH – log k_{obs} profile. It is noteworthy that both k_1 and k_2 mechanisms are concentration independent (i.e. the observed rate constant, k_{obs}, does not vary with concentration) whereas $k_2$cat displays a strong concentration dependence, reaching a maximum k_{obs} value at pH = pK_a (50:50 boronic acid/boronate). The overall pH – log k_{obs} profile shows a key distinctive feature, in that the concentration-dependent mechanism is only present at pH values near the pK_a of the boronic acid. At either very acidic (low pH) or very basic conditions (high pH), the concentration dependence is lost and only the Kuivila-type acid- and base-catalysed processes prevail.

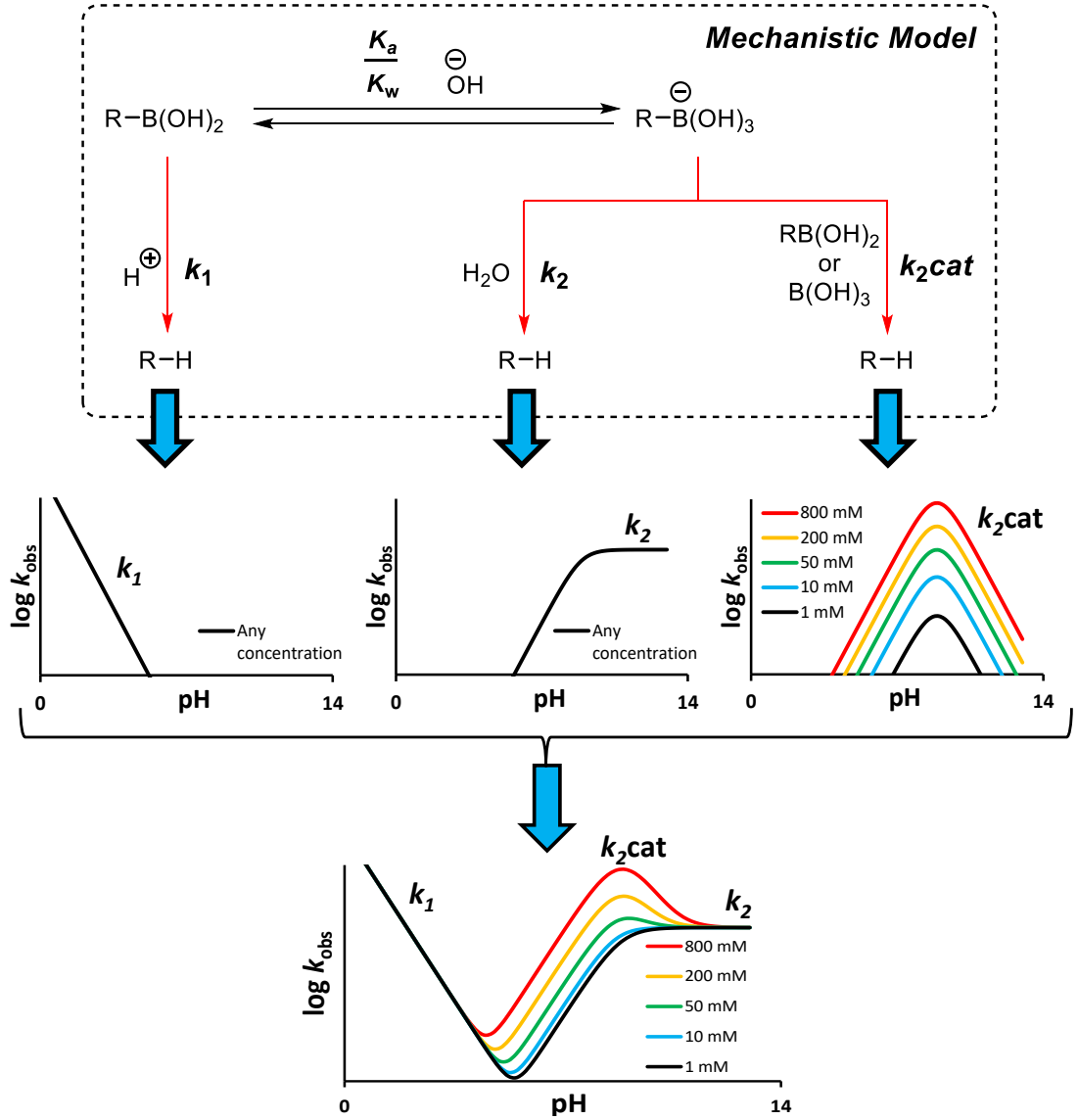

Figure 2.8 Simple mechanistic model for the simulation of pH – log k_{obs} profiles for non-basic boronic acids, showing the representative simulation plots for each individual process (k_1, k_2, $k_2$cat) and their combination to give the overall pH – log k_{obs} profile.

Using the model, the experimental data acquired for the protodeboronation of 3-thienyl boronic acid (**50**) at various initial boronic acid concentrations was successfully simulated and rate constants extracted (Figure 2.9). A good fit was obtained across the entire pH range, including the concentration-dependent region at pH = pK_a. However minor deviations from the fit are observed at near neutral pH values, particularly for reactions performed at low initial boronic acid concentrations ($[RB(OH)_2]_0$ = 50 mM, Figure 2.9). This effect may arise from the presence of a trace metal catalysed protodeboronation pathway, previously proposed by Kuivila.[61,b]

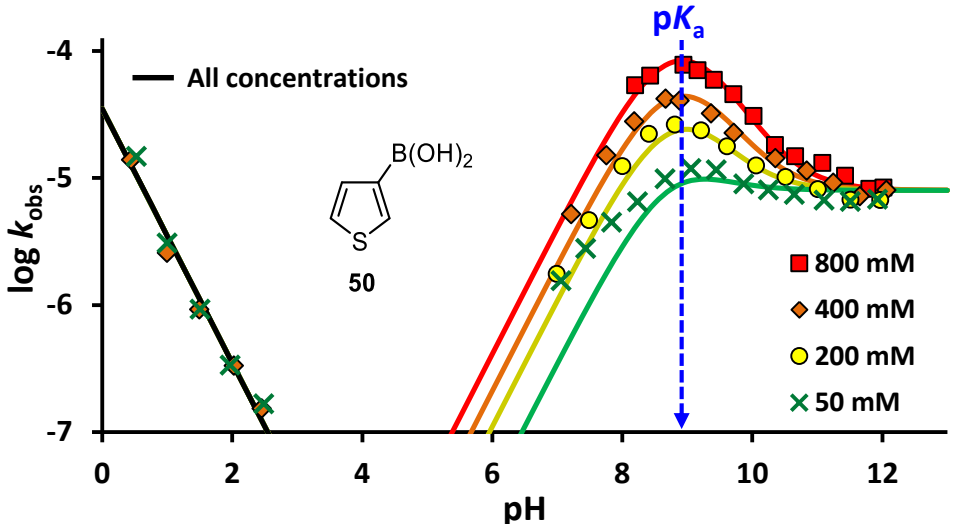

Figure 2.9 pH – log k_{obs} profile for pseudo first-order protodeboronation of 3-thienyl boronic acid (**50**) in H_2O at 90 °C. Markers = experimental data. Solid lines = simulation fittings using mechanistic model (see Figure 2.8). pK_a = 8.91 (determined by ^{11}B NMR pH titration at 90 °C), k_1 = 3.3 x 10^{-5} s^{-1}, k'_2 = 7.8 x 10^{-6} s^{-1}, $k_2$cat = 4.0 x 10^{-4} M^{-1} s^{-1}.

2.2.1.3. Kinetic isotope effect studies

With a working model in hand, we sought to investigate the effect of solvent hydrogen isotope composition (H_2O and D_2O) on the rates of protodeboronation of 3-thienyl boronic acid (**50**). Reaction rates were obtained in H_2O and D_2O, separately, at two initial boronic acid concentrations (50 and 400 mM) in alkaline conditions (pH 5 – 13). Differences in the autoionisation constants (K_W) for H_2O and D_2O, due to different zero-point energies, make interpretation of a co-plotted pH– and pD – log k_{obs} profile troublesome.[158] For example, consider two separate solutions of pure H_2O and D_2O with identical hydron[c] concentrations (i.e. pH = pD): Although hydron concentrations are equal, the different autoionisation constants (K_W) for each solution result in different hydroxide (or deuteroxide) concentrations

[b] Since the primary focus was centred on simulation of the $k_2$cat process, additional protodeboronation pathways were not incorporated into the model at this time.
[c] Hydron is a term for a monohydrogen cation of charge +1, comprising of protons and deuterons.

(i.e. pOH ≠ pOD). A more intuitive plot can be constructed by standardising the data in terms of hydroxide concentration. This can be achieved by plotting pH and (pD + ΔpK_W) together on the x-axis, where ΔpK_W is the difference between the autoionisation constants of H_2O and D_2O at 90 °C (Figure 2.10). Simulation of all the rate data using the mechanistic model (refer to Figure 2.8) provides an easy comparison of individual rate constants and calculation of KIE values for both base-catalysed (KIE = 2.0) and self/autocatalysed (KIE = 1.4) protodeboronation pathways, and indicates both mechanisms involve a rate-limiting proton-transfer. Although the values are relatively small for primary KIEs, the computed transitions states show rather complex hydrogen/deuterium bonding effects which may be responsible for the reduced values (refer to Figure 2.7).

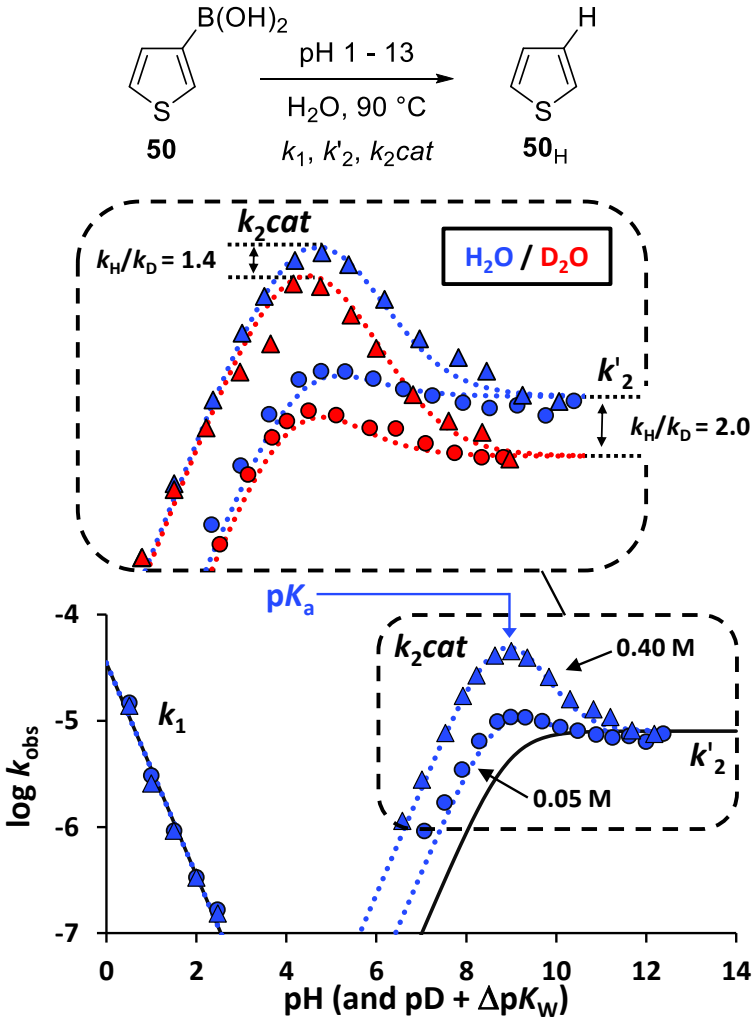

Figure 2.10 Effect of pH and concentration on the rate of protodeboronation of 3-thienyl boronic acid (**50**). Markers = experimental data (blue = H_2O, red = D_2O). Dotted lines = simulation fitting using mechanistic model (see Figure 2.8). pK_a = 8.91 (H_2O) or 9.68 (D_2O), determined by ^{11}B NMR pH titration at 90 °C. Simulation fitting in H_2O: pK_a = 8.91, k_1 = 3.3 x 10^{-5} s^{-1}, k'_2 = 7.8 x 10^{-6} s^{-1}, $k_2$cat = 4.5 x 10^{-4} M^{-1} s^{-1} (for solid black line, $k_2$cat = 0). Simulation fitting in D_2O: pK_a = 9.68, k'_2 = 3.9 x 10^{-6}, $k_2$cat = 3.2 x 10^{-4} M^{-1} s^{-1}.

2.2.2. Disproportionation

2.2.2.1. 3-thienyl boronic acid disproportionation and crossover studies

In addition to self- and autocatalytic protodeboronation, another concentration-dependent process was observed in the reaction of 400 mM 3-thienyl boronic acid (**50**) in H_2O at 90 °C (left, Figure 2.6). Reaction monitoring by ^{11}B NMR revealed the formation of a new boron species over the course of a few hours, which was then observed to decay into protodeboronation products. Acidification of a reaction aliquot after 5 hours (bottom spectrum, Figure 2.11) revealed the new signal to be pH dependent, much like the boronic acid, but with a greater chemical shift range (2.17 ppm at pH 8.95, and to 39.40 ppm at pH 5.00). The large downfield shift in the acidified sample was representative of a borinic acid chemical shift, a boron species consisting of two aryl groups attached to boron ($R_2B(OH)$).[159]

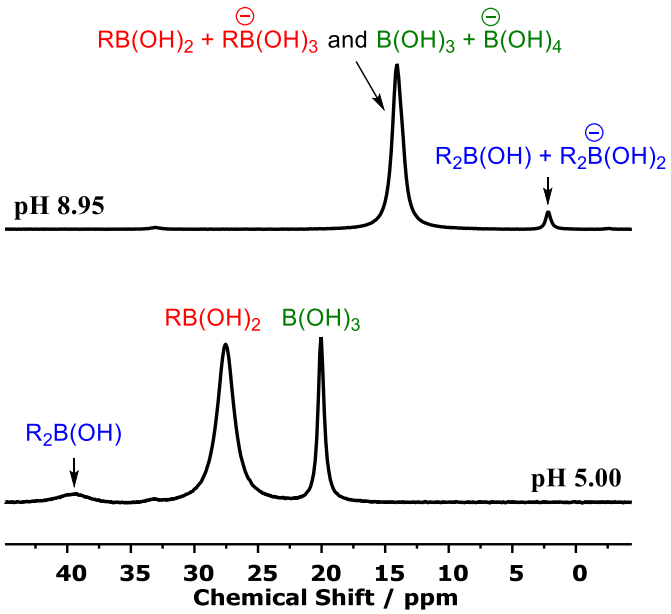

Figure 2.11 Top: ^{11}B NMR spectrum after reaction of 3-thienyl boronic acid (**20**) at pH 8.95 in H_2O at 90 °C for 5 h. Bottom: ^{11}B NMR spectrum of the same sample following acidification with AcOH to pH 5.00.

The formation of a borinic acid (or borinate, i.e. $R_2B(OH)_2^-$) species was speculated to form *via* disproportionation of two molecules of boronic acid. Similar disproportionation processes are well known for the magnesium-based Grignard reagents, through what has been termed the 'Schlenk equilibrium'.[160] Other organometallic cross-coupling partners, such as Negishi (Zn) and Stille (Sn) reagents, are also known to participate in the exchange of aryl or alkyl groups in their preparation or under reaction conditions.[161] A crossover experiment was designed to investigate the exchange of aryl groups across boron by reacting 200 mM isotopically enriched [^{10}B]-3-thienyl boronic acid ([^{10}B]-**50**) with 200 mM [^{11}B]-$B(OH)_3$ with

200mM KOD (pD ≈ pK_a ≈ 9.68) in D_2O at 90 °C. Reaction monitoring with ^{10}B NMR displayed the expected decay of boronic acid ([^{10}B]-**50**) and the minor, but transient, formation of the borinic acid species ([^{10}B]-**50**$_{borinic}$). Similarly, ^{11}B NMR analysis displayed the transient formation of [^{11}B]-3-thienyl boronic acid ([^{11}B]-**50**), and very minor levels of [^{11}B]-3-thienyl borinic acid ([^{11}B]-**50**$_{borinic}$) which indicates transfer of the 3-thienyl group between all boron species (Figure 2.12).

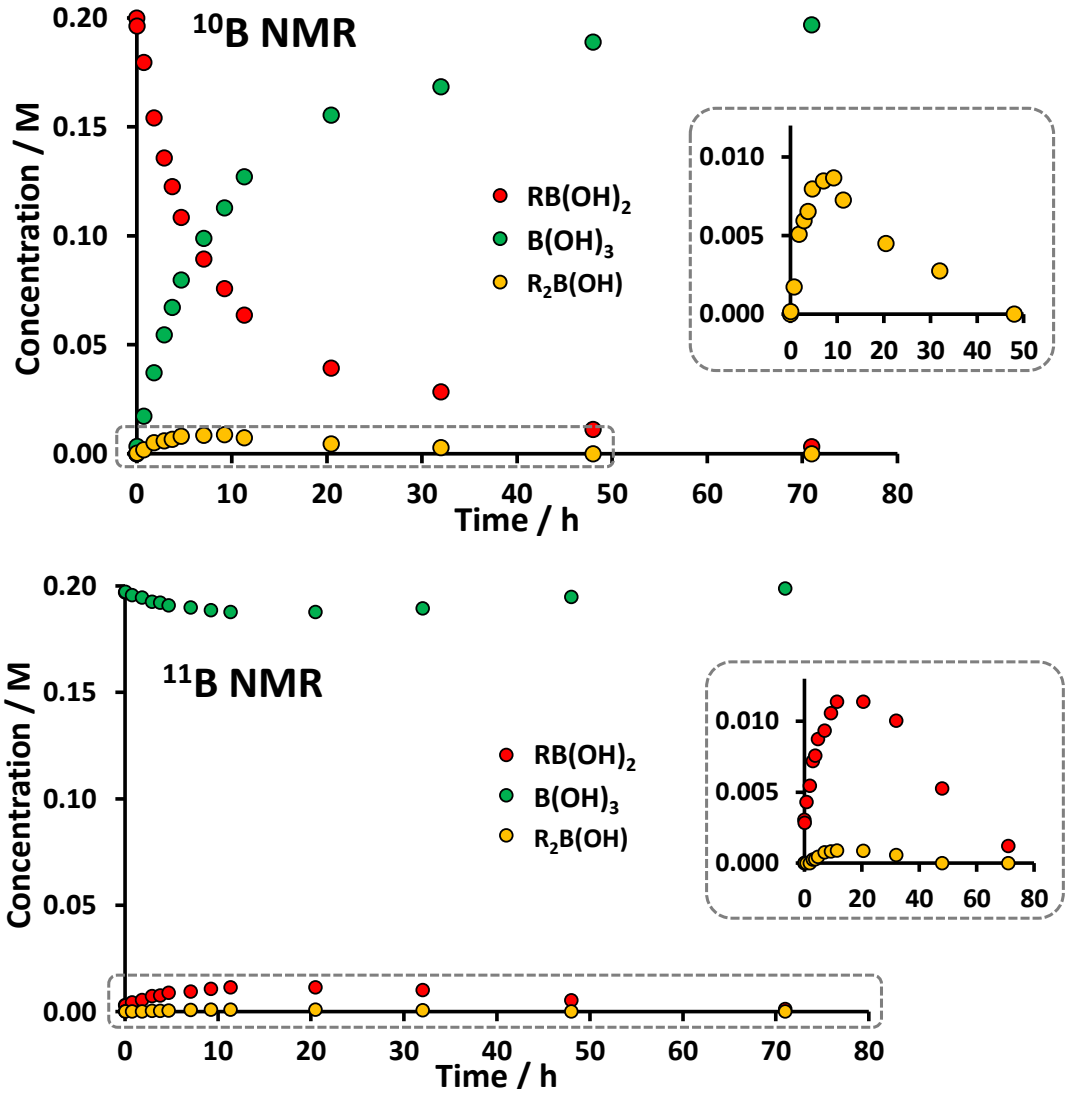

Figure 2.12 Protodeboronation and crossover of [^{10}B]-3-thienyl boronic acid ([^{10}B]-**50**) analysed by simultaneous ^{10}B NMR (top) and ^{11}B NMR (bottom).

2.2.2.2. 2-furyl boronic acid disproportionation

Further disproportionation studies were conducted with 2-furyl boronic acid (**51**) (400 mM) with 0.5 equiv. KOD at 70 °C. A new solvent system, 1:1 D_2O/d_8-dioxane, was employed to maintain sufficient solubility at high reaction concentrations and to allow convenient analysis by ^{1}H and ^{11}B NMR. The temporal concentration data indicated a two-step process,

initially forming 2-furyl borinic acid (**51**$_{borinic}$), which underwent further reaction to give a new boron species (for ^{1}H and ^{11}B NMR spectra, see Appendix section 8.4.). The new species displayed a similar pH-dependent chemical shift to that of boronic acid and borinic acid in both ^{1}H and ^{11}B NMR spectra and was ultimately assigned as trifurylborane (**51**$_{borane}$); a further disproportionation product of borinic acid. After several days all species decay to the protodeboronated products; boric acid and d_1-furan (**51**$_D$). Borinic acid forms rapidly within the first hour and is then consumed as borane is formed. Interestingly, significant amounts of the borane species can be observed after several days under the reaction conditions (Figure 2.13).

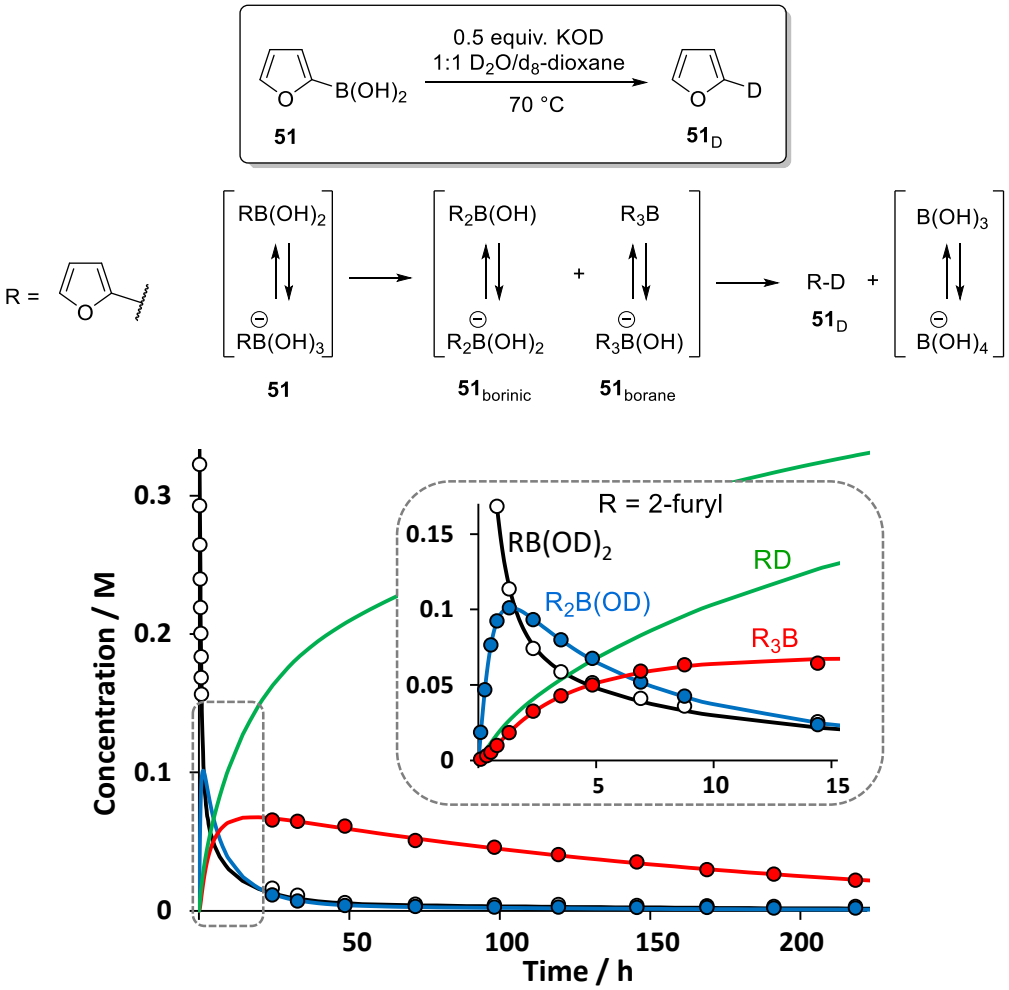

Figure 2.13 Temporal concentration plot for the disproportionation of 2-furyl boronic acid (**51**) (400 mM) with 0.5 equiv. KOD in 1:1 D_2O/d_8-dioxane at 70 °C. Markers = experimental data from *in situ* ^{1}H NMR spectroscopy. Lines = simulation fitting, see Experimental 6.4.3.2 for model and further details. Protodeboronation product, d_1-furan, was volatile under the reaction conditions and was not monitored.

DFT studies were employed (AGL) to investigate the potential mechanism of disproportionation. Given that disproportionation was maximised at pH (or pD) values close

to the boronic acid pK_a, we initially envisaged an analogue of the self- and autocatalytic protodeboronation mechanism ($k_2$cat), in which the aryl group of the boronate migrates to the Lewis acidic boron center of a boronic acid (to form borinic acid/borinate) rather than to the Brønsted acidic proton of the boron hydroxyl group (to form protodeboronated products) (Figure 2.14).

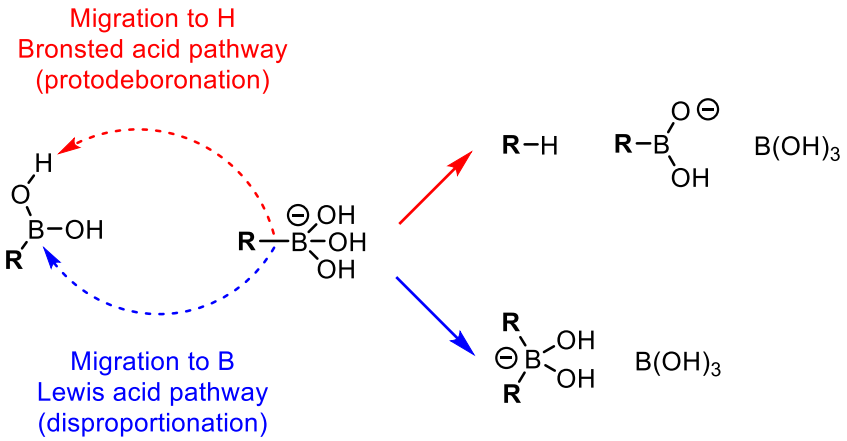

Figure 2.14 Analogy between bimolecular protodeboronation ($k_2$cat) and disproportionation.

However, the computed activation barrier for the 2-furyl migration from **51**$_{OH}$ to the boron centre of **50** was calculated to be greater than that for migration to the proton of the boron hydroxyl group (22.5 kcal mol^{-1} and 20.3 kcal mol^{-1}, respectively) and thus protodeboronation would outweigh disproportionation if only these transition states were operative. Therefore an alternative disproportionation process was considered whereby a cyclic boroxine-ate complex can form *via* condensation of two molecules of boronic acid and one molecule of boronate, followed by aryl migration, and finally hydrolysis to release borinic acid (**51**$_{borinic}$), boronic acid (**51**) and boric acid (B(OH)$_3$) (top, Scheme 2.1). The rate-limiting barrier for 2-furyl migration was calculated to be 19.1 – 19.4 kcal mol^{-1}. Interestingly, a similar process for the formation of borane (**51**$_{borane}$) would require reaction between a borinic acid and a boronate, which cannot involve a cyclic boroxine due to lack of hydroxyl groups at boron. Instead, a dimer intermediate was computed with a free energy barrier of 18.9 kcal mol^{-1} (bottom, Scheme 2.1).

Considering the computed mechanisms for disproportionation, a model consisting of reversible disproportionation and irreversible protodeboronation (through k_2 and $k_2$cat mechanisms) was used to simulate the temporal concentration data, from which a good fit was achieved (solid lines, Figure 2.13, see Experimental 6.4.3.2 for simulation details)

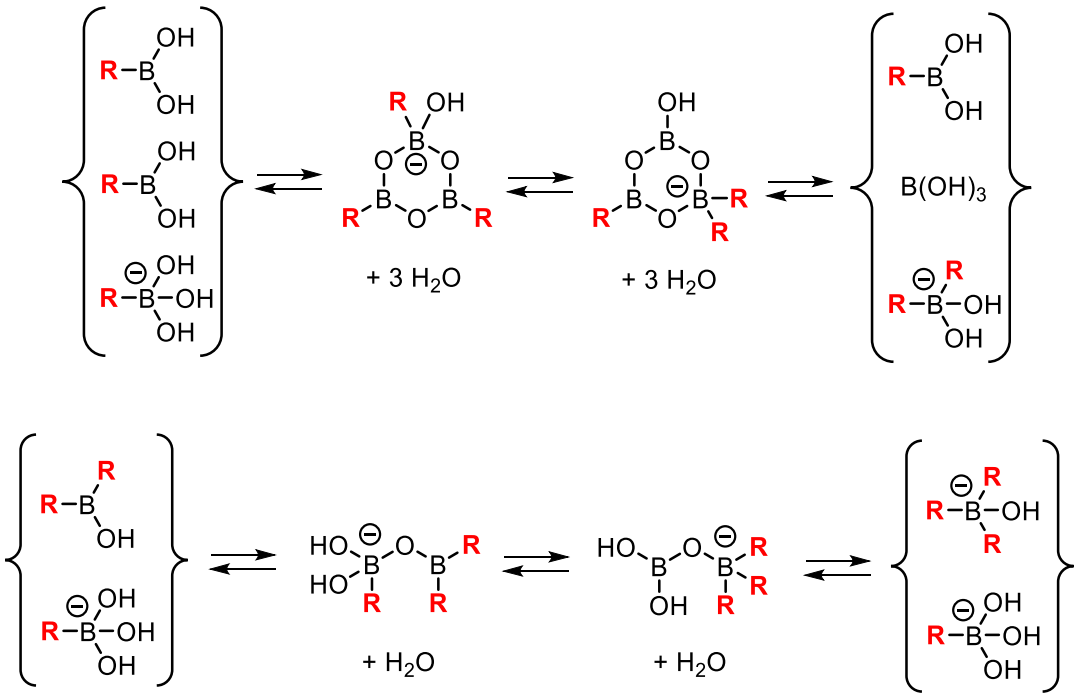

Scheme 2.1 Disproportionation to form borinic and borane products through boroxine and dimer transition states.

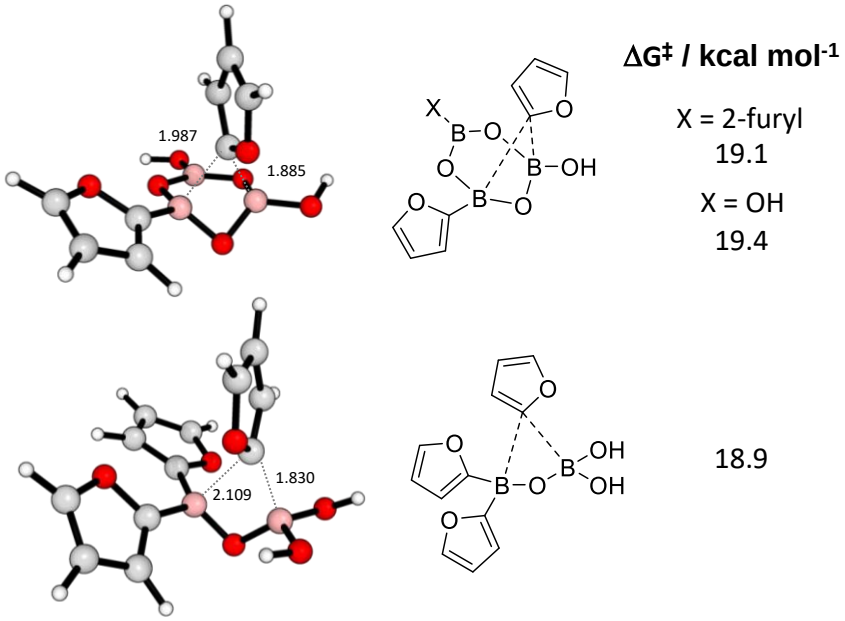

Figure 2.15 Computed transition states for furyl migration to form borinic acid through a boroxine intermediate, and borane through a dimer intermediate.

2.3. Other non-basic boronic acids

2.3.1. Heteroaromatic, vinyl and cyclopropyl boronic acids

With a working mechanistic model in hand, and with a good understanding of the concentration-dependent effects, we sought to obtain full pH – log k_{obs} profiles for the protodeboronation of some non-basic boronic acids, including 3-thienyl, 2-furyl, 2-thienyl, 1-tosyl-2-pyrrolyl, vinyl and cyclopropyl boronic acids (**50** – **55**). Reactions were carried out with 50 mM initial boronic acid to ensure ample signal by NMR analysis while minimising disproportionation processes. Also, we chose to employ an organic-aqueous solvent blend (1:1 H_2O/dioxane) to ensure sufficient reagent and product solubility throughout the reaction. An arbitrary threshold was set for data inclusion, in which only reaction half-lives less than 80 days were included in the simulation fittings (threshold at log k_{obs} = -7, see dashed grey lines in Figure 2.16).[d] pK_a values for boronic acids **50** – **55** were determined by ^{11}B NMR and inputted into the model prior to automated iteration of the rate constants (k_1, k_2 and $k_2$cat) to minimise the SSE. In all cases, a good overlap between experimental and simulated data were obtained (rate and equilibrium constants displayed in Table 2.1).

In comparison to 3-thienyl boronic acid, all 2-heteroaromatic boronic acids (**51 – 53**) displayed greater reactivity across the entire pH scale. Higher tendencies for protodeboronation of 2-heteroaryl boronic acids has been noted in previous studies, but only in acid-catalysed conditions.[148,162] The base-catalysed mechanism (k_2) is generally more efficient than the acid-catalysed mechanism (k_1), and the rates rise considerably in the order 3-thienyl, 2-furyl, 2-thienyl, 1-tosyl-2-pyrolyl. For 1-tosyl-2-pyrrolyl boronic acid, a pK_a value could not be determined through ^{11}B NMR pH titration due to rapid protodeboronation ($t_{½}$ < 3 min) and therefore the value was included in the automated iteration and optimisation during the simulation fitting. Both vinyl and cyclopropyl boronic acids (**54** and **55**) display surprising stability towards protodeboronation, with the only detectable levels of protodeboronation in strong acid or base (pH < 2 and pH > 10). Despite the relatively low reaction concentrations, bimolecular self- and autocatalytic protodeboronation ($k_2$cat) was present, particularly for substrates that display slow base-catalysed (k_2) mechanisms. Interestingly, this indicates the propensity for self- and autocatalytic protodeboronation is less sensitive to changes in the aryl or alkyl fragment in comparison to the acid and base-catalysed mechanisms.

[d] At the threshold rate (log k_{obs} = -7), reactions display less than 2% conversion after reaction for 48 h, thus it is difficult to determine if protodeboronation is the dominant process below this point.

Table 2.1 Equilibrium and rate constants used in the simulation of pH – log k_{obs} profiles for the protodeboronation of **50** – **55** in 1:1 H_2O/dioxane at 70 °C**.**

Entry	$RB(OH)_2$	pK_a[a]	*log* k_1	*log* k_2	*log* $k_2$cat
1	3-thienyl, **50**	11.04	−5.95	−6.01	−4.21
2	2-furyl, **51**	10.29	−3.71	−4.98	−3.32
3	2-thienyl, **52**	10.38	−4.44	−3.92	≤ −3.54[c]
4	1-tosyl-2-pyrolyl, **53**	9.64[b]	−3.41	−2.34	≤ −2.07[c]
5	Vinyl, **54**	11.21	−5.57	−6.02	−3.90
6	Cyclopropyl, **55**	12.72	−5.95	−6.10	−5.01

[a] pK_a determined by ^{11}B NMR pH titration at 70 °C (unless otherwise stated). [b] pK_a determined by iterative fitting of rate data. [c] Value not required for satisfactory simulation; a greater value results in ≥5% change in SSE between experimental and simulated data across the full profile.

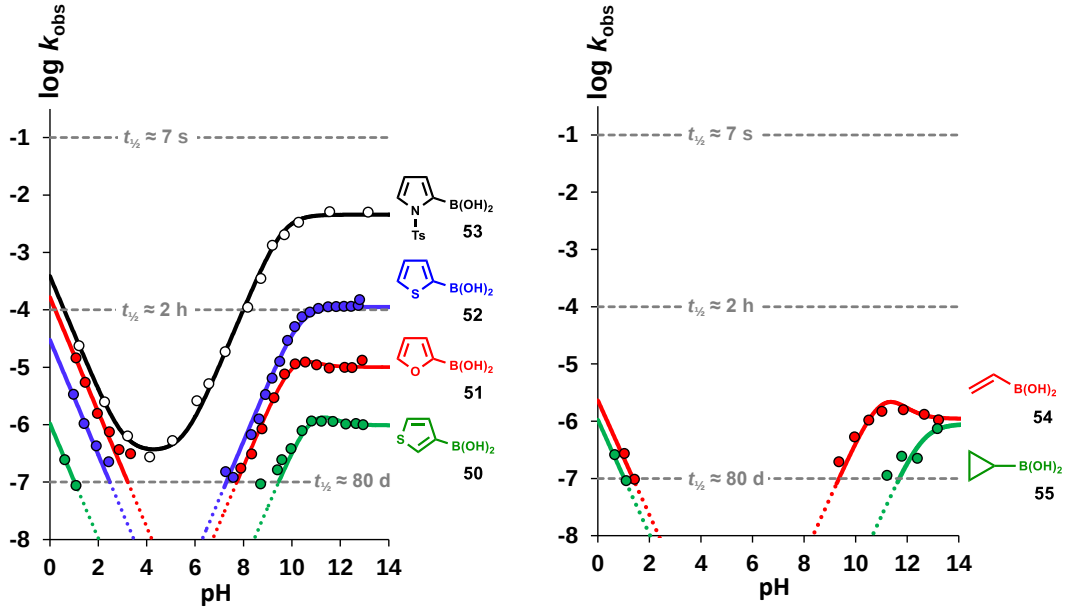

Figure 2.16 pH – log k_{obs} profiles for the pseudo first-order protodeboronation of heteroaromatic boronic acids (**50 – 55**) in 1:1 H_2O/dioxane at 70 °C. Markers = experimental data. Solid lines = simulation fitting using mechanistic model in Figure 2.8, and simulation parameters in Table 2.1.

2.3.2. Alkyl boronic acids

A range of simple alkyl boronic acids were also investigated under identical reaction conditions (1:1 H_2O/dioxane, 70 °C), including methyl (**56**), cyclobutyl (**57**) and cyclohexyl (**58**) boronic acids. All reagents displayed extremely slow reactions ($t_{½}$ > months), which made it difficult to determine if protodeboronation was the major pathway of decomposition, rather than other side reactions such as boronic acid oxidation. Since much of the data lies below the arbitrary threshold (log $k_{obs} \leq -7$), the experimental data was not simulated with the general model (for data, see Experimental 6.4.1.8.).

2.3.3. Bis-boronic acids

Bis-boronic acids are a unique class of substrate containing two boronic acid functional groups. These compounds have been utilised in copolymerisation cross-couplings, whereby protodeboronation limits the number average molecular weight of the polymer.[163] 2,5-thiophenediylbisboronic acid (**59**) was selected and protodeboronation rates obtained in alkaline pH. A unique mechanistic model was constructed to simulate the protodeboronation kinetics consisting of two aqueous association constants, K_a-mono and K_a-bis, to form mono-boronate ($\mathbf{59}_{OH}$-mono) and bis-boronate ($\mathbf{59}_{OH}$-bis) species respectively, and two standard base-catalysed processes from each component (k'_2-mono and k'_2-bis) (Figure 2.17).

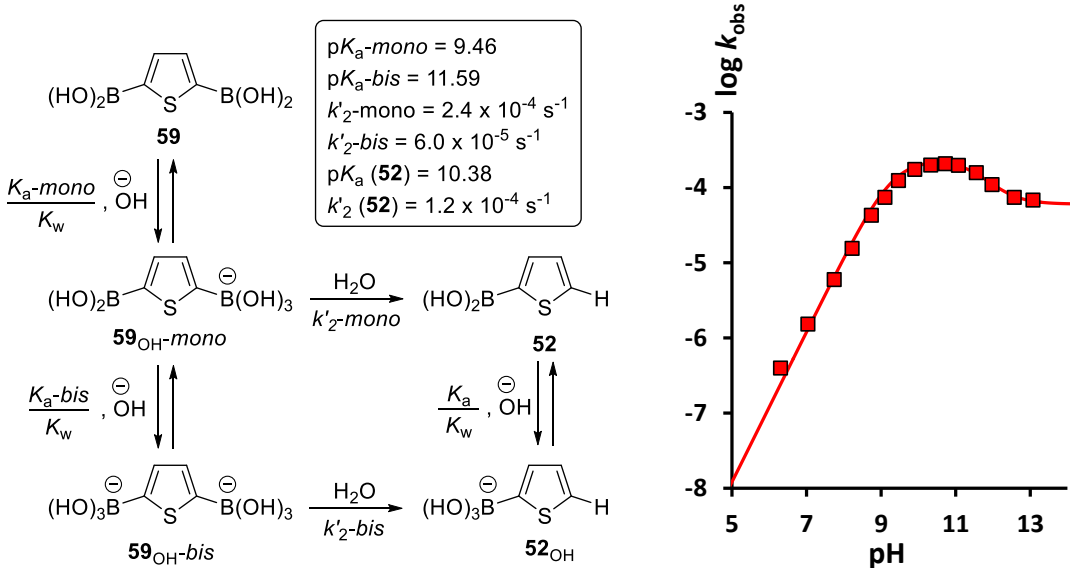

Figure 2.17 Mechanistic model for the protodeboronation of 2,5-thiophenedilyboronic acid (**59**) and 2-thienylboronic acid (**52**) (50 mM, 1:1 H_2O/dioxane, 70 °C) (left). Rate and equilibrium constants obtained through simulation of pH – log k_{obs} data (right). Markers = experimental data. Solid line = simulation fitting using model described above.

Simulation of the experimental results gave evidence that the mono-boronate ($\mathbf{59}_{OH}$-mono) reacts twice as fast as 2-thienyl boronate ($\mathbf{52}_{OH}$) indicating that the presence of the spectator boronic acid group in $\mathbf{59}_{OH}$-mono has a small impact on the overall rate of protodeboronation, while also having an effect on the Lewis acidity at boron (pK_a-mono (**59**) - pK_a (**52**) = -0.92). In contrast, bis-boronate ($\mathbf{59}_{OH}$-bis), when statistically normalised according to the number of reactive boronate groups, reacts 8 times slower than mono-boronate ($\mathbf{59}_{OH}$-mono) and thus indicates that the presence of a spectator boronate group mildly suppresses protodeboronation, and also decreases Lewis acidity at boron (pK_a-bis (**59**) - pK_a (**52**) = +1.21). From this data, it can be seen that strongly alkaline conditions (pH > pK_a-bis) may be beneficial in reducing the amount of protodeboronation in reactions that utilise bis-boronic acids, particularly in polymerisation cross-couplings.

2.4. Summary

Protodeboronation of 4-methoxylphenyl boronic acid (**28**) was investigated between pH 5 - 13 in H_2O at 90 °C, and no significance dependence on salt or counterion effects were found. pH – log k_{obs} profiles were augmented by the leaching of boric acid from borosilicate glassware which was resolved by switching to quartz glass vessels. A concentration-

dependent mechanism was detected in the alkaline pH region and studied in more detail with 3-thienyl boronic acid (**50**). The concentration-dependent process reached a maximal rate at a pH value equal to the pK_a of the boronic acid. In depth KIE and DFT studies elucidated this mechanism to involve rate-limiting proton transfer, in which a boronic acid delivers a proton to a boronate. An analogous autocatalytic process was identified, whereby boric acid can act as a proton source. Disproportionation processes were also evident for 3-thienyl (**50**) and 2-furyl boronic acids (**51**) under similar reaction conditions leading to the formation of new boron species; borinic acid and borane.

In a new solvent system (1:1 H_2O/dioxane, 70 °C), pH – log k_{obs} profiles for some simple non-basic heteroaryl, vinyl and cyclopropyl boronic acids (**50** – **55**) were successfully simulated using a mechanistic model considering three protodeboronation pathways; acid-catalysed (k_1), base-catalysed (k_2) and self-/autocatalysed protodeboronation ($k_2$cat). 2-heteroaryl boronic acids displayed much higher levels of reactivity than 3-thienyl boronic acid across the entire pH range. On the other hand, vinyl (**54**) and cyclopropyl (**55**) boronic acids were only reactive in very acidic or basic conditions, with half-lives of many weeks. A small range of alkyl boronic acids were investigated and displayed the highest levels of stability across the entire pH range, with half-lives typically greater than many months.

A bis-boronic acid, 2,5-thiophenediylboronic acid (**59**), was also studied under alkaline conditions (pH 5 – 13). A unique mechanistic model was required for the successful simulation of the obtained pH – log k_{obs} profile, which considered two aqueous association constants (K_a-mono and K_a-bis) and two base-catalysed processes (k'_2-mono and k'_2-bis). Relative to 2-thienyl boronate (**52**$_{OH}$), mono-boronate (**59**$_{OH}$-mono) reacts twice as fast, whereas bis-boronate (**59**$_{OH}$-bis) reacts 8 times slower. Thus, the presence of a spectator boronic acid or boronate group in bis-boronic acids has only a small impact on the reactivity.

Chapter 3

Protodeboronation of Basic Heteroaromatic Boronic Acids

3.1. Mechanistic model and experimental data

3.1.1. General mechanistic model for basic heteroaromatic boronic acids

The mechanistic model used in the previous chapter (Figure 2.8) is limited to boronic acids that display only one pH-dependent equilibrium (the boronic acid-boronate equilibrium, K_a). We have previously seen that this can be extended to two aqueous association equilibria for bis-boronic acids (Figure 2.17). However, further modifications are required to produce a more general mechanistic model that can encompass a broader range of substrates – namely basic heteroaromatic boronic acids. For example, pyridyl (and other basic heterocyclic motifs) contain a basic nitrogen atom within the aromatic ring which can act as a Brønsted base and abstract a proton from the system to form a protonated heterocycle (equilibrium defined as K_{aH}). Considering both pH-dependent equilibria, K_a and K_{aH}, a new speciation model can be constructed for basic boronic acids, involving the following three species: an *N*-protonated form ($\mathbf{X}_{H+}$), a neutral form (**X**), and a boronate form ($\mathbf{X}_{OH}$). Two additional equilibria are also included to aid discussion, but are not kinetically distinguished in the modelling. These include pre-equilibrium between boronate ($\mathbf{X}_{OH}$) and hydroxide to form a dianionic intermediate ($\mathbf{X}_{O-}$, K_3), and a second pre-equilibrium between the neutral species (**X**) and autoionised water to form a zwitterionic water adduct ($\mathbf{X}_{ZW}$, K_4). Additionally, new protodeboronation pathways were required to provide successful simulation of the pH – log k_{obs} profiles for a range of basic heteroaromatic boronic acids. These additional pathways are presented in advance of the analysis to help simplify the discussion in later sections. Along with the previously discussed acid-catalysed (k_1), base-catalysed (k_2) and self-/autocatalysed ($k_2$cat) pathways, a further three pathways were required including: a Perrin-type mechanism involving base-catalysed protonolysis of $\mathbf{X}_{OH}$ (K_3k_3), pH-independent fragmentation of $\mathbf{X}_{ZW}$ (k_4), and finally pH-independent protodeboronation of $\mathbf{X}_{H+}$ by water (k_5). Figure 3.1 provides a visual description of the general mechanistic model, and also displays the individual pH – log k_{obs} profiles that result from each protodeboronation pathway. In a similar manner to before (section 2.2.1.2), the mathematical combination of all six protodeboronation processes and calculation of the three-state speciation allows the construction of an overall rate equation, and can ultimately provide a method of simulating the experimental pH – log k_{obs} data. The six protodeboronation processes are mathematically described in Equation 3.1, and can be condensed by using Equation 2.4 and subsuming water/equilibrium terms to afford Equation 3.2.

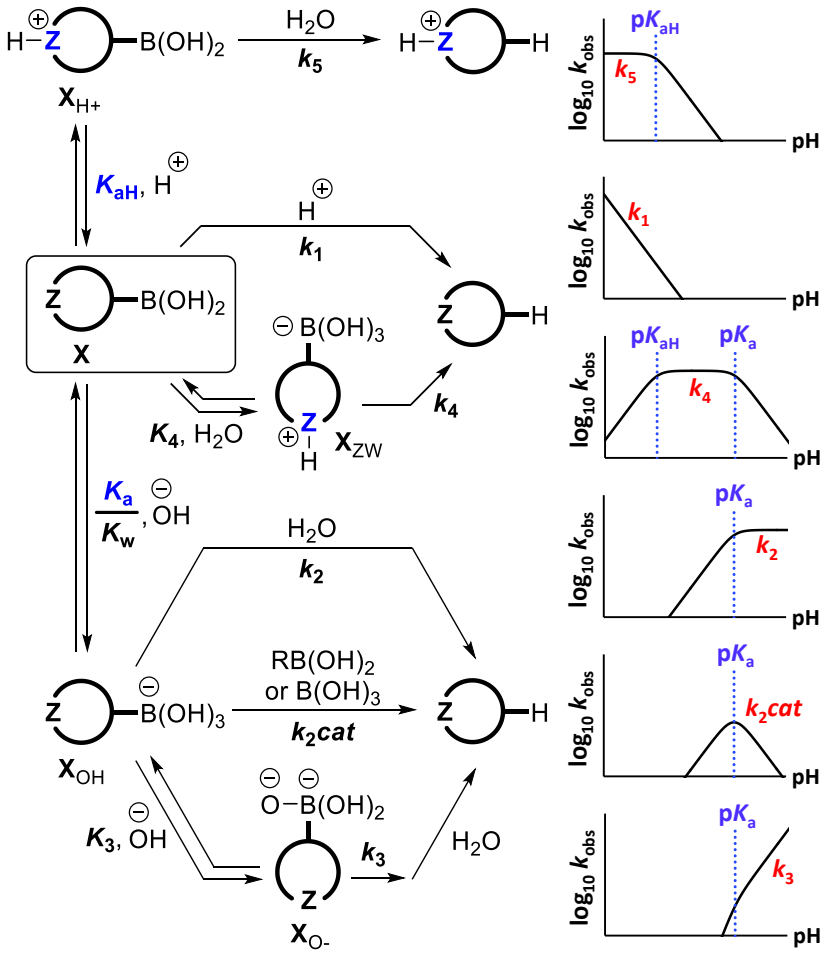

Figure 3.1 General mechanistic model for the protodeboronation of basic boronic acids, and the individual pH – log k_{obs} profiles for each mechanism.

$$let\ [\mathrm{RB(OH)_2}] = [\mathbf{X}];\ \ [\mathrm{RB(OH)_3^-}] = [\mathbf{X_{OH}}];\ \ [\mathrm{RB(OH)_2H^+}] = [\mathbf{X_{H+}}];$$

$$rate = k_1[\mathbf{X}][\mathrm{H^+}] + k_2[\mathbf{X_{OH}}][\mathrm{H_2O}] + k_2cat[\mathbf{X_{OH}}]([\mathbf{X}] + [\mathrm{B(OH)_3}])$$
$$+ K_3k_3[\mathbf{X_{OH}}][\mathrm{OH^-}] + K_4k_4[\mathbf{X}][\mathrm{H_2O}] + k_5[\mathbf{X_{H+}}][\mathrm{H_2O}] \qquad (3.1)$$

$$using\ equation\ (1.4)\ and\ subsuming\ water/equilbrium\ terms, i.e.\ k'_x = K_xk_x[\mathrm{H_2O}]$$

$$rate = k_1[\mathbf{X}][\mathrm{H^+}] + k'_2[\mathbf{X_{OH}}] + k_2cat[\mathbf{X_{OH}}][\mathrm{C}] + k'_3[\mathbf{X_{OH}}][\mathrm{OH^-}]$$
$$+ k'_4[\mathbf{X}] + k'_5[\mathbf{X_{H+}}] \qquad (3.2)$$

The overall boron concentration ($[\mathbf{X}]_{total}$) can be expressed as the sum of the individual concentrations for all three speciation modes (Equation 1.8).

$$[\mathbf{X}]_{tot} = [\mathbf{X}] + [\mathbf{X_{OH}}] + [\mathbf{X_{H+}}] \qquad (3.3)$$

An overall rate equation concerning the total boron concentration (Equation 3.4) can be expressed in terms of equibrilium constants and hydronium ion concentration by applying extended Henderson-Hasselbalch equations. Using logarithms, this can be expressed in more intuitive terms of pH, pK_W, pK_a and pK_{aH} (Equation 3.5; for full derivation see section 8.3.).

$$rate = k_{\text{obs}}[\mathbf{X}]_{tot} \tag{3.4}$$

$$k_{\text{obs}} = \frac{k_1 10^{-\text{pH}} + k'_4}{1 + 10^{\text{p}K_{\text{aH}}-\text{pH}} + 10^{\text{pH}-\text{p}K_{\text{a}}}} + \frac{k'_2 + k_2 cat[\text{C}] + k'_3 10^{\text{pH}-\text{p}K_W}}{1 + 10^{\text{p}K_{\text{a}}-\text{pH}} + 10^{\text{p}K_{\text{aH}}+\text{p}K_{\text{a}}-2\text{pH}}} + \frac{k'_5}{1 + 10^{\text{pH}-\text{p}K_{\text{aH}}} + 10^{2\text{pH}-\text{p}K_{\text{aH}}-\text{p}K_{\text{a}}}} \tag{3.5}$$

Using Equation 3.5, the empirical rate (k_{obs}) can be analysed as a function of pH, using up to nine constants (pK_a, pK_{aH}, pK_w, k_1, k'_2, $k_2$cat, k'_3, k'_4, k'_5) to vary the profile shape.

3.1.2. pH – log k_{obs} profiles and simulations

pH – log k_{obs} profiles were experimentally obtained for a variety of basic heteroaromatic boronic acids (**60** – **71**, Table 3.1). Using the general mechanistic model, simulated profiles were fitted to the experimental data through iterative fitting of rate and equilibrium constants between pH 1 – 13, by minimisation of the SSE between experimental and simulated profiles. In many cases, pK_a values were determined by ^{11}B NMR pH titration and values were 'locked' during simulation of experimental data. pK_a values that could not be measured experimentally, due to rapid protodeboronation, were obtained through iterative fitting of the simulated pH – log k_{obs} profile. For basic substrates (containing a basic nitrogen atom), pK_{aH} values were determined by ^{1}H NMR titrations at 25 °C and an empirical correction factor was used to compensate for the temperature difference (ΔpK_{aH} 70-25 °C = 0.46).

3.1.2.1. Overview of simulations

For the range of heteroaromatic boronic acids tested, a wide variety of different, but distinctive, profiles were observed. 2-pyridyl boronic acids (**44**, **69** and **70**) displayed near inverse pH – log k_{obs} profiles compared to non-basic boronic acids, and were successfully simulated with a single rate term (k'_4). In these cases, maximum rates of protodeboronation are present at pH values that favour neutral boronic acid (**X**) (i.e. neutral pH), whereas protodeboronation is greatly reduced at pH values that favour boronate ($\mathbf{X}_{OH}$) or *N*-protonated species ($\mathbf{X}_{H+}$) (i.e. very high or very low pH). It is noteworthy to mention that protodeboronation rates are extraordinarily fast in comparison to the previously studied non-basic boronic acids (e.g.: 2-pyridyl boronic acid (**44**) at pH 7, $t_{½}$ = 24 s). For the least basic,

6-(trifluoromethyl)-2-pyridyl boronic acid (**70**) ($pK_{aH} \leq 0.6$), very low pH values are not enough to generate significant *pyridinium* (*N*-protonated species, $\mathbf{X}_{H+}$) formation, and thus attenuation of protodeboronation is not observed in the acidic region. 5-thiazolyl boronic acid (**66**) and 5-pyrazolyl boronic acids (**67** and **68**) also displayed high levels of reactivity and required combination of base-catalysed and neutral mechanisms (k'_2 and k'_4) for simulation.

Table 3.1 Equilibrium and rate constants used in the simulation of pH – log k_{obs} profiles for the protodeboronation of **44** and **60 – 70** in 1:1 H_2O/dioxane at 70 °C.

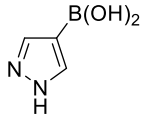
60

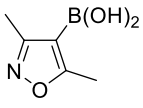
61

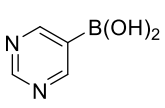
62

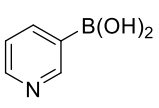
63

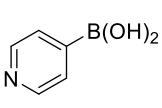
64

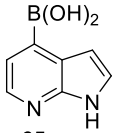
65

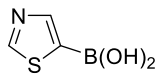
66

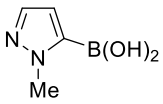
67

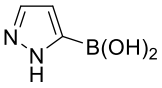
68

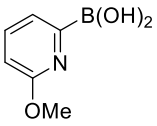
69

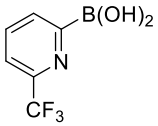
70

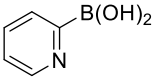
44

RB(OH)$_2$	pK_{aH}[a]	pK_a[b]	*log* k_1	*log* k'_2	*log* $k_2$cat	*log* k'_3	*log* k'_4	*log* k'_5
60	1.26 (1.70)	11.61	-3.16	≤ -6.02[d]	-3.27	-3.72	-6.60	≤ -5.68[d]
61	0.04[e] (<0.50)	10.45	-5.51	-4.01	-2.00	-2.62	-6.38	≤ -4.61[d]
62	0.14[e] (<0.60)	8.18	≤ -4.82[d]	-5.04	-3.44	≤ -4.75[d]	-5.44	≤ -4.83[d]
63	3.60 (4.22)	9.76	≤ -3.10[d]	-6.05	-3.60	≤ -5.59[d]	-5.71	≤ -6.70[d]
64	3.36[e] (3.82)	8.94	≤ -3.76[d]	-5.93	-3.78	≤ -5.78[d]	-5.71	-5.77
65	2.95[e] (3.41)	9.90	≤-5.64[d]	-6.24	-3.95	≤ -6.60[d]	-6.89	-7.07
66	1.62 (1.85)	8.41[c]	≤ -2.60[d]	-2.02	≤ -1.58[d]	≤ -2.21[d]	-1.83	≤ -4.22[d]
67	1.08 (1.62)	8.82	≤ -4.22[d]	-3.87	-3.49	≤ -3.94[d]	-3.78	≤ -5.31[d]
68	1.36 (2.00)	9.11	≤ -4.58[d]	-4.35	-3.19	≤ -3.93[d]	-4.28	≤ -5.84[d]
69	3.16 (3.60)	9.54[c]	≤ -1.36[d]	≤ -6.72[d]	≤ -2.33[d]	≤ -6.04[d]	-2.41	≤ -4.52[d]
70	-1.06[e] (<-0.6)	8.49[c]	≤ -2.06[d]	≤ -6.32[d]	≤ -1.84[d]	≤ -4.82[d]	-2.75	≤ -0.06[d]
44	3.52 (3.86)	10.76[c]	≤ -0.74[d]	≤ -4.26[d]	≤ -0.67[d]	≤ -3.74[d]	-1.60	≤ -4.24[d]

[a] pK_{aH} in parentheses determined by ^{1}H NMR pH titration at 25 °C; pK_aH at 70 °C from iterative fitting of rate data (unless stated). [b] pK_a determined by ^{11}B NMR pH titration at 70 °C (unless stated). [c] pK_a from iterative fitting of rate data. [d] value not required for satisfactory simulation; greater values induce ≥5% change in SSE between simulation and data across the full profile. [e] pK_{aH} fixed at empirical offset (-0.46 units) based on compounds **44**, **60, 63**, and **66 – 69**.

The 3-pyridyl boronic acid (**63**) and 5-pyrimidyl boronic acid (**62**) were much less reactive, and simulation of their pH – log k_{obs} profiles required combination of base-catalysed mechanisms (k'_2 and $k_2$cat) and a neutral mechanism (k'_4). In a similar manner to the 2-pyridyl boronic acids, 3-pyridyl boronic acid (**63**) displayed attenuation of protodeboronation

at pH values below its pK_{aH}. 4-pyridyl boronic acids (**64** and **65**) displayed similar reactivity to 3-pyridyl/5-pyrimidyl boronic acids (**62** and **63**) yet no attenuation of protodeboronation was observed at pH values below their pK_{aH}. This feature was unique to 4-pyridyl motifs and required an extra mechanism involving protodeboronation of the *pyridinium* species *via* water (k'_5) to successfully simulate pH – log k_{obs} data (top, Figure 3.1). Lastly, 4-isoxazolyl and 4-pyrazolyl boronic acids (**60** and **61**) displayed the most complex profiles, requiring combination of almost all protodeboronation pathways (k_1, k'_2, $k_2$cat, k'_3, k'_4). These were the only substrates that required contribution from the dianionic boronate mechanism (k'_3), which has only been proposed for electron deficient 2,6-disubstituted aryl boronic acids.[82]

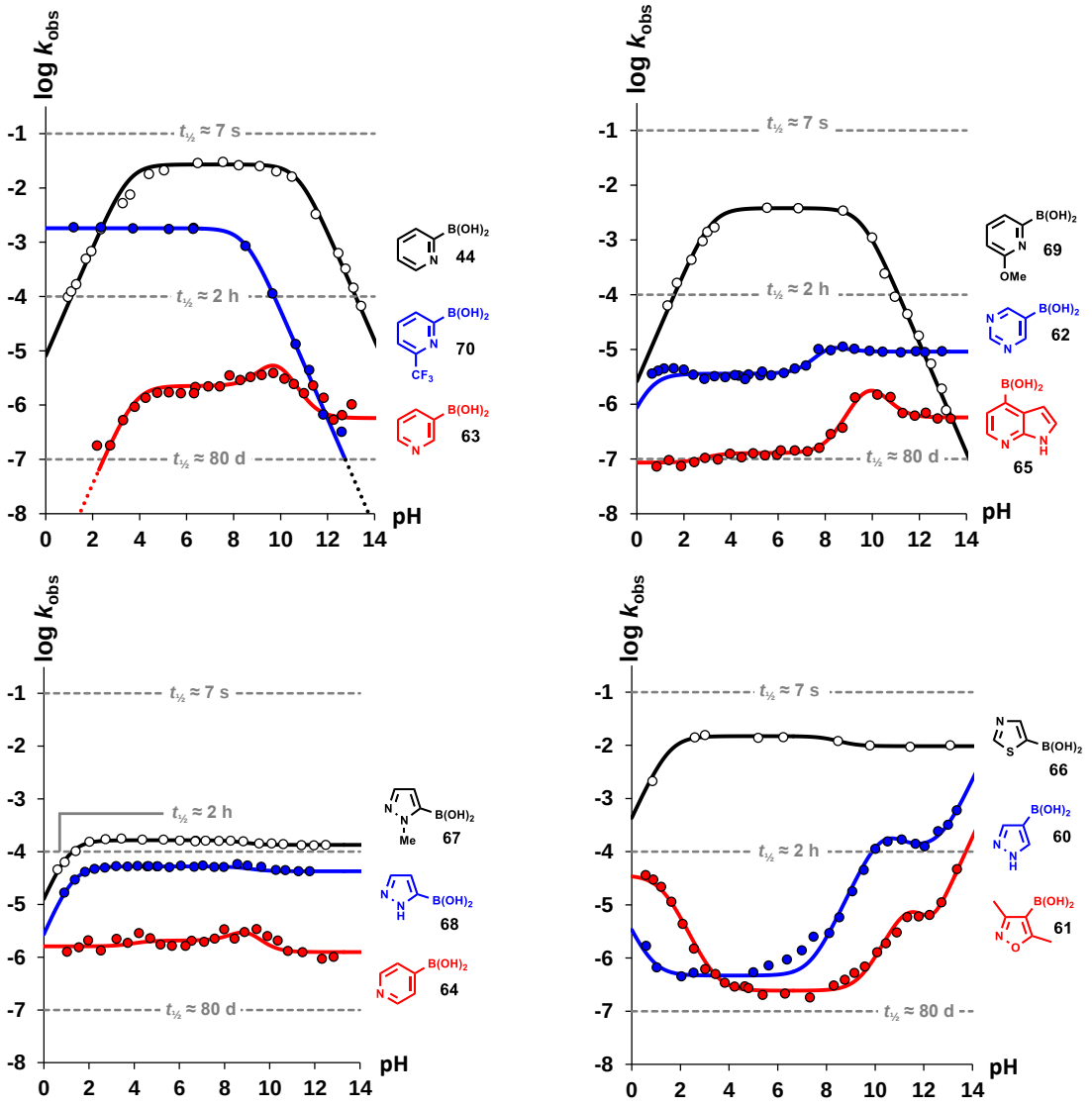

Figure 3.2 pH – log k_{obs} profiles for the pseudo first-order protodeboronation of heteroaromatic boronic acids (**44**, **60** – **70**) in 1:1 H_2O/dioxane at 70 °C. Markers = experimental data. Solid lines = simulation fitting using mechanistic model in Figure 3.1 and Table 3.1.

3.2. Mechanisms of protodeboronation

To aid the understanding of the obtained pH – log k_{obs} profiles for basic heteroaromatic boronic acids, the mechanisms of protodeboronation were studied in detail with ^{11}B NMR, DFT calculations, and the effect of Lewis acidic additives on particular substrates.

3.2.1. Zwitterionic water-adducts (X_{ZW}, k_4)

3.2.1.1. ^{11}B NMR studies

For all studied heteroaromatic boronic acids, successful simulation of pH – log k_{obs} profiles required the inclusion of a neutral mechanism (k'_4) stemming from the neutral boronic acid species (**X**). This is particularly interesting when compared to non-basic boronic acids, which typically display standard acid- and base-catalysed mechanisms and thus display greatest stability at neutral pH values. Conversely, heteroaromatic boronic acids display a varying level of reactivity at neutral pH values depending on the exact heteroaromatic group and position. For example, 2-pyridyl boronic acids (**44**, **69** and **70**) react rapidly at pH ~6, and simulation of the pH – log k_{obs} profiles could be satisfactorily described solely by a neutral mechanism (k'_4). Thus the standard Kuivila-type acid- and base-catalysed mechanisms (k_1 and k'_2) are not significant between pH 1 – 13 for these substrates. Moreover, hydronium and hydroxide ions (H^+ and OH^-) both act as strong inhibitors for the protodeboronation of 2-pyridyl boronic acid (**44**) by modifying the speciation to the seemingly unreactive *N*-protonated ($\mathbf{X}_{H+}$) or boronate ($\mathbf{X}_{OH}$) species. Consequently, 2-pyridyl boronic acid (**44**) protodeboronates within seconds at pH ~6, yet is stable for many hours at pH ~13 (1:1 H_2O/dioxane, 70 °C).

To aid understanding, the aqueous cleavage of the C-B bond for the 2-pyridyl boronic acid neutral species was studied by DFT (AGL). Free energy barriers for the protodeboronation of neutral boronic acids (**44, 69** and **70**) were calculated to be too high (46-48 kcal mol^{-1}) to account for the observed rates, regardless of the potential contribution to direct hydrolysis by dynamic water fluctuation.[164,165] This suggests the neutral boronic acids could not themselves be the reactive species, and that other species are responsible for the reactivity. To examine the exact speciation further, ^{11}B NMR spectra of 2-pyridyl species were obtained in the pH region where maximum protodeboronation rates were observed (pH 6 – 7, rt). Interestingly for 2-pyridyl boronic acid (**44**), ^{11}B NMR displayed a sharp signal at 1.55 ppm, and no signal at the expected region for a sp^2 hybridised neutral boronic acid (approx. 28 ppm). From this, it can be concluded that another species must be dominant, which we suspected to be a zwitterionic water-adduct ($\mathbf{X}_{ZW}$). We hypothesised this species may form by the rapid and

reversible capture of autoionised water at both Brønsted-basic nitrogen and Lewis-acidic boron atoms within basic heteroaromatic boronic acids (K_4). This effect is analogous to that found in amino-acids (albeit with Brønsted-acidic and Brønsted-basic sites), and is well-known to result in the formation of zwitterionic species that are predominant at neutral pH values in aqueous solution.[166] Given that the connectivity and hybridisation of the boron centre is very similar for both boronate ($\mathbf{X}_{OH}$) and zwitterionic water-adduct ($\mathbf{X}_{ZW}$), it can be assumed that the ^{11}B chemical shift for both species are also likely to be similar (~ 1 ppm). Using this assumption, the ^{11}B chemical shift of 2-pyridyl boronic acid (**44**) indicates near quantitative presence of zwitterionic water-adduct (>95%) under the reaction conditions (1:1 H_2O/dioxane, pH 6.5, rt). Similar analysis of the ^{11}B NMR spectra for 6-substituted-2-pyridyl boronic acids (**69** and **70**) displayed intermediate chemical shifts (**69** ≈ 20 ppm, **70** ≈ 26 ppm) indicating the electron demand of the 6-substituent plays an important role in the equilibrium position of the neutral and zwitterionic species (Figure 3.3).

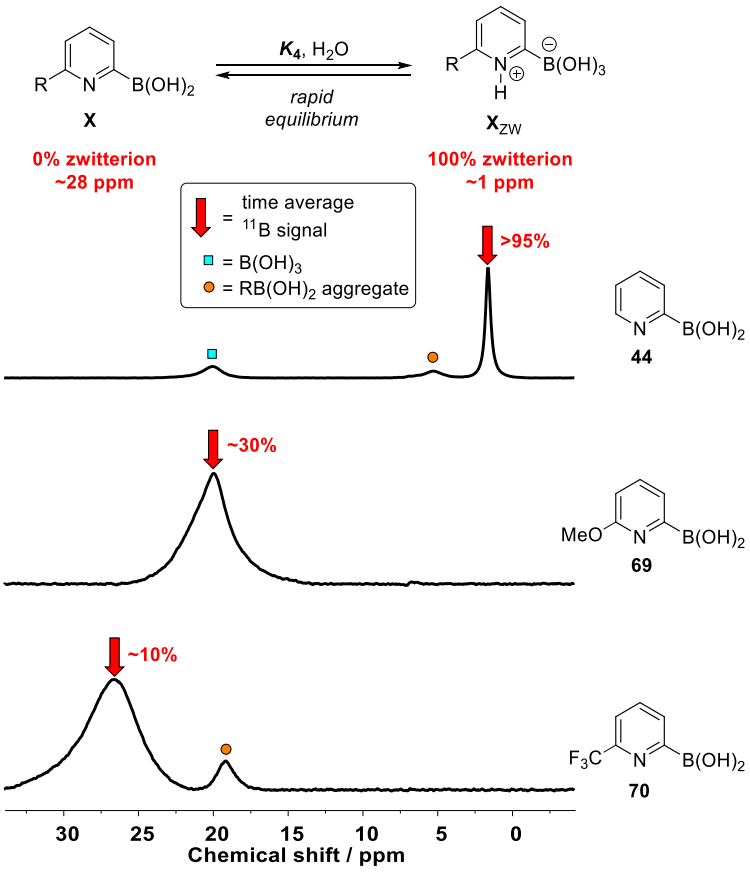

Figure 3.3 ^{11}B NMR spectra of **44**, **69** and **70** in AcO^-/AcOH buffer (0.01 M $RB(OH)_2$, pH 6.5, rt). Signals correspond to time-average chemical shifts between neutral species (**X**, 28 ppm) and zwitterionic species ($\mathbf{X}_{ZW}$, 1 ppm).

For many other basic heteroaromatic boronic acids, water autoionised equilibria with zwitterionic water-adducts were not easily detected by ^{11}B NMR ($\delta_B \geq 27$ ppm, pH 5 – 7, no buffer, 70 °C) with the only exception being the 5-pyrazole systems (**67** and **68**) which displayed minor upfield shifts (**67**, δ_B = 25.11 ppm; **68**, δ_B = 25.42 ppm). Using the same method, the percentage of zwitterionic water-adduct was calculated to be relatively low in all cases (Table 3.2). On the contrary, zwitterion speciation has been previously reported for 3- and 4-pyridyl boronic acids (**63** and **64**) by UV-vis spectrophotometry in purely aqueous solvents and calculated to be majority zwitterion (75 – 90%).[167] However, the differences in solvent systems may explain the large differences observed in our studies.

Table 3.2 Zwitterion percentages at pH 5.0 – 5.5 determined by ^{11}B NMR at 70 °C.

Entry	$RB(OH)_2$	δ_B / ppm	% zwitterion[a]
1	4-pyrazolyl, **60**	27.38	<5%
2	3,5-dimethylisoxazolyl, **61**	27.23	<5%
3	5-pyrimidyl, **62**	27.50	<5%
4	3-pyridyl, **63**	27.91	<5%
5	4-pyridyl, **64**	27.31	<5%
6	4-azaindolyl, **65**	27.56	<5%
7	5-thiazolyl, **66**	27.07[b]	<5%
8	1-Methyl-5-pyrazolyl, **67**	25.11	~10%
9	5-pyrazolyl, **68**	25.42	~10%
10	6-methoxy-2-pyridyl, **69**	19.91[b]	~30%
11	6-(trifluoromethyl)-2-pyridyl, **70**	26.02[b]	~10%
12	2-pyridyl, **44**	1.55[b]	>95%

[a] Zwitterion percentage calculated assuming the signal limits; boronic acid (28 ppm) and zwitterion (1 ppm). %zwitterion = (δ_B – 1) / (28 – 1) × 100. [b] Spectrum acquired at pH 6.0 - 6.5 ($AcOH/AcO^-$ buffer) at 25 °C.

3.2.1.2. Computational studies

Protodeboronation of the zwitterionic water-adducts was probed by DFT studies (AGL). 2-pyridyl zwitterionic water-adducts (**44**$_{ZW}$, **69**$_{ZW}$ and **70**$_{ZW}$) displayed a unique unimolecular fragmentation mechanism. The transition state shows a hydrogen bond between the proton situated on the basic nitrogen and the oxygen situated on boron, in effect, solvating the departing boric acid fragment (**44**$_{ZW}$, Figure 3.4). This mode of intramolecular stabilisation was crucial in affording a low energy barrier to fragmentation of the C-B bond (26.0 kcal mol^{-1}). However an alternative mechanism involving a bimolecular reaction with water was also found to be feasible, with a similar energy barrier (25.9 kcal mol^{-1}) (**44**$_{ZW}$ + H_2O, Figure 3.4). Interestingly, DFT studies indicate a much higher energy barrier (32.5 kcal mol^{-1}) for

the unimolecular fragmentation of 3-pyridyl boronic acid zwitterionic water-adduct (**63**$_{ZW}$). Understandably, an equivalent mode of intramolecular stabilisation is not apparent for **63**$_{ZW}$ due to the increased distance between the protonated nitrogen and boronate group, compared to the 2-pyridyl analogue (**44**$_{ZW}$). This is in agreement with the experimental data, which displays the 2-pyridyl zwitterionic-water adduct (**44**$_{ZW}$) to be over 4 orders of magnitude more reactive than the 3-pyridyl zwitterionic-water adduct (**63**$_{ZW}$) at pH ~6 (see pH – log k_{obs} profiles for **44** and **63**, Figure 3.2).

5-thiazolyl and 5-pyrazolyl boronic acids (**66 – 68**) display somewhat surprising levels of reactivity under neutral pH conditions given that zwitterion populations are low (~10% or less) and that the basic nitrogen atoms are remote from the boron centre. DFT calculations (AGL) support these findings, displaying much less favourable generation of the zwitterionic water-adducts, yet transition states for their fragmentation are comparable in energy to the 2-pyridyl systems due to other stabilising effects. For the thiazolium boronate (**66**$_{ZW}$) a strong interaction between the oxygen atom (located on boron) and the S-C antibonding orbital provides substantial stabilisation of the departing boric acid fragment (**66**$_{ZW,}$ Figure 3.4). Analogous noncovalent interactions have previously been reported by Meanwell and co-workers.[168] For 5-pyrazolium boronates (**67**$_{ZW}$ and **68**$_{ZW}$), similar transition state stabilisation is observed through highly polarised bonds (C-H bond of the *N*-methyl for **67**$_{ZW}$, and N-H bond for **68**$_{ZW}$, Figure 3.4) and allows similar modes of stabilisation during fragmentation. Unlike the 2-pyridyl systems, thiazolyl and pyrazolyl boronic acids remain reactive in alkaline conditions (pH > pK_a, see pH – log k_{obs} profiles in Figure 3.2). Although the zwitterions are converted into boronates in alkaline pH, the modes of transition state stabilisation remain present for 5-thiazolyl and 5-pyrazolyl boronates. However, this stabilisation is attenuated due to the decreased polarisation of orbitals and bonds in the boronate species, compared to the zwitterionic water-adducts. Nevertheless, this attenuation is counterbalanced with a higher concentration of boronate at high pH (~100%), relative to zwitterion at neutral pH (~10% maximum) resulting in similar observed rates of protodeboronation in both neutral and alkaline pH regions.

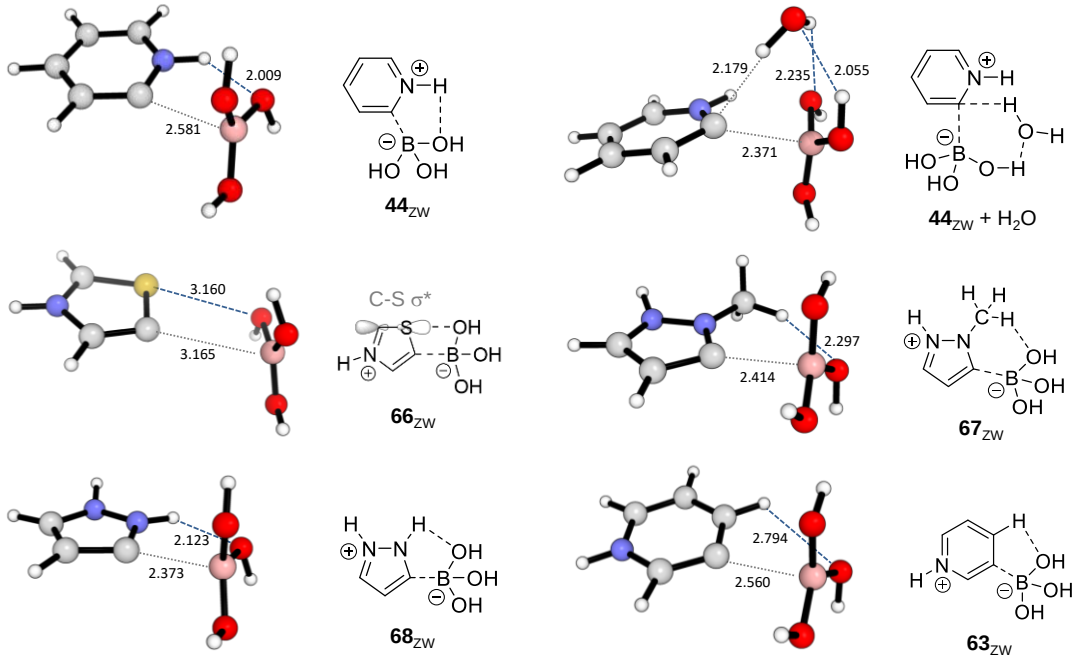

Figure 3.4 Transition state structures for protodeboronation *via* zwitterionic water-adduct fragmentation (k_4).

3.2.1.3. Lewis acid additives

For the 2-pyridyl boronic acid (**44**), concentration-dependent signals were detected and presumed to be aggregate species of the form $[RB(OH)_2]_n$, albeit at insignificant levels ($\delta_B \approx$ 6 ppm, see Figure 3.3). Although insignificant at low concentrations (10 mM), at higher reaction concentrations the signal becomes more pronounced and thus we sought to determine the effect of the concentration on the rate of protodeboronation. At two different initial boronic acid concentrations (50 and 200 mM), the protodeboronation of 2-pyridyl boronic acid (**44**) under neutral pH conditions (1:1 H_2O/dioxane, 70 °C, pH 6.2-6.9) was monitored by ^{1}H NMR. The reaction kinetics revealed reduced rate constants for protodeboronation at higher initial boronic acid concentrations, suggesting that aggregates form an unreactive reservoir of boronic acid, acting to reduce the proportion of zwitterionic water-adduct ($\mathbf{X}_{ZW}$) and in turn attenuate protodeboronation. Interestingly, pseudo first-order kinetics were obtained in both cases, suggesting that the product (boric acid) may also participate in aggregation equilibria. This was confirmed by the reaction of 50 mM 2-pyridyl boronic acid (**44**) in the presence of added 150 mM boric acid, which displayed an identical reaction profile to that of 200 mM 2-pyridyl boronic acid (**44**) (Table 3.3).

We turned our attention to stronger Lewis acid additives, namely metals, to determine if protodeboronation rates of 2-pyridyl boronic acid could be inhibited further. Four additives were tested, including $MgCl_2$, $Sc(OTf)_3$, $ZnCl_2$ and $CuCl_2$. From these additives, $MgCl_2$

displayed no effect whereas the remaining three additives displayed significant suppression in the rate of protodeboronation. The greatest suppression was observed with 2 equiv. $CuCl_2$, which increased the half-life of 2-pyridyl boronic acid (**44**) protodeboronation by a factor of 24. The mode of inhibition was speculated to be sequestration of the reactive zwitterionic water-adduct ($\mathbf{X}_{ZW}$) by Cu to form an unreactive Lewis acid adduct ($\mathbf{X}_{M}$) (Scheme 3.1). However the literature reports that Cu may act as a transmetalating stepping-stone in some reactions and thus irreversible transmetalation was also considered.[100] The reaction kinetics could not be monitored *in situ* due to problematic paramagnetic broadening of NMR signals. Therefore, the mode of inhibition was tested by addition of 2,2'-bipyridine during a $CuCl_2$-attenuated reaction, which resulted in immediate reinstatement of rapid protodeboronation (entry H, Figure 3.5), indicating irreversible transmetalation of Cu (for boron) is not responsible for the rate suppression.

The hybridisation at boron for the Lewis acid adduct ($\mathbf{X}_{M}$) was determined by ^{11}B NMR. Analysis of the 2-pyridyl boronic acid (**44**) in the presence of $ZnCl_2$ at neutral pH (entry F, Table 3.3) displayed a boronate-like signal (δ_B = 1.5 ppm). Thus, it is proposed that the addition of Lewis acid additives results in the presence of a new equilibrium to form a Lewis acid adduct, whereby the proton (N-H^+) is replaced by the Lewis acid (Scheme 3.1).

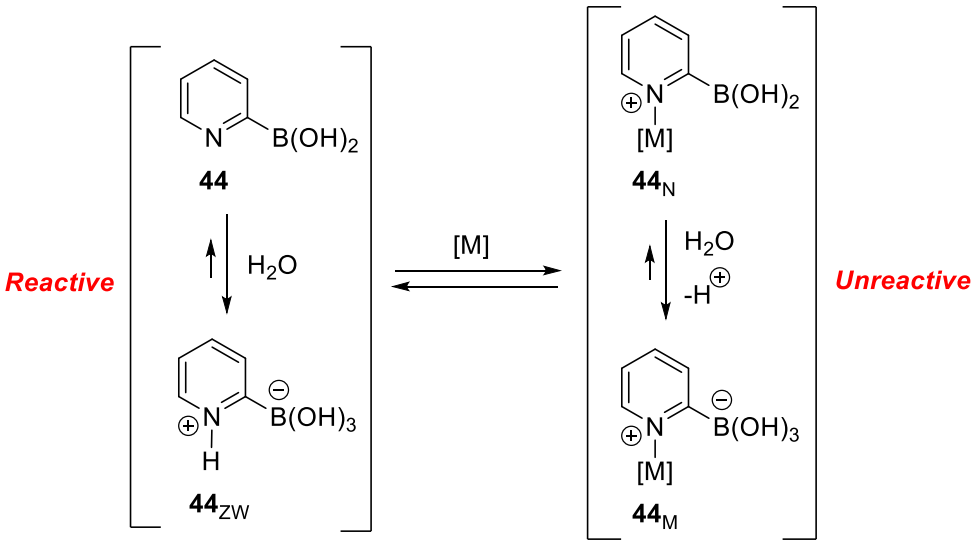

Scheme 3.1 Proposed equilibrium formation of zwitterionic Lewis acid adduct.

This reversible complexation leads to a reduced concentration of $\mathbf{44}_{ZW}$ and thus a suppressed protodeboronation rate. Lewis acid coordination at the basic nitrogen clearly removes the intramolecular stabilisation observed in the zwitterionic state (hydrogen bond between N-H^+ and boric acid fragment, see Figure 3.4) but also must not provide an analogous mode of stabilisation.

Table 3.3 Effect of Lewis acid additives on the protodeboronation kinetics of **44** and **66** – **68** at pH 6.2 – 6.9 in 1:1 H_2O/dioxane at 70 °C.

Entry	[RB(OH)$_2$]	Additive (conc)	k_{obs} 10^3 / s^{-1}	$t_{½}$
A	**44**, 0.05 M	None	27.9	25 s
B	**44**, 0.20 M	None	20.8	33 s
C	**44**, 0.05 M	$B(OH)_3$ (0.15 M)	20.0	34 s
D	**44**, 0.05 M	$MgCl_2$ (0.10 M)	28.8	24 s
E	**44**, 0.05 M	$Sc(OTf)_3$ (0.10 M)	12.9	53 s
F	**44**, 0.05 M	$ZnCl_2$ (0.10 M)	8.4	82 s
G	**44**, 0.05 M	$CuCl_2$ (0.10 M)	1.20	10 min
H	**44**, 0.05 M	$CuCl_2$ (0.10 M)[a]	16.9	41 s
I	**66**, 0.05 M	None	14.4	48 s
J	**66**, 0.05 M	$ZnCl_2$ (0.10 M)	50.5	14 s
K	**67**, 0.05 M	None	0.184	63 min
L	**67**, 0.05 M	$ZnCl_2$ (0.10 M)	2.20	5 min
M	**68**, 0.05 M	None	0.068	169 min
N	**68**, 0.05 M	$ZnCl_2$ (0.10 M)	0.902	13 min

[a] Bipy (0.20 M) added at 80 s.

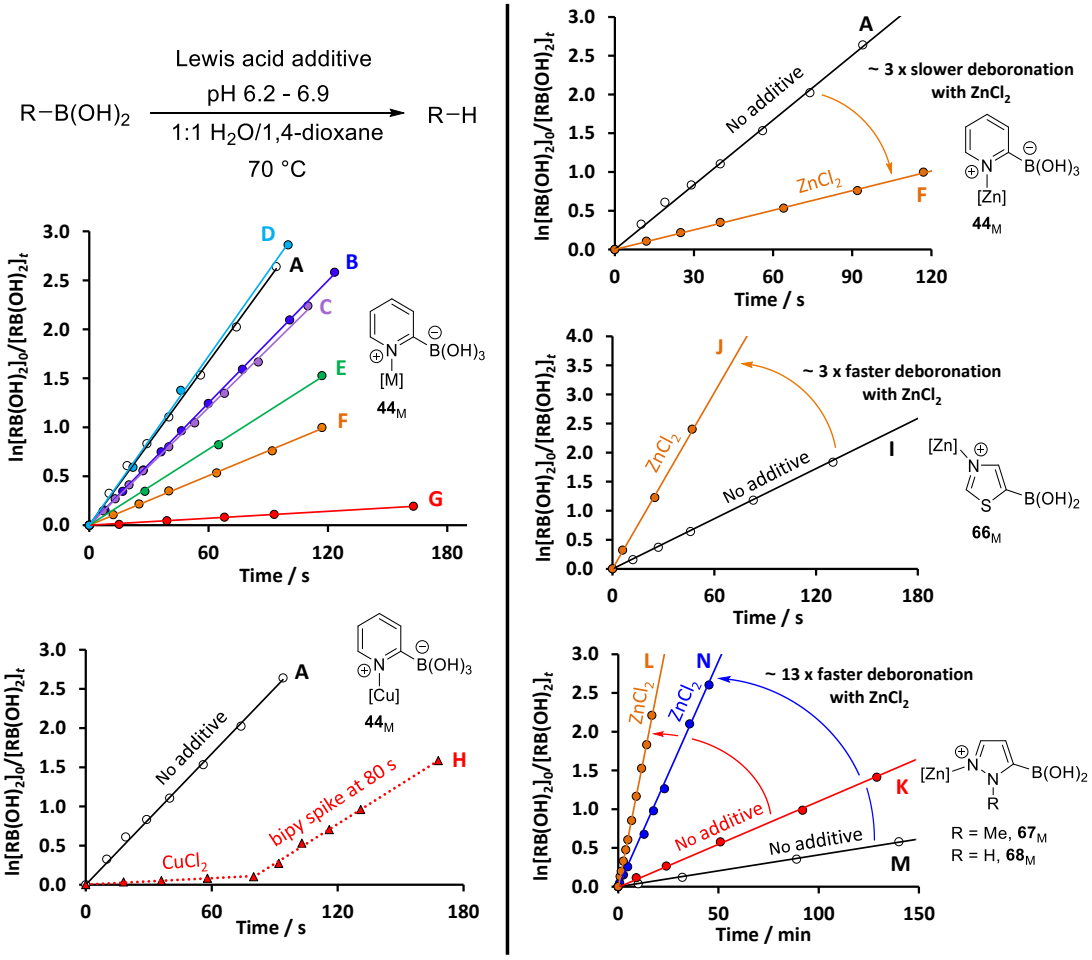

Figure 3.5 First-order log plots for the protodeboronation of **44** in the presence of various Lewis acid additives, and **66** – **68** in the presence of $ZnCl_2$.

The effect of $ZnCl_2$ on the reaction of 5-thiazolyl and 5-pyrazolyl systems was also investigated under neutral pH conditions. Remarkably, the opposite trends were observed to the 2-pyridyl system, whereby an increase in the rate of protodeboronation was observed (3-fold for **66**, 13-fold for **67** and **68**). As previously mentioned, the 5-thiazolyl and 5-pyrazolyl boronic acids display different modes of intramolecular activation compared to $\mathbf{44}_{ZW}$ (see Figure 3.4). Instead of reducing these interactions as in the 2-pyridyl system, the addition of $ZnCl_2$ to 5-thiazolyl boronic acid (**66**) can exacerbate the effect of the C-S antibonding orbital, leading to a greater transition state stabilisation and faster protodeboronation. Similarly, for the 5-pyrazole boronic acids (**68** and **69**), *N*-complexation by Zn results in faster protodeboronation, and can augment the stabilising effects of the polarised *N*-methyl and N-H groups.

3.2.2. 4-pyridinium protonolysis (X_{H+}, k_5)

pH – log k_{obs} profiles of many heteroaromatic boronic acids with measurable pK_{aH} values display an attenuation in the rate of protodeboronation at pH values below the substrate pK_{aH} value (see Figure 3.2). This effect can be explained by the respeciation of the reactive zwitterionic water-adducts ($\mathbf{X}_{ZW}$) into unreactive protonated heteroaromatic species ($\mathbf{X}_{H+}$). Interestingly, the 4-pyridyl systems (**64** and **65**) were clearly an exception to this trend as the log k_{obs} value remains constant as the pH migrates through and below the pK_{aH} (3.36 and 2.95), indicating that an additional protodeboronation mechanism involving the pyridinium species ($\mathbf{X}_{H+}$) is present. A characteristic plateau of the log k_{obs} value in this region (pH < pK_{aH}) further indicates the process to be pH-independent (i.e. no involvement of H^+ or OH^- in rate-determining step). A mechanism consisting of attack at the boron atom of $\mathbf{64}_{H+}$ by water to form a dipolar or carbenoid intermediate is supported by DFT studies (AGL) (Figure 3.6).[71,150] Although the barrier for this process is rather high in energy (45.1 kcal mol^{-1}), it is similar in energy for the protodeboronation under neutral conditions.

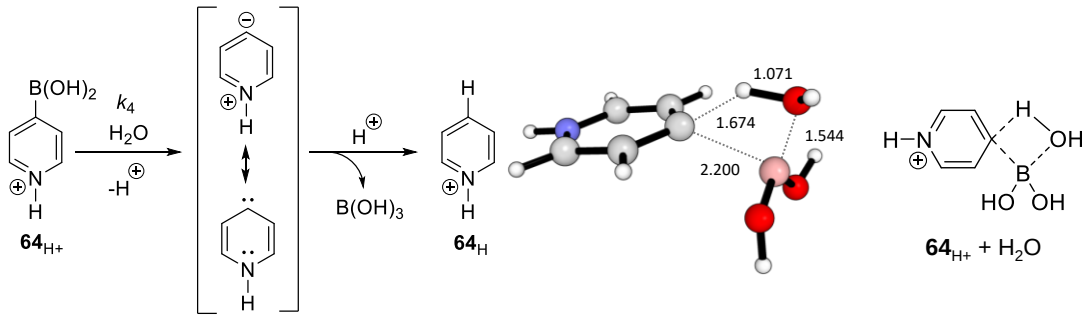

Figure 3.6 Protodeboronation of pyridinium species ($\mathbf{64}_{H+}$) by water, pathway k_4 (left), and the corresponding transition state structure (right).

3.2.3. Boronate deprotonation (X_{O^-}, k_3)

A mechanism involving base-catalysed decomposition of the boronate was required for kinetic simulation of both 4-pyrazolyl and 4-isoxazolyl boronic acids (**60** and **61**) in highly alkaline conditions (pH > 12). This mechanism has previously been proposed by Perrin for 2,6-disubstituted electron deficient aryl boronic acids but not for heteroaromatic substrates.[82] The pH – log k_{obs} profiles for these two substrates confirm the first-order dependence on hydroxide and on boronate species ($\mathbf{X}_{OH}$) with an increase in log k_{obs} with a positive unit gradient after the k_2-plateau (see Figure 3.2). In principle, if boronate deprotonation is a rapid and reversible process, a second pH rate plateau would be expected if high enough pH value were explored, at which point boronates ($\mathbf{60}_{OH}$ and $\mathbf{61}_{OH}$) are converted into dianionic species ($\mathbf{60}_{O^-}$ and $\mathbf{61}_{O^-}$). On the other hand, a rate-limiting deprotonation (or other rate-limiting process involving boronate and hydroxide) would display a continuous unit gradient to infinitely high pH. However, due to limitations with solution homogeneity and pH electrode limits, such pH values could not be obtained. These considerations are explored in-depth for some polyfluorophenyl boronic acids in the following chapter (*vide infra*, section 4.2.)

DFT calculations (AGL) indicate that protodeboronation through the dianionic pathway (k_3) requires the heterocycle to provide transition state stabilisation for the deprotonated boronates ($\mathbf{60}_{O^-}$ and $\mathbf{61}_{O^-}$) and for the resulting carbanion arising from C-B fragmentation. For the 4-pyrazolyl system, this effect arises through an intramolecular interaction between the C-N σ* orbital and the boric acid fragment (34.7 kcal mol^{-1}, $\mathbf{60}_{O^-}$), and similarly a C-O σ* orbital for the 4-isoxazolyl system (34.3 kcal mol^{-1}, $\mathbf{61}_{O^-}$) (Figure 3.7). This mechanism might also be expected for the structurally similar 5-pyrazolyl boronic acids (**66** and **65**), however simulation of their pH – log k_{obs} profiles did not require a contribution from this mechanism (see Figure 3.2). DFT studies reveal that while the 5-pyrazolyl dianion can stabilise the boronate by interactions with the adjacent N-H, it cannot provide stabilisation of the resulting carbanion following C-B fragmentation. Thus, a dianionic pathway (k'_3) pathway is not observed for the 5-pyrazolyl boronic acids.

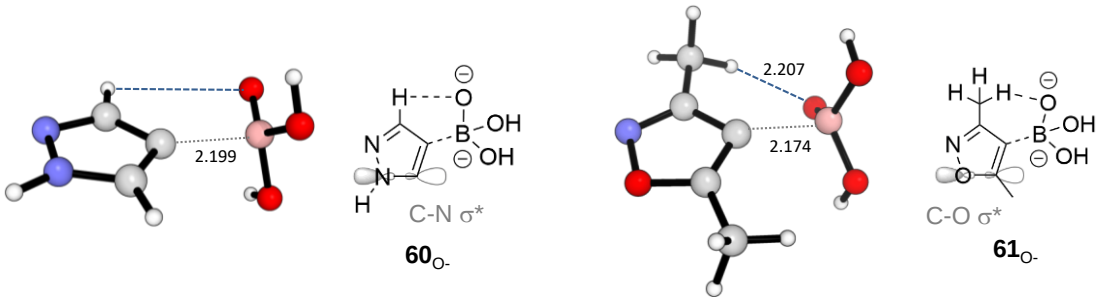

$\mathbf{60}_{O^-}$ $\mathbf{61}_{O^-}$

Figure 3.7 Transition state structures for protodeboronation (k'_3) of $\mathbf{60}_{O^-}$ and $\mathbf{61}_{O^-}$.

3.3. Summary

Protodeboronation rates for a range of heteroaromatic boronic acids were investigated between pH 1 – 13 (1:1 H_2O/dioxane, 70 °C). A diverse range of pH – log k_{obs} profiles were obtained, which were simulated using a general mechanistic model consisting of a 3-fold speciation ($\mathbf{X}_{H+}$, $\mathbf{X}$, $\mathbf{X}_{OH}$) and various protodeboronation pathways (k_1, k_2, $k_2$cat, k_3, k_4, k_5). Contrary to popular belief, many heteraromatic boronic acids undergo very slow protodeboronation, even under strongly alkaline condition, whereas some substrates displayed very high rates of protodeboronation within specific pH regions.

^{11}B NMR studies reveal the presence of a pH-independent equilibrium between boronic acid and zwitterionic water-adducts which are key in describing the observed reactivity at neutral pH values for some basic heteroaromatic boronic acids. For 2-pyridyl (**44**), 5-thiazolyl (**66**), and 5-pyrazolyl boronic acids (**67** and **68**), very fast rates of protodeboronation are observed under neutral pH and DFT studies have revealed that their zwitterionic water-adducts display modes of intramolecular stabilisation that allow facile C-B fragmentation.

For the 2-pyridyl boronic acid (**14**), Lewis acid additives were found to attenuate protodeboronation by complexation at the basic nitrogen centre, thus lowering the reactive zwitterionic water-adduct concentration and removing intramolecular stabilisation. This effect was maximised with 2 equiv. $CuCl_2$, which displayed a 24-fold decrease in the rate of protodeboronation. On the other hand, 5-thiazolyl and 5-pyrazole boronic acids (**66** – **68**) decomposed faster with 2 equiv. $ZnCl_2$, due to complexation at the basic nitrogen atom which augments boronate stabilisation during the transition state (exacerbating intramolecular stabilisation).

Unique protodeboronation pathways were observed for 4-pyridyl systems, in which the protonated pyridinium species ($\mathbf{X}_{H+}$) is responsible for moderate protodeboronation rates in acidic pH conditions (pH < pK_{aH}). Similarly, unique protodeboronation pathways were required for the successful simulation of 4-pyrazole and 3,5-dimethyl-4-isoxazolyl boronic acids (**60** and **61**) whereby rapid protodeboronation occurs in strongly alkaline conditions (pH > 12). DFT calculations support the formation, and subsequent fragmentation, of a dianionic species ($\mathbf{X}_{O-}$) assisted by C-N or C-O σ* orbitals.

Chapter 4

Protodeboronation of Polyfluorophenyl Boronic Acids

4.1. Preliminary studies

4.1.1. Overview

Polyfluorophenyl boronic acids have been applied in various chemical processes that go beyond that of simple aromatic boronic acids. Their unique properties have been exploited in Lewis acid catalysis, metabolite chemosensing and drug design.[49,127,169] However, these valuable reagents have also been reported to be particularly prone to protodeboronation. Thus, efforts have been put towards circumventing their decomposition during cross-coupling reactions by using active pre-catalysts or silver additives.[81] In addition, several studies have focussed on understanding their reactivity (*vide supra*, section 1.5.3.3)[79,80,82]. In particular, Perrin conducted detailed studies for some 2,6-disubstituted electron-deficient aryl boronic acids, encompassing a range of polyfluorinated substrates, whereby even at room temperature, many substrates displayed half-lives in the range of minutes to seconds.[82] From this study, a linear dependence between pH and log k_{obs} (between pH 7 – 12) was observed for 2,4,6-trifluorophenyl boronic acid. Crucially, a lack of rate saturation was explained by the presence of a base-mediated mechanism in which hydroxide catalyses the protodeboronation of the aryl boronate ($\mathbf{X}_{OH}$), by deprotonation to form a dianionic intermediate ($\mathbf{X}_{O-}$) (Scheme 4.1). Perrin was unable to determine if deprotonation of $\mathbf{X}_{OH}$ or fragmentation of $\mathbf{X}_{O-}$ is rate limiting, and did not monitor rates of protodeboronation above pH 12.

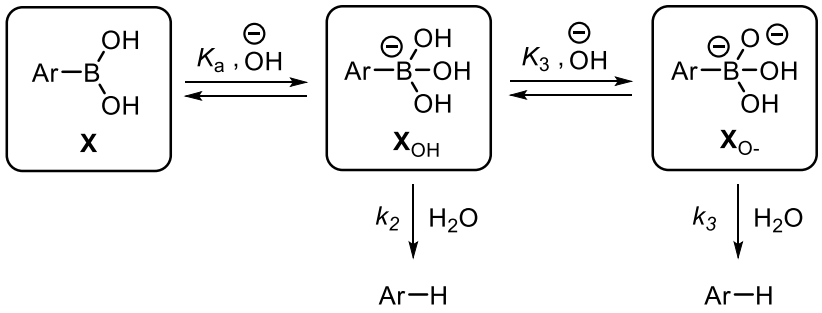

Scheme 4.1 Equilibria and protodeboronation pathways proposed for polyfluorophenyl boronic acid decomposition.

It is noteworthy to mention that in our earlier studies with basic heteroaromatic boronic acids, **60** and **61** both displayed characteristics of a Perrin-type mechanism (k'_3) in their pH – log k_{obs} profiles, where a positive unit gradient can be observed between pH 12 – 13, and was supported by computational studies (*vide supra*, section 3.2.3.). However, this process has not been observed for any tested basic or non-basic boronic acid within our substrate scope.

4.2. Mechanistic investigations

4.2.1. pH – log k_{obs} profile for 2,6-difluorophenyl boronic acid

We suspected that Perrin's results could have been explained with a simple Kuivila-type base-catalysed mechanism (k'_2) and that rate saturation had not been observed as sufficiently alkaline conditions were not attained (pH > 12). This is particularly plausible as *ortho*-substituents are well known to decrease the Lewis acidity of boronic acids through unfavourable steric interactions.[5] In other words, hydroxide association at boronic acid (**X**) to form boronate ($\mathbf{X}_{OH}$) may have been incomplete under the conditions investigated previously. Therefore, we sought to construct a pH – log k_{obs} profile for the 2,6-difluorophenyl boronic acid (**71**) employing our previously established conditions (1:1 H_2O/dioxane, 70 °C). Inconsistent with Perrin's interpretation, the profile displayed a single base-catalysed process, with rate saturation between pH 9.5 – 13.3 (Figure 4.1).

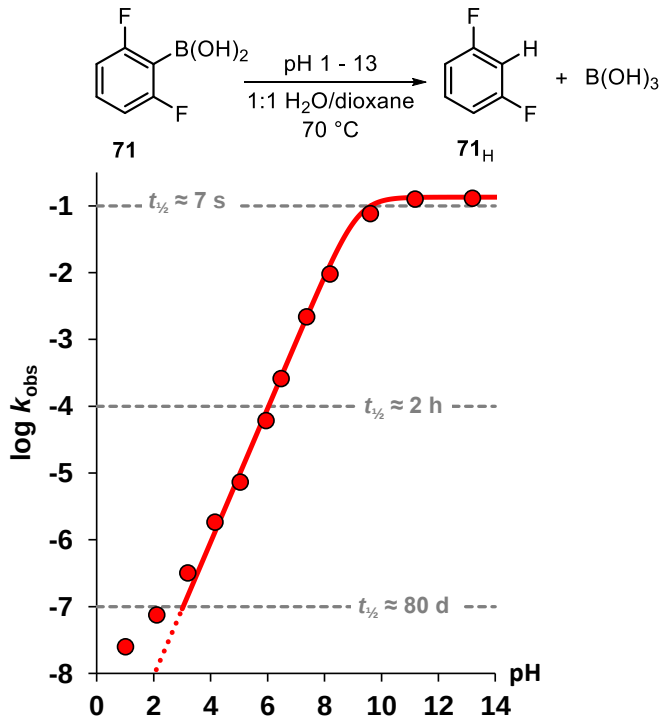

Figure 4.1 pH – log k_{obs} profile for the pseudo first-order protodeboronation of 2,6-difluorophenylboronic acid (**71**). Markers = experimental data. Solid line = simulation using the general mechanistic model (see Figure 3.1) comprising of one rate constant and one equilibrium constant (k'_2 = 0.13; pK_a = 9.16).

As predicted, reaction rates under alkaline conditions were very fast ($t_{½}$ ≈ 5 s, pH > 10). Unlike the previous profiles observed for non-basic boronic acids, no acid-catalysed process was detected, even at pH 1, presumably due to the inability of the electron-deficient species to undergo S_EAr-type protonation. Although the profile shape is very indicative of a Kuivila-

type base-catalysed process (k'_2), it is important to note that in principle, the same shape profile can be constructed for a Perrin-type mechanism (k'_3) given two conditions:

1) $k'_3 \approx k'_2$
2) $pK_3 \approx pK_a$ (and that rate saturation is observable for both equilibria, i.e.: $pK_x << 13$)

However, simulation of the experimental data with the general mechanistic model indicates that the rate saturation is observed with an equilibrium process consisting of a pK_x value of 9.15. Such a value seems plausible for hydroxide association constant at boron (i.e. a pK_a value) given the values previously determined for many non-basic and basic heteroaromatic boronic acids (see Table 3.1). On the other hand, equilibrium constants for the deprotonation of boronate (K_3) have not been reported in aqueous solution and thus are expected to be large and outside of the measurable pH window ($pK_3 >> 13$). Therefore, based only on the extrapolated equilibrium constant, it seems likely that the 2,6-difluorophenyl boronic acid (**71**) does *not* react via a Perrin-type process (k'_3), and thus a Kuivila-type mechanism (k'_2) must be considered in more detail.

4.2.2. Hydroxide dependence

To determine conclusively if the observed rate profile (above pH ~9.5) is due to boronate saturation ($\mathbf{X}_{OH}$, k'_2) or dianionic species saturation ($\mathbf{X}_{O^-}$, k'_3), a plot of protodeboronation rates against equivalents of hydroxide was constructed. In principle, a Kuivila-type mechanism (k'_2) would require only 1 equiv. of hydroxide to reach total saturation of the protodeboronation rate, whereas a Perrin-process (k'_3) would require at least 2 equiv. of hydroxide (*vide infra*, section 4.2.6.). Reaction of 2,6-difluorophenylboronic (**71**) (50 mM, 1:1 H_2O/dioxane, 70 °C) with varying amounts of KOH (0 – 2.8 equiv) revealed rate saturation at 1 equiv. KOH, supporting a Kuivila-type base-catalysed mechanism (k'_2) (Figure 4.2).

Considering the temperature disparity between Perrin's reaction conditions and ours, the hydroxide dependence was additionally examined for pentafluorophenyl boronic acid (**72**) at room temperature (1:1 H_2O/dioxane, 21 °C), which also displayed rate saturation between 1 - 3 equiv. KOH (Figure 4.3). Therefore, the hydroxide dependence studies eliminate a rate-limiting event comprising of formation *or* reaction of a dianionic species ($\mathbf{X}_{O^-}$), thus a Perrin-type mechanism (k'_3) can be dismissed for 2,6-difluorophenyl boronic acid (**71**).

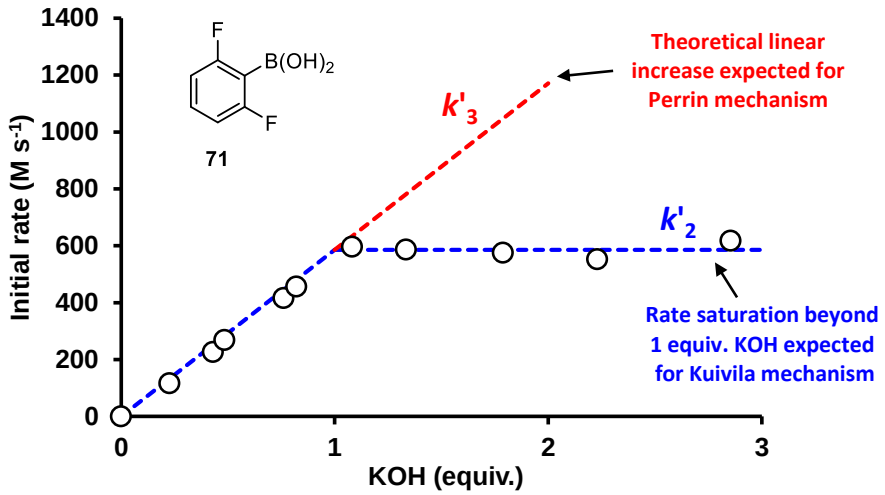

Figure 4.2 Initial rates of protodeboronation with various equivalents of KOH for 2,6-difluorophenyl boronic acid (**71**) (50 mM, 1:1 H_2O/dioxane, 70 °C). White circles = experimental data obtained by SF-IR (performed by Dr Marc Reid, University of Edinburgh). Blue dotted line indicates theoretical saturation after 1 equiv. of KOH. Red line indicates theoretical linear increase of rate with increasing KOH, expected for a Perrin-type mechanism (k'_3).

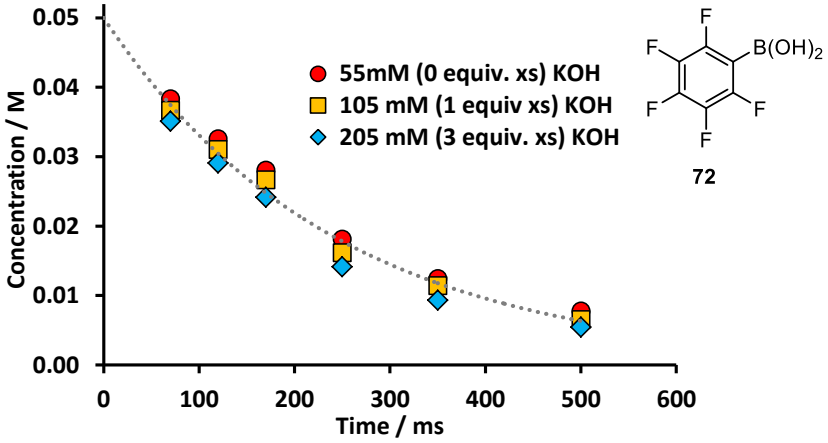

Figure 4.3 Temporal concentration data for the protodeboronation of pentafluorophenyl boronic acid (**72**) (50 mM, 5 mM TFA, 1:1 H_2O/dioxane, 21 °C) with various amounts of KOH. Excess (xs) KOH calculated using $[KOH]_{added} - ([RB(OH)_2]_{initial} + [TFA])$. Grey dotted line = simultaneous first-order simulation fitting to all data sets (k = 4.28 ± 0.20).

4.2.3. Rates of protodeboronation for polyfluorophenyl boronic acids

With confidence that the protodeboronation rate is saturated beyond 1 equiv. of hydroxide, we sought to acquire protodeboronation kinetics for a full scope of fluorinated aromatic boronic acids under a single set of reaction conditions consisting of: KOH (2 equiv.), carboxylate internal standard (0.1 equiv., TFA or PPA); 1:1 H_2O/dioxane; 70 °C (Table 4.1). The substrate scope included all isomers of mono-, di-, tri- and tetra-fluorophenyl boronic acids, some with additional substitution (OMe, CF_3, NO_2), and some non-fluorinated substrates including a few substrates utilised in Kuivila's original studies (Figure 4.4).[61] An

excess of base was crucial in ensuring that kinetics were obtained at boronate saturation (i.e. boronic acid is quantitatively converted to boronate), thus simplifying the analysis of observed rate constants (k_{obs}).

Given the previously reported kinetic data and observations by Perrin, we anticipated that the elevated reaction temperature would result in exceptionally fast reaction rates for heavily fluorinated species (i.e. pentafluorophenylboronic acid), whereas monofluorinated species (i.e. 4-fluorophenylboronic acid) were expected to require several days to react.[80,82] Therefore, we required a range of reaction monitoring techniques to encompass a wide range of reactivities. For very slow reactions ($t_{½}$ > 1 day), reactions were carried out in sealed J Young's valve NMR tubes over several days, whereas moderate reactions rates ($t_{½}$ between 1 h – 1 day) were monitored by manual quenching of reaction solutions into strong acid (all monitored by ^{1}H or ^{19}F NMR spectroscopy). Stopped-flow infrared (SF-IR) spectroscopy with complete thermostating was utilised for *in situ* reaction monitoring of rapid reactions ($t_{½}$ between 50 ms and 30 min), which can exploit the aromatic C-F stretches present in all polyfluorophenyl compounds (large extinction coefficients and located at convenient wavenumbers). For further precision, rapid quench-flow (RQF) apparatus was utilised for exceptionally fast reactions ($t_{½}$ between 2 ms – 60 s), and samples analysed by ^{19}F NMR spectroscopy. Clean pseudo first-order decay of starting material was observed for all fast reactions ($t_{½}$ < 1 day). However, due to solubility and evaporation issues, product formation could not be reliably monitored. On the other hand, slower reactions ($t_{½}$ > 1 day) displayed side reactions including oxidation and potential polymerisation (noted by Kuivila)[61] and resulted in unreliable extrapolation of rate constants through starting material consumption. However in these cases, the protodeboronated product could be reliably monitored providing reactions were carried out in a sealed vessel and that initial rates were used (avoiding evaporation/solubility issues).

Table 4.1 Measured equilibrium constants and rate constants for the protodeboronation of **28** and **71** – **99**).

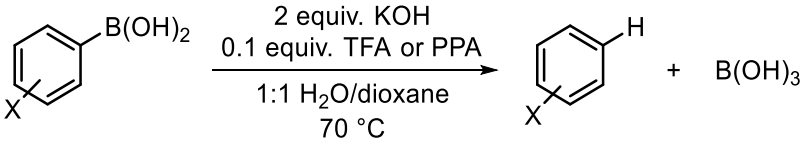

Entry	RB(OH)$_2$	Abbreviation	pK_a[a]	log k_{obs}	$t_{½}$
1	**73**	Phenyl	11.25	-7.39	196 d
2	**28**	4-MeO	11.78	-6.63	34 d
3	**74**	2-F	10.14	-5.00	19 h
4	**75**	3-F	10.46	-7.40	199 d
5	**76**	4-F	10.97	-7.23	134 d
6	**77**	2,3-F	9.51	-3.92	95 min
7	**78**	2,4-F	10.02	-4.60	8 h
8	**79**	2,5-F	9.34	-4.20	3 h
9	**80**	3,4-F	10.34	-7.13	109 d
10	**81**	3,5-F	9.78	-7.08	97 d
11	**82**	2,3,4-F	9.06	-3.53	39 min
12	**83**	2,3,5-F	8.74	-2.95	10 min
13	**84**	2,4,5-F	9.00	-3.76	66 min
14	**85**	3,4,5-F	9.44	-6.77	47 d
15	**71**	2,6-F	9.15[b]	-0.87	5 s
16	**86**	2,3,4,5-F	8.91[b]	-2.41	3 min
17	**87**	2,3,6-F	8.66[b]	0.47	260 ms
18	**88**	2,4,6-F	9.03[b]	-0.26	1 s
19	**89**	2,3,4,6-F	8.39[b]	1.02	70 ms
20	**90**	2,3,5,6-F	7.97[b]	1.79	11 ms
21	**72**	2,3,4,5,6-F	7.67[b]	2.43	3 ms
22	**91**	2-F-4-MeO	10.78	-5.25	32 h
23	**92**	2-F-4-CF_3	9.04	-4.03	2 h
24	**93**	2-F-5-NO_2	8.22[b]	-3.10	15 min
25	**94**	2,6-F-4-MeO	9.56[b]	-1.01	7 s
26	**95**	2,3,5,6-F-4-MeO	8.33[b]	1.88	9 ms
27	**96**	3,5-CF_3	9.38	-6.81	52 d
28	**97**	3,5,-NO_2	7.91	-4.92	16 h
29	**98**	4-Me	11.78	-6.80	51 d
30	**99**	3-Cl	10.56	-6.85	57 d

[a] pK_a determined by ^{11}B NMR pH titration at 70 °C (unless stated). [b] pK_a extrapolated from simulation of rate data.

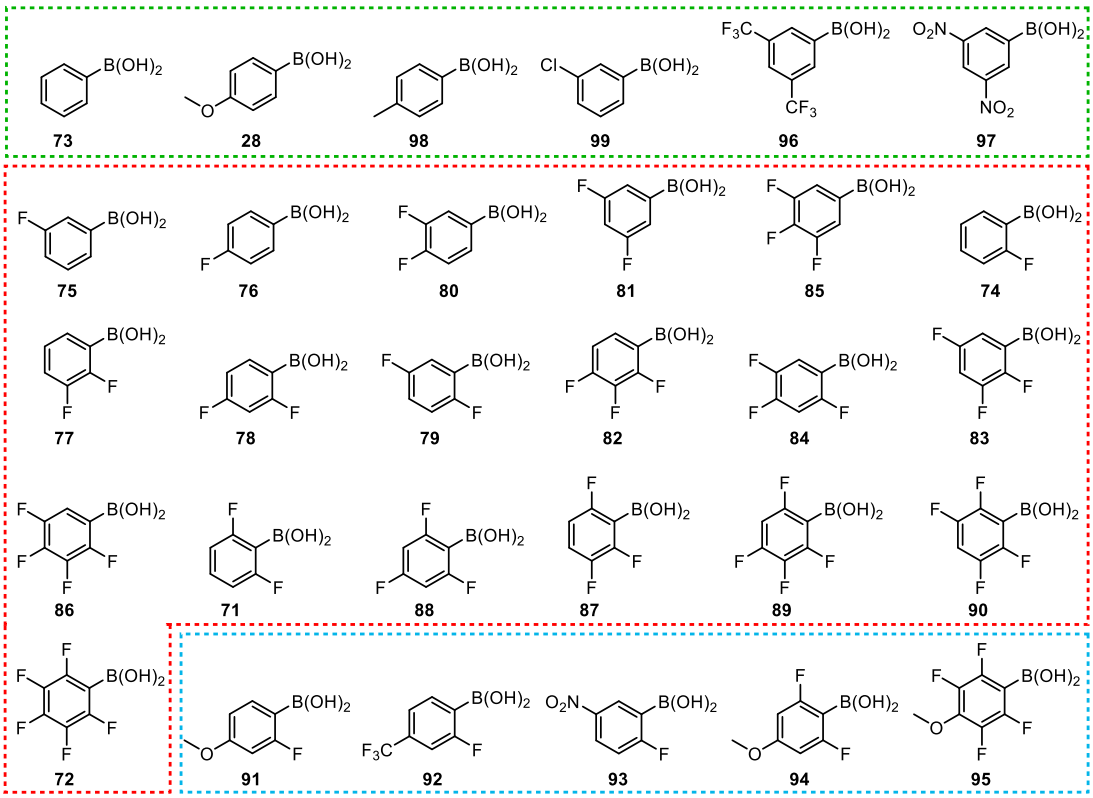

Figure 4.4 Substrate scope used in this study. Green box highlights substrates without fluorine substitution. Red box highlights substrates with only fluorine substitution. Blue box highlights substrates with fluorine and other substituents.

Across the substrate scope, a very diverse range of reactivity was observed, spanning 10 orders of magnitude between benzene boronic acid (**73**) ($t_{½}$ ≈ 200 days) and pentafluorophenyl boronic acid (**72**) ($t_{½}$ ≈ 3 ms). As previously reported, not only does the level of fluorine substitution have an impact of substrate stability, but also the substitution position.[79,80,82] Three distinct reactivity classes were visualised including:

1) Lower reactivity substrates – typically with no *ortho*-fluoro substitution
2) Moderate reactivity substrates – typically with single *ortho*-fluoro substitution
3) Higher reactivity substrates – typically with di*ortho*-fluoro substitution

Within the more reactive categories (substrates with at least one *ortho*-fluoro substituent), any additional fluorine substitution (*ortho*, *meta* or *para)* resulted in an increased protodeboronation rate. Notably, a strong additive trend can be extrapolated with these reactive substrates, whereby (on average) the addition of an *ortho*, *meta* or *para* fluorine results in a 30,000-fold, 12-fold or 3-fold rate increase, respectively. Similarly, the addition of other electron-withdrawing substituents (CF_3, NO_2) to *ortho*-fluoro substituted regents results in an increased protodeboronation rate (compare entry 3 with entries 23 and 24; Table 4.1), whereas an electron-donating group (MeO) has little impact (compare entry 3, 15 and

20 with entries 22 and 25-26; Table 4.1). The same trend is not so apparent for the lower reactivity class, as many substrates without *ortho*-fluorine substitution (including those with no fluorine substitution) display very similar rates of protodeboronation ($t_{½}$ ≈ 100 – 200 days) with no significant rate change upon *meta* or *para* substitution. The only significant exception to this generalisation was 3,5-dinitrophenyl boronic acid (**97**, $t_{½}$ = 16 h), which is discussed in full detail (*vide infra*, section 4.2.4.4.)

4.2.4. LFER analysis of rate data

4.2.4.1. Kuivila's Hammett analysis

Using the obtained rate data, we focused on constructing a LFER profile to aid understanding of the mechanism(s) in action, and to compare this to previously reported data. In Kuivila's studies, base-catalysed protodeboronation rates were correlated with various LFER parameters, and the best correlation was obtained with the original Hammett σ values (Figure 4.5).[61] It is important to note that the observed rate constants obtained by Kuivila were converted into absolute rate constants using pK_a values reported by Polvey, using a different solvent system and temperature (3:1 H_2O/methanol, 25 °C) compared to the reaction conditions (H_2O, 90 °C).[61] Regardless of these limitations, qualitative information can be extracted. The gradient of the plot (ρ = −2.3) indicates stabilisation of the transition state with electron-donating substituents (*p*-Me, *p*-MeO etc.). In other words, a small positive charge develops in the benzene ring at the transition state. For the small set of *ortho*-substituted aryl boronic acids examined by Kuivila, the Taft equation was employed, however, non-linear correlations indicated other factors may play a role in the reactivity of this subset of substrates.

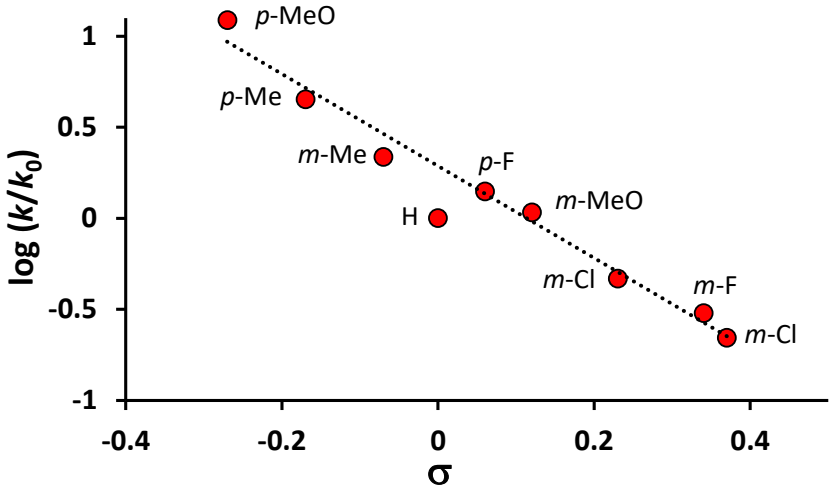

Figure 4.5 Reconstructed Hammett plot for the protodeboronation of substituted phenyl boronic acids at 90 °C by Kuivila and co-workers.[61]

4.2.4.2. Modified Hammett analysis

Hammett analysis is usually conducted for systems containing only a single non-hydrogen substituent in either the *meta* or *para* position of a phenyl system. However, it has been demonstrated in past studies that multiple substituents can be tolerated within the analysis for some reactions.[170,171] The total Hammett σ value for a poly-substituent system can be calculated by summing the individual substituent σ values. However, limitations to this theory have been proposed: large and adjacent substituents may exhibit significant steric clash whereas others may display favourable hydrogen-bonding interactions.[171] In each case, the substituents can be forced into unusual conformations which impact their electronic contribution. Deviations in the additivity have been observed in Hammett's early work, but these deviations appear to be minor for small substituents such as methyl groups.[172] Of course, many of the polyfluorophenyl boronic acids include adjacent substituents which may impact the additivity assumption when conducting a Hammett analysis. However, we anticipated that the size and limited degrees of freedom for a fluorine substituent may help to maintain an additive trend.

Many of the polyfluorophenyl boronic acids used in the substrate scope contain *ortho*-fluorine substitution. The inability to use *ortho*-substituents in a standard Hammett analysis eliminates the opportunity to correlate the entire substrate scope into a single, classical LFER plot. To overcome this we envisaged a modification of a Hammett analysis, whereby a theoretical Hammett σ value for an *ortho*-fluorine substituent (σ_o(F)) can be calculated and optimised through an iterative regression fitting to the experimental rate data. Such an analysis seemed viable given the additive increase in the protodeboronation rate upon installation of an *ortho*-fluorine substituent (~30,000-fold increase in k_{obs}, for example compare entry 14 with 16; Table 4.1). Furthermore, the additive trend for σ values is maintained for di*ortho*-fluoro substituted compounds (for example, compare entry 3 with 15; Table 4.1). Unlike *meta* and *para* substituents, it is important to note that an σ_o(F) value may not be a pure description of electronic effects (and more likely a combination of electronic, steric and neighbouring effects) however qualitative results can still be extracted and used to find trends in reactivity.

A regression analysis of the entire data set was optimised through iterative fitting of the σ_o(F) value (=1.10) while using standard Hammett σ values for *meta* and *para* substituents, which turn out to be very revealing (top, Figure 4.6).

Two distinct regions of linearity were observed:

1) $\sigma < 0.80$, which displays a plateau region ($\rho \approx 0$) encompassing many substrates without *ortho*-fluoro substitution (lower reactivity compounds).
2) $\sigma > 0.80$, which displays a positive gradient ($\rho \approx 4.1$) encompassing the *ortho*- and di*ortho*-fluoro substituted (moderate to high reactivity) compounds.

The same analysis was conducted using both Brown's σ^+ and Yoshioka's σ^- values, however the strongest correlation was observed for standard Hammett σ values.[173,174] Surprisingly, the Hammett analysis conducted by Kuivila was not reproduced in our experiments. Nevertheless, the large positive gradient ($\rho = 4.1$, $\sigma > 0.8$) found in our Hammett analysis is the reverse trend observed in Kuivila's studies ($\rho = -2.3$, $-0.27 < \sigma < 0.37$), and indicates that unique (non Kuivila-type) mechanisms of protodeboronation are likely to be in action for substrates with large positive σ values.

4.2.4.3. Swain-Lupton analysis

The LFER study was further improved with a Swain-Lupton modification, whereby field (*F*) and resonance (*R*) values for substituents can be optimised by varying the ratio of each component (*f* and *r*). In a similar manner to before, iterative fitting of an *ortho*-fluorine substituent ($\sigma_o^{SL}(F) = 1.24$) and the ratio of field and resonance effects ($f = 0.69$ and $r = 0.31$, constrained so that $f + r = 1$) afforded an optimised LFER plot (bottom, Figure 4.6). The analysis particularly improved the data scatter in the region where $\sigma > 0.8$. It is noteworthy that substrates containing both fluorine and other substituents (blue squares, Figure 4.6) displayed particular scatter in the modified Hammett analysis; substrates with classically electron-donating groups (4-MeO) are predicted to be less reactive than experimentally observed, whereas electron-withdrawing groups (CF_3, NO_2) are predicted to be more reactive than observed. With the optimised *f* and *r* values, the Swain-Lupton analysis resolves this observation by reducing the electronic contribution through resonance. For example, this analysis renders the 4-MeO substituent almost 'electronically neutral' ($\sigma_p(MeO) = -0.27$ whereas $\sigma_p^{SL}(MeO) = 0.03$).

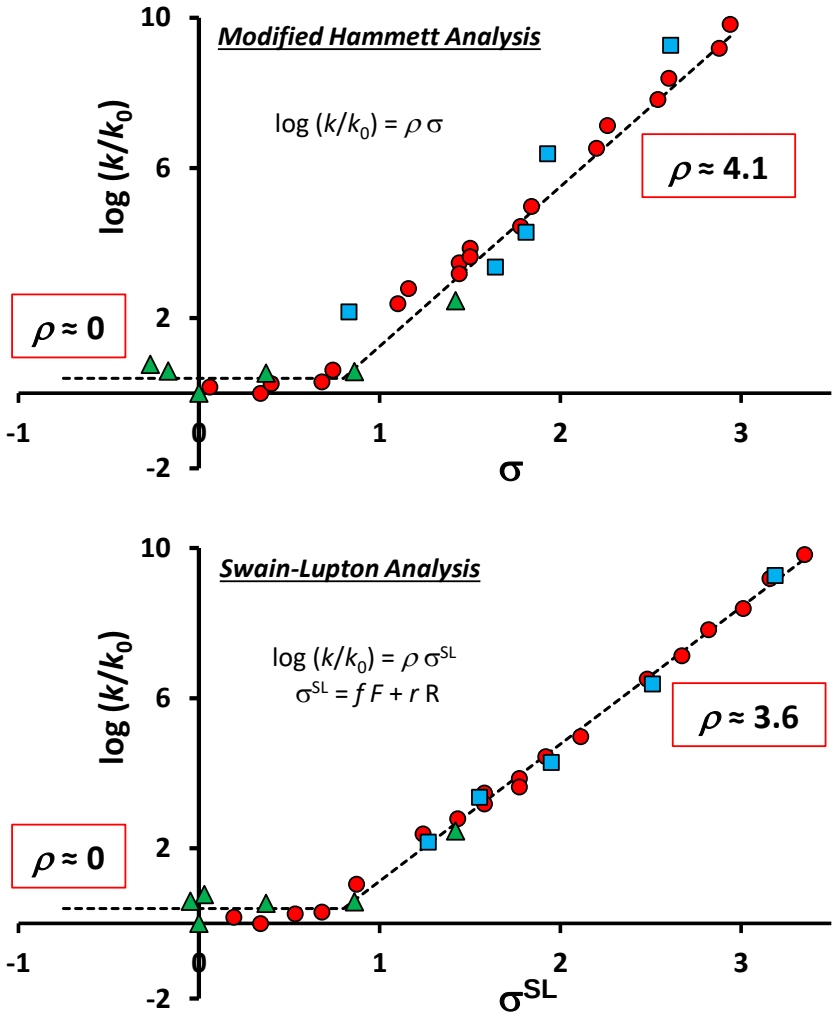

Figure 4.6 LFER analysis for the protodeboronation of **28**, **71** – **99**. Top: Modified Hammett analysis, σ_o(F) = 1.10. Bottom: Modified Swain-Lupton analysis, σ_o^{SL}(F) =1.24, f = 0.69, r = 0.31. Red circles = substrates with fluorine substituents only. Blue squares = substrates with fluorine and other substituents. Green triangles = substrates without fluorine substituents.

4.2.4.4. Reactivity without ortho-substituents

Although the Swain-Lupton analysis displays trends in reactivity, it is important to note that the strong correlations observed at $\sigma^{SL} > 0.8$ (ρ = 3.6) is dominated by substrates containing *ortho*-fluorine substitution. Thus, it is difficult to determine whether steric, electronic or both factors are responsible for the high levels of reactivity observed for these species. To test this, we sought to synthesise a highly electron-deficient aryl boronic acid with a $\sigma^{SL} > \sim 1$ that contains **no** *ortho*-substituents. To avoid steric inhibition of resonance, we also focused on ensuring substituents were not adjacent (i.e. not 3,4-disubstituted). This leaves only two possible substitution patterns; a single *para* substituent or two *meta* substituents. The single *para* substituent pattern would require a very powerful electron-withdrawing group, of which only a few esoteric examples exist.[175] Therefore we turned our attention to a 3,5-

di*meta* substituted system and selected 3,5-dinitrophenyl boronic acid (**97**) as a suitable candidate (σ^{SL} = 1.42). Synthesis and then protodeboronation of **97** under the standard reaction conditions (1:1 H_2O/dioxane, 2 equiv. KOH, 70 °C) revealed a good correlation with the Swain-Lupton analysis, reacting at a similar rate to *ortho*-fluorophenyl boronic acid (**74**). This finding indicates that an *ortho*-fluorine substituent may act merely as a powerful electron-withdrawing group, and have little steric effect (or other specific *ortho* effects) during the protodeboronation mechanism. In other words, *ortho* substitution is not a prerequisite for the mechanism that proceeds when $\sigma^{SL} > 0.8$.

4.2.5. KIE studies

4.2.5.1. Independent rate KIE experiments

KIE experiments were conducted to elucidate further mechanistic details for the protodeboronation of 4-methoxyphenylboronic acid (**28**) and 2,6-difluorophenylboronic acid (**71**). These two reagents were specifically selected as they exhibit very different σ^{SL} values, and thus are located in different mechanistic regimes of the Swain-Lupton plot. Independent rate KIEs were obtained for both substrates by comparison of reaction rates in either H_2O or D_2O (1:1 L_2O/dioxane, 2 equiv. KOL, 0.1 equiv. TFA, 70 °C). A KIE was observed for 4-methoxyphenyl boronic acid (**28**) (independent rate KIE = 4.3) whereas no significant KIE was measured for 2,6-difluorophenylboronic acid (**71**) (independent rate KIE = 1.0) (Figure 4.7), indicating that each substrate reacts through a different protodeboronation mechanism. The large and normal KIE for 4-methoxyphenyl boronic acid (**28**) supports the concerted mechanism proposed by Kuivila and co-workers.[61] On the other hand, the absence of a KIE for the 2,6-difluorophenyl boronic acid (**71**) eliminates a concerted mechanism with water, and indicates little or no proton transfer during the rate-limiting event.

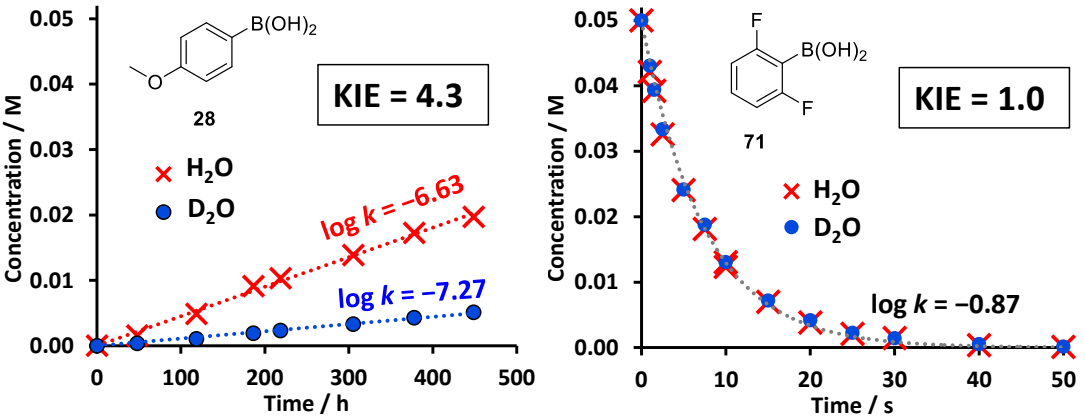

Figure 4.7 Temporal concentration data for the protodeboronation of 4-methoxyphenyl boronic acid (**28**) and 2,6-difluorophenyl boronic acid (**71**) in 1:1 L_2O/dioxane at 70 °C. Markers = experimental data. Dotted lines = first-order simulation fittings.

4.2.5.2. Competition KIE experiments

To further investigate the mechanism, 4-methoxyphenyl boronic acid (**28**) was reacted in a solvent mixture consisting of 1:1:2 H_2O/D_2O/dioxane, and the formation of d_0- and d_1-anisole ($\mathbf{28}_H$ and $\mathbf{28}_D$) analysed by ^1H NMR (left, Figure 4.8). The product H/D partitioning ([d_0-anisole]/[d_1-anisole]) was equal to the independent rate KIE (H/D partitioning = rate KIE = 4.3) which indicates protonation occurs in the rate-limiting event, further supporting a concerted reaction between aryl boronate and water, as proposed by Kuivila.

2,6-difluorophenyl boronic acid (**71**) was reacted under the same conditions, whereby 1,3-difluorobenzene ($\mathbf{71}_H$) and d_1-1,3-difluorobenzene ($\mathbf{71}_D$) products were easily quantified using ^{19}F NMR due to sufficient isotope shifts in the NMR spectra (right, Figure 4.8). Interestingly, a small but measurable H/D partitioning was observed and was greater than the independent rate KIE (H/D partitioning = 1.25, rate KIE = 1.00). These findings show that the protonation step must come after the rate-limiting event, a process not consistent with Kuivila's base-catalysed mechanism.

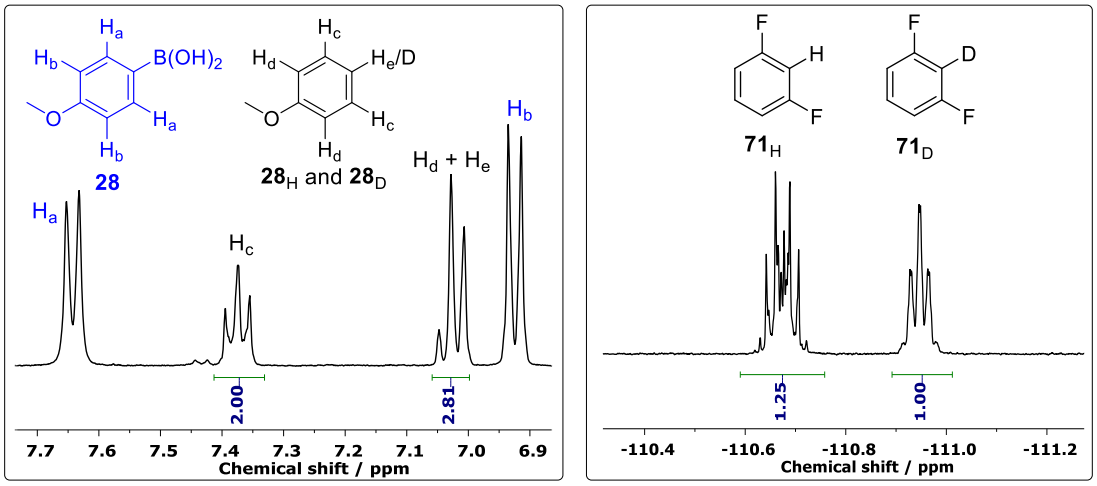

Figure 4.8 Individual reaction of 4-methoxyphenyl boronic acid (**28**) and 2,6-difluorophenyl boronic acid (**71**) (right) in 1:1:2 H_2O/D_2O/dioxane at 70 °C displaying the product partitioning of proto- and deutero-products, analysed by ^1H (left) or ^{19}F (right) NMR. See section 6.6.4. for details on H/D partitioning calculations.

4.2.6. Eyring analysis

Protodeboronation rates for 2,6-difluorophenyl boronic acid (**71**) were conducted at a variety of temperatures which, when employed in an Eyring equation, provides activation parameters. The form of the Eyring analysis is dependent on the reaction molecularity, which has been determined using the KIE data (*vide supra*, section 4.2.4.). The independent rate KIE provides conclusive evidence for the absence of extensive proton transfer in the RLS,

and thus indicates a unimolecular transition state. With the determined reaction molecularity, protodeboronation reactions were performed between 21 and 70 °C (1:1 H_2O/dioxane, 2 equiv. KOH, 0.1 equiv. TFA), and the resulting activation parameters ($\Delta H^{‡}$ = −23.2 kcal mol^{-1}, $\Delta S^{‡}$ = +4.7 cal K^{-1} mol^{-1}) indicate a dissociative transition state (Figure 4.9).

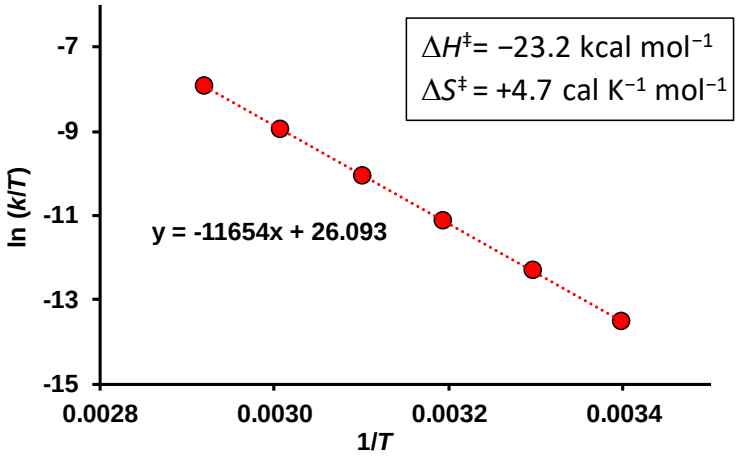

Figure 4.9 Eyring analysis for the protodeboronation of 2,6-difluorophenyl boronic acid (**71**) (50 mM, 2 equiv. KOH, 0.1 equiv. TFA, 1:1 H_2O/dioxane, 21 – 70 °C).

4.2.7. Mechanistic proposals

With the acquired experimental data, it is evident that both 4-methoxyphenyl boronic acid (**28**) and 2,6-difluorophenyl boronic acid (**71**) undergo unique base-catalysed mechanisms. Simple analysis and simulation of their pH – log k_{obs} profiles does not provide sufficient information to distinguish the different base-catalysed processes proposed by Kuivila and Perrin. For 4-methoxyphenyl boronic acid (**28**), Kuivila's results are consistent with a concerted mechanism between aryl boronate and water (k'_2, pathway **I**, Scheme 4.10). This has been further supported by the independent rate and competition KIE studies (*vide supra*, sections 4.2.4. and 4.2.5.), which indicate proton transfer is involved in the rate-limiting step of the reaction. In contrast for 2,6-difluorophenyl boronic acid (**71**), the dependency of the reaction rate on hydroxide concentration displayed full rate saturation at 1 equivalent of KOH, which eliminates a Perrin-type mechanism (k'_3, pathway $\mathbf{II_a}$ or $\mathbf{II_b}$, Scheme 4.10). Additionally, the absence of an independent rate KIE confirms water is not involved in the rate-limiting step, and thus a Kuivila mechanism (k'_2, pathway **I**, Scheme 4.10) can also be eliminated. Competition KIE studies reveal a small partitioning of H and D products that is not equal to the independent rate KIE, indicating that protonation must come after the rate-limiting event. Using the KIE studies to confirm that water is not involved in the rate-limiting step, the Eyring analysis can be meaningfully interpreted and the resulting activation

parameters indicate a dissociative transition state. Finally, a complete LFER analysis for all isomers of polyfluorophenyl boronic acids shows that the protodeboronation rates of mono- and di*ortho*-fluorine substituted boronic acids can be accelerated with further substitution of electron withdrawing groups (F, CF_3, NO_2).

All of the considered data is in agreement with rate-limiting unimolecular fragmentation of aryl boronate to form an aryl anion, followed by rapid protonation by water (k_2^{Ar-}, pathway **III**, Scheme 4.10). Table 4.2 displays a summary of the experimental findings and how, in turn, it can be used to eliminate the relevant mechanisms proposed in Scheme 4.2.

Table 4.2 Summary of which mechanisms are supported by individual experimental data.

Mechanism	Rate saturation at 1 equiv. KOH	ρ = +ve	Independent rate KIE = 1	Rate KIE ≠ Competition KIE	Dissociative mechanism[a]
I (Kuivila)	✓	×	×	×	×
II_a (Perrin)	×	?	×	×	×
II_b (Perrin)	×	✓	×	✓	×
III (new)	✓	✓	✓	✓	✓

[a] Based on the Eyring analysis, assuming water is not involved in the rate-limiting step.

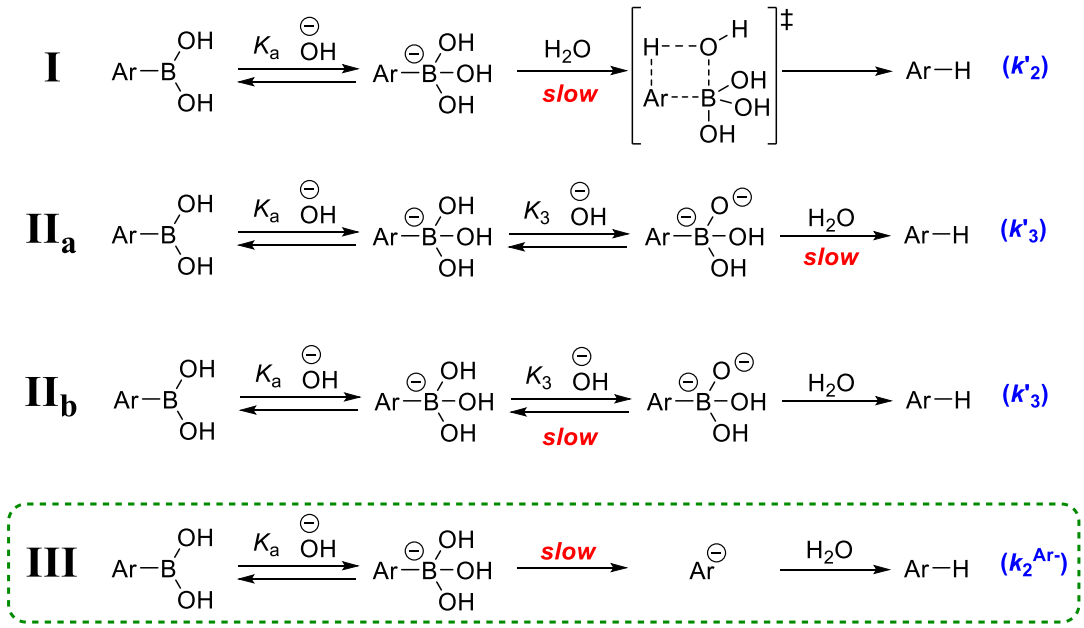

Scheme 4.2 Base-catalysed protodeboronation pathways proposed by Kuivla (**I**), Perrin (**II_a** or **II_b**) and a new mechanism proposed on the basis of experimental data in this study (**III**).

Since the aryl anion mechanism (k_2^{Ar-}) cannot be kinetically distinguished from a Kuivila-type base-catalysed mechanism (k'_2) by pH – log k_{obs} simulation using the general mechanistic model used in Chapter 3 (*vide supra*, section 3.1.1), this process will be labelled as a "k_2" process, but is distinguished in the text with superscript notation as k_2^{Ar-}.

4.2.7.1. Re-examination of LFER analysis

Aryl anions have been postulated as intermediates in several reactions including the base-catalysed halogen shift of aryl halides,[176] alkali cleavage of 2,6-dihalobenzaldehydes,[177] cleavage of 2-halobenzophenones with KNH_2,[178,179] thermal decarboxylation reactions,[180] and hydrogen isotope exchange in 2-fluorobenzenes.[181] Many of these aryl anion mechanisms are noted to be enhanced by *ortho*-halogen substituents, much like the observations for protodeboronation of polyfluorophenyl boronic acids. One study by Bunnett is particularly relevant, involving the aqueous decarboxylation of 2,6-dinitrobenzoates.[182,183] *Para* substituents were varied and the rates plotted against the original Hammett σ values, which displayed a moderate correlation (left, Figure 4.10). However, examination of the Hammett plot shows that the 4-MeO substituent is underestimated in this analysis; an effect that was also observed in the Hammett plot for the protodeboronation of polyfluorophenyl boronic acids (compare entries 22,25 and 26 with entries 3,15 and 20, Table 4.1). Because this effect was previously remedied in the protodeboronation studies by employing a Swain-Lupton analysis, we conducted the same analysis for Bunnett's decarboxylation data. Using identical parameter coefficients to those employed in the protodeboronation studies (f =0.69, r = 0.31), an improved correlation was observed (right, Figure 4.10).

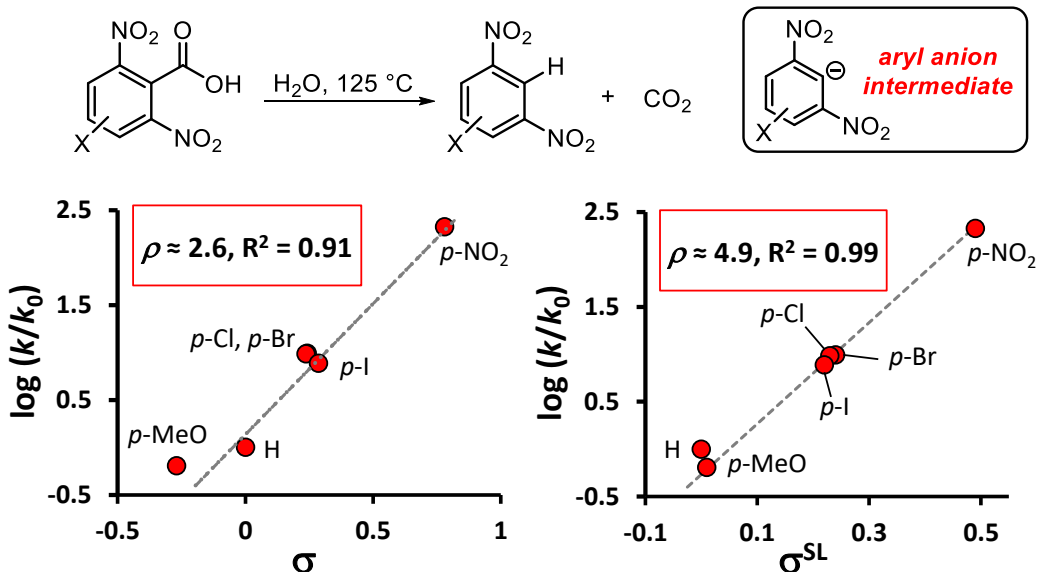

Figure 4.10 LFER analysis of the decarboxylation of 4-substituted 2,6-dinitrobenzoates by Bunnett.[182] Left: Hammett analysis. Right: Swain-Lupton analysis, f = 0.69, r = 0.31.

Using the original Hammett σ values to correlate the reactivity of an aryl anionic transition state is a sub-optimal model. This is because Hammett analysis is based on σ values derived from the ionisation of benzoic acids, which can be efficiently (de)stabilised by substituents through resonance effects in the aromatic π-system (top scheme, Figure 4.11). Conversely, an aryl anionic transition state holds a negative charge in an orbital perpendicular to the aromatic π-system, and thus the resonance contribution of a substituent has, comparatively, a reduced influence on (de)stabilising the transition state en route to aryl anion formation (bottom scheme, Figure 4.11). Thus, it can be rationalised that *field effects have a more significant role than resonance effects in the stabilisation of aryl anionic transition states*. The Swain-Lupton analysis addresses this issue by weighting the field and resonance contributions of each substituent in a ~2:1 ratio.

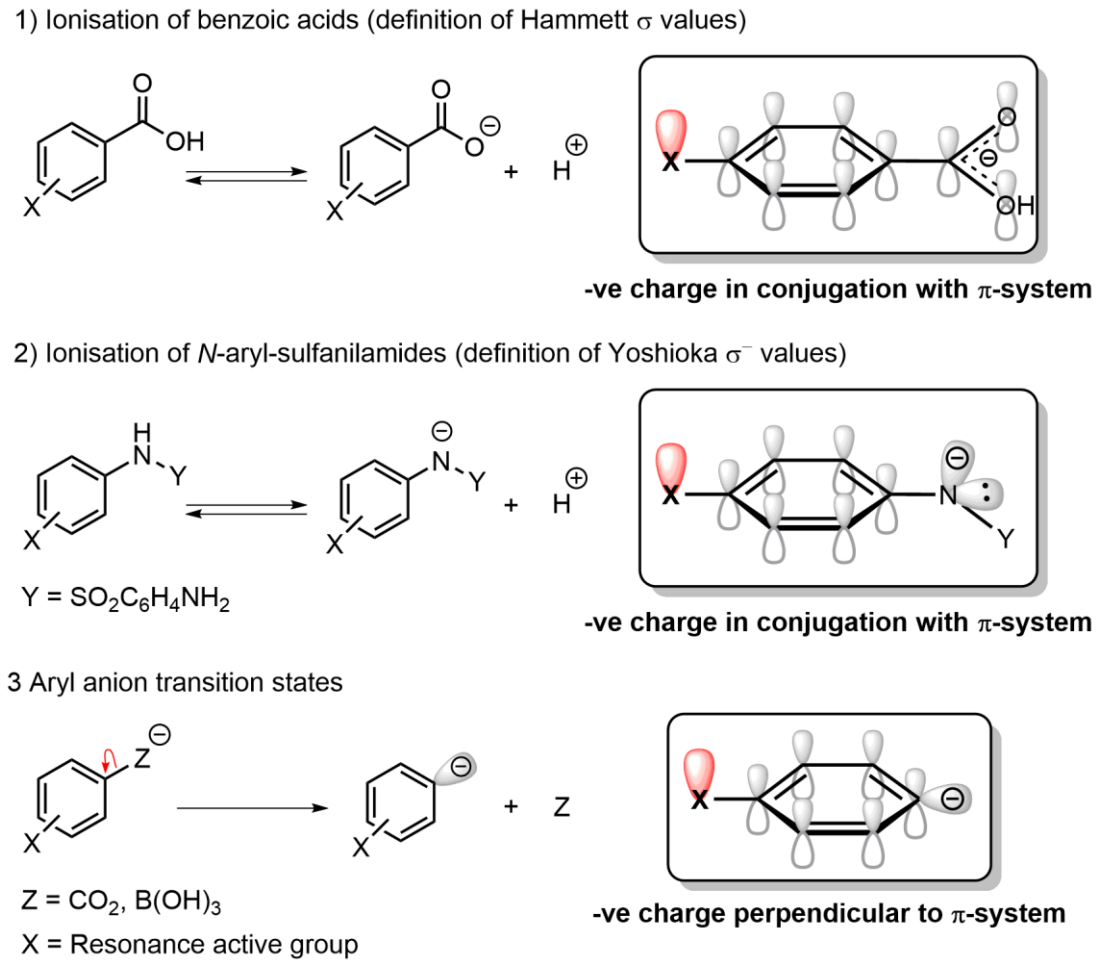

Figure 4.11 Reaction scheme for the ionisation of benzoic acids (top), and for the unimolecular fragmentation to form an aryl anion. MO pictures are a visual aid, displaying if the negative charge is in conjugation with the π-system, and thus sensitive to substituent resonance effects. The orbital depicted on the substituent (in red) can represent a lone pair (electron-donating group) or an empty orbital on an electron deficient atom (electron-withdrawing group).

It would seem plausible that the utilised Swain-Lupton parameters (f = 0.69, r = 0.31) used in the correlation of the protodeboronation and decarboxylation rate data may work as a general parameter for the correlation of other aryl anionic mechanisms. However, to date, the number of studies which propose aryl anionic mechanisms do not include enough experimental data to allow for similar in-depth analyses.

4.2.7.2. Re-examination of KIE studies

In addition to the LFER analysis, Bunnett and coworkers also performed detailed reaction kinetics to determine an independent rate KIE and activation parameters (independent rate KIE = 1.00, $\Delta S^{\ddagger}$ = +25 cal K^{-1} mol^{-1}), which are pleasingly similar to that obtained for protodeboronation of 2,6-difluorophenyl boronic acid (**71**) (independent rate KIE = 1.00, $\Delta S^{\ddagger}$ = +5 cal K^{-1} mol^{-1}).[182] Bunnett did not perform competition KIE experiments (reactions in 50:50 H_2O/D_2O), however, one may initially consider such an experiment to exhibit a large primary $^1H/^2H$ KIE (H/D partitioning >> 1) as the aryl anion selectively protonates by reaction with either H_2O or D_2O. A similar outcome was expected for the protodeboronation of polyfluorophenyl boronic acids, yet competition studies revealed a surprisingly small value (partitioning H/D = 1.25). This value can be explained by the Hammond-Leffler postulate: the protonation step is expected to be very exothermic, thus the energy (and geometry) of the transition state is likely to be much similar in energy (and geometry) to the aryl anion (relative to the products), resulting in a diminished KIE. Although the competition KIE is small, it is important to note that it is not equal to independent rate KIE (=1.00), and thus supports an aryl anion pathway ($k_2^{Ar^-}$).

4.3. Computational studies

The computational studies in this section were performed by Dr Marc Reid, University of Edinburgh.

Quantum chemical calculations were employed to support the experimental evidence for rate limiting unimolecular fragmentation of polyfluorophenyl boronates, and to provide easily accessible parameters that may help describe, and ultimately predict, the reactivity of these substrates. Firstly, we sought to correlate the relative reaction rates to the intrinsic energy differences (ΔE) calculated for the unimolecular fragmentation of boronates (Scheme 4.3).

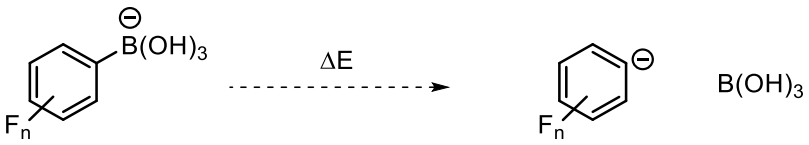

Scheme 4.3 Unimolecular fragmentation process used to in the quantum chemical calculations of the in intrinsic energy differences (ΔE).

Albeit a rather simple model, the obtained ΔE values correlated well with the experimental reactivity of substrates. For example, 4-methoxyphenyl boronic acid (**28**) was found to have a large intrinsic energy difference (ΔE = 43.82 kcal mol^{-1}), whereas pentafluorophenyl boronic acid (**72**) had the lowest (ΔE = 17.49 kcal mol^{-1}). For the full range of polyfluorophenyl boronic acids, the ΔE values were in qualitative agreement with the earlier Swain-Lupton analysis, and thus a plot of ΔE against the relative logarithmic rates of protodeboronation produced a similar profile whereby a linear correlation for *ortho*-fluoro and di*ortho*-fluoro substituted compounds can be observed (Figure 4.12).

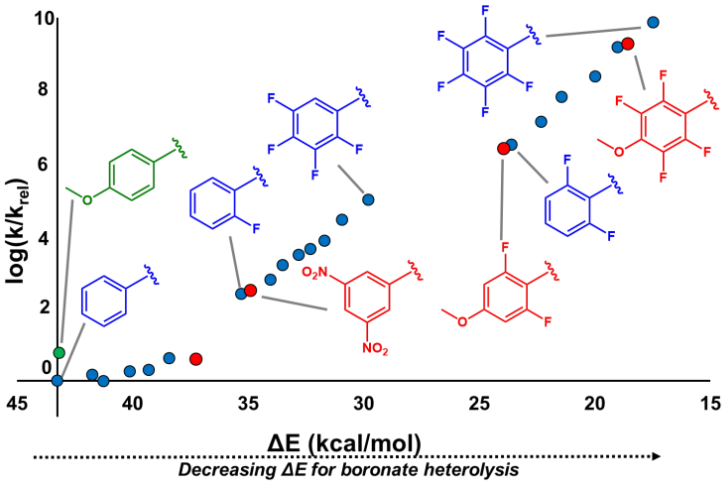

Figure 4.12 Correlation of relative protodeboronation rates with the intrinsic energy difference upon fragmentation of aryl boronate (ΔE).

With the calculated ΔE data, it was apparent that similar conclusions could be derived solely from the relative C-B bond orders for the aryl boronates. Wiberg Bond Indices (WBIs) were calculated for a subset of aryl boronates, which revealed the expected increase in protodeboronation rate with *decrease* in C-B WBI (left, Figure 4.13). Additionally, Natural Bonding Order (NBO) analysis allowed charges on boron and *ipso* carbon to be calculated. Interestingly, a strong correlation was observed for charges on boron, but not for carbon (right, Figure 4.13). Nonetheless, the simple-to-derive parameters provide a convincing method for the prediction of polyfluorophenylboronic acid protodeboronation, and may provide a simple method to access the reactivity of some other *ortho*-EWG substituted aryl boronic acids (e.g.: Cl, Br and NO_2).

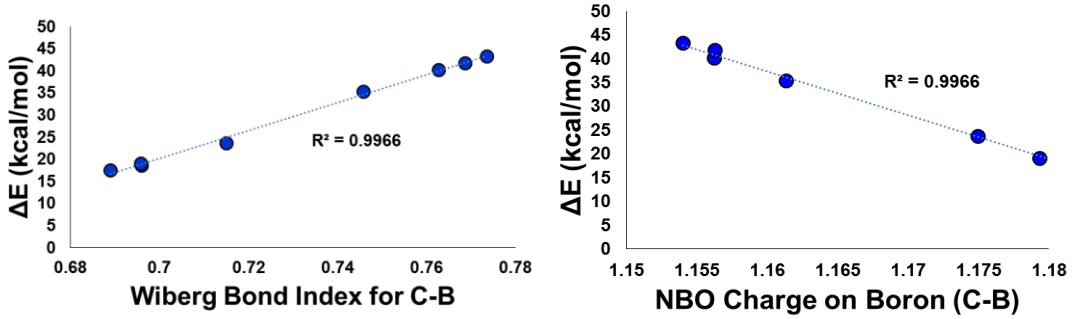

Figure 4.13 Correlation of intrinsic energy differences upon fragmentation of aryl boronate (ΔE) with Wiberg Bond Index for C-B bond (left) and NBO charge on boron (right).

4.4. LFER analysis for equilibrium data (pK_a)

The aqueous association constants (pK_a) were determined for all polyfluorophenyl boronic acids and non-fluorinated boronic acids (**28** and **71** – **99,** Table 4.1). ^{11}B NMR pH titrations were used for stable substrates ($t_{½}$ > 1 h), whereas extrapolation of pH – log k_{obs} data was required for rapidly reacting substrates ($t_{½}$ < 1 h). In a similar manner to that described previously (*vide supra*, section 4.2.3.2) we sought to correlate the equilibrium constants using a modified Hammett analysis, employing a theoretical Hammett σ value for an *ortho*-fluorine substituent (σ_o(F)). As previously seen with the modified Hammett analysis with rate data, this approach was deemed viable as the addition of an *ortho*-fluoroine was approximately additive (~1.00 pK_a unit decrease upon installation of an *ortho*-fluorine substituent). Regression analysis to all the measured pK_a values was optimised through iterative fitting of the σ_o(F) value, and using standard Hammett σ values for *meta* and *para* substituents (Figure 4.14). A strong correlation was observed across the entire data set (σ_o(F) = 0.45, R^2 = 0.98), with a positive gradient (ρ = 2.2). Interestingly, the additive trend for *ortho*-fluorine substituents diminishes with high fluorine substitution (ΔpK_a (**72**) – (**86**) = 0.52), and thus these substrates are the most significant outliers in the correlation. Although this is likely caused by steric effects, it is important to note that many 2,6-difluoro substituted substrates map to the correlation very well. Therefore, it is not the *ortho* substitution alone that causes a loss of the additivity trend, but the presence of both *ortho* and *meta* substituents. The repulsion between adjacent fluorine atoms (*ortho* and *meta*) may bring about greater steric contributions, and thus these substrates are less Lewis acidic than predicted through the modified Hammett analysis.

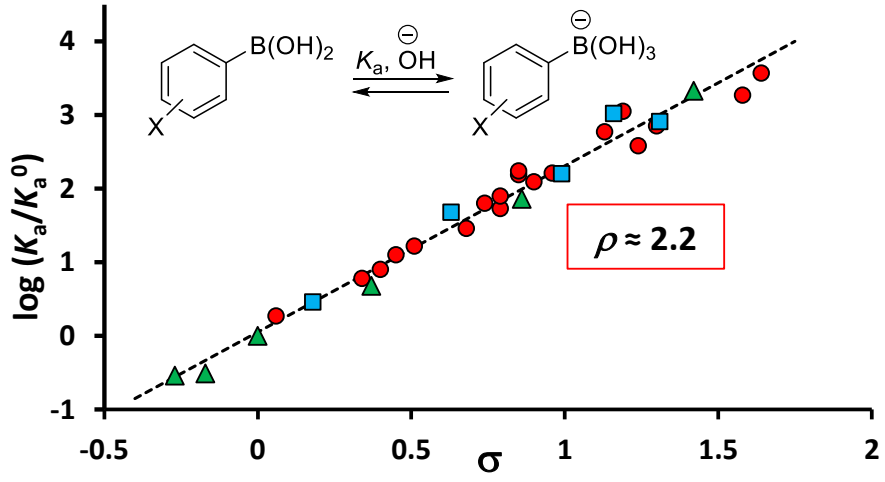

Figure 4.14 Modified Hammett analysis for the aqueous association constant (K_a) of boronic acids (1:1 H_2O/dioxane, 70 °C) using σ_o(F) = 0.45. Red circles = substrates with fluorine substituents only. Blue squares = substrates with fluorine and other additional substituents. Green triangles = substrates without fluorine substituents.

4.5. Summary

Protodeboronation rates for an extensive range of polyfluorophenyl and other aryl boronic acids were examined under alkaline conditions (pH ~13.3, 1:1 H_2O/dioxane, 70 °C), and correlated with various LFER parameters. Although classed as non-basic boronic acids, some of the polyfluorophenyl boronic acids display extraordinary reactivity. Compounds without o*rtho*-fluorine substitution were stable for many days, whereas *ortho*-fluorine substituents display a significant increase in reactivity. In particular, di*ortho*-fluorine substituted compounds react between seconds to milliseconds depending on the specific *meta* and *para* substituents. The entire substrate scope was correlated on a Swain-Lupton plot (modified to encompass *ortho*-fluorine substituents) and indicated a new mechanistic regime for the *ortho*- and di*ortho*-fluorinated substrates.

For 4-methoxyphenyl boronic acid (**28**) KIE studies are in agreement with rate-limiting concerted reaction with water, as proposed by Kuivila (k'_2). On the other hand, hydroxide dependence on the rate of protodeboronation for 2,6-difluorophenyl boronic acid (**71**) revealed complete rate saturation beyond 1 equiv. of KOH, conflicting with previous mechanistic proposals by Perrin. Detailed KIE studies for 2,6-difluorophenyl boronic acid (**71**) indicate water is not involved in the rate-limiting event, while Eyring analysis suggests a dissociative transition state. All the experimental evidence are in agreement with rate-limiting aryl boronate fragmentation to form an aryl anion, followed by rapid protonation. This mechanism was further supported with quantum chemical calculations, whereby the intrinsic energy differences (ΔE) between aryl boronate and the fragmentation products provide a strong correlation with the relative rates of protodeboronation. Furthermore, simple calculation of the C-B bond order (WBIs) or the charge on boron (NBO analysis) supply equally strong correlations.

The optimised Swain-Lupton parameters (f = 0.69, r = 0.31) were used to correlate previously reported data for the aqueous decarboxylation of 2,6-dinitrobenzoates, which has also been proposed to go through an aryl anionic transition state. An improved correlation (relative to a standard Hammett analysis) was obtained and thus the Swain-Lupton parameters may have application in other reactions that display aryl anion intermediates.

Aqueous association constants (K_a) were experimentally determined by ^{11}B NMR pH titrations or extrapolated through simulation of the rate data. A modified Hammett analysis provided a good correlation with the relative pK_a values, and can be utilised as a predictive tool for the determination of pK_a values for a wide range of aryl boronic acids.

Chapter 5

Conclusions and Future Work

5.1. Conclusions

Mechanistic studies into the protodeboronation of a wide range of boronic acids have been performed between pH 1 and 13 (1:1 H_2O/dioxane, 70 °C), and subsequently several protodeboronation pathways have been identified. A general mechanistic model was developed and used as an exploratory tool to simulate the experimentally obtained pH – log k_{obs} profiles, and ultimately used to extract equilibrium constants (K_{aH} and K_a) and rate constants ($k_1 – k_5$) from the experimental data. While there is no overall trend to describe the reactivity of all substrates, boronic acids can be divided into distinct categories based on inherent structural features (non-basic aromatics, basic aromatics, *ortho*-fluorine substitution etc.). Each category of boronic acid can be evaluated for likely speciation (**X**, $\mathbf{X}_{OH}$ or $\mathbf{X}_{H+}$), and thus the likely mechanisms of protodeboronation ($k_1 – k_5$) can be predicted. Consequently, this allows assessment of the stability (or instability) of a substrate at a given pH or in the presence of certain additives. Figure 5.1 provides a visual schematic summary, displaying the general structures of boronic acid in each category and the corresponding characteristic pH – log k_{obs} profiles, indicating the regions of (in)stability.

5.1.1. Non-basic boronic acids

Non-basic aromatic and heteroaromatic boronic acids (**28** and **50** – **55**) follow on from previous studies by Kuivila, in which the reactivity is dictated by simple acid- and base-catalysed protodeboronation (k_1 and k_2). 2-heteroaryl boronic acids are found to be more reactive than regioisomeric 3-heteroaryl boronic acids. Vinyl and cyclopropyl boronic acids (**54** and **55**) displayed the greatest stability across the entire pH profile (along with other alkyl boronic acids) thus cross-coupling conditions, rather than inherent reagent instability, are most likely responsible for their anecdotal decomposition.[135,184] Concentration-dependent processes dominate at high reaction concentrations, resulting in self/autocatalytic protodeboronation ($k_2$cat) and disproportionation processes. These processes are maximised at pH values equal to the pK_a of the boronic acid (i.e. 50% boronic acid and 50% boronate). In particular, 2-furyl boronic acid (**51**) undergoes rapid disproportionation to form borinic acid and borane species, which appear to be stable in solution for several days.

5.1.2. Basic heteroaromatic boronic acids

Contrary to popular perception, many basic heterocyclic boronic acids undergo very slow aqueous protodeboronation, even at very high pH. Nonetheless, 2-pyridyl, 5-thiazolyl and 5-pyrazolyl boronic acids (**44** and **66** – **68**) can undergo rapid protodeboronation. Most surprising is that these substrates display the fastest protodeboronation rates at neutral pH,

whereby the speciation is shifted towards reactive zwitterionic water-adducts ($\mathbf{X}_{ZW}$). These species display unique modes of intramolecular stabilisation during C-B bond fragmentation, provided by pyridinium NH (**44**), S-C σ* orbitals (**66**) or highly polarised NMe or NH bonds (**67**or **68**) (k'_4). Conversely, at very low or very high pH, the 2-pyridyl boronic acid speciation is shifted away from the reactive zwitterionic water-adduct, and thus the rates of protodeboronation are greatly attenuated. This is not true for 5-thiazolyl and 5-pyrazolyl systems, which remain reactive under alkaline conditions. Lewis acid additives ($B(OH)_3$, $Sc(OTf)_3$, $ZnCl_2$ and $CuCl_2$) were found to attenuate protodeboronation rates for 2-pyridyl boronic acid (**44**) by lowering the zwitterion concentration, and may explain the beneficial effects of particular metal additives in the coupling of 2-pyridyl boronic acids.[76,94,100] On the other hand, Lewis acids exacerbate protodeboronation rates for 5-thiazolyl and 5-pyrazolyl boronic acids (**66** – **68**), where complexation to the remote basic nitrogen augments boronate stabilisation during the TS.

Other basic heteroaromatic boronic acids display unique modes of protodeboronation. For example, 4-pyridyl boronic acids (**64** and **65**) undergo a unique reaction of pyridinium ($\mathbf{X}_{H+}$) with water (k'_5). Also 4-pyrazolyl and 4-isoxazolyl boronic acids (**60** and **61**) display a unique mode of reactivity in highly alkaline conditions (pH > 12). DFT studies reveal operation of a Perrin-type protodeboronation pathway in which C-N or CO σ* orbitals facilitate formation of a dianionic species ($\mathbf{X}_{O-}$), and subsequent C-B fragmentation (k'_3).

5.1.3. Polyfluorophenyl boronic acids

Protodeboronation rates for a range of polyfluorophenyl boronic acids were investigated (2 equiv. KOH, 0.1 equiv. TFA or PPA, 1:1 H_2O/dioxane, 70 °C), which spanned over 9 orders of magnitude in reactivity. The extent and position of fluorine substitution was crucial for determining substrate stability. *Ortho*-fluorine or di*ortho*-fluorine substituted compounds displayed the highest levels of reactivity ($t_{½}$ ≈ 24 h to 3 ms), whereas substrates without *ortho*-fluorine substitution were the most stable ($t_{½}$ > 24 h). Correlation of the entire substrate scope on a modified Swain-Lupton plot revealed that *ortho*-fluorine substituted substrates undergo a unique base-catalysed mechanism of protodeboronation.[61] Hydroxide dependence, KIE studies and Eyring analysis all support rate-limiting aryl boronate fragmentation (k_2^{Ar-}). Intrinsic energy differences (ΔE) between aryl boronate and fragmentation products, Wiberg Bond Indices and Natural Bonding Order analysis (charge on boron) were all in qualitative agreement with the Swain-Lupton analysis, providing a simple tool for the prediction of boronic acid reactivity via the aryl anion protodeboronation pathway (k_2^{Ar-}).

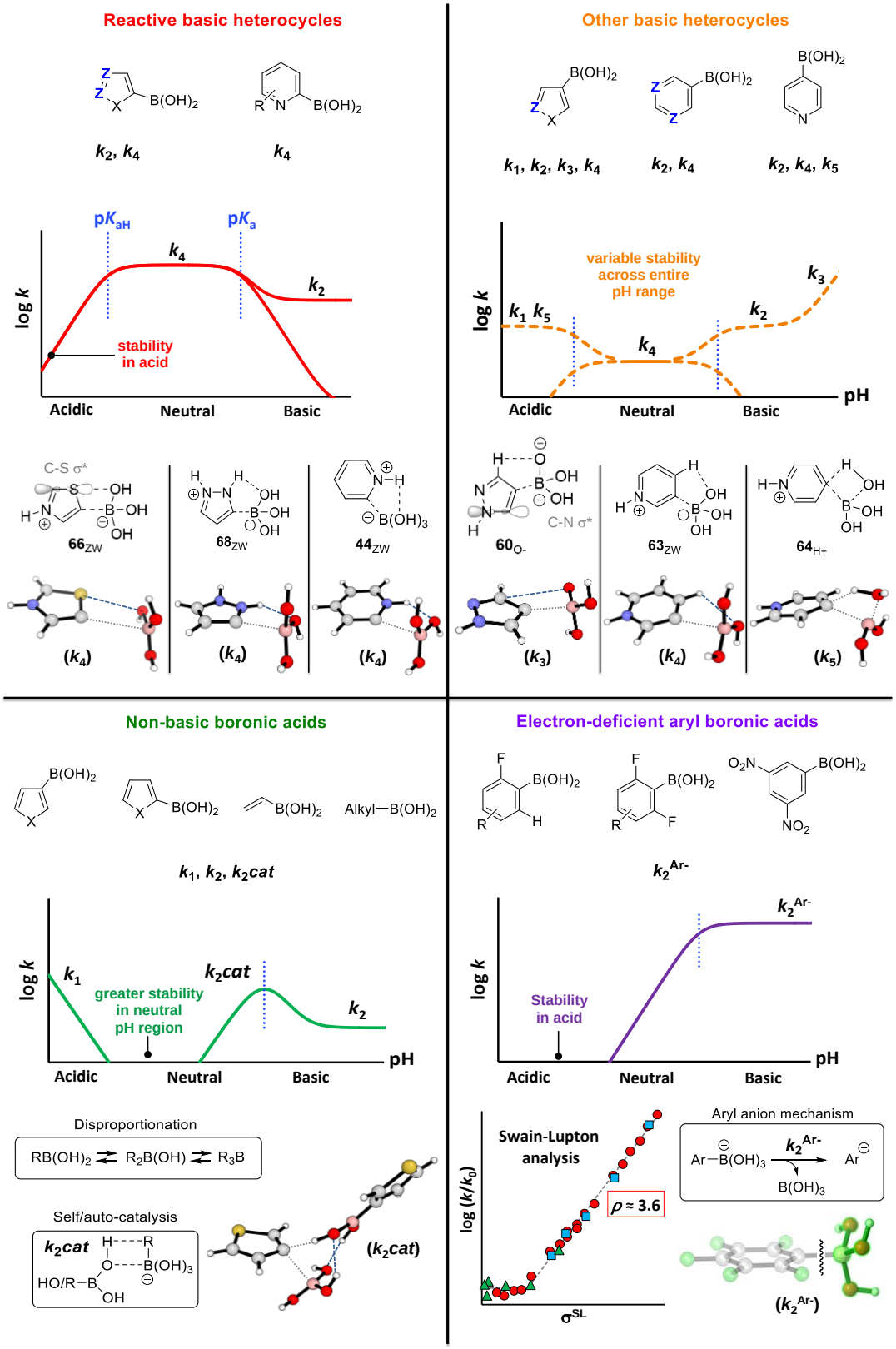

Figure 5.1 Schematic relationships for protodeboronation rate (log *k*) and pH (arbitrary scales) allowing the classification of boronic acids according to structure and presence of basic sites (Z = N_{Ar} or C, however only one site needs to be basic) and the associated protodeboronation mechanism(s) (k_1 – k_5).

5.2. Future Work

5.2.1. Non-basic boronic acids

Overall, non-basic alkyl, aryl and heteroaryl boronic acids are relatively stable to direct protodeboronation, requiring strong acid or base to invoke detectable reactivity. However, the concentration-dependent processes (at pH ≈ pK_a) have significant implications for the abundance of reactions that utilise boronic acids in mildly basic aqueous solutions. We have shown that self/autocatalytic protodeboronation can enhance protodeboronation rates over an order of magnitude, in which the boronic acid (or boric acid) acts as a proton source. This transition state is held together with an intricate network of hydrogen bonds, which can potentially be mimicked with other proton sources. Further investigations in this area may reveal common reagents which may induce rapid protodeboronation rates for even some of the most stable boronic acids. In particular, reagents with the capability to form hydrogen bonding networks with an aryl boronate might be necessary to invoke significant protodeboronation. This may go towards explaining why carboxylic acids have been employed in some deliberate protodeboronation reactions.[185]

5.2.2. Basic heteroaromatic boronic acids

Although an extensive range of basic heteroaromatic boronic acids were investigated, many other important motifs were not addressed, including 2-pyrimidyl (**100**) and 2-imidazolyl boronic acids (**101**). Less basic (or more electron-deficient) 2-pyridyl boronic acids are more stable under neutral pH values, seemingly due to a reduction in zwitterion concentration. A similar rationale could be made for 2-pyrimidyl boronic acid, which will comparatively be less basic than pyridyl analogues. On the other hand, 2-imidazolyl boronic acid, which has not be successfully synthesised or isolated to date, is expected to be much more basic and resemble the structure of 5-pyrazole boronic acids (**67** and **68**). By considering the expected zwitterionic transition states, it might be expected that the secondary adjacent aromatic nitrogen atoms in $\mathbf{100}_{ZW}$ and $\mathbf{101}_{ZW}$ can provide unique (de)stabilisation features which dictate the rate of protodeboronation. In particular, DFT studies may help to reveal the reactivity of these zwitterionic water-adducts, and may provide solutions to their preparation and application.

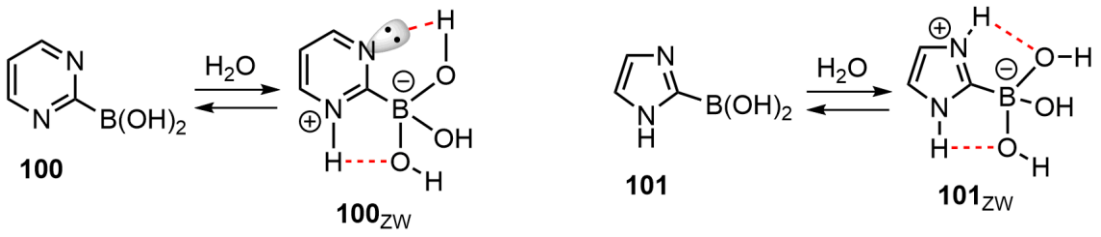

Figure 5.2 Proposed zwitterionic water-adduct structures for 2-pyrimidyl and 2-imidazolyl boronic acids, displaying the potential additional modes of stability through hydrogen-bonds.

Additionally, Lewis acids have been found to attenuate protodeboronation rates for 2-pyridyl boronic acids. This finding maybe crucial in explaining the beneficial effect of some metals (Ag and Cu) in cross-coupling reactions of troublesome substrates.[94,100] Therefore, further research to elucidate highly efficient and readily available Lewis acid additives would provide new methods for the successful coupling of 2-pyridyl (and similar) motifs. An interesting concept would involve using these findings to provide alternative methods for the preparation of 2-pyridyl boronic acids. In particular, the isolation of a Lewis acid-boronic acid adduct would, in principle, provide a bench-stable reagent that could be utilised directly in cross-coupling reactions.

5.2.3. Polyfluorophenyl boronic acids

While LFER plots and quantum chemical calculations have provided a method for the reliable prediction of polyfluorophenyl boronic acid reactivity, the study has been limited to *ortho*-fluorine substituents. A similar analysis can be conducted for other *ortho*-EWG substituents (Cl, Br, I, CF_3, NO_2 etc.) to extend the predictive capabilities of the model. As previously seen for the polyfluorinated systems, computational parameters (WBIs and NBO analysis) may give a meaningful insight into the stability of a wide range of substrates. In particular, preliminary studies have displayed *ortho*-nitrophenyl boronic acid (**102**) is very reactive ($t_{½}$ < ~5 min, 1:1 H_2O/dioxane, 70 °C, data not shown) when compared to other *ortho*-substitued substrates (*ortho*-fluorophenyl boronic acid (**94**), $t_{½}$ = 19 h). Thus, with a similar additive trends in reactivity, di*ortho*-nitrophenyl boronic acid (**103**) would be anticipated to react within microseconds. However, steric factors must be reconsidered when moving to larger substituents, and could be experimentally probed by investigating some mixed di*ortho* substituted systems, containing one fluorine substituent and a variable alkyl group (Figure 5.3).

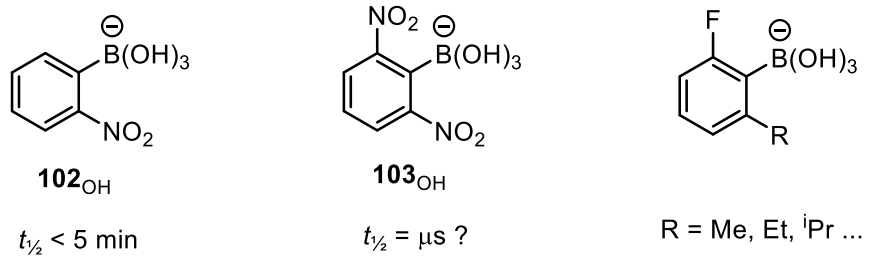

Figure 5.3 Other potentially reactive boronic acids that may protodeboronate through an aryl anion type mechanism (k_2^{Ar-}).

Lastly, some polyfluorophenyl boronic acids have been employed as Lewis acid catalysts in Friedel-Crafts alkylations.[48,127] Although not fully confirmed, it appears that highly Lewis acidic boronic acids (i.e. low pK_a) display the greatest efficiency in these reactions, and thus heavily fluorinated substrates are commonly employed. However, as observed in Chapter 4, these species are also highly prone to protodeboronation. An obvious solution would entail the use of a *stable, yet Lewis acidic* substrate. From our protodeboronation studies, the 3,5-dinitrophenyl boronic acid (**97**) displayed a similar Lewis acidity to pentafluorophenyl boronic acid (**72**) but with over a million-fold increase in stability under basic conditions. Therefore, the use of these substrates in Lewis acid catalysed reactions may prove fruitful if investigated.

Chapter 6

Experimental

6.1. General experimental details

6.1.1. Techniques

Unless otherwise stated, all reactions were performed in oven-dried glassware under an inert nitrogen atmosphere, using standard Schlenk-line techniques. Where required, needles and other glassware were dried in an oven (200 °C) and cooled under vacuum and purged with an inert atmosphere of nitrogen prior to use. The removal of solvents in vacuo was achieved using a rotary evaporator with a water bath (temperature range of 25-50 °C), or at 0.5 torr on a high vacuum line at 25 °C. All NMR tubes used as reaction vessels were prewashed sequentially with concentrated HCl, distilled water, saturated NaOH in ^{i}PrOH, distilled water, dilute HCl, distilled water (3 times) and acetone (3 times) to remove any contaminants.

6.1.2. Reagents and solvents

All commercial reagents were obtained from Sigma-Aldrich, FluoroChem, Fisher Scientific, Acros Organics, Alfa Aesar, Cambridge Isotopes Limited or Goss Scientific Limited. Isotopically labelled boron reagents ([^{10}B]–boric acid and [^{11}B]–boric acid) were purchased from Sigma-Aldrich. Unless otherwise stated below, all boronic acid and boronic acid MIDA ester reagents were obtained from Sigma-Aldrich, Fisher Scientific or Alfa Aesar, and were used without further purification.

Exceptions: 3,5-dinitrophenylboronic acid (**97**) was synthesised in-house (see section 6.2.3.). 3-thienyl boronic acid (**50**) (Sigma-Aldrich), 2,6-difluorophenyl boronic acid (**71**) (FluoroChem) and 4-methoxyphenyl boronic acid (**28**) (Sigma-Aldrich) were all recrystallized from H_2O or D_2O prior to KIE experiments. 2-pyridine boronic acid MIDA ester (**44**$_{MIDA}$) (Sigma-Aldrich) was found to decompose during storage and was therefore purified by flash chromatography (MeCN) before use in all experiments.

Anhydrous organic solvents were obtained from a solvent purification system (MBraun SPS 800) situated in the School of Chemistry, University of Edinburgh. These solvents were dispensed using gas-tight syringes under a positive pressure of nitrogen. Commercial grade solvents were used for extractions, TLC analysis and flash column chromatography. Distilled water was obtained through a double distillation system.

Deuterated solvents for NMR analysis were purchased from Sigma-Aldrich, Cambridge Isotopes Limited, and Goss Scientific Limited.

A solvent blend of H_2O/1,4-dioxane used in many experiments was obtained by mixing H_2O (500 mL, 499 g) with 1,4-dioxane (533 mL, 517 g) (Sigma-Aldrich) at 21 °C to give a total volume of 1 L. The concentration of H_2O in the new solvent blend was calculated to be $\left(\frac{55.4\ \text{M}}{2}\right) = 27.8\ \text{M}$.[186]

Expansion of the solvent mixture at 70 °C was determined by the following procedure:

10 mL of H_2O/1,4-dioxane solvent mixture was measured out into a graduated flask at room temperature (21 °C). The flask was sealed and heated to 70 °C for 30 min in an oil bath. The flask was unsealed and the new volume was recorded (10.35 ± 0.01 mL, 3.5 % increase in volume). Thus, the concentration of H_2O in the H_2O/1,4-dioxane solvent mixture at 70 °C was calculated to be = $\left(\frac{55.4\ \text{M}}{2\ \text{x}\ 1.035}\right) = 26.8\ \text{M}$. This approximately results in a 1:1 H_2O/1,4-dioxane (v/v %) mixture and therefore is referred to as '1:1 H_2O/1,4-dioxane' throughout the thesis.

6.1.3. Chromatography

TLC analysis was performed on Macherey-Nagel POLYGRAM® SIL G/UV silica gel plates (0.2 mm) using the indicated solvent system. Preparative thin-layer chromatography was performed on Merck Silica Gel 60 F254 precoated aluminum-backed plates using the indicated solvent system. Compounds were visualised by UV fluorescence (λ = 254 nm) or by treatment with a $KMnO_4$ solution followed by brief heating. Flash column chromatography was performed with Merck silicagel 60 (40 – 63 μm).

6.1.4. Analysis

6.1.4.1. pH analysis

pH measurements were carried out using a Hannah Instruments portable pH meter (HI 9125), equipped with a Sigma-Aldrich® micro pH combination electrode (Z113441, 183 mm length, 3.5 mm O.D.). The pH meter was calibrated to FIXANAL® buffer concentrate solutions at pH 4 (citric acid/NaOH/NaCl solution), pH 7 (KH_2PO_4/Na_2HPO_4) and pH 10 ($Na_2B_4O_9$/NaOH) with automatic temperature compensation.

6.1.4.2. NMR spectroscopy

Unless otherwise stated, NMR spectra were recorded at 27 °C, except $^{10}B/^{11}B$ NMR spectra which were recorded at 70 °C. ^{1}H, ^{10}B, ^{11}B, $^{13}C\{^{1}H\}$ and ^{19}F NMR spectra were recorded on JEOL GX 300, Eclipse 300, Bruker Ascend 400 or Bruker Ascend 500 spectrometers. ^{1}H and $^{13}C\{^{1}H\}$ spectra were referenced to residual solvent signals, or to a TMS internal

standard. ^{10}B, ^{11}B and ^{19}F spectra were externally referenced to ($BF_3.OEt_2$). Coupling constants, *J*, were calculated to the nearest 0.1 Hz using MestreNova (versions 9 and 10). The following abbreviations (and their combinations) are used to label the multiplicities: s (singlet), d (doublet), t (triplet), q (quartet), sept (septet), m (multiplet), app (apparent) and br (broad). NMR spectra were recorded using Norrell® 502, Norrell® S400 and Norrell® 200-QTZ (quartz) NMR sample tubes.

^{10}B, ^{11}B and ^{19}F NMR spectra contained large background signals. These were removed by applying a backward linear prediction function (MestreNova - Toeplitz method, 0 to 16, 32k basis points and 24 coefficients). ^{10}B and ^{11}B baselines were corrected carefully to ensure integrations were not affected (Whittaker smoother function, typically 40-80 Hz filter).

6.1.4.3. IR spectroscopy

Characterisation was performed on Shimadzu IRAffinity-1 FTIR spectrophotometer with an ATR diamond cell. IR spectra were recorded in the range of 3500-500 cm^{-1}.

6.1.4.4. Mass spectrometry

HRMS was performed by the Mass Spectrometry department at the University of Edinburgh using a Finnigan MAT 900 XLP high-resolution mass spectrometer.

6.1.4.5. Elemental analysis

Elemental analysis was performed by Elemenetal Analysis Service at the London Metropolitan University using a Carlo Erba FLASH 2000 Elemental Analyser.

6.1.5. Kinetic simulations

Kinetic simulations of pseudo first-order temporal concentration data was performed using Excel (2013) (section 6.3.). Multi-step simulations were performed on DynoChem (2011).

6.1.6. Rapid quench-flow (RQF) apparatus

Rapid quench-flow experiments were performed with a Hi-Tech Scientific RQF-63 Quench-Flow unit, which employs three syringes that are held in a thermostatted water bath. A solution of boronic acid from one syringe was mixed with a solution of KOH from a second syringe. The reaction mixtures were allowed to age for various time periods and were quenched by mixing with HCl from a third syringe. Reagents and quench solutions were loaded and incubated in the thermostatted reagent bath at 70 °C for a minimum of 10 min before mixing reagents. Both ‘continuous’ and ‘delay’ modes were utilised to acquire a full range of quench times for the entire scope of polyfluorophenyl boronic acids used in the

study. Delay loop volumes ranging from 20 – 350 μL provided quench times of 2 – 100 ms for the 'continuous' mode setup, and a standard delay loop with a volume of 350 μL was used for the 'delay' mode setup. Quenched reaction solutions were analysed by ^{19}F NMR to determine substrate consumption.

6.1.7. Stopped-flow infrared (SF-IR) analysis

The stopped-flow infrared experiments were performed on a novel piece of equipment within the Lloyd-Jones research group, designed and manufactured in collaboration with TgK Scientific (left, Figure 6.1). Reagents (A and B) are rapidly driven into a mixing chamber by an electronic stepping motor (TgK), and then pass into a 20 μL analysis chamber which is thermostatted with water circulation (top right, Figure 6.1). In this chamber, the reaction mixture sits above a 2 × 2 mm^2 ATR-IR diamond crystal which is irradiated with IR for the analysis of reaction kinetics (bottom right, Figure 6.1).

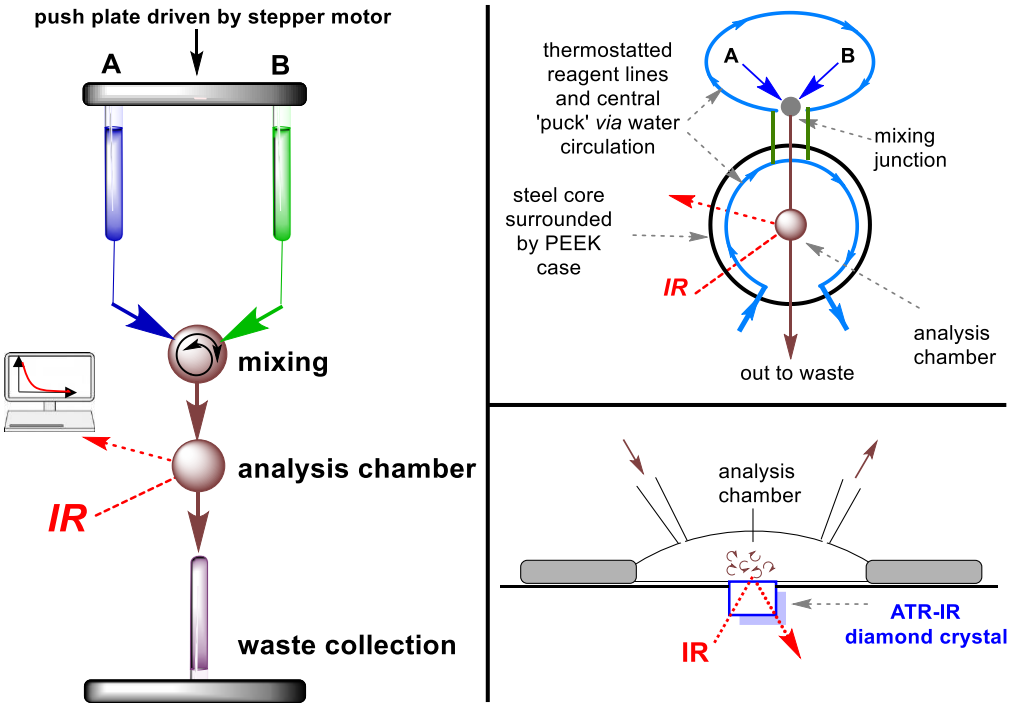

Figure 6.1 Left: Schematic representation of the SF-IR setup. Top right: Schematic representation of the analysis chamber casing. Bottom right: Schematic representation of analysis chamber and the directional flow of reagents.

Water circulation for temperature regulation was controlled by a Lauda™ Alpha RA 8 water circulator. Additional temperature control was provided on the surface on the Specac Golden Gate *via* a Specac heating unit, capable of regulating the temperature of the area around the ATR diamond crystal. The Vertex80 IR instrument was controlled *via* Bruker™ OPUS™ software (v. 7.2). The TgK syringe pump was controlled *via* TgK KinetaDrive software.

6.2. Synthetic procedures

6.2.1. [^{10}B]-3-thienyl boronic acid

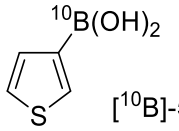

[^{10}B]-**50**

6.2.1.1. Preparation of [^{10}B]-B(O^{i}Pr)$_3$

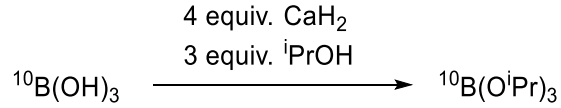

To an oven dried round-bottomed flask, purged with nitrogen, was added [^{10}B]-boric acid (0.08 mol, 4.92 g) and calcium hydride (0.32 mol, 14.60 g, 93% w/w). Anhydrous isopropanol (0.24 mol, 14.53 g) was added dropwise down a condenser and over a stream of nitrogen. After bubbling had ceased, the mixture was heated to 90 °C overnight. After cooling to room temperature, volatiles were pumped off *in vacuo* and trapped at -78 °C. The trapped contents were distilled under reduced pressure (50 °C at 30 mm Hg) to give the title compound as a colourless oil (9.13 g, 60%) **^{1}H NMR** (400 MHz, $CDCl_3$) δ = 4.35 (sept, *J* = 6.2 Hz, 3H), 1.15 (d, *J* = 6.2 Hz, 18H). **^{13}C{^{1}H} NMR** (100 MHz, $CDCl_3$) δ = 64.90, 24.54. **^{10}B NMR** (43 MHz, $CDCl_3$) δ = 17.52.

^{10}B incorporation was not determined for this material, however analysis of [^{10}B]-**50** during cross-over tests confirmed high abundance. Contaminated with approx. 10% of isopropanol.

Data is consistent with that expected based on published data for the same compound with natural abundance ^{10}B/^{11}B (20/80).[187]

6.2.1.2. Preparation of [^{10}B]-3-thienyl boronic acid ([^{10}B]-50)

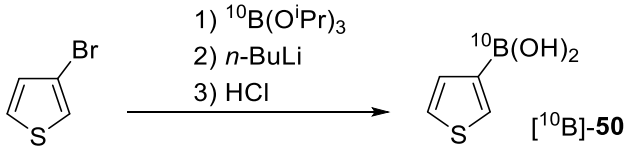

[^{10}B]-**50**

To an oven dried multi-neck round-bottomed flask, purged with nitrogen and a magnetic stirrer bar, was added 3-bromothiophene (22.3 mmol, 3.63 g), [^{10}B]-triisopropylborate (26.7 mmol, 5.00 g) and dry THF (30 mL). A solution of *n*-butyllithium (24.5 mmol, 11.3 mL of a 2.17 M solution in hexanes) was added dropwise at -78 °C and stirred for 30 mins, before being allowed to warm to room temperature and stirred for a further 30 mins. The mixture

was quenched with 0.1 M HCl to pH 2 and extracted with EtOAc (3 x 100 mL). The extracts were dried over Na_2SO_4 and concentrated under reduced pressure. The crude product was purified by column chromatography on silica gel (1:1 Hexane/EtOAc, R_f = 0.35) to give a white solid (1.11 g, 40%). **^{1}H NMR** (400 MHz, DMSO-d_6) δ = 7.91 (dd, *J* = 2.7 Hz, *J* = 1.1 Hz, 1H), 7.42 (dd, *J* = 4.8 Hz *J* = 2.7 Hz, 1H), 7.38 (dd, *J* = 4.8 Hz *J* = 1.1 Hz, 1H). **^{13}C{^{1}H} NMR** (100 MHz, DMSO-d_6) δ = 135.84, 133.03, 126.15 (*ipso*-carbon bonded to boron atom was not observed). **^{10}B NMR** (43 MHz, DMSO-d_6) δ = 26.62. **HRMS (EI)** *m/z* calcd. for $C_4H_5O_2{}^{10}B_1S_1$ 127.01342, found 127.01322.

^{10}B incorporation was not determined for this material, however analysis of [^{10}B]-**50** during cross-over tests confirmed high abundance.

Data is consistent with that expected based on published data for the same compound with natural abundance ^{10}B/^{11}B (20/80).[188]

6.2.2. 6-(trifluoromethyl)-2-pyridine boronic acid MIDA ester

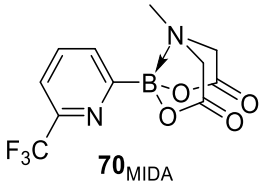

70$_{MIDA}$

1.2.2.1 Preparation of 6-(trifluoromethyl)-2-pyridine boronic acid MIDA ester (70$_{MIDA}$)

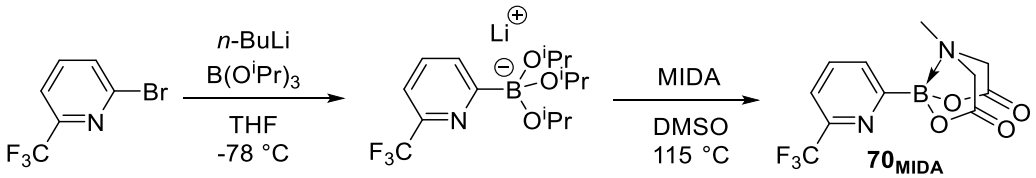

To an oven dried multi-neck round-bottomed flask, purged with nitrogen and a magnetic stirrer bar, was added 2-bromo-6-(trifluoromethyl)pyridine (9.84 mmol, 2.22 g), triisopropylborate (11.4 mmol, 2.75 mL) and dry THF (20 mL). A solution of *n*-butyllithium (9.72 mmol, 4.48 mL of a 2.17 M solution in hexanes) was added dropwise at -78 °C and stirred for 1 h, before being allowed to warm to room temperature and stirred for a further 1 h. Separately, to a multi-neck round-bottomed flask equipped with water-cooled short-path distillation apparatus and thermometer was added *N*-methyliminodiacetic acid (16.7 mmol, 2.46 g) and DMSO (20 mL). The mixture was stirred and heated to 115 °C before adding the boronate mixture dropwise (ca. 1 h). The mixture was cooled to 50 °C and the DMSO was

removed via distillation (down to a maximum vacuum of 1 mTorr at 50 °C). After cooling, the residue was absorbed onto Celite from an acetonitrile suspension. The crude product was purified by column chromatography on silica gel (1:1 Hexane/EtOAc, R_f = 0.38) to give a white solid (1.85 g, 62%). **^{1}H NMR** (400 MHz, DMSO-d_6) δ = 8.05 (app t, J = 7.7 Hz, 1H), 7.88-7.80 (m, 2H), 4.44 (d, J = 17 Hz, 2H), 4.09 (d, J = 17 Hz, 2H), 2.58 (s, 3H). **^{13}C{^{1}H} NMR** (126 MHz, DMSO-d_6) δ = 168.96, 162.87 (br, tentatively assigned as carbon bonded to boron atom), 146.67 (q, $^{2}J_{C\text{-}F}$ = 33.2 Hz), 137.09, 130.35, 121.76 (q, $^{1}J_{C\text{-}F}$ = 273.2 Hz), 119.93 (q, $^{3}J_{C\text{-}F}$ = 2.8 Hz), 62.04, 47.09. **^{11}B NMR** (128 MHz, DMSO-d_6) δ = 9.23. **^{19}F NMR** (376 MHz, DMSO-d_6) δ = −66.60. **HRMS (EI)** *m/z* calcd. for $C_{11}H_{10}O_4N_2B_1F_3$ 302.06802, found 302.06661.

Data is consistent with that found in the literature.[189]

6.2.3. 3,5-dinitrophenyl boronic acid

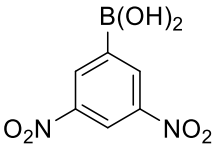

97

6.2.3.1. Preparation of 3,5-dinitrophenyl boronic acid (97)

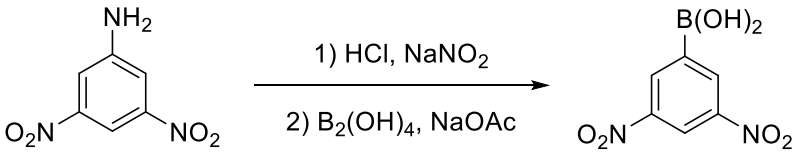

97

Experimental procedure taken from literature.[190]

To a suspension of aniline (10 mmol, 1.83 g) in water (30 mL) at rt was added HCl (12 M, 2.08 mL) and the reaction mixture was stirred for 10 min before being cooled to 0 °C. A solution of $NaNO_2$ (12 mmol, 828 mg) in water (5 mL) was added dropwise and the reaction mixture stirred for 30 minutes. Tetrahydroxydiboron (20 mmol, 1.79 g), NaOAc (20 mmol, 1.64 g) and water (30 mL) were added to the reaction mixture which was warmed to rt and stirred for 60 min. K_2CO_3 sat. was added to the reaction mixture until pH 8, then followed by EtOAc (200 mL). The mixture was extracted with sorbitol/Na_2CO_3 (1M solution in water, 2 x 100 mL). The combined aqueous layers were washed with EtOAc (2 x 100 mL) and then acidified until pH 1 with HCl (6 M). The aqueous layer was extracted with EtOAc (3 x 100 mL) and the combined organic layers washed with water (2 x 100 mL) and brine (100 mL),

dried over magnesium sulfate, filtered and concentrated under vacuum to give a brown oil (778 mg). The crude material (50 mg) was purified by preparative TLC (EtOAc + 1% TFA, R_f = 0.50). The product was washed from the silica with EtOAc (50 mL) and filtered. The filtrate was washed with NaH_2PO_4 (1 M, 2 x 50 mL) and brine (50 mL), dried over magnesium sulfate, filtered and concentrated under vacuum to give a brown oil (40 mg, 2%). **^{1}H NMR** (500 MHz, 9:1 CD_3CN/D_2O) δ = 8.92 (t, *J* = 2.3 Hz, 1H), 8.86 (d, *J* = 2.3 Hz, 2H). **^{11}B NMR** (160 MHz, 9:1 CD_3CN/D_2O) δ = 27.02. **^{13}C{^{1}H} NMR** (125 MHz, 9:1 CD_3CN/D_2O) δ = 149.26, 134.70, 121.14 (carbon *ipso* to boron atom not observed). **HRMS (EI)** *m*/*z* for $C_6H_5BN_2O_6$ not observed - see literature for complications observed during mass spectrometry analysis of electron-deficient boronic acids.[191] Derivatization to the boronic acid pinacol ester was achieved with the addition of 1 equiv. pinacol to the boronic acid in MeCN, which was successfully analysed by HRMS (EI); *m*/*z* calc. for [M^+] $C_{12}H_{15}N_2O_6B$: 294.10177, found 294.10163. **ν_{max} (neat)/cm^{-1}** 3095.75, 1620.21, 1585.49, 1529.55, 1462.04, 1431.18, 1400.32, 1338.70, 1303.88, 1267.23, 1220.94, 1170.79, 1122.57, 1074.35, 1033.85, 1001.06, 916.19, 889.18, 867.97, 850.61, 813.96, 775.38, 758.02, 727.16, 711.73, 686.66, 607.58, 592.15, 559.36. **Elemental analysis** calc. for $C_6H_5BN_2O_6$: C, 34.01; H, 2.38; N, 13.22. Found: C, 34.29; H, 2.29; N, 13.41.

6.3. Reaction monitoring: General details

6.3.1. Calculating rate constants

Reaction progress was analysed using either ^{1}H, ^{11}B, ^{19}F NMR spectroscopy or *in situ* SF-IR spectroscopy. For one-point kinetics, pseudo-first-order decay was assumed and the observed rate constant (k_{obs}) was extracted using the following equation:

$$t \times k_{\mathrm{obs}} = \frac{\ln[\mathrm{RB(OH)_2}]_0}{\ln[\mathrm{RB(OH)_2}]_t}$$

where t = time (seconds), k_{obs} = observed rate constant, $[RB(OH)_2]_0$ = initial total substrate concentration, $[RB(OH)_2]_t$ = substrate concentration at time t.

For multiple-point kinetics, temporal concentration data was fitted to a simulated first-order decay equation through variation of an observed rate constant (k_{obs}) to minimise the sum square error (SSE) using Excel Solver (Excel 2013).

$$[\mathrm{RB(OH)_2}]_t = \frac{[\mathrm{RB(OH)_2}]_0}{e^{tk_{obs}}}$$

Reference spectra were used to calculate the initial concentration of substrate, and were obtained by analysis of a reaction mixture aliquot before mixing of reagents (or before adjusting pH of reaction mixtures). The start of kinetic timings are indicated in the procedures with the following notation: (t=0).

For reactions where the pH was measured, the pH of reaction mixtures were rapidly adjusted upon the addition of concentration KOH or HCl (no more than 3 seconds were required to give stable pH readings). At the pH extremes (solutions at very high or very low pH), the addition of aqueous KOH or HCl to the reaction solution resulted in a dilution of no more than 2% in concentration.

pH – log k_{obs} profiles were constructed from a series of rate constants obtained typically 10-20 reactions ranging from pH 1 to 13. The exact procedures used are described in full detail in section 6.3.3.

6.3.2. Buffers

A range of substituted phenols and carboxylic acids were employed as buffers for various reactions. Their usable pH range (1:1 H_2O/dioxane, 70 °C) is indicated in parentheses below:

Phenol (11.1-12.0), 2-chlorophenol (9.6-10.1), 2-nitrophenol (8.1-8.6), 3,5-bis(trifluoromethyl)phenol (8.8-9.3), 2,4,6-trichlorophenol (7.2-7.7), acetic acid (6.2-6.9), methoxyacetic acid (5.0-5.5), methyliminodiacetic acid (3.0-3.6).

4 equivalents (relative to boronic acid or MIDA ester) of buffer was sufficient in maintaining a constant pH (± 0.1 pH).

6.3.3. General procedures

Various procedures were used to obtain rate data for the construction of temporal concentration plots, and in turn, pH – log k_{obs} profiles. Many procedures have variables such as buffers, quench solutions, temperature etc. The conditions employed can be found in Table 6.3 and in the Appendix (section 8.5.). General procedures are listed below;

6.3.3.1. General procedure A – One point kinetics (H_2O, 90 °C)

To an oven dried multi-neck round-bottomed flask was added the desired boronic acid (1.25 mmol), H_2O (25 mL) and a magnetic stirrer bar under an inert nitrogen atmosphere. The reaction mixture was stirred, equipped with a calibrated pH electrode, and heated to 90 °C in an oil bath for 10 minutes. Concentrated solutions of HCl or KOH were added (8 M, 2-10 μL at a time) to adjust the pH (t=0). The pH was modified ~0.5 units at a time, transferring an aliquot (0.5 mL) into a NMR tube and then into a 90 °C oil bath on each occasion. After a given time period, samples were quenched by placing the NMR tubes into ice and then adding saturated $NaOAc_{(aq)}$ or AcOH (50 μL) to neutralise the solution. Substrate consumption was determined by ^{11}B NMR spectroscopy.

6.3.3.2. General procedure B – One point kinetics (H_2O/dioxane, 70 °C)

To an oven dried multi-neck round-bottomed flask was added boronic acid (1.25 mmol), 1:1 H_2O/dioxane (25 mL) and a magnetic stirrer bar under an inert nitrogen atmosphere. The reaction mixture was stirred, equipped with a calibrated pH electrode, and heated to 70 °C in an oil bath for 10 minutes. Concentrated solutions of HCl or KOH were added (8 M, 2-10 μL at a time) to adjust the pH (t=0). The pH was modified ~0.5 units at a time, transferring an aliquot (0.5 mL) into a NMR tube and then into a 70 °C oil bath, on each occasion. After a given time period, samples were quenched by placing the NMR tubes into ice and then adding saturated $NaOAc_{(aq)}$ or AcOH (50 μL) to neutralise the solution. Substrate consumption was determined by ^{1}H or ^{11}B NMR spectroscopy.

6.3.3.3. General procedure C – One point kinetics using MIDA esters

To an oven dried multi-neck round-bottomed flask was added boronic acid MIDA ester (1.25 mmol), 1:1 H_2O/dioxane (23.75 mL), dioxane (0.625 mL) and a magnetic stirrer bar under an inert nitrogen atmosphere. The reaction mixture was stirred, equipped with a calibrated pH electrode, and heated to 70 °C in an oil bath for 10 minutes. KOH (0.625 mL, 8 M) was added and stirred for 2-3 seconds before adding the appropriate amount of HCl or buffer to obtain the desired pH (*t*=0). Concentrated solutions of HCl or KOH were added (8 M, 2-10 μL at a time) to adjust the pH. The pH was modified ~0.5 units at a time, transferring an aliquot (0.5 mL) into a NMR tube and then into a 70 °C oil bath on each occasion. After a given time period, samples were quenched by placing the NMR tubes into ice and then adding the specified quench solution (50 μL). Substrate consumption was determined by ^{1}H NMR spectroscopy.

6.3.3.4. General procedure D – Multi-point kinetics

To a 20 mL glass vessel was added boronic acid (0.25 mmol), H_2O (5 mL) and a magnetic stirrer bar. The reaction mixture was stirred, equipped with a calibrated pH electrode and heated to 90 °C for 10 minutes. Concentrated solutions of HCl or KOH were added (8 M, 2-10 μL at a time) to adjust the pH to the desired value (*t*=0). Aliquots (0.25 mL) were periodically quenched with saturated $NaOAc_{(aq)}$ or AcOH (50 μL) to neutralise the solution. Substrate consumption was determined by ^{11}B NMR spectroscopy.

6.3.3.5. General procedure E – Multi-point kinetics using MIDA esters

To a 20 mL glass vessel was added H_2O, dioxane, and KOH (1 mmol, 8 M) to give a solvent composition of 1:1 H_2O/dioxane with a total volume of 5 mL. The reaction mixture was stirred, equipped with a calibrated pH electrode and heated to 70 °C for 10 minutes before adding boronic acid MIDA ester (0.25 mmol). The reaction mixture was stirred for 2-3 seconds before adding the appropriate amount of HCl or buffer to obtain the desired pH (*t*=0). Aliquots (0.25 mL) were removed periodically and quenched into the specified quench solution (50 μL). Substrate consumption was determined by ^{1}H NMR spectroscopy.

6.3.3.6. General procedure F – Multi-point kinetics (J-Young's valve NMR tube)

Boronic acid (0.25 mmol) was dissolved in a pre-mixed solvent blend consisting of 1:1 H_2O/dioxane (4.94 mL), dioxane (62.5 μL) and internal standard (TFA or PPA, 0.025 mmol). 0.50 mL of the reaction mixture was transferred into a nitrogen-flushed J-Young's

valve NMR tube, followed by KOH (12.5 μL, 8 M). The NMR tube was sealed and analysed by NMR spectroscopy at 70 °C (*t*=0 spectrum), before being placed immediately into an oil bath at 70 °C. After given time periods (ranging from every 6 hours, to every 4 days depending on the rate of protodeboronation), the sample was reanalysed by NMR spectroscopy at 70 °C and immediately returned to an oil bath at 70 °C.

Substrates containing fluorine nuclei were monitored by ^{19}F NMR, using TFA as an internal standard to calculate boronic acid consumption and product formation.

Substrates without fluorine nuclei were monitored by ^{1}H NMR, thus propionic acid (0.025 mmol, 1.9 μL) was used as an internal standard (instead of TFA) to calculate boronic acid consumption and product growth.

Note: product formation was successfully tracked given that product concentrations were low (< 10 mM), avoiding solubility issues.

6.3.3.7. General procedure G – Multi-point kinetics (manual quenching)

To a 20 mL glass vessel was added boronic acid (0.25 mmol) and a pre-mixed solvent blend consisting of 1:1 H_2O/dioxane (4.94 mL), dioxane (62.5 μL) and TFA (0.025 mmol, 1.9 μL). The reaction mixture was stirred and heated to 70 °C in an oil bath for 10 min. 0.50 mL was transferred to an NMR tube for analysis by ^{19}F NMR (*t*=0 spectrum). To the remaining reaction mixture was added KOH (56.3 μL, 8 M) (*t*=0). The solution was vigorously stirred for a few seconds and 0.25 mL aliquots were transferred into individual NMR tubes and immediately placed into an oil bath at 70 °C. Samples were periodically quenched with the addition of quench solution (280 μL)*. Boronic acid consumption was calculated relative to the TFA internal standard signal in the ^{19}F NMR spectra. Product growth was not calculated due to poor solubility and/or evaporation of polyfluoroaromatics under the reaction conditions.

*Quench solution = HCl (12 M, 30 μL), D_2O (125 μL) and dioxane (125 μL)

6.3.3.8. General procedure H – Multi-point kinetics (Rapid quench-flow)

Boronic acid (1 mmol) and TFA (0.1 mmol, 7.7 μL) were dissolved in the 1:1 H_2O/dioxane (10 mL) to give a 0.1 M solution of boronic acid, which was analysed by ^{19}F NMR (*t*=0 spectrum) before being loaded into the first reagent syringe on the rapid quench-flow apparatus with the reagent water bath at 70 °C. A solution of KOH in 1:1 H_2O/dioxane (0.2 M) was loaded into the second reagent syringe, and a quench solution of HCl in 1:1 H_2O/dioxane (0.4 M) into the quench syringe. After thermal equilibration to 70 °C (10 min),

the reagents were mixed and reacted for various time periods (ranging from 2 milliseconds to 30 seconds) before quenching with the quench solution. Boronic acid consumption was calculated relative to the TFA internal standard signal in the ^{19}F NMR spectra. Product growth was not calculated due to poor solubility and/or evaporation of polyfluoroaromatics under the reaction conditions.

Exceptions: For substrates **89, 90** and **95**; an increase in TFA (1.1 mmol, 84 μL) was required to keep the boronic acid stable while thermally equilibrating to 70 °C, and thus a higher concentration of KOH solution (0.3 M) was required to give a constant excess of KOH under the reaction conditions. Also a higher concentration of HCl (0.5 M) was required to ensure immediate quenching.

For substrate **72**; an increase in TFA (1.1 mmol, 84 μL) plus an additional HCl (2.0 mmol, 167 μL of 12 M solution) was required to keep the boronic acid stable while thermally equilibrating to 70 °C, and thus a higher concentration of KOH (0.5 M) was required to give a constant excess of KOH under the reaction conditions. Also a higher concentration of HCl (1 M) was required to ensure immediate quenching.

6.3.3.9. General procedure I – Multi-point kinetics (SF-IR analysis)

SF-IR procedures were performed by Dr Marc Reid, University of Edinburgh

To a 5 mL graduated flask was added boronic acid (0.5 mmol), TFA (0.05 mmol) and 1:1 H_2O/dioxane to make a 5 mL solution. The solution was transferred to a syringe and loaded into the reagent chamber of the SF-IR apparatus. A solution of KOH in 1:1 H_2O/dioxane (various concentrations) was transferred to a syringe and loaded into the second reagent chamber of the SF-IR apparatus. The reagent were mixed[e] and monitored over several minutes.

Spectra were collected using a *single-sided* interferogram acquisition method. During kinetic experiments, only the reference and sample interferograms were collected. Following each reaction, ATR-IR difference spectra were generated from the collected raw data in OPUS. Integration of peaks in the region around 1400 cm^{-1} (suspected C–F bond stretches) were used to generate the boronate decay and arene evolution profiles.

[e] Reagents are mixed in a 1:1 ratio, resulting in a dilution to give a 50 mM solution of boronic acid.

6.4. Reaction monitoring: Chapter 2

6.4.1. pH – log k_{obs} profiles and simulations

6.4.1.1. 4-methoxyphenyl boronic acid (28) at various initial concentrations using borosilicate glass vessels in H_2O, 90 °C

pH – log k_{obs} profiles for the protodeboronation of 4-methoxyphenyl boronic acid (**28**) (H_2O, 90 °C) at various initial boronic acid concentrations (10 – 200 mM) were constructed from multiple reactions performed using general procedure A. Reactions were carried out in borosilicate glassware (Norell® 5 mm S400 NMR sample tubes).

6.4.1.2. 4-methoxyphenyl boronic acid (28) and salt effects in H_2O, 90 °C

pH – log k_{obs} profiles for the protodeboronation of 4-methoxyphenyl boronic acid (**28**) (H_2O, 90 °C) in the presence of KNO_3 and/or KCl salts were constructed from multiple reactions performed using general procedure A ($[RB(OH)_2]_0$ = 50 mM). Salt was charged to the reaction vessel at the same time as boronic acid. Reactions were carried out in borosilicate glassware (Norell® 5 mm S400 NMR sample tubes).

6.4.1.3. 4-methoxyphenyl boronic acid (28) and counterion effects in H_2O, 90 °C

pH – log k_{obs} profiles for the protodeboronation of 4-methoxyphenyl boronic acid (**28**) (H_2O, 90 °C) with various hydroxide bases were constructed from multiple reactions performed using general procedure A ($[RB(OH)_2]_0$ = 50 mM), substituting the use of KOH (for pH adjustments) with the following bases: LiOH, CsOH and NMe_4OH. Reactions were carried out in borosilicate glassware (Norell® 5 mm S400 NMR sample tubes).

6.4.1.4. 4-methoxyphenyl boronic acid (28) at various initial concentrations using quartz glass vessels in H_2O, 90 °C

pH – log k_{obs} profiles for the protodeboronation of 4-methoxyphenyl boronic acid (**28**) (H_2O, 90 °C) at various initial boronic acid concentrations (10 – 200 mM) were constructed from multiple reactions performed using general procedure A. Reactions were carried out in quartz glassware (Norrell® 200-QTZ NMR sample tubes).

6.4.1.5. 3-thienyl boronic acid (50) at various initial concentrations using quartz glass vessels in H_2O, 90 °C

pH – log k_{obs} profiles for the protodeboronation of 3-thienyl boronic acid (**50**) (H_2O, 90 °C) at various initial boronic acid concentrations (50 – 800 mM) were constructed from multiple

reactions performed using general procedure A. Reactions were carried out in quartz glassware (Norrell® 200-QTZ NMR sample tubes).

6.4.1.6. KIE studies for 3-thienyl boronic acid (50) in H_2O or D_2O, 90 °C

pH – log k_{obs} and pD – log k_{obs} profiles were constructed from multiple reactions performed using general procedure A. For pD – log k_{obs} profiles, 3-thienyl boronic acid was recrystallized from D_2O before use and the reaction solvent (H_2O) was replaced with D_2O. Experimentally measured pD values were corrected using the standard correction factor, $pD_{real} = pH_{measured} - 0.4$ (note that the correction offset does not affect the KIE values extracted from the simulation fittings).[192] Experimental data was simulated using the simple mechanistic model (Figure 2.8), considering rate constants k_1, k_2, and k_{2cat} and equilibrium constants $K_{a(H2O)}$ or $K_{a(D2O)}$. Fitting of experimental results in both H_2O and D_2O allowed the extraction of equilibrium constants in both solvents. An equilibrium isotope effect was calculated to be $K_H/K_D = 0.83$.

6.4.1.7. Thienyl, furyl, pyrrolyl, vinyl and cyclopropyl boronic acids (50 – 55) in 1:1 H_2O/dioxane, 70 °C

pH – log k_{obs} profiles for the protodeboronation of **50** – **55** were constructed from multiple reactions performed using general procedure B. All reactions used an initial boronic acid concentration of 50 mM, with the exception of cyclopropyl boronic acid (**55**) which used a 400 mM initial boronic acid concentration.

1-tosyl-2-pyrroyl boronic acid (**53**) was released *in situ* from the corresponding MIDA boronate. The pH – log k_{obs} profile was constructed using general procedure C (without quench) for data points below pH 9, and general procedure E (with KOH quench) for data points above pH 9.

The pH – log k_{obs} data is listed, with the accompanying procedures, in the Appendix (section 8.5.).

The pH – log k_{obs} profiles were simulated using the simple mechanistic model described in Figure 2.8 and Table 2.1.

6.4.1.8. Alkyl boronic acids (56 – 58) in 1:1 H_2O/dioxane, 70 °C

Rate data for the protodeboronation of methyl, cyclobutyl or cyclohexyl boronic acids (**56** – **58**) were obtained using general procedure B. Data was not plotted or simulated using the mechanistic model. Reactions used an initial boronic acid concentration of 50 mM, with the exception of cyclobutyl boronic acid (**57**) which used a 200 mM initial boronic acid

concentration. Most of the data fell below the threshold limit (log k_{obs} = −7) and thus was not plotted or simulated using the general mechanistic model.

6.4.1.9. 2,5-thiophenediylbisboronic acid (59) in 1:1 H_2O/dioxane, 70 °C

pH – log k_{obs} profile for the protodeboronation of 2,5-thiophenediylbisboronic acid (**59**) was constructed from multiple reactions performed using general procedure B. The pH-log k_{obs} profile was modelled considering two equilibria (pK_a-mono = monoboronate formation, and pK_a-bis = diboronate formation) and two rate constants (k'_2-mono = protodeboronation of the monoboronate, and k'_2-bis = protodeboronation of the diboronate). From this model, values for the equilibrium constants and rate constants were extracted (pK_a-mono = 9.46 ; pK_a-bis = 11.59 ; k'_2-mono = 2.4 x 10^{-4} ; k'_2-bis = 6.0 x 10^{-5}) which displays the monoboronate is approximately 4 times more prone to protodeboronation than the diboronate.

6.4.2. Reaction kinetics for 3-thienyl boronic acid

6.4.2.1. 400 mM 3-thienyl boronic acid (50) in H_2O, 90 °C, pH 8.9

Temporal concentration data for the protodeboronation of 3-thienyl boronic acid (**50**) (H_2O, 90 °C) with an initial boronic acid concentration of 400 mM was performed using the following procedure:

To an oven dried multi-neck round-bottomed flask was added 3-thienyl boronic acid **50** (1.28 g, 10 mmol), H_2O (25 mL) and a magnetic stirrer bar under an inert nitrogen atmosphere. The reaction mixture was stirred, equipped with a calibrated pH electrode, and heated to 90 °C in an oil bath for 10 minutes. The pH was adjusted with 8M KOH (625 μL) to give a reaction solution pH of 8.9 (t=0). Aliquots (10 x 0.5 mL) were transferred into separate NMR tubes (Norrell® 200-QTZ NMR sample tubes) and immediately into a 90 °C oil bath. At various time points (between 1 to 30 h), aliquots were quenched by placing the NMR tubes into ice and then adding saturated $NaOAc_{(aq)}$ (50 μL) to neutralise the solution. Substrate consumption was determined by ^{11}B NMR spectroscopy.

6.4.2.2. 50 mM 3-thienyl boronic acid (50) and 350 mM $^{10}B(OH)_3$ in H_2O, 90 °C, pH 8.9

To an oven dried multi-neck round-bottomed flask was added 3-thienyl boronic acid (**50**) (160 mg, 1.25 mmol), $^{10}B(OH)_3$ (534 mg, 8.75 mmol), H_2O (25 mL) and a magnetic stirrer bar under an inert nitrogen atmosphere. The reaction mixture was stirred, equipped with a calibrated pH electrode, and heated to 90 °C in an oil bath for 10 minutes. The pH was adjusted with 8M KOH (563 μL) to give a reaction solution pH of 8.9 (t=0). Aliquots (10 x

0.5 mL) were transferred into separate NMR tubes (Norrell® 200-QTZ NMR sample tubes) and immediately into a 90 °C oil bath. At various time points (between 1 to 30 h), aliquots were quenched by placing the NMR tubes into ice and adding saturated $NaOAc_{(aq)}$ (50 μL) to neutralise the solution. Substrate consumption was determined by ^{11}B NMR spectroscopy.

6.4.3. Disproportionation kinetics

6.4.3.1. 3-thienyl boronic acid (50) crossover experiments

To a 20 mL glass vessel equipped with a magnetic stirrer was added [^{10}B]-3-thienyl boronic acid (127 mg, 1.00 mmol), [^{11}B]-boric acid (62.0 mg, 1.00 mmol), KOD (20 μL of a 10 M solution, 1.00 mmol, pD ≈ 9.68), and D_2O (5 mL). The solution was stirred and heated to 90 °C. Aliquots (250 μL) were periodically removed and quenched with AcOH (100 μL) and 1,4-dioxane (150 μL). Quenched aliquots were analysed by ^{11}B and ^{10}B NMR. Quenching gave sufficient peak separation in both ^{10}B and ^{11}B NMR spectra, allowing quantitative integration. ^{11}B NMR displayed the transient formation of [^{11}B]-boronic acid through boron-boron exchange (see Figure 2.12).

6.4.3.2. 2-furyl boronic acid (51) disproportionation experiments

2-furyl boronic acid (**51**) (22.4 mg, 0.20 mmol) was added to a 5 mm NMR tube and dissolved in D_2O (0.25 mL) and d_8-1,4-dioxane (0.25 mL). KOD (10 M, 10 μL) was added to the solution and mixed vigorously. The NMR tube was placed into a preheated (70 °C) NMR spectrometer for reaction monitoring (simultaneous ^1H and ^{11}B NMR). ^{11}B NMR spectra show the formation of two new boron species. The intensity of the new signals correlate with the formation (and decay) of new signals in the ^1H NMR spectra. Distinct signals were observed for the formation and decay of the presumed borinic acid and borane species in the ^1H NMR (see Figure 2.13). The protodeboronated product, d_1-furan, was volatile under the reaction conditions and could not be quantified, thus the residual solvent signal was used as an internal standard to quantify the formation of all species.

Temporal concentration data was modelled with DynoChem, using the model shown below (Figure 6.2). Many of the rate constants, such as the nominal termolecular processes, are steps that have been telescoped for simplification, and should not be used in isolation. pH was assumed to be constant and therefore –ate equilibria are ignored from the modelling, thus the equilibria constants should not be interpreted in isolation or in a quantitative manner. See Appendix (section 8.4.) for ^1H and ^{11}B NMR spectra.

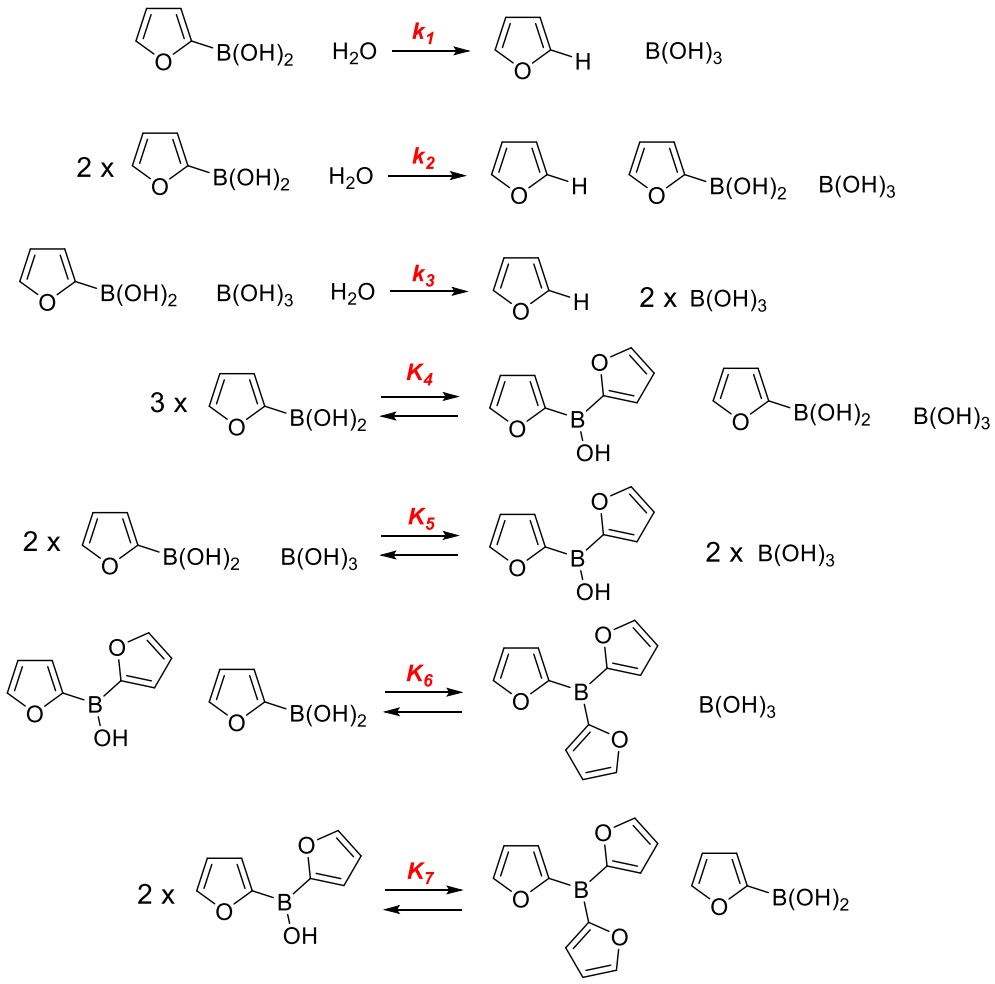

Figure 6.2 Model for the disproportionation and protodeboronation of 2-furyl boronic acid (**51**).

Table 6.1 Equilibrium and rate constants used for the modelling of disproportionation and protodeboronation of 2-furyl boronic acid (**51**).

Rate or equilibrium	Value / x 10^5	units
k_1	3.64 x 10^{-7}	$mol^{-1}\ dm^3\ s^{-1}$
k_2	2.68 x 10^{-7}	$mol^{-2}\ dm^6\ s^{-1}$
k_3	6.18 x 10^{-6}	$mol^{-2}\ dm^6\ s^{-1}$
K_4	2.71 x 10^{-1}	-
k_4	7.86 x 10^{-4}	$mol^{-2}\ dm^6\ s^{-1}$
K_5	1.52 x 10^{1}	-
k_5	5.49 x 10^{-3}	$mol^{-2}\ dm^6\ s^{-1}$
K_6	5.10 x 10^{-1}	-
k_6	2.17 x 10^{-4}	$mol^{-1}\ dm^3\ s^{-1}$
K_7	4.54	-
k_7	1.80 x 10^{-4}	$mol^{-1}\ dm^3\ s^{-1}$

6.4.4. Boric acid leaching experiments

The formation of tetrahydroxyborate, $B(OH)_4^-$, from the hydrolysis of borosilicate glassware in alkaline conditions was performed using the following procedure:

Aqueous KOH (1 M) (0.5 mL) was added to a Norell® 5 mm S400 NMR sample tube. The sample was placed into a preheated (90 °C) NMR spectrometer for reaction monitoring. The sample was monitored by ^{11}B NMR, acquiring spectra every 30 minutes for 12 hours.

6.5. Reaction monitoring: Chapter 3

6.5.1. pH – log k_{obs} profiles and simulation

6.5.1.1. Basic heteroaromatic boronic acids in H_2O/dioxane, 70 °C

pH – log k_{obs} profiles for the protodeboronation of **44** and **60** – **70** were constructed from multiple procedures depending on the exact reagent and pH. The pH – log k_{obs} data is listed, with the accompanying procedures, in the Appendix (section 8.5.)

The pH – log k_{obs} profiles were simulated using the general mechanistic model described in Figure 3.1 and Table 3.1.

6.5.2. Lewis acid additives

6.5.2.1. Addition of Lewis acid additives to 2-pyridine boronic acid (44)

The following procedure was utilised for the addition of the following Lewis acid additives: 150 mM $B(OH)_3$, 200 mM $MgCl_2$, 200 mM $Sc(OTf)_3$ and 200 mM $ZnCl_2$.

To a 20 mL glass vessel was added H_2O, 1,4-dioxane, and KOH (312.5 μL, 2.5 mmol) to give a solvent composition of 1:1 H_2O/1,4-dioxane with a total volume of 5 mL. The reaction mixture was stirred, equipped with a calibrated pH electrode and heated to 70 °C for 10 minutes before adding 2-pyridine boronic acid MIDA ester ($\mathbf{44}_{MIDA}$) (58.5 mg, 0.25 mmol). The reaction mixture was stirred for 1 minute before adding AcOH (144 μL, 2.5 mmol) and Lewis acid additive (if necessary). Aliquots (0.25 mL) were removed periodically and quenched into aqueous 1 M KOH (0.25 mL). Samples were filtered before substrate consumption was determined by ^{1}H NMR spectroscopy.

Exception: In a repeat of one experiment (without Lewis acid additives), the 2-pyridine boronic acid MIDA ester concentration was increased 4-fold to give an initial boronic acid concentration of 200 mM. The quantities of other reagents were not modified from the above procedure.

6.5.2.2. Addition of $CuCl_2$ to 2-pyridine boronic acid (44)

To a 20 mL glass vessel was added H_2O, 1,4-dioxane, and KOH (312.5 μL, 2.5 mmol) to give a solvent composition of 1:1 H_2O/1,4-dioxane with a total volume of 5 mL. The reaction mixture was stirred, equipped with a calibrated pH electrode and heated to 70 °C for 10 minutes before adding 2-pyridine boronic acid MIDA ester ($\mathbf{44}_{MIDA}$) (58.5 mg, 0.25 mmol). The reaction mixture was stirred for 1 minute before adding AcOH (144 μL, 2.5 mmol) and $CuCl_2$ (67.2 mg, 0.50 mmol). Aliquots (0.25 mL) were removed periodically and

quenched into aqueous 1 M HCl (0.25 mL). Samples were filtered before substrate consumption was determined by ^{11}B NMR spectroscopy (^{1}H NMR spectroscopy proved inadequate due to paramagnetic broadening).

In a repeat of the above reaction, 2,2-bipyridine (bipy, 156 mg, 1 mmol) was added 80 s after the addition of AcOH and $CuCl_2$. Aliquots were quenched and analysed in the same manner as above.

6.5.2.3. Addition of $ZnCl_2$ to 5-thiazole boronic acid (66)

To a 5 mL volumetric flask was added 5-thiazole boronic acid MIDA ester (**66**$_{MIDA}$) (60 mg, 0.25 mmol), which was dissolved in 1:1 H_2O/1,4-dioxane (0.76 mL). To a 20 mL glass vessel was added H_2O, 1,4-dioxane, and KOH (312.5 μL, 2.5 mmol) to give a solvent composition of 1:1 H_2O/1,4-dioxane with a total volume of 4.24 mL, which was stirred, equipped with a calibrated pH electrode and heated to 70 °C for 10 minutes before adding 5-thiazole boronic acid MIDA ester solution, immediately followed with AcOH (144 μL, 2.5 mmol) and Lewis acid additive (if necessary). Aliquots (0.25 mL) were removed periodically and quenched into aqueous 1 M HCl (0.25 mL). Samples were filtered before substrate consumption was determined by ^{1}H NMR spectroscopy.

6.5.2.4. Addition of $ZnCl_2$ to 5-pyrazole boronic acids (67 and 68)

To a 20 mL glass vessel was added H_2O, 1,4-dioxane, and KOH (312.5 μL, 2.5 mmol) to give a solvent composition of 1:1 H_2O/1,4-dioxane with a total volume of 5 mL. The reaction mixture was stirred, equipped with a calibrated pH electrode and heated to 70 °C for 10 minutes before adding boronic acid MIDA ester (0.25 mmol), AcOH (144 μL, 2.5 mmol) and Lewis acid (if necessary). Aliquots (0.25 mL) were removed periodically and quenched into aqueous 1 M HCl (0.25 mL). Samples were filtered before substrate consumption was determined by ^{1}H NMR spectroscopy.

6.6. Reaction monitoring: Chapter 4

6.6.1. pH – log k_{obs} profiles and simulation

6.6.1.1. 2,6-difluorophenyl boronic acid (71) in 1:1 H_2O/dioxane, 70 °C

The pH – log k_{obs} profile for the protodeboronation of 2,6-difluorophenyl boronic acid (**71**) (1:1 H_2O/dioxane, 70 °C) was constructed from multiple reactions using one of three procedures, depending on the reaction pH. Table 6.2 notes the procedure used for each reaction, and the relevant procedures are described below.

Table 6.2 pH – log k_{obs} data for the protodeboronation of 2,6-difluorophenyl boronic acid (**71**)

Entry	pH	log k_{obs}
1	13.20	−0.89[a]
2	11.19	−0.90[a]
3	9.61	−1.12[a]
4	8.20	−2.02[a]
5	7.38	−2.66[a]
6	6.48	−3.59[b]
7	5.95	−4.22[b]
8	5.04	−5.14[b]
9	4.16	−5.74[c]
10	3.20	−6.50[c]
11	2.11	−7.13[c]
12	1.01	−7.60[c]

[a] Multi-point kinetics using a buffered system. [b] One-point kinetics using a buffered system. [c] One-point kinetics using an unbuffered system.

Procedure for buffered systems

To a 20 mL glass vessel was added 2,6-difluorophenyl boronic acid (**71**) (39.5 mg, 0.25 mmol), buffer* (1 mmol), and TFA (2 μL, 0.025 mmol), followed by 1:1 H_2O/dioxane (4.875 mL), dioxane (62.5 μL) and a magnetic stirrer. The reaction mixture was stirred, equipped with a calibrated pH electrode and heated to 70 °C for 10 minutes in an oil bath. 0.50 mL of the reaction mixture was transferred to an NMR tube for analysis by ^{19}F NMR (t=0 spectrum). To the remaining reaction mixture was added KOH (56.3 μL, 8 M), and 0.25 mL aliquots were transferred periodically (every 5 to 20 seconds) into individual vials containing quench solution (280 μL)**. Boronic acid consumption was calculated relative to

the TFA internal standard signal in the ^{19}F NMR spectra. Product growth was not calculated due to poor solubility of polyfluoroaromatics in the reaction solvent.

*Different buffers were utilised to achieve various pH solutions. These included phenol (pH 11.19), 2-chlorophenol (pH 9.61), 2-nitrophenol (pH 8.20) and acetic acid (pH 7.38). In all cases, pH fluctuations were smaller than ±0.05 pH units over the course of the reaction.

**Quench solution = HCl (12 M, 30 μL), D_2O (125 μL) and dioxane (125 μL)

Procedure for one-point kinetics using buffered systems

To a 20 mL glass vessel was added 2,6-difluorophenyl boronic acid (**71**) (39.5 mg, 0.25 mmol), acetic acid (1 mmol), and TFA (2 μL, 0.025 mmol), followed by 1:1 H_2O/dioxane (4.875 mL), dioxane (62.5 μL) and a magnetic stirrer. The reaction mixture was stirred, equipped with a calibrated pH electrode and heated to 70 °C for 10 minutes in an oil bath. 0.50 mL of the reaction mixture was transferred to an NMR tube for analysis by ^{19}F NMR (*t*=0 spectrum). To the remaining reaction mixture was added KOH (8 M) dropwise to increase the pH stepwise. A 0.25 mL aliquot was transferred into a NMR tube at pH 6.48, 5.95 and 5.04, which were all heated to 70 °C in an oil bath (*t*=0). After 24 hours, sample were quenched with the addition of quench solution (280 μL)**. Boronic acid consumption was calculated relative to the TFA internal standard signal in the ^{19}F NMR spectra. Product growth was not calculated due to poor solubility of polyfluoroaromatics in the reaction solvent.

**Quench solution = HCl (12 M, 30 μL), D_2O (125 μL) and dioxane (125 μL)

Procedure for one-point kinetics using non-buffered systems

To a 20 mL glass vessel was added 2,6-difluorophenyl boronic acid (**71**) (39.5 mg, 0.25 mmol) and TFA (2 μL, 0.025 mmol), followed by 1:1 H_2O/dioxane (5 mL) and a magnetic stirrer. The reaction mixture was stirred, equipped with a calibrated pH electrode and heated to 70 °C for 10 minutes in an oil bath. 0.50 mL of the reaction mixture was transferred to an NMR tube for analysis by ^{19}F NMR (*t*=0 spectrum). To the remaining reaction mixture was added HCl (8 M) dropwise to decrease the pH stepwise. A 0.25 mL aliquot was transferred into a NMR tube at pH 4.16, 3.20, 2.11 and 1.01, which were all heated to 70 °C in an oil bath (*t*=0). After 37 hours, sample were diluted with the 1:1 D_2O/dioxane (250 μL). Boronic acid consumption was calculated relative to the TFA internal standard signal in the ^{19}F NMR spectra. Product growth was not calculated due to poor solubility of polyfluoroaromatics in the reaction solvent.

6.6.2. Hydroxide dependence

6.6.2.1. 2,6-difluorophenyl boronic acid (71)

Temporal concentration data for the protodeboronation of 2,6-difluorophenyl boronic acid (**71**) was obtained using general procedure I, using between 0.2 and 2.8 equiv. KOH.

For reactions with more than 1 equiv. KOH, temporal concentration data was simulated with a first-order decay equation. Reactions with less than one equiv. KOH displayed pseudo zero-order profiles, and the first 20% conversion was used to extrapolate an initial rate using linear regression (Excel 2013).

6.6.2.2. Pentafluorophenyl boronic acid (72)

Pentafluorophenylboronic acid (**72**) was reacted with various amounts of KOH using the rapid quench-flow apparatus, using the following procedure:

Pentafluorophenylboronic acid (2 mmol, 424 mg) and TFA (1.8 mmol, 138 μL) were dissolved in the 1:1 H_2O/dioxane (20 mL) to give a 0.1 M solution of boronic acid, which was analysed by ^{19}F NMR (t=0 spectrum) before being loaded into the first reagent syringe on the rapid quench-flow apparatus (21 °C). A solution of KOH in 1:1 H_2O/dioxane (0.2 M, 0.3 M or 0.5 M) was loaded into the second reagent syringe, and a quench solution of HCl in 1:1 H_2O/dioxane (0.4 M, 0.5 M or 1 M) into the quench syringe. The reagents were mixed and reacted for various time periods (ranging from 70 to 500 milliseconds) before quenching with the quench solution. Boronic acid consumption was calculated relative to the TFA internal standard signal in the ^{19}F NMR spectra. Product growth was not calculated due to poor solubility of polyfluoroaromatics in the reaction solvent.

Rate constants (k_{obs}) were obtained by fitting the temporal concentration data of all reactions to a first-order decay equation. A fitting error of 5% was deduced from the SSE for all reactions, and thus it was acknowledged that no significant variation of the rate was observed with increasing hydroxide concentration.

6.6.3. Protodeboronation rates for substrate scope

The experimental procedures utilised to obtain rate data for substrates **28** and **71 – 99** are reported in Table 6.3. Superscript notation indicates the general procedure and specific conditions and analytical methods used for each log k_{obs} value. Swain-Lupton values (σ^{SL}) were calculated from the modified Swain-Lupton constants (F and R),[175] and with the optimised ratio of field (f = 0.69) and resonance (r = 0.31) contributions (see section 4.2.3.3.)

Table 6.3 log k_{obs} and σ^{SL} data for polyfluorophenyl and other aryl boronic acids

Entry	Substrate	Abbreviation	log k_{obs}	$\sigma^{SL} = (F \times f) + (R \times r)$
1	**73**	Phenyl	-7.39[a]	0
2	**28**	4-OMe	-6.62[a]	0.03
3	**74**	2-F	-5.00[c]	1.24
4	**75**	3-F	-7.40[a]	0.34
5	**76**	4-F	-7.23[a]	0.19
6	**77**	2,3-F_2	-3.92[c]	1.58
7	**78**	2,4-F_2	-4.60[c]	1.43
8	**79**	2,5-F_2	-4.20[c]	1.58
9	**80**	3,4-F_2	-7.13[a]	0.53
10	**81**	3,5-F_2	-7.08[a]	0.68
11	**82**	2,3,4-F_3	-3.53[c]	1.77
12	**83**	2,3,5-F_3	-2.95[c]	1.92
13	**84**	2,4,5-F_3	-3.76[c]	1.77
14	**85**	3,4,5-F_3	-6.77[a]	0.87
15	**71**	2,6-F_2	-0.87[d]	2.48
16	**86**	2,3,4,5-F_4	-2.41[c]	2.11
17	**87**	2,3,6-F_3	0.47[d]	2.82
18	**88**	2,4,6-F_3	-0.26[d]	2.67
19	**89**	2,3,4,6-F_4	1.02[d]	3.01
20	**90**	2,3,5,6-F_4	1.79[d]	3.16
21	**72**	2,3,4,5,6-F_5	2.43[d]	3.35
22	**91**	2-F-4-OMe	-5.25[c]	1.27
23	**92**	2-F-4-CF_3	-4.03[c]	1.55
24	**93**	2-F-5-NO_2	-3.10[c]	1.95
25	**94**	2,6-F_2-4-OMe	-1.01[d]	2.51
26	**95**	F_4-4-OMe	1.88[d]	3.19
27	**96**	3,5-CF_3	-6.81[b]	0.86
28	**97**	3,5-NO_2	-4.92[b]	1.42
29	**98**	4-Me	-6.80[b]	-0.05
30	**99**	3-Cl	-6.85[b]	0.37

[a] General procedure F – log k_{obs} value obtained from initial rate of product formation. [b] General procedure F – log k_{obs} value obtained from starting material consumption. [c] General procedure G. [d] General procedure H.

6.6.4. KIE studies

6.6.4.1. 4-methoxyphenyl boronic acid (28)

4-methoxyphenyl boronic acid (**28**) (0.25 mmol) was dissolved in the desired solvent blend (see Table 6.4). Propionic acid (0.025 mmol, 1 M in H_2O, 25 μL) and KOH/D (0.50 mmol) were added and the solution was stirred for 1 min before transferring 0.5 mL in a J-Young's valve NMR tube. The NMR tube was sealed and analysed by ^{1}H NMR at 70 °C (*t*=0 spectrum), before being placed immediately into an oil bath at 70 °C. After given time periods (approximately every 3-4 days), the sample was reanalysed by ^{1}H NMR at 70 °C and immediately returned to an oil bath at 70 °C.

Table 6.4 Quantities of reagents and solvents used in KIE experiments to give 0.05 M reaction solutions of boronic acid.

Reaction solvent	$RB(OL)_2$	L_2O	Dioxane	KOL
H_2O/dioxane	L=H, 38.0 mg	H_2O, 2.44 g	2.67 g	KOH (8 M), 62.5 μL
D_2O/dioxane	L=D, 38.5 mg	D_2O, 2.72 g	2.67 g	KOD (10 M), 50 μL
1:1:2 H_2O/D_2O/dioxane	L=D, 38.5 mg	H_2O, 1.19 g D_2O, 1.39 g	2.67 g	KOH (8 M), 62.5 μL

For reactions carried out in H_2O/dioxane and D_2O/dioxane, the formation of protodeboronated material was monitored relative to the propionic acid internal standard. Initial rates were obtained (linear regression of temporal concentration data) and converted to pseudo first-order rate constants by division of initial boronic acid concentration (50 mM). $k_H = 2.36 \times 10^{-7}$, $k_D = 5.40 \times 10^{-8}$, KIE = $k_H/k_D = 4.4$.

For the reaction carried out in 1:1:2 H_2O/D_2O/dioxane, the ratio of proto- and deutero-deboronation product was determined after reacting for 450 hours at 70 °C. The ratio of products was calculated using ^{1}H NMR by comparing the integral values of protons H_c (7.37 ppm) with H_d and H_e at (7.03 ppm) (see Figure 4.8).

$$\text{Partitioning KIE} = \frac{[d_0 - anisole]}{[d_1 - anisole]} = \frac{0.81}{0.19} = 4.3$$

6.6.4.2. 2,6-difluorophenyl boronic acid (71)

2,6-difluorophenylboronic acid (**71**) (1 mmol) and TFA (0.1 mmol, 7.7 μL) were dissolved in the desired solvent blend (see Table 6.5) to give a 0.1 M solution of boronic acid, which was loaded into the first reagent syringe on the rapid quench-flow apparatus with the reagent water bath at 70 °C. A solution of KOH/D (0.2 M, see Table 6.5) was loaded into the second

reagent syringe, and a quench solution of H/DCl (0.4 M) into the quench syringe. After thermal equilibration to 70 °C (10 min), the reagents were mixed and reacted for various time periods before quenching with the quench solution. The consumption of boronic acid was determined using ^{19}F NMR (*t*=0 spectrum obtained by NMR analysis of the boronic acid reagent solution before the addition of KOH).

Table 6.5 Quantities of reagents and solvents used in KIE experiments to give 0.05 M reaction solutions of boronic acid upon mixing of the two reagents syringes using the rapid quench-flow apparatus.

Solvent	$RB(OL)_2$	L_2O	Dioxane	KOL	Quench
H_2O/dioxane	L=H, 158 mg	H_2O, 2.44 g	5.33 g	KOH (0.2 M) in 1:1 H_2O/dioxane	HCl (0.4 M) in 1:1 H_2O/dioxane
D_2O/dioxane	L=D, 160 mg	D_2O, 5.53 g	5.33 g	KOD (0.2 M) in 1:1 D_2O/dioxane	DCl (0.4 M) in 1:1 D_2O/dioxane
1:1:2 H_2O/D_2O /dioxane	L=D, 160 mg	H_2O, 2.50 g D_2O, 2.76 g	5.33 g	KOH (0.2 M) in (1:1 H_2O/D_2O)/dioxane	HCl (0.4 M) in (1:1 H_2O/D_2O)/dioxane

For reactions carried out in H_2O/dioxane and D_2O/dioxane, the consumption of boronic acid was monitored relative to the TFA internal standard, and the temporal concentration data was fitted to a pseudo first-order decay to obtain a pseudo first-order rate constant. $k_H = k_D = 0.130$, KIE = 1.0. For the reaction carried out in 1:1:2 H_2O/D_2O/dioxane, the ratio of proto- and deutero- deboronation product was determined after a reaction time of 30 seconds at 70 °C. The ratio of products were calculated using ^{19}F NMR whereby distinct signals are observed for the proto- and deutero-product at -110.67 ppm and -110.95 ppm respectively, which displayed a partitioning KIE of 1.25 (see Figure 4.8).

$$\text{Partitioning KIE} = \frac{[d_0 - difluorobenzene]}{[d_1 - difluorobenzene]} = \frac{1.25}{1.00} = 1.25$$

6.6.5. Eyring analysis

Temporal concentration data for the protodeboronation of 2,6-difluorophenyl boronic acid (**71**) was obtained between 21 – 70 °C (using general procedure G).

Eyring analysis was achieved by constructing a plot of 1/T *versus* ln (*k*/T) using the linear Eyring equation (Equation 6.1) where *R* = gas constant (8.314 J mol^{-1} K^{-1}), $\Delta H^{\ddagger}$ = enthalpy of activation (J mol^{-1}), $\Delta S^{\ddagger}$ = entropy of activation (J mol^{-1} K^{-1}), k_B = Boltzmann constant (1.38×10^{-23} J K^{-1}).

$$\ln\left(\frac{k}{T}\right) = -\frac{\Delta H^{\ddagger}}{R}.\frac{1}{\mathrm{T}} + \left(\frac{\Delta S^{\ddagger}}{\mathrm{R}} + \ln\left(\frac{k_B}{h}\right)\right) \qquad (6.1)$$

6.7. pK_a and pK_{aH} titrations

6.7.1. pK_a of 3-thienyl boronic acid at various H_2O/dioxane compositions

3-thienyl boronic acid (**50**) (160 mg, 1.25 mmol) was dissolved in the appropriate solvent (H_2O/1,4-dioxane, see Figure 6.3) to give a 0.05 M solution was stirred and heated (90 °C) in an oil bath for 15 minutes. The flask was equipped with a calibrated pH electrode. KOH (8 M) was added portion-wise (2-10 μL at a time) to increment the pH. The amount of KOH added and the pH of the solution were recorded after each addition of KOH. A plot of pH *versus* "total mmol of KOH added" produces a set of pH titration curves (Figure 6.3). pK_a values were extracted using the mid-point of the linear buffering region (where pH = pK_a).

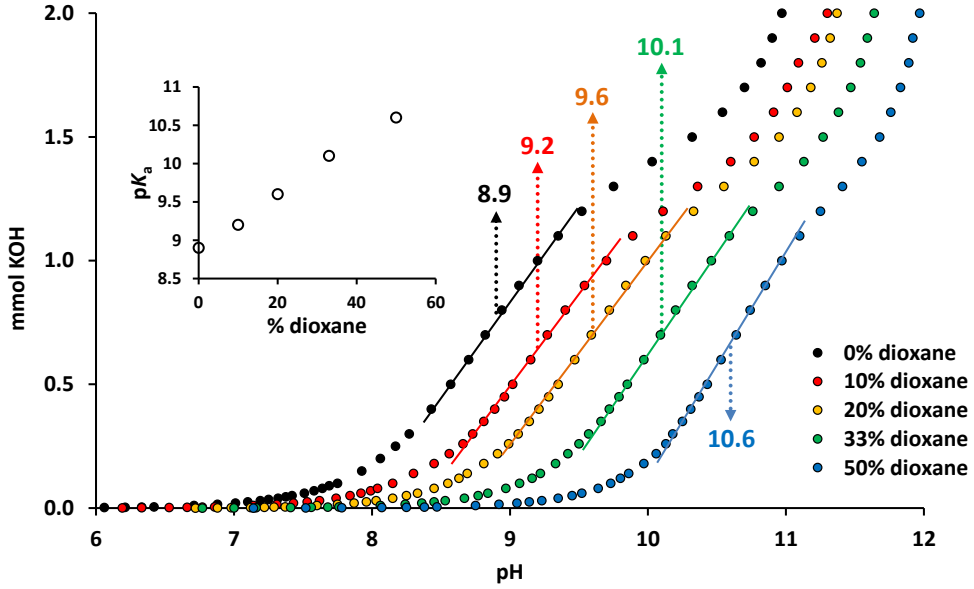

Figure 6.3 pK_a titration of 3-thienyl boronic acid (**50**) between 0 – 50 % volume dioxane at 90 °C.

6.7.2. pK_a titrations using ^{11}B NMR

6.7.2.1. Procedure for ^{11}B NMR pH titrations

pK_a values for stable boronic acids ($t_{½}$ > 1 h) were determined by ^{11}B NMR titration using the following procedure:

The desired boronic acid (1.25 mmol) was dissolved in the appropriate solvent (H_2O or 1:1 H_2O/1,4-dioxane, 25 mL) to give a 0.05 M solution. The solution was stirred and heated (70 or 90 °C) in an oil bath for 15 minutes. The flask was equipped with a calibrated pH electrode. KOH (8 M) was added portion-wise (2-20 μL at a time) to increment the pH. The pH was modified no more than 0.5 pH units at a time, transferring an aliquot (0.5 mL) into a

NMR tube on each occasion. Samples were heated to 70 °C within the NMR instrument for 5 minutes before recording ^{11}B NMR spectra.

Chemical shifts were converted into % boronate assuming a linear relationship, and using chemical shift limits as 0% boronate and 100% boronate. The pH – % boronate plot was simulated using the Henderson-Hasselbalch equation to extract the pK_a value. The SSE was minimised using Excel Solver.

$$\text{Henderson-Hasselbalch equation} \quad \text{pH} = \text{p}K_a + \log\left(\frac{[\text{B}^-]}{[\text{B}]}\right)$$

A representative example is shown below (For all titration plots, see Appendix section 8.2.).

pH	Chemical shift /ppm	% Boronate
6.01	27.42	0.00
9.76	26.69	3.06
10.23	25.06	9.90
10.46	23.41	16.81
10.63	21.62	24.32
10.76	19.69	32.41
10.88	18.00	39.50
11.01	16.07	47.59
11.13	13.69	57.57
11.27	11.90	65.07
11.45	9.58	74.80
11.65	7.64	82.94
11.90	5.94	90.06
12.20	4.72	95.18
12.74	3.76	99.20
13.01	3.57	100.00

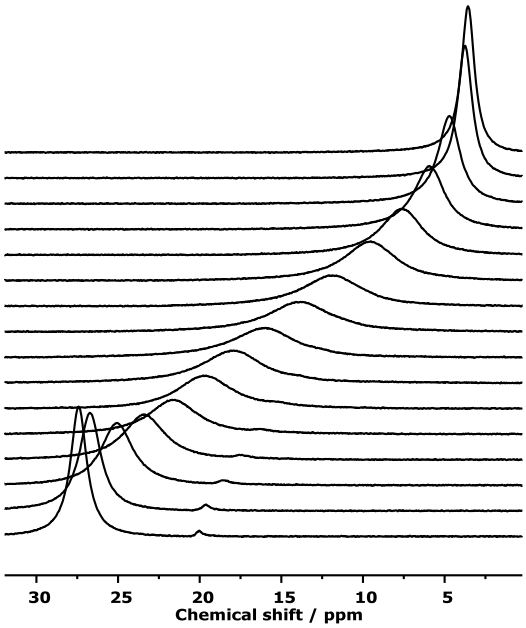

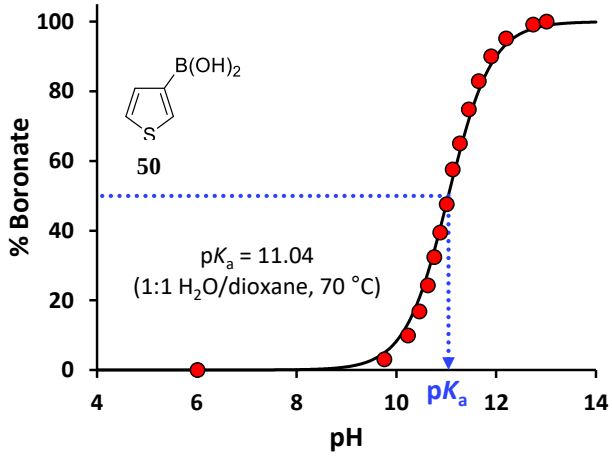

Figure 6.4 Representative pK_a titration of **50** displaying a table of pH and chemical shift values (top left), stacked ^{11}B NMR spectra at various pH values (top right) and the corresponding Henderson-Hasselbalch simulation (bottom).

6.7.3. pK_a extrapolation of rapidly reacting boronic acids

6.7.3.1. Rapidly reacting heteroaromatic boronic acids

Standard ^{11}B NMR titrations were not suitable for many substrates due to rapid protodeboronation rates ($t_{½}$ < 1 h). For some heteroaromatic boronic acids (refer to Table 3.1) pK_a values were extrapolated from iterative fitting of rate data using the general mechanistic model (see Figure 3.1 and Table 3.1).

6.7.3.2. Rapidly reacting polyfluorophenyl boronic acids

For some polyfluorophenyl boronic acids (refer to Table 4.1), pK_a values were determined by monitoring the rate of protodeboronation under neutral or acidic pH values, whereby the rate of protodeboronation is reduced due to a reduction in the boronate concentration (Table 6.6). Assuming the obtained rate constant under the standard conditions (k_{max}, 2 equiv. KOH, pH ≈ 13.3) is representative of a maximum rate of protodeboronation (i.e. ~100% boronate), the reduction in the observed rate constant at lower pH (k_{slow}) is proportional to the change in boronate concentration.

$$\text{mol fraction of boronate} = \frac{k_{slow}}{k_{max}}$$

Therefore, using the Henderson-Hasselbalch equation, the ratio of rate constants (k_{slow}/k_{max}), and the reaction pH of the slower reaction (pH$_{slow}$), a pK_a value can be determined using the following equation:

$$\text{p}K\text{a} = \text{pH}_{slow} - \log\left(\frac{[\text{B}^-]}{[\text{B}]}\right) = \text{pH}_{slow} - \log\left(\frac{\left(\frac{k_{slow}}{k_{max}}\right)}{1 - \left(\frac{k_{slow}}{k_{max}}\right)}\right)$$

For example, for the pentafluorophenyl boronic acid (**72**); k_{max} (pH 13.30) = 300, k_{slow} (pH 2.25) = 1.15 x 10^{-3}.

$$\text{p}K\text{a} = 2.25 - \log\left(\frac{\left(\frac{0.00115}{300}\right)}{1 - \left(\frac{0.00115}{300}\right)}\right) = 2.25 - \log(3.83 \times 10^{-6}) = 2.25 - (-5.42) = 7.67$$

Table 6.6 Rate constants and extrapolated pK_a values for reactive aryl boronic acids.

Substrate	Abbreviation	log k_{max} (pH)	log k_{slow} (pH)	p*K*a
86	2,3,4,5-F	-2.41 (13.30)	-3.28 (7.38)	8.91
71	2,6-F	-0.886 (13.30)	-2.67 (7.38)	9.15
87	2,3,6-F	0.431 (13.30)	-2.20 (6.01)	8.66
88	2,4,6-F	-0.264 (13.30)	-1.97 (7.34)	9.03
89	2,3,4,6-F	0.993 (13.30)	-1.40 (6.00)	8.39
90	2,3,5,6-F	1.79 (13.30)	-4.17 (2.01)	7.97
72	2,3,4,5,6-F	2.48 (13.30)	-2.94 (2.25)	7.67
94	2,6-F-4-MeO	-1.01 (13.30)	-3.20 (7.38)	9.56
95	2,3,5,6-F-4-MeO	-1.88 (13.30)	-4.16 (2.30)	8.33
93	2-F-4-NO2	-3.10 (130.30)	-3.96 (7.42)	8.22

Temporal concentration data for all reactions can be found in the Appendix (section 8.1.) Procedures for reactions at low pH values (to obtain k_{slow} values) are described below:

Procedure 1 - reactions at pH 6.00 to 6.01

To a 20 mL glass vessel was added 1:1 H_2O/dioxane (4.94 mL), dioxane (62.5 μL), AcOH (43 μL, 0.75 mmol), KOAc (24.5 mg, 0.25 mmol) and TFA (1.9 μL, 0.025 mmol). The solvent mixture was stirred and heated to 70 °C in an oil bath for 10 min. The solvent mixture was equipped with a calibrated pH electrode. The desired boronic acid (0.25 mmol) was added to the solvent mixture, followed immediately with the transfer of a 0.25 mL aliquot into the quench solution (280 μL)*, which was analysed by ^{19}F NMR (*t*=0 spectrum, no more than 10 seconds between addition of solid and first quench). 0.25 mL aliquots were periodically quenched into the quench solution*. Boronic acid consumption was calculated relative to the TFA internal standard signal in the ^{19}F NMR spectra. Product growth was not calculated due to poor solubility of polyfluoroaromatics in the reaction solvent.

The pH of the reaction mixtures were monitored over time and displayed no more than a ±0.05 pH fluctuation from start to finish. The range of measured pH values were averaged to give a single pH value.

*Quench solution = HCl (12 M, 30 μL), D_2O (125 μL) and dioxane (125 μL).

Procedure 2 - reactions at pH 2.01 to 2.30

Reaction mixtures at pH 2.01 to 2.30 were achieved using the above procedure (procedure 1), but without the addition of AcOH or KOAc to the solvent mixture. Although not formally buffered, pH fluctuations were smaller than ±0.05 pH units over the course of the reaction.

Procedure 3 - reactions at pH 7.34 to 7.42

Reaction mixtures at pH 7.34 to 7.42 were achieved using the above procedure (procedure 1), but without the addition of AcOH, and with an increased amount of KOAc to the solvent mixture. Although not formally buffered, pH fluctuations were smaller than ±0.05 pH units over the course of the reaction.

6.7.4. pK_{aH} titrations using ^{1}H NMR

pK_{aH} values for basic heteroaromatic boronic acids were extrapolated from iterative fitting of rate data using the general model described in Figure 3.1 and Table 3.1. In addition, pK_{aH} values were also experimentally determined in 1:1 H_2O/dioxane at 25 °C using ^{1}H NMR.

6.7.4.1. Procedure for ^{1}H NMR pH titrations at 25 °C

To a 20 mL glass vessel was added the desired boronic acid (0.25 mmol) and 1:1 H_2O/1,4-dioxane (5 mL) at 25 °C. The reaction mixture was stirred and equipped with a calibrated pH electrode. KOH (5 μL of 1M solution) was added, the pH recorded, and an aliquot (0.5 mL) was transferred to an NMR tube for analysis. HCl (8 M) was added portion-wise (2-20 μL at a time) to decrease the pH. The pH was modified no more than 1 pH unit at a time, transferring an aliquot (0.5 mL) into a NMR tube on each occasion. Samples were analysed at 25 °C within the NMR instrument by ^{1}H NMR.

For many substrates, multiple ^{1}H signals are observed, however only one signal (with the largest chemical shift difference between pH extremes) was used in the pK_{aH} titration calculations. Chemical shifts were converted into % $N_{Ar}H^+$ (% protonated species) assuming a linear relationship, and using chemical shift limits as 0% $N_{Ar}H^+$ and 100% $N_{Ar}H^+$. The pH - % $N_{Ar}H^+$ plot was simulated using the Henderson-Hasselbalch equation to extract the pK_{aH} value. The SSE was minimised using Excel Solver.

6.7.4.2. Notes for partial ^{1}H NMR pH titrations at 25 °C

4-isoxazolyl boronic acid (**61**) and 5-pyrimidine boronic acid (**62**) displayed partial time-averaged chemical shifts between pH 0.21 and pH 6.20 at 25 °C, and thus a confident pK_{aH} value could not be obtained. A Henderson-Hasselbalch fitting was applied to the partial titration data while optimising a hypothetical value for the chemical shift at 100% $N_{Ar}H^+$ to provide a maximum value for the pK_{aH} (see Appendix section 8.2. for pK_a plots).

6.7.4.3. Procedure for ^{1}H NMR pH titrations with prior MIDA ester hydrolysis

pK_{aH} titrations for compounds **44**, **66**, **67**, **69** and **70** were obtained by prior *in-situ* hydrolysis of the corresponding MIDA boronate, using the procedure described below.

To a 20 mL glass vessel was added the desired boronic acid MIDA ester (0.25 mmol) and 1:1 H_2O/1,4-dioxane (5 mL) at 25 °C. The reaction mixture was stirred and equipped with a calibrated pH electrode. KOH (0.20 mmol, 25 μL of 8M solution) was added and the reaction mixture was stirred for 1 minute before adding AcOH (0.20 mmol, 11.5 μL). The pH was recorded and an aliquot (0.5 mL) transferred to an NMR tube for analysis. HCl (8 M) was added portion-wise (2-20 μL at a time) to decrease the pH. The pH was modified approximately 1 pH unit at a time, transferring an aliquot (0.5 mL) into a NMR tube on each occasion. Samples were analysed at 25 °C within the NMR instrument by ^{1}H NMR.

Analysis of the experimental data described in the previous procedure (section 6.7.4.1.) was used to produce the pH - % $N_{Ar}H^+$ plots (refer to Appendix section 8.2.). 6-(trifluoromethyl)-2-pyridine boronic acid (**70**) did not display a time-averaged signal between pH 1.22 and pH 7.14 at 25 °C, and a pK_{aH} value could not be obtained. Substrates **44** and **69** displayed a maximum migration in chemical shift of 0.65 ppm during pK_{aH} titrations, and thus assuming a similar chemical shift migration for substrate **70**, and assuming an accuracy of 0.01 ppm, a maximum pK_{aH} value for substrate **70** (at 25 °C, 1:1 H_2O/1,4-dioxane) can be calculated using the Henderson-Hasselbalch equation:

$$\mathrm{p}K_a(\max) = \mathrm{pH} - \log\left(\frac{[\mathrm{B}]}{[\mathrm{BH}^+]}\right) = 1.22 - \log\left(\frac{0.65 - 0.01}{0.01}\right) = 1.22 - 1.82 = -0.60$$

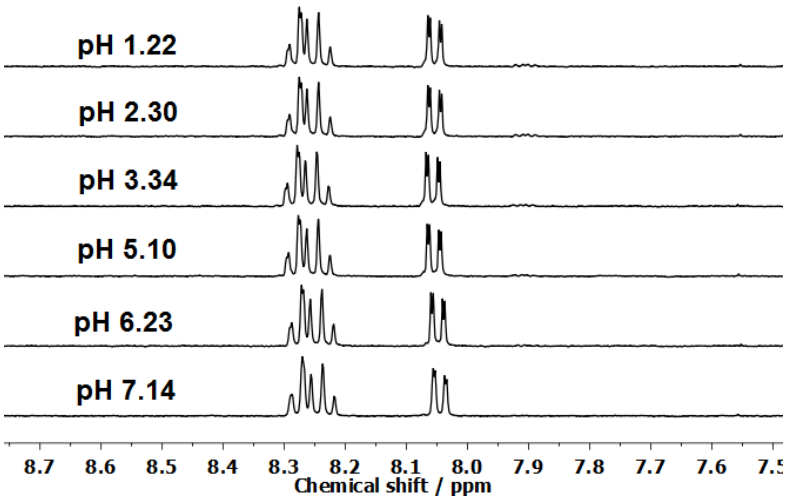

Figure 1. ^{1}H NMR spectra of **70** in 1:1 H_2O/dioxane at 25 °C.

6.8. Computational details

Computational studies were performed by Dr Andrew Leach (John Moores University) and Dr Marc Reid (University of Edinburgh), and were used to support various aspects of the experimental data presented in this thesis.

6.8.1. General information: Chapter 2 and 3

DFT calculations were performed using M06L/6-311++G**, incorporating solvation free energies computed as single points employing the same level of theory and the PCM formalism. This level of theory have been shown to be in good agreement with experimental data for other boron-based reagents, including MIDA boronate hydrolysis.[115] M06/6-311+G**//B3LYP/6-31+G** was used for selected species, incorporating solvation via single point using B3LYP/6-31+G* combined with the PCM formalism as implemented in Gaussian03. This level of theory has been utilised for boronic acids.[156,193] Calculations were performed in Gaussian09 (unless stated otherwise) at 298 K and 1 atm. Ideal gas derived corrections from 1 M standard state to 25 M H_2O gave best agreement with experimental data and are used throughout.

6.8.2. General information: Chapter 4

DFT calculations were performed using B3LYP/6-31+G*, incorporating solvation free energies computed as single points employing the same level of theory and the PCM formalism. Calculations were performed in Gaussian09 (unless stated otherwise) at 298 K and 1 atm. Boronate anions were subjected to a conformer search using MarvinSketch (v 15.7.6.) *Conformers* plug in, using MMFF94 forcefield to minimise each conformer. All settings were set to default values. Each boronate was further optimised using DFT (Gaussian09 quantum chemistry program package). Each DFT-optimised boronate was subject to a single point energy calculation employing Möller-Plesset perturbation theory (MP2) in conjunction with the 6-311+G basis set for all atoms, and the IEFPCM solvent model for 1,4-dioxane. Similarly to the boronate anions, the related aryl anion structures, as well as boric acid itself, were optimised employing the MP2/6-311+G(d,p)/PCM (1,4-dioxane) // B3LYP/6-31+G(d,p)/PCM(1,4-dioxane) level of theory. NOTE – no conformer searches were necessary when processing the aryl anions or boric acid. Using the DFT-optimised geometries, Natural Bonding Orbital (NBO) analysis was employed at the MP2/6-311+G(d,p)/PCM (1,4-dioxane) // B3LYP/6-31+G(d,p)/PCM(1,4-dioxane) level of theory using NBO (v 3.1.) as implemented in Gaussian09.

6.9. Simulation fittings: General information

6.9.1. Autoionisation of water

The autoionisation constant for water (K_w) varies depending on solvent composition and temperature.[157,158] For purely aqueous reactions in H_2O (or D_2O), the following values were used in simulation fittings:

pK_w (H_2O, 90 °C) = 12.43 pK_w (D_2O, 90 °C) = 13.28

The pK_w value of the H_2O/1,4-dioxane solvent mixture was not determined at 70 °C. However, literature data at 25 °C (52% wt 1,4-dioxane)[194] and the known trend of purely aqueous systems with temperature indicate the true value is likely to be between 13.5 - 14.5 (refer to literature pK_w data below).

pK_w of H_2O (25 °C) = 14.00, pK_w of H_2O (70 °C) = 12.81, pK_w of H_2O (52% wt 1,4-dioxane, 25 °C) = 15.76

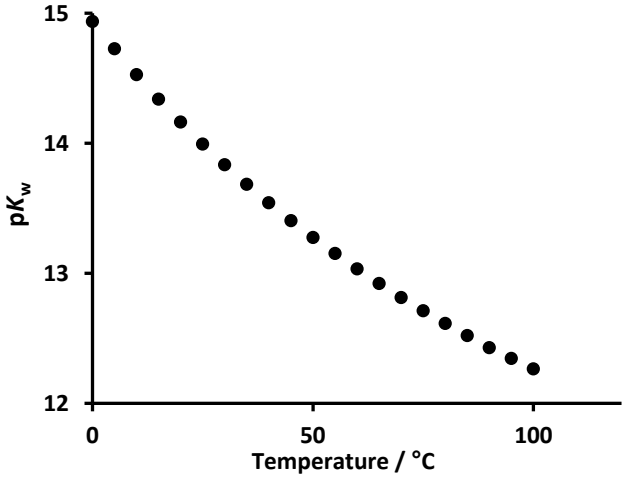

Figure 2. Dependence on pKw of H2O with temperature.

Chapter 7

References

1 H. C. Brown and G. Zweifel, *J. Am. Chem. Soc.*, 1961, **83**, 3834–3840.
2 T. Onak, *Organoborane Chemistry*, Academic Press Inc., London, 1975, pp 19-135.
3 P. Muller, *Pure Appl. Chem.*, 1994, **66**, 1077–1184.
4 J. P. Lorand and J. O. Edwards, *J. Org. Chem.*, 1959, **24**, 769–774.
5 D. G. Hall, *Boronic Acids: Preparation and Applications in Organic Synthesis, Medicine and Materials*, Wiley VCH: Weinheim, Germany, 2nd ed., 2011.
6 R. E. Zeebe, A. Sanyal, J. D. Ortiz and D. A. Wolf-Gladrow, *Mar. Chem.*, 2001, **73**, 113–124.
7 N. Miyaura, K. Yamada and A. Suzuki, *Tetrahedron Lett.*, 1979, **20**, 3437–3440.
8 C. S. Cho and S. Uemura, *J. Organomet. Chem.*, 1994, **465**, 85–92.
9 D. M. T. Chan, K. L. Monaco, R.-P. P. Wang and M. P. Winters, *Tetrahedron Lett.*, 1998, **39**, 2933–2936.
10 D. A. Evans, J. L. Katz and T. R. West, *Tetrahedron Lett.*, 1998, **39**, 2937–2940.
11 P. Y. S. Lam, C. G. Clark, S. Saubern, J. Adams, M. P. Winters, D. M. T. Chan and A. Combs, *Tetrahedron Lett.*, 1998, **39**, 2941–2944.
12 L. S. Liebeskind and J. Srogl, *J. Am. Chem. Soc.*, 2000, **122**, 11260–11261.
13 M. Sakai, H. Hayashi and N. Miyaura, *Organometallics*, 1997, **16**, 4229–4231.
14 M. Sakai, M. Ueda and N. Miyaura, *Angew. Chem. Int. Ed.*, 1998, **37**, 3279–3281.
15 A. Takezawa, K. Yamaguchi, T. Ohmura, Y. Yamamoto and N. Miyaura, *Synlett*, 2002, 1733–1735.
16 A. F. Littke and G. C. Fu, *Angew. Chem. Int. Ed.*, 2002, **41**, 4176–4211.
17 G. Altenhoff, R. Goddard, C. W. Lehmann and F. Glorius, *J. Am. Chem. Soc.*, 2004, **126**, 15195–15201.
18 A. F. Littke, C. Dai and G. C. Fu, *J. Am. Chem. Soc.*, 2000, **122**, 4020–4028.
19 D. Zim, A. S. Gruber, G. Ebeling, J. Dupont and A. L. Monteiro, *Org. Lett.*, 2000, **2**, 2881–2884.
20 A. Fihri, D. Luart, C. Len, A. Solhy, C. Chevrin and V. Polshettiwar, *Dalton Trans.*, 2011, **40**, 3116–3121.
21 J. P. Wolfe, R. A. Singer, B. H. Yang and S. L. Buchwald, *J. Am. Chem. Soc.*, 1999, **121**, 9550–9561.
22 N. Marion and S. P. Nolan, *Acc. Chem. Res.*, 2008, **41**, 1440–1449.
23 A. Suzuki, *J. Organomet. Chem.*, 1999, **576**, 147–168.
24 N. Miyaura, *J. Organomet. Chem.*, 2002, **653**, 54–57.
25 G. B. Smith, G. C. Dezeny, D. L. Hughes, A. O. King and T. R. Verhoeven, *J. Org. Chem.*, 1994, **59**, 8151–8156.
26 A. O. Aliprantis and J. W. Canary, *J. Am. Chem. Soc.*, 1994, **116**, 6985–6986.
27 K. Matos and J. A. Soderquist, *J. Org. Chem.*, 1998, **63**, 461–470.
28 A. A. C. Braga, N. H. Morgon, G. Ujaque and F. Maseras, *J. Am. Chem. Soc.*, 2005, **127**, 9298–9307.
29 C. Amatore, A. Jutand and G. Le Duc, *Chem. Eur. J.*, 2011, **17**, 2492–2503.
30 B. P. Carrow and J. F. Hartwig, *J. Am. Chem. Soc.*, 2011, **133**, 2116–2119.
31 A. A. Thomas and S. E. Denmark, *Science*, 2016, **352**, 329–332.
32 A. B. Lerner, T. E. H. H. Lee, J. C. Sheehan and G. P. Hess, *J. Am. Chem. Soc.*, 1955, **77**, 1067–1068.
33 B. Castro, J. R. Dormoy, G. Evin and C. Selve, *Tetrahedron Lett.*, 1975, **16**, 1219–1222.
34 K. Ishihara, S. Ohara and H. Yamamoto, *J. Org. Chem.*, 1996, **61**, 4196–4197.
35 K. Ishihara, S. Ohara and H. Yamamoto, *Macromolecules*, 2000, **33**, 3511–3513.
36 K. Ishihara, S. Ohara and H. Yamamoto, *Org. Synth.*, 2002, **79**, 176–185.
37 T. Maki, K. Ishihara and H. Yamamoto, *Synlett*, 2004, 1355–1358.
38 R. M. Al-Zoubi, O. Marion and D. G. Hall, *Angew. Chem. Int. Ed.*, 2008, **47**, 2876–2879.
39 H. Zheng and D. G. Hall, *Tetrahedron Lett.*, 2010, **51**, 3561–3564.

40 H. Zheng, M. Lejkowski and D. G. Hall, *Tetrahedron Lett.*, 2013, **54**, 91–94.
41 H. Zheng, R. McDonald and D. G. Hall, *Chem. Eur. J.*, 2010, **16**, 5454–5460.
42 Y.-L. Liu, L. Liu, Y.-L. Wang, Y.-C. Han, D. Wang and Y.-J. Chen, *Green Chem.*, 2008, **10**, 635–640.
43 R. Sanz, A. Martínez, D. Miguel, J. M. Álvarez-Gutiérrez and F. Rodríguez, *Adv. Synth. Catal.*, 2006, **348**, 1841–1845.
44 K. Namba, H. Yamamoto, I. Sasaki, K. Mori, H. Imagawa and M. Nishizawa, *Org. Lett.*, 2008, **10**, 1767–1770.
45 M. Yasuda, T. Somyo and A. Baba, *Angew. Chem. Int. Ed.*, 2006, **45**, 793–796.
46 Y. Tamaru, M. Kimura and M. Fukasaka, *J. Am. Chem. Soc.*, 2005, **67**, 4592–4593.
47 A. B. Zaitsev, S. Gruber and P. S. Pregosin, *Chem. Commun.*, 2007, 4692.
48 J. A. McCubbin, H. Hosseini and O. V. Krokhin, *J. Org. Chem.*, 2010, **75**, 959–962.
49 C. L. Ricardo, X. Mo, J. A. McCubbin and D. G. Hall, *Chem. Eur. J.*, 2015, **21**, 4218–4223.
50 P. F. Bross, R. Kane, A. T. Farrell, S. Abraham, K. Benson, M. E. Brower, S. Bradley, J. V. Gobburu, A. Goheer, S.-L. Lee, J. Leighton, C. Y. Liang, R. T. Lostritto, W. D. McGuinn, D. E. Morse, A. Rahman, L. A. Rosario, S. L. Verbois, G. Williams, Y.-C. Wang and R. Pazdur, *Clin. Cancer Res.*, 2004, **10**, 3954–3964.
51 X.-Y. Pei, Y. Dai and S. Grant, *Clin. Cancer Res.*, 2004, **10**, 3839–3852.
52 K. Lacina, P. Skládal and T. D. James, *Chem. Cent. J.*, 2014, **8**, 1–17.
53 G. Springsteen and B. Wang, *Chem. Commun.*, 2001, 1608–1609.
54 E. Karakuş, M. Üçüncü, R. C. Eanes and M. Emrullahoğlu, *New J. Chem.*, 2013, **37**, 2632–2635.
55 D. C. Klonoff, *J. Diabetes Sci. Technol.*, 2012, **6**, 1242–1250.
56 H. Kobayashi, M. Ogawa, R. Alford, P. L. Choyke and Y. Urano, *Chem. Rev.*, 2010, **110**, 2620–2640.
57 P. W. Miller, N. J. Long, R. Vilar and A. D. Gee, *Angew. Chem. Int. Ed.*, 2008, **47**, 8998–9033.
58 G. E. Smith, H. L. Sladen, S. Biagini and P. J. Blower, *Dalt. Trans.*, 2011, **40**, 6196–6205.
59 O. Jacobson, D. O. Kiesewetter and X. Chen, *Bioconjug. Chem.*, 2015, **26**, 1–18.
60 A. D. Ainley and F. Challenger, *J. Chem. Soc.*, 1930, 2171–2180.
61 H. G. Kuivila, J. F. Reuwer and J. A. Mangravite, *Can. J. Chem.*, 1963, **41**, 3081–3090.
62 H. G. Kuivila and K. V. Nahabedian, *J. Am. Chem. Soc.*, 1961, **83**, 2159–2163.
63 J. J. Molloy, R. P. Law, J. W. B. Fyfe, C. P. Seath, D. J. Hirst and A. J. B. Watson, *Org. Biomol. Chem.*, 2015, **13**, 3093–102.
64 C. W. Muir, J. C. Vantourout, A. Isidro-Llobet, S. J. F. Macdonald and A. J. B. Watson, *Org. Lett.*, 2015, **17**, 6030–6033.
65 X. Chen, C. E. Goodhue and J.-Q. Yu, *J. Am. Chem. Soc.*, 2006, **128**, 12634–12635.
66 D. J. Wallace and C. Chen, *Tetrahedron Lett.*, 2002, **43**, 6987–6990.
67 S.-M. Zhou, M.-Z. Deng, L.-J. Xia and M.-H. Tang, *Angew. Chem. Int. Ed.*, 1998, **37**, 2845–2847.
68 M. Lemhadri, H. Doucet and M. Santelli, *Synth. Commun.*, 2006, **36**, 121–128.
69 T. Ishiyama, K. Ishida and N. Miyaura, *Tetrahedron*, 2001, **57**, 9813–9816.
70 A. J. J. Lennox and G. C. Lloyd-Jones, *Chem. Soc. Rev.*, 2014, **43**, 412–443.
71 A. A. Fuller, H. R. Hester, E. V Salo and E. P. Stevens, *Tetrahedron Lett.*, 2003, **44**, 2935–2938.
72 A. Lützen and M. Hapke, *Eur. J.Org. Chem.*, 2002, 2292–2297.
73 Y. Yang, A. Hörnfeldt and S. Gronowitz, *Chem. Scr.*, 1988, **28**, 275–279.
74 D. M. Knapp, E. P. Gillis and M. D. Burke, *J. Am. Chem. Soc.*, 2009, **131**, 6961–3.
75 F. C. Fischer and E. Havinga, *Recl. Trav. Chim. Pays-Bas*, 1965, **84**, 1954–1955.
76 K. Chen, R. Peterson, S. K. Math, J. B. LaMunyon, C. A. Testa and D. R. Cefalo,

Tetrahedron Lett., 2012, **53**, 4873–4876.
77 K. Deshayes, R. D. Broene, I. Chao, C. B. Knobler and F. Diederich, *J. Org. Chem.*, 1991, **56**, 6787–6795.
78 A. N. Cammidge and K. V. L. Crépy, *J. Org. Chem.*, 2003, **68**, 6832–6835.
79 H. J. Frohn, N. Y. Adonin, V. V. Bardin and V. F. Starichenko, *Z. Anorg. Allg. Chem.*, 2002, **628**, 2834–2838.
80 N. Y. Adonin, A. Y. Shabalin and V. V. Bardin, *J. Fluor. Chem.*, 2014, **168**, 111–120.
81 T. Kinzel, Y. Zhang and S. L. Buchwald, *J. Am. Chem. Soc.*, 2010, **132**, 14073–14075.
82 J. Lozada, Z. Liu and D. M. Perrin, *J. Org. Chem.*, 2014, **79**, 5365–5368.
83 M. Sana, G. Leroy and C. Wilante, *Organometallics*, 1991, **10**, 264–270.
84 H. R. Snyder, J. A. Kuck and J. R. Johnson, *J. Am. Chem. Soc.*, 1938, **60**, 105–111.
85 J. R. Johnson and M. G. Van Campen, *J. Am. Chem. Soc.*, 1938, **60**, 121–124.
86 K. S. Webb and D. Levy, *Tetrahedron Lett.*, 1995, **36**, 5117–5118.
87 A. J. J. Lennox and G. C. Lloyd-Jones, *Isr. J. Chem.*, 2010, **50**, 664–674.
88 C. Adamo, C. Amatore, I. Ciofini, A. Jutand and H. Lakmini, *J. Am. Chem. Soc.*, 2006, **128**, 6829–6836.
89 G. C. Fu, *Acc. Chem. Res.*, 2008, **41**, 1555–1564.
90 K. L. Billingsley, K. W. Anderson and S. L. Buchwald, *Angew. Chem. Int. Ed.*, 2006, **45**, 3484–3488.
91 K. Billingsley and S. L. Buchwald, *J. Am. Chem. Soc.*, 2007, **129**, 3358–3366.
92 N. Kudo, M. Perseghini and G. C. Fu, *Angew. Chem. Int. Ed.*, 2006, **45**, 1282–1284.
93 N. Y. Adonin, D. E. Babushkin, V. N. Parmon, V. V. Bardin, G. A. Kostin, V. I. Mashukov and H. J. Frohn, *Tetrahedron*, 2008, **64**, 5920–5924.
94 J. Chen and A. Cammers-Goodwin, *Tetrahedron Lett.*, 2003, **44**, 1503–1506.
95 T. Korenaga, T. Kosaki, R. Fukumura, T. Ema and T. Sakai, *Org. Lett.*, 2005, **7**, 4915–4917.
96 Y. Nishihara, H. Onodera and K. Osakada, *Chem. Commun.*, 2004, 192–193.
97 D. Imao, B. W. Glasspoole, V. S. Laberge and C. M. Crudden, *J. Am. Chem. Soc.*, 2009, **131**, 5024–5025.
98 G. Zou, Y. K. Reddy and J. R. Falck, *Tetrahedron Lett.*, 2001, **42**, 7213–7215.
99 N. Leconte, A. Keromnes-Wuillaume, F. Suzenet and G. Guillaumet, *Synlett*, 2007, 204–210.
100 J. Z. Deng, D. V. Paone, A. T. Ginnetti, H. Kurihara, S. D. Dreher, S. A. Weissman, S. R. Stauffer and C. S. Burgey, *Org. Lett.*, 2009, **11**, 345–347.
101 K. Semba and Y. Nakao, *J. Am. Chem. Soc.*, 2014, **136**, 7567–7570.
102 K. Dirrich, T. Bube, R. Sfurmer and R. W. Hoffmann, *Angew. Chem. Int. Ed. Engl.*, 1986, **25**, 1028–1030.
103 H. G. Kuivila, A. H. Keough and E. J. Soboczenski, *J. Org. Chem.*, 1953, **19**, 780–783.
104 D. S. Matteson and A. A. Kandil, *Tetrahedron Lett.*, 1986, **27**, 3831–3834.
105 H. Steinberg and D. L. Hunter, *Ind. Eng. Chem.*, 1957, **49**, 174–181.
106 R. A. Bowie and O. C. Musgrave, *J. Chem. Soc.*, 1963, 3945–3949.
107 D. X. Yang, S. L. Colletti, K. Wu, M. Song, G. Y. Li and H. C. Shen, *Org. Lett.*, 2009, **11**, 381–384.
108 S. Goggins, E. Rosevere, C. Bellini, J. C. Allen, B. J. Marsh, M. F. Mahon and C. G. Frost, *Org. Biomol. Chem.*, 2014, **12**, 47–52.
109 K. L. Billingsley and S. L. Buchwald, *Angew. Chem. Int. Ed.*, 2008, **47**, 4695–4698.
110 Y. Yamamoto, M. Takizawa, X.-Q. Yu and N. Miyaura, *Angew. Chem. Int. Ed.*, 2008, **47**, 928–931.
111 E. P. Gillis and M. D. Burke, *J. Am. Chem. Soc.*, 2008, **130**, 14084–14085.
112 T. Mancilla, R. Contreras and B. Wrackmeyer, *J. Organomet. Chem.*, 1986, **307**, 1–6.

113 G. R. Dick, E. M. Woerly and M. D. Burke, *Angew. Chem. Int. Ed.*, 2012, **51**, 2667–2672.
114 B. E. Uno, E. P. Gillis and M. D. Burke, *Tetrahedron*, 2009, **65**, 3130–3138.
115 J. A. Gonzalez, O. M. Ogba, G. F. Morehouse, N. Rosson, K. N. Houk, A. G. Leach, P. H.-Y. Cheong, M. D. Burke and G. C. Lloyd-Jones, *Nat. Chem.*, 2016, 1–9.
116 E. Vedejs, R. W. Chapman, S. C. Fields, S. Lin and M. R. Schrimpf, *J. Org. Chem.*, 1995, **60**, 3020–3027.
117 G. A. Molander and N. Ellis, *Acc. Chem. Res.*, 2007, **40**, 275–286.
118 G. A. Molander and A. R. Brown, *J. Org. Chem.*, 2006, **71**, 9681–9686.
119 G. A. Molander and P. E. Gormisky, *J. Org. Chem.*, 2008, **73**, 7481–5.
120 A. J. J. Lennox and G. C. Lloyd-Jones, *J. Am. Chem. Soc.*, 2012, **134**, 7431–7441.
121 G. A. Molander and B. Biolatto, *J. Org. Chem.*, 2003, **68**, 4302–4314.
122 C. Y. Lee, S. J. Ahn and C. H. Cheon, *J. Org. Chem.*, 2013, **78**, 12154–12160.
123 H. Ihara and M. Suginome, *J. Am. Chem. Soc.*, 2009, **131**, 7502–7503.
124 T. G. Elford, S. Nave, R. P. Sonawane and V. K. Aggarwal, *J. Am. Chem. Soc.*, 2011, **133**, 16798–16801.
125 S. Roesner and V. K. Aggarwal, *Can. J. Chem.*, 2012, **90**, 965–974.
126 S. Roesner, D. J. Blair and V. K. Aggarwal, *Chem. Sci.*, 2015, **6**, 3718–3723.
127 C. L. Ricardo, X. Mo, J. A. McCubbin and D. G. Hall, *Chemistry*, 2015, **21**, 4218–4223.
128 H. Zheng and D. G. Hall, *Aldrichimica Acta*, 2014, **47**, 41–51.
129 N. Gernigon, R. M. Al-Zoubi and D. G. Hall, *J. Org. Chem.*, 2012, **77**, 8386–8400.
130 R. D. Kimbrough, *Environ. Health Perspect.*, 1976, **14**, 51–56.
131 M. M. Hansen, R. A. Jolly and R. J. Linder, *Org. Process Res. Dev.*, 2015, **19**, 1507–1516.
132 H. G. Kuivila, J. F. Reuwer and J. A. Mangravite, *J. Am. Chem. Soc.*, 1964, **2164**, 2666–2670.
133 C. Liu, X. Li, Y. Wu and J. Qiu, *RSC Adv.*, 2014, **4**, 54307–54311.
134 C. Liu, X. Li and Y. Wu, *RSC Adv.*, 2015, **5**, 15354–15358.
135 G. Barker, S. Webster, D. G. Johnson, R. Curley, M. Andrews, P. C. Young, S. A. Macgregor and A.-L. Lee, *J. Org. Chem.*, 2015, **80**, 9807–9816.
136 F. Shen, S. Tyagarajan, D. Perera, S. W. Krska, P. E. Maligres, M. R. Smith and R. E. Maleczka, *Org. Lett.*, 2016, **18**, 1554–1557.
137 N. Miyaura and A. Suzuki, *Chem. Rev.*, 1995, **95**, 2457–2483.
138 K. V Nahabedian and H. G. Kuivila, *J. Am. Chem. Soc.*, 1961, **83**, 2167–2174.
139 H. G. Kuivila and K. V Nahabedian, *J. Am. Chem. Soc.*, 1961, **83**, 2164–2166.
140 L. P. Hammett and A. J. Deyrup, *J. Am. Chem. Soc.*, 1932, **54**, 2721–2739.
141 N. A. Rebacz and P. E. Savage, *Phys. Chem. Chem. Phys.*, 2013, **15**, 3562–9.
142 H. R. Devlin and I. J. Harris, *Ind. Eng. Chem. Fundam.*, 1984, **23**, 387–392.
143 C. Eaborn, *J. Chem. Soc.*, 1956, 4858–4864.
144 C. Eaborn and K. C. Pande, *J. Chem. Soc.*, 1961, 297–301.
145 C. Eaborn and J. A. Waters, *J. Chem. Soc.*, 1961, 542–547.
146 C. Eaborn and K. C. Pande, *J. Chem. Soc.*, 1961, 3715–3718.
147 N. V Pechishcheva, E. V Osintseva, L. K. Neudachina, Y. G. Yatluk, L. I. Leont'ev, K. Y. Shunyaev and A. A. Vshivkov, *Dokl. Chem.*, 2006, **408**, 65–69.
148 R. D. Brown, A. S. Buchanan and A. A. Humffray, *Aust. J. Chem.*, 1965, **18**, 1521–1525.
149 R. D. Brown, A. S. Buchanan and A. A. Humffray, *Aust. J. Chem.*, 1965, **18**, 1513–1520.
150 K. W. Ratts, R. K. Howe and W. G. Phillips, *J. Am. Chem. Soc.*, 1969, **91**, 6115–6121.
151 M. Charton, *Can. J. Chem.*, 1960, **38**, 2493–2499.
152 M. Charton, *J. Am. Chem. Soc.*, 1969, **91**, 6649–6654.

153 M. Charton, *J. Am. Chem. Soc.*, 1969, **91**, 615–618.
154 S. Licht, *Anal. Chem.*, 1985, **57**, 514–519.
155 J. S. Renny, L. L. Tomasevich, E. H. Tallmadge and D. B. Collum, *Angew. Chem. Int. Ed.*, 2013, **52**, 11998–12013.
156 G. Noonan and A. G. Leach, *Org. Biomol. Chem.*, 2015, **13**, 2555–2560.
157 W. Marshall and E. Franck, *J. Phys. Chem. Ref. Data*, 1981, **10**, 295–304.
158 R. E. Mesmer and D. L. Herting, *J. Solution Chem.*, 1978, **7**, 901–912.
159 T. E. Cole and B. D. Haly, *Organometallics*, 1992, **11**, 652–657.
160 W. Schlenk and W. Schlenk, *Berichte d. D. Chem. Gesellschaft.*, 1929, **62**, 920–924.
161 A. J. Blake, J. Shannon, J. C. Stephens and S. Woodward, *Chem. Eur. J.*, 2007, **13**, 2462–2472.
162 D. Florentin, M. C. Fournie-Zaluksi, M. Callanquin and B. P. Roques, *J. Heterocycl. Chem.*, 1976, **13**, 1265–1272.
163 L. Ji, R. M. Edkins, L. J. Sewell, A. Beeby, A. S. Batsanov, K. Fucke, M. Drafz, J. A. K. Howard, O. Moutounet, F. Ibersiene, A. Boucekkine, E. Furet, Z. Liu, J. F. Halet, C. Katan and T. B. Marder, *Chem. Eur. J.*, 2014, **20**, 13618–13635.
164 H. Gunaydin and K. N. Houk, *J. Am. Chem. Soc.*, 2008, **130**, 15232–15233.
165 P. L. Geissler, *Science*, 2001, **291**, 2121–2124.
166 H. Howard-Lock, C. Lock, M. Martins, P. Smalley and R. Bell, *Can. J. Chem.*, 1985, **64**, 1215–1219.
167 F. C. Fischer and E. Havinga, *Recl. Trav. Chim. Pays-Bas*, 2010, **93**, 21–24.
168 B. R. Beno, K. S. Yeung, M. D. Bartberger, L. D. Pennington and N. A. Meanwell, *J. Med. Chem.*, 2015, **58**, 4383–4438.
169 J. Wang, M. Sánchez-Roselló, J. L. Aceña, C. Del Pozo, A. E. Sorochinsky, S. Fustero, V. A. Soloshonok and H. Liu, *Chem. Rev.*, 2014, **114**, 2432–2506.
170 P. J. Bray and R. G. Barnes, *J. Chem. Phys.*, 1957, **27**, 551–560.
171 H. H. Jaffe, *Chem. Rev.*, 1953, **53**, 191–261.
172 L. P. Hammett, *J. Am. Chem. Soc.*, 1937, **59**, 96–103.
173 H. C. Brown and Y. Okamoto, *J. Am. Chem. Soc.*, 1957, **79**, 1913–1917.
174 M. Yoshioka, K. Hamamoto and T. Kubota, *Bull. Chem. Soc. Jpn.*, 1962, **35**, 1723–1728.
175 C. Hansch, A. Leo and R. W. Taft, *Chem. Rev.*, 1991, **91**, 165–195.
176 J. F. Bunnett, *Acc. Chem. Res.*, 1972, **5**, 139–147.
177 J. F. Bunnett, J. H. Miles and K. V. Nahabedian, *J. Am. Chem. Soc.*, 1961, **83**, 2512–2516.
178 J. F. Bunnett and B. F. Hrutfiord, *J. Org. Chem.*, 1962, **27**, 4152–4156.
179 J. F. Bunnett, D. S. Connor and K. J. O'Reilly, *J. Org. Chem.*, 1979, **44**, 4197–4199.
180 B. R. Brown, *Q. Rev. Chem. Soc.*, 1951, **5**, 131–146.
181 A. Streitwieser and J. A. Hudson, *J. Am. Chem. Soc.*, 1968, **90**, 648–651.
182 P. Segura, J. F. Bunnett and L. Villanova, *J. Org. Chem.*, 1985, **50**, 1041–1045.
183 P. Segura, *J. Org. Chem.*, 1985, **50**, 1045–1053.
184 V. A. Kallepalli, K. A. Gore, F. Shi, L. Sanchez, G. A. Chotana, S. L. Miller, R. E. Maleczka and M. R. Smith, *J. Org. Chem.*, 2015, **80**, 8341–8353.
185 S. Ahn, C. Lee, N. Kim and C. Cheon, *J. Org. Chem.*, 2014, **79**, 7277–7285.
186 W. Wagner and A. Pruss, *J. Phys. Chem. Ref. Data*, 2002, **31**, 387–535.
187 T. E. Cole, R. Quintanilla and S. Rodewald, *Synth. React. Inorg. Met. Chem.*, 1990, **20**, 55–63.
188 T. Leermann, F. R. Leroux and F. Colobert, *Org. Lett.*, 2011, **13**, 4479–4481.
189 G. R. Dick, D. M. Knapp, E. P. Gillis and M. D. Burke, *Org. Lett.*, 2010, **12**, 2314–2317.
190 W. Erb, A. Hellal, M. Albini, J. Rouden and J. Blanchet, *Chem. Eur. J.*, 2014, **20**, 6608–6612.
191 L. Wang, C. Dai, S. K. Burroughs, S. L. Wang and B. Wang, *Chem. Eur. J.*, 2013, **19**,

7587–7594.
192 P. K. Glasoe and F. A. Long, *J. Phys. Chem.*, 1960, **64**, 188–190.
193 J. M. Lee, P. Helquist and O. Wiest, *J. Am. Chem. Soc.*, 2012, **134**, 14973–14981.
194 L. G. Hepler, E. M. Woolley and D. G. Hurkot, *J. Phys. Chem.*, 1970, **74**, 3908–3913.

Chapter 8

Appendix

8.1. Temporal concentration plots

A representative temporal concentration plot is shown for the protodeboronation of boronic acids that were analysed using a general procedure utilising multiple point kinetics. Additionally, temporal concentration plots used for the calculation of pK_a values in section 6.7.3.2 are also displayed. All of the temporal concentration plots were obtained in 1:1 H_2O/dioxane at 70 °C at the stated reaction pH. The dotted black line shows the first-order simulation, and is used to obtain a k_{obs} value (see section 6.3.1.).

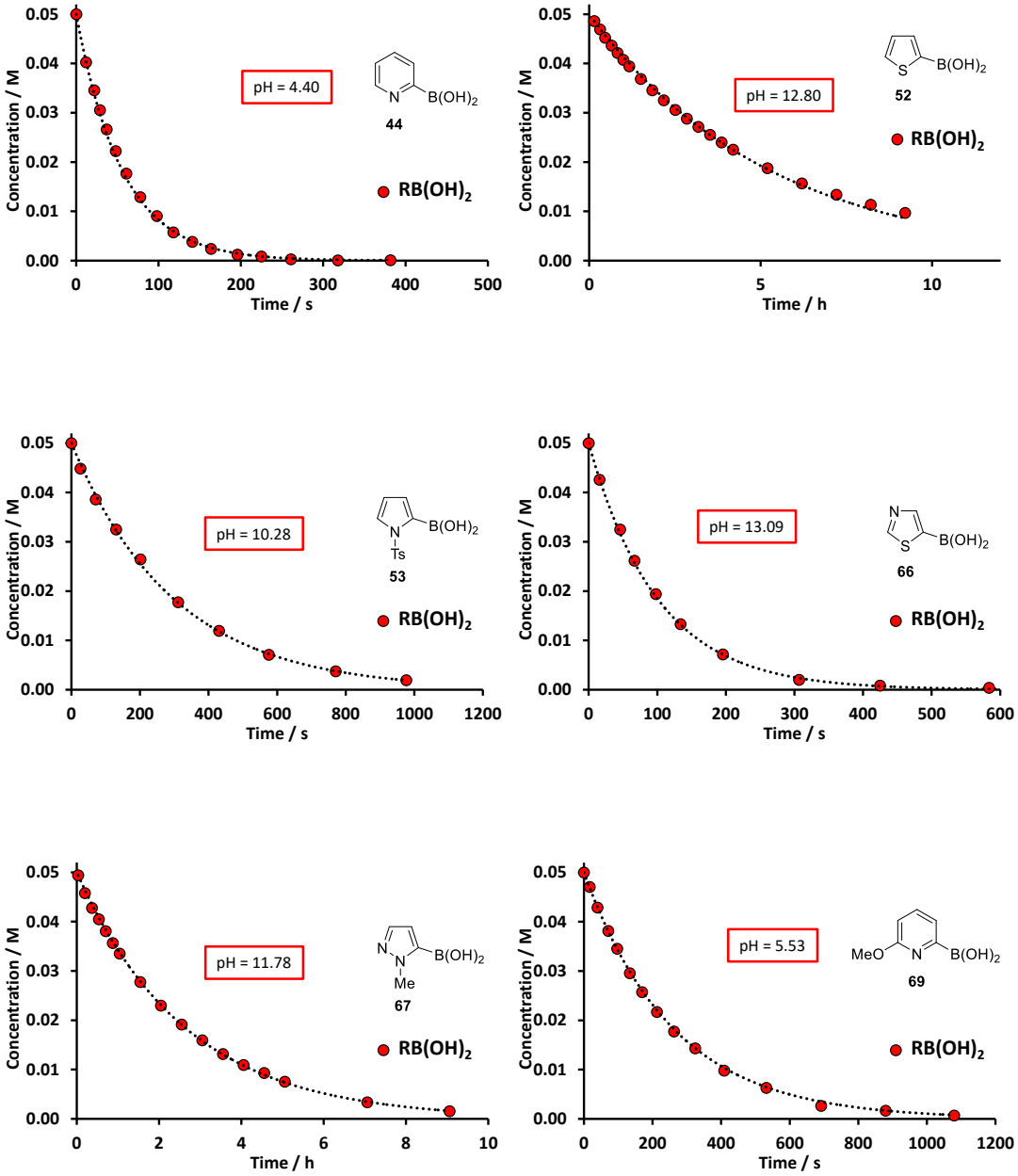

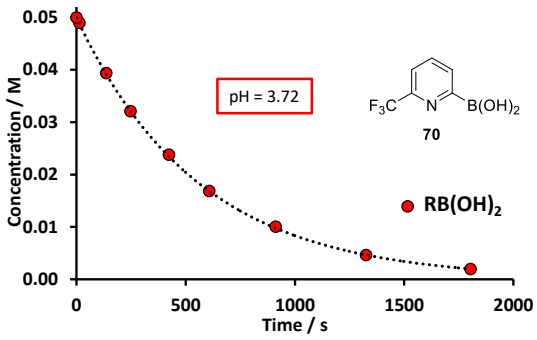
Concentration / M
Time / s
pH = 3.72
70
RB(OH)2

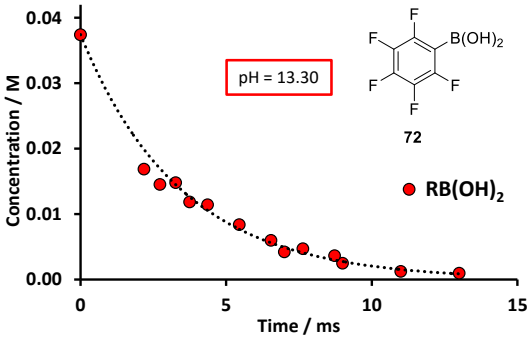
Concentration / M
Time / ms
pH = 13.30
72
RB(OH)2

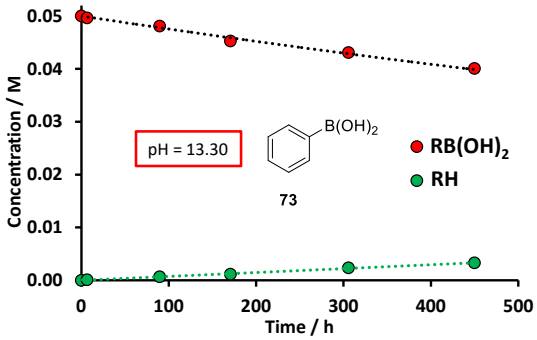
Concentration / M
Time / h
pH = 13.30
73
RB(OH)2
RH

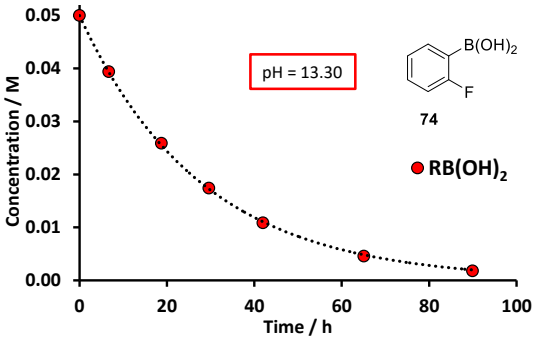
Concentration / M
Time / h
pH = 13.30
74
RB(OH)2

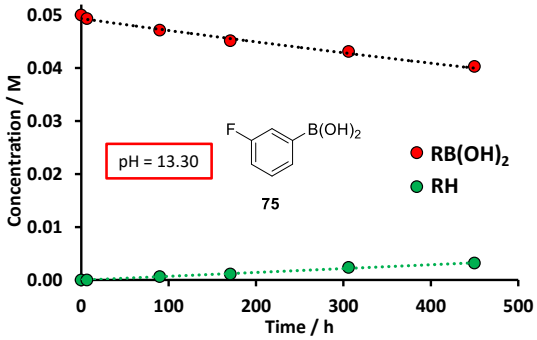
Concentration / M
Time / h
pH = 13.30
75
RB(OH)2
RH

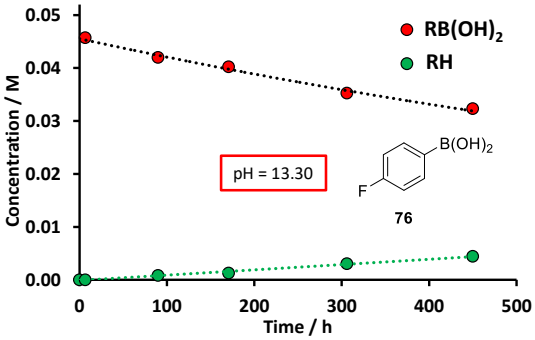
Concentration / M
Time / h
RB(OH)2
RH
pH = 13.30
76

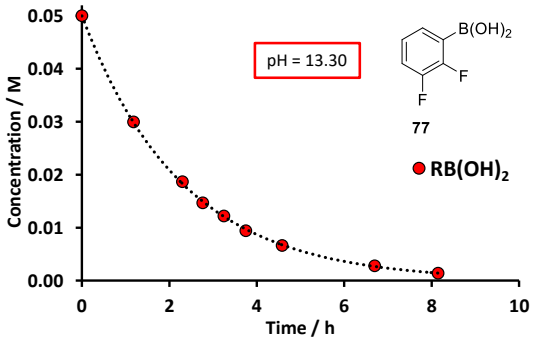
Concentration / M
Time / h
pH = 13.30
77
RB(OH)2

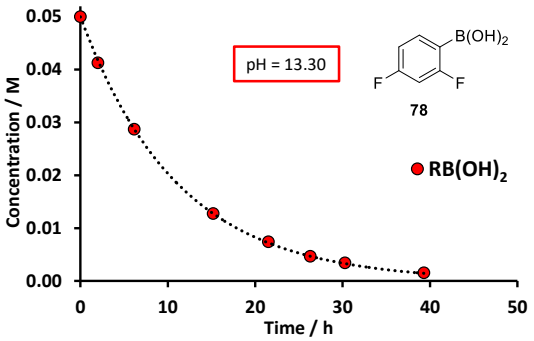
Concentration / M
Time / h
pH = 13.30
78
RB(OH)2

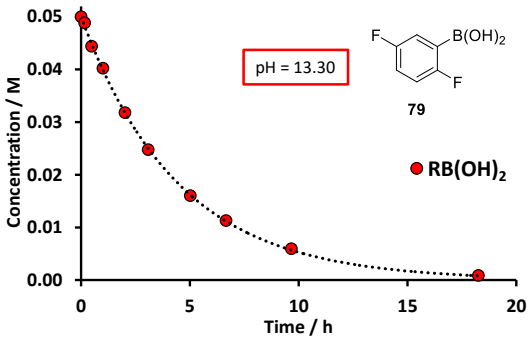
Concentration / M
Time / h
pH = 13.30
79
RB(OH)2

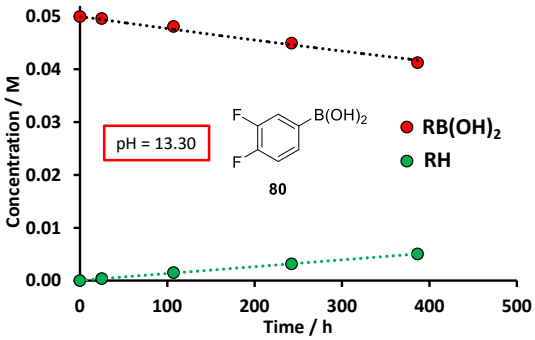
Concentration / M
Time / h
pH = 13.30
80
RB(OH)2
RH

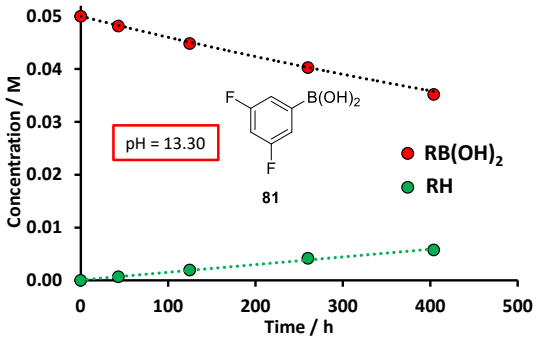
Concentration / M
Time / h
pH = 13.30
81
RB(OH)2
RH

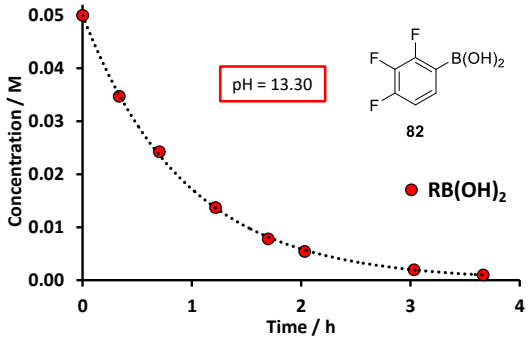
Concentration / M
Time / h
pH = 13.30
82
RB(OH)2

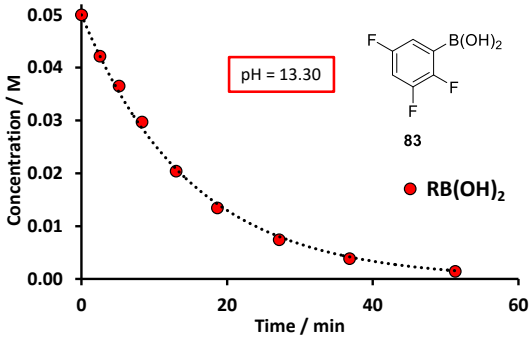
Concentration / M
Time / min
pH = 13.30
83
RB(OH)2

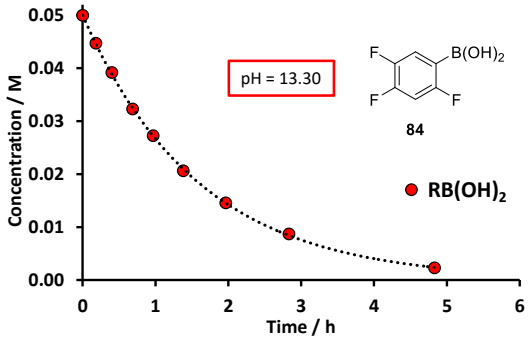
Concentration / M
Time / h
pH = 13.30
84
RB(OH)2

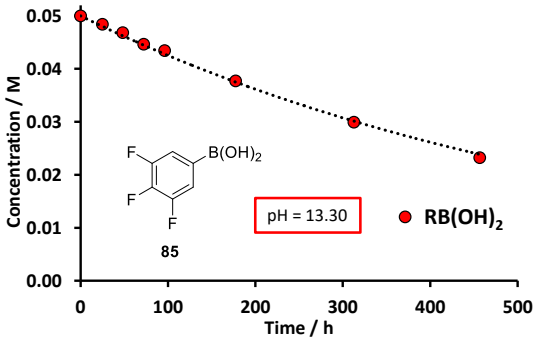
Concentration / M
Time / h
pH = 13.30
85
RB(OH)2

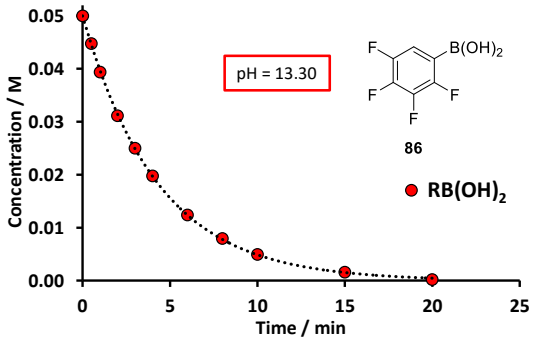
Concentration / M
Time / min
pH = 13.30
86
RB(OH)2

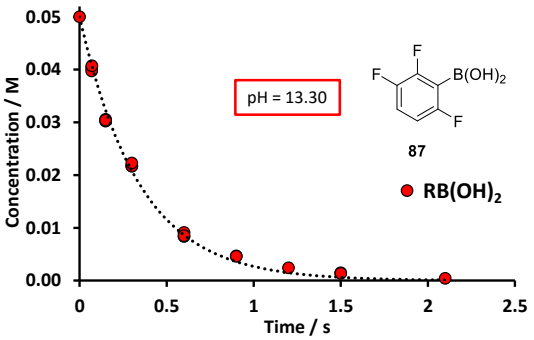
Concentration / M
Time / s
pH = 13.30
87
RB(OH)2

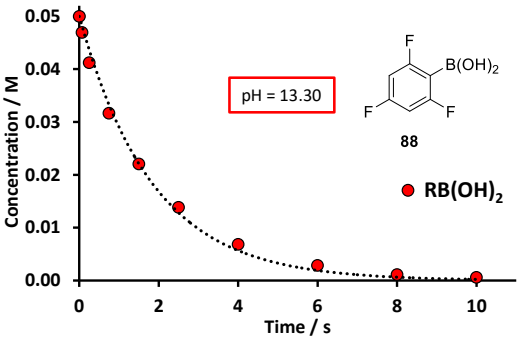
Concentration / M
Time / s
pH = 13.30
88
RB(OH)2

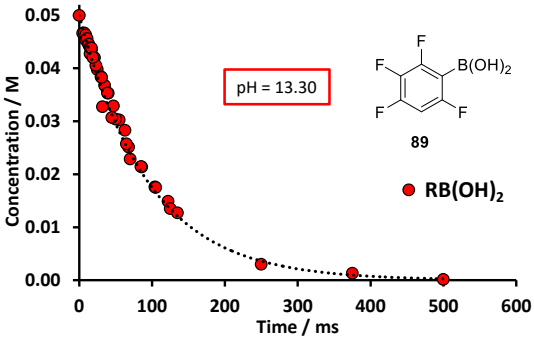
Concentration / M
Time / ms
pH = 13.30
89
RB(OH)2

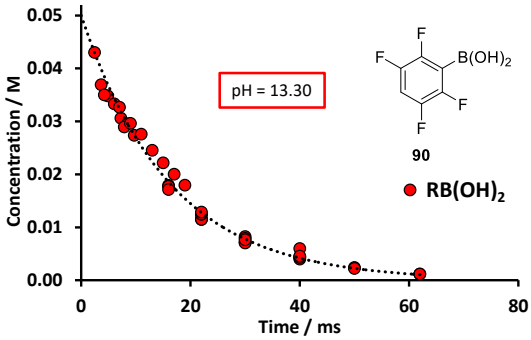
Concentration / M
Time / ms
pH = 13.30
90
RB(OH)2

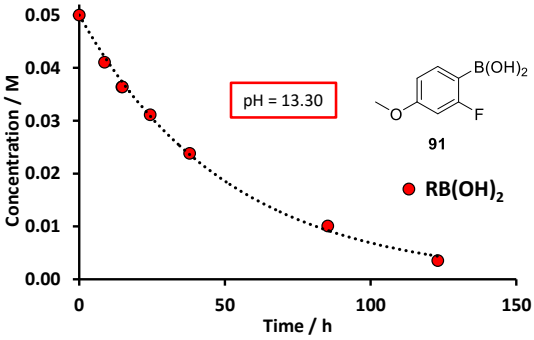
Concentration / M
Time / h
pH = 13.30
91
RB(OH)2

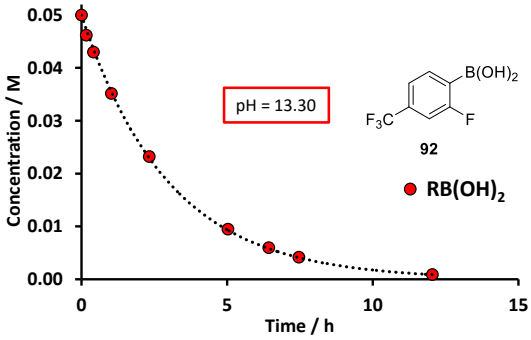
Concentration / M
Time / h
pH = 13.30
92
RB(OH)2

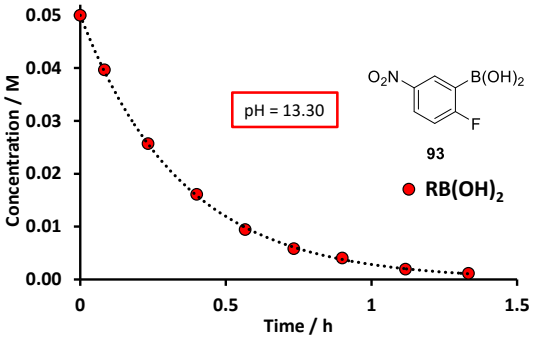
Concentration / M
Time / h
pH = 13.30
93
RB(OH)2

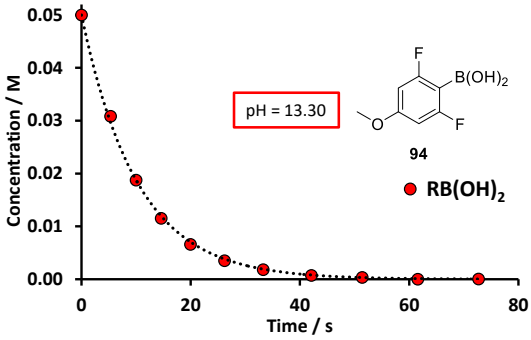
Concentration / M
Time / s
pH = 13.30
94
RB(OH)2

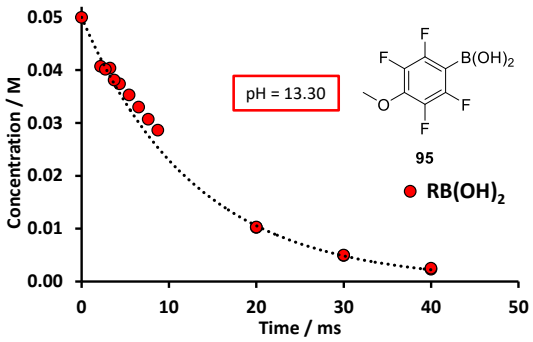
pH = 13.30
95
RB(OH)2
Concentration / M
Time / ms

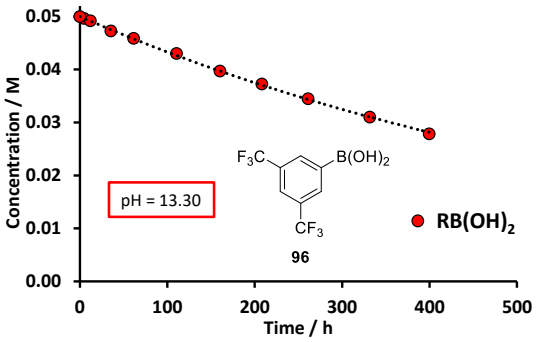
pH = 13.30
96
RB(OH)2
Concentration / M
Time / h

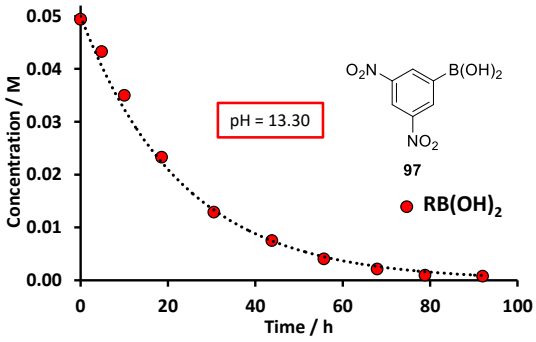
pH = 13.30
97
RB(OH)2
Concentration / M
Time / h

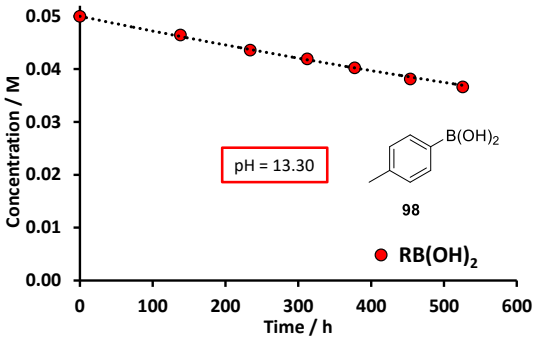
pH = 13.30
98
RB(OH)2
Concentration / M
Time / h

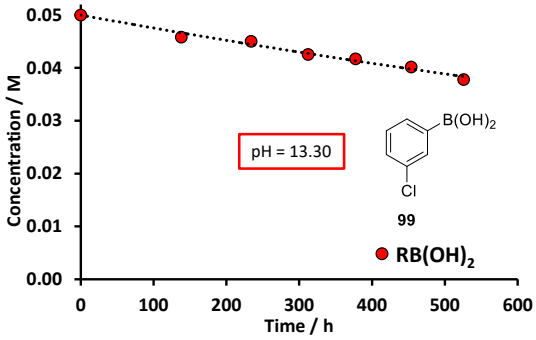
pH = 13.30
99
RB(OH)2
Concentration / M
Time / h

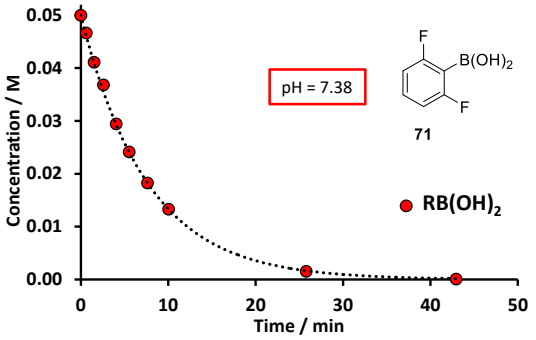
pH = 7.38
71
RB(OH)2
Concentration / M
Time / min

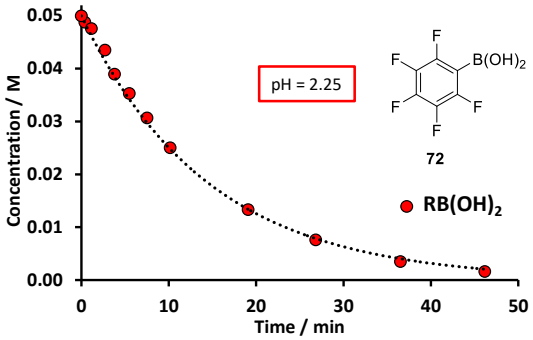
pH = 2.25
72
RB(OH)2
Concentration / M
Time / min

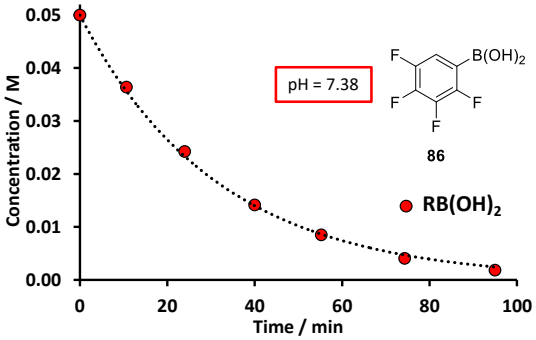
pH = 7.38
86
RB(OH)2
Concentration / M
Time / min

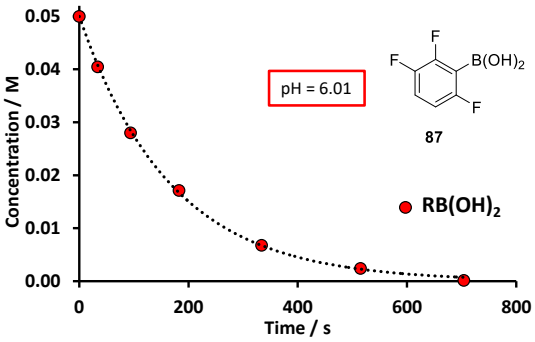
Concentration / M
Time / s
pH = 6.01
87
RB(OH)2

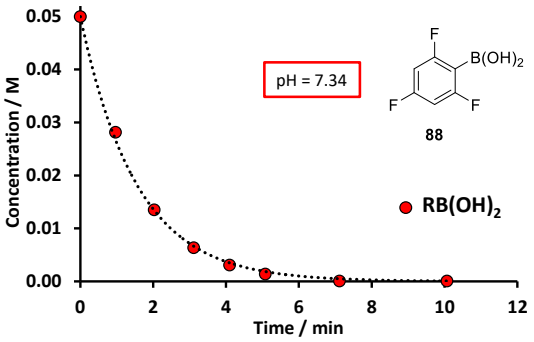
Concentration / M
Time / min
pH = 7.34
88
RB(OH)2

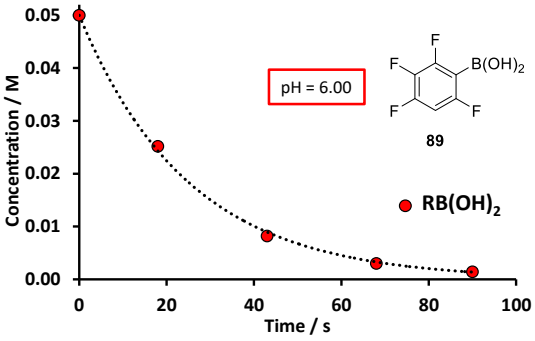
Concentration / M
Time / s
pH = 6.00
89
RB(OH)2

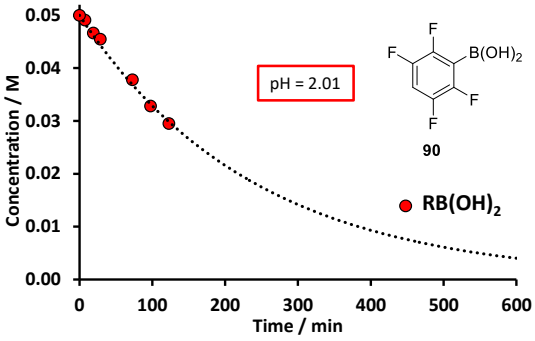
Concentration / M
Time / min
pH = 2.01
90
RB(OH)2

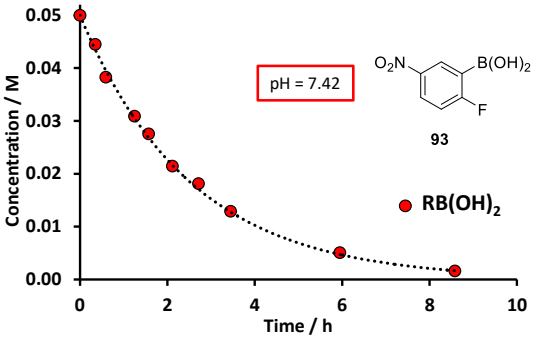
Concentration / M
Time / h
pH = 7.42
93
RB(OH)2

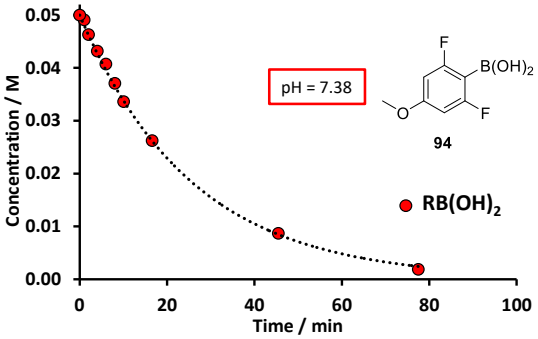
Concentration / M
Time / min
pH = 7.38
94
RB(OH)2

8.2. NMR pH titrations

8.2.1. pK_a titrations in H_2O at 90 °C

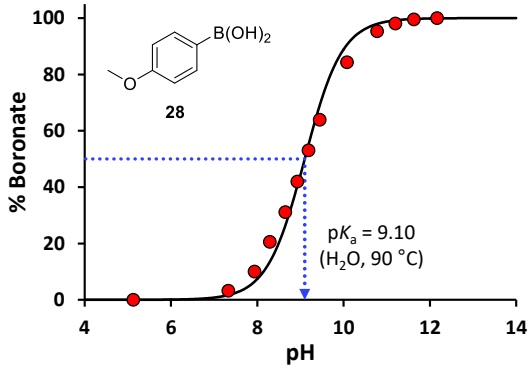

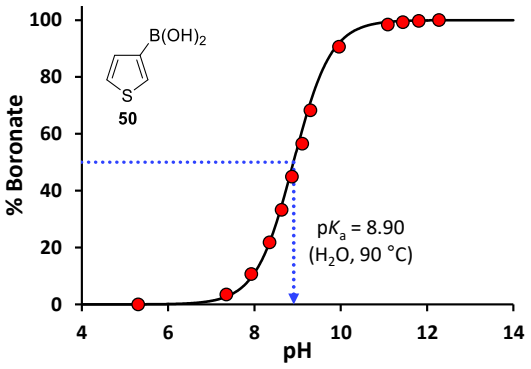

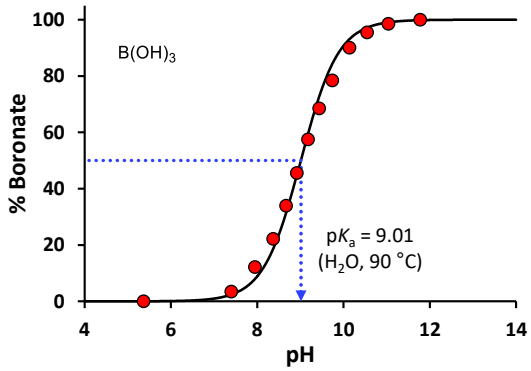

8.2.2. pK_a titrations in 1:1 H_2O/dioxane at 70 °C

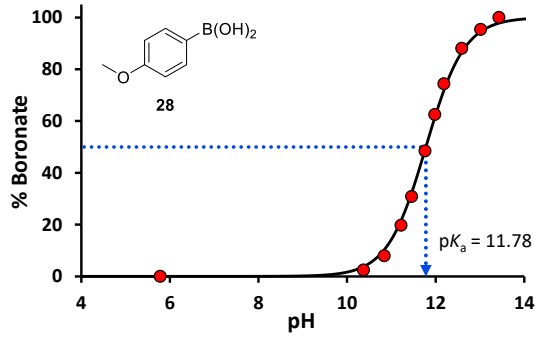

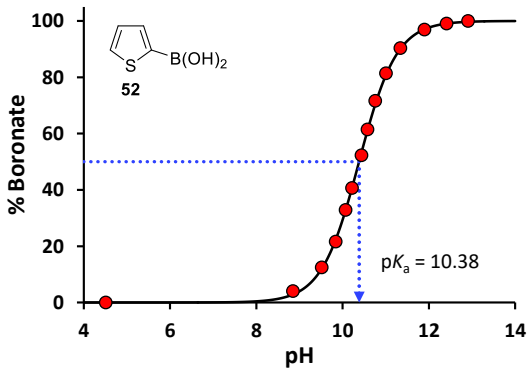

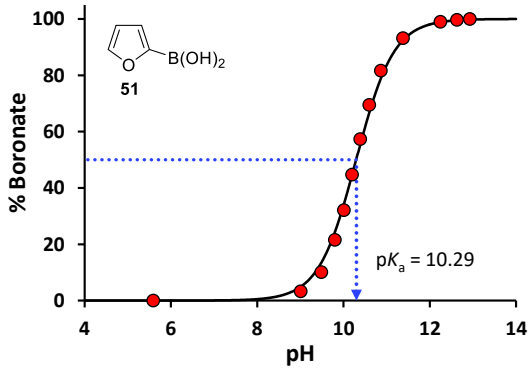

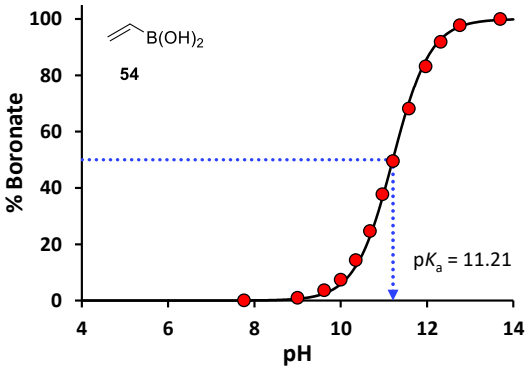

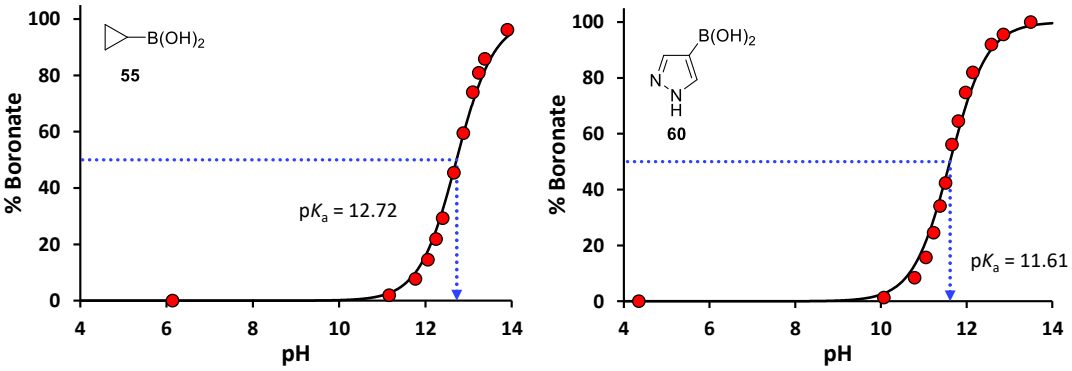
B(OH)2
55
% Boronate
pH
pKa = 12.72

B(OH)2
N
N
H
60
% Boronate
pH
pKa = 11.61

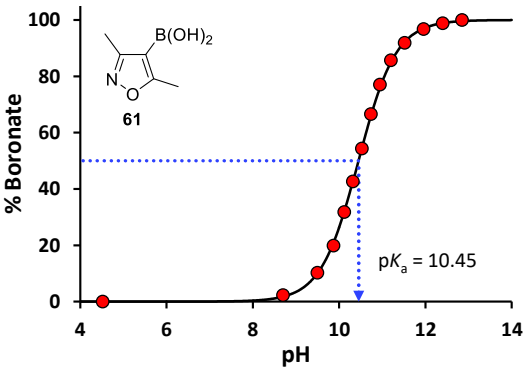
B(OH)2
N
O
61
% Boronate
pH
pKa = 10.45

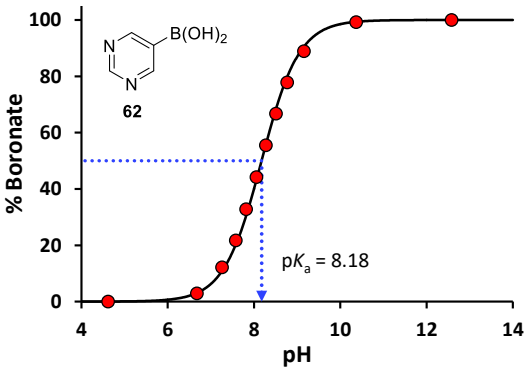
B(OH)2
N
N
62
% Boronate
pH
pKa = 8.18

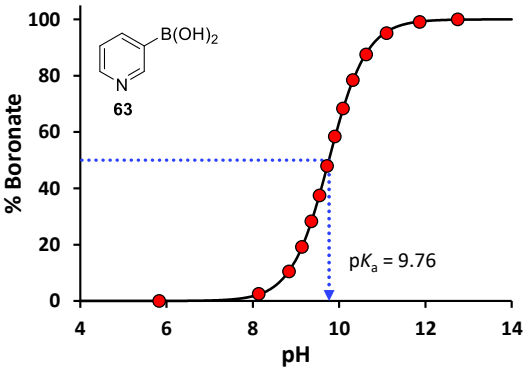
B(OH)2
N
63
% Boronate
pH
pKa = 9.76

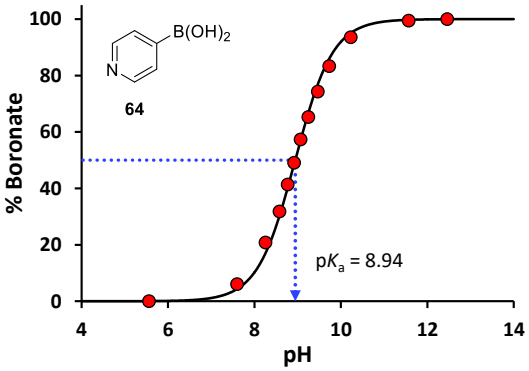
B(OH)2
N
64
% Boronate
pH
pKa = 8.94

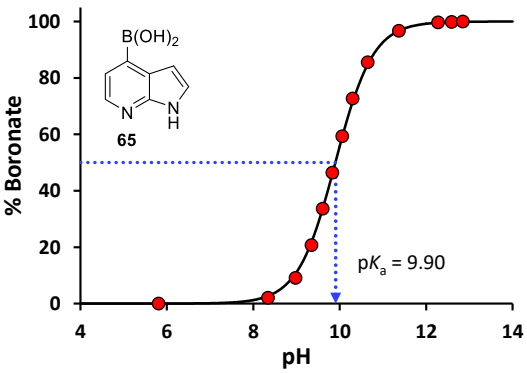
B(OH)2
N
N
H
65
% Boronate
pH
pKa = 9.90

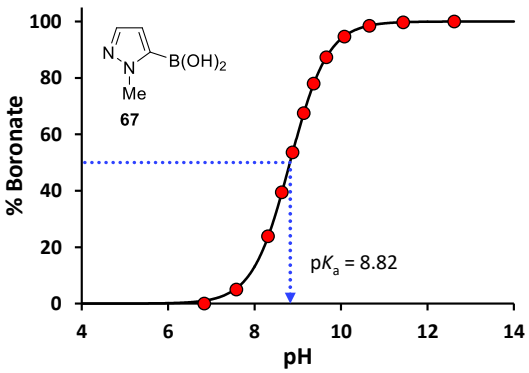
B(OH)2
N
N
Me
67
% Boronate
pH
pKa = 8.82

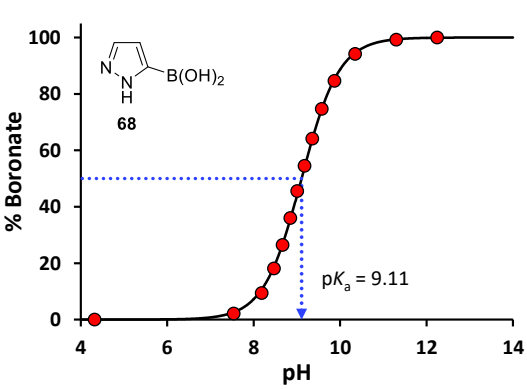
% Boronate
pH
68
pK_a = 9.11

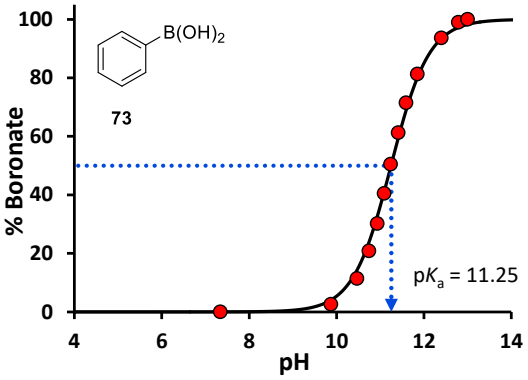
% Boronate
pH
73
pK_a = 11.25

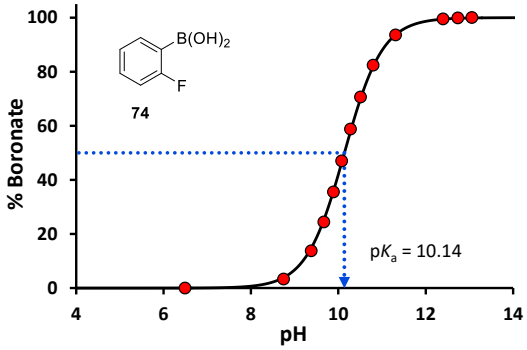
% Boronate
pH
74
pK_a = 10.14

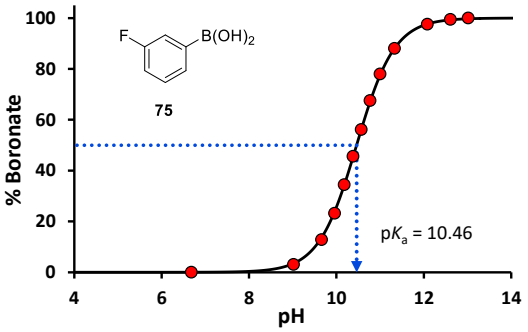
% Boronate
pH
75
pK_a = 10.46

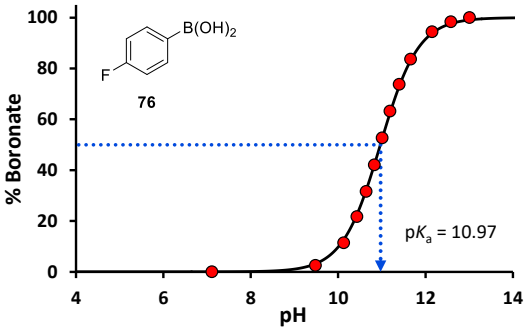
% Boronate
pH
76
pK_a = 10.97

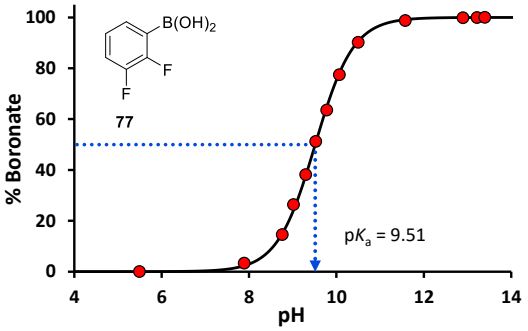
% Boronate
pH
77
pK_a = 9.51

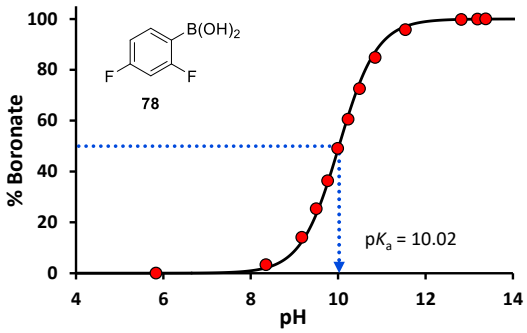
% Boronate
pH
78
pK_a = 10.02

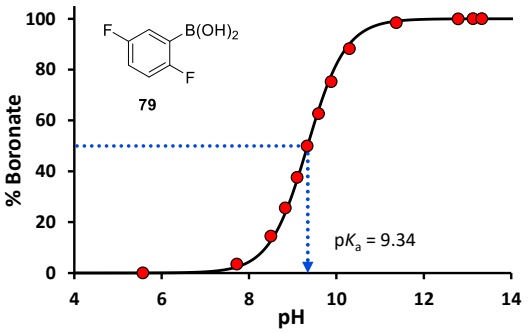
% Boronate
pH
79
pK_a = 9.34

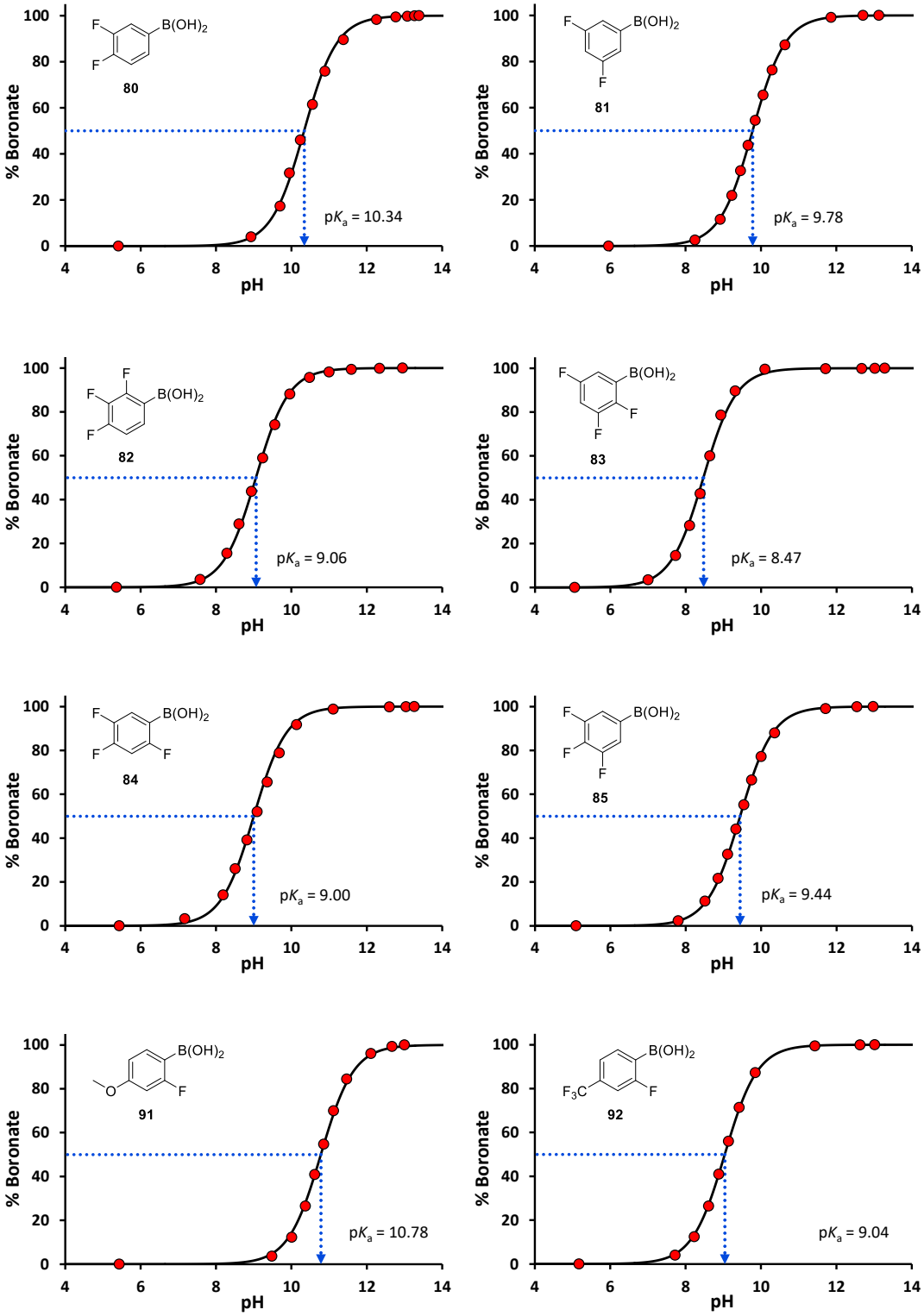
% Boronate
pH
80
pK_a = 10.34
81
pK_a = 9.78
82
pK_a = 9.06
83
pK_a = 8.47
84
pK_a = 9.00
85
pK_a = 9.44
91
pK_a = 10.78
92
pK_a = 9.04

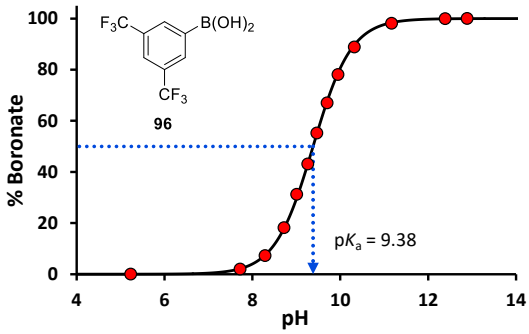
% Boronate
pH
F_3C
$B(OH)_2$
CF_3
96
pK_a = 9.38

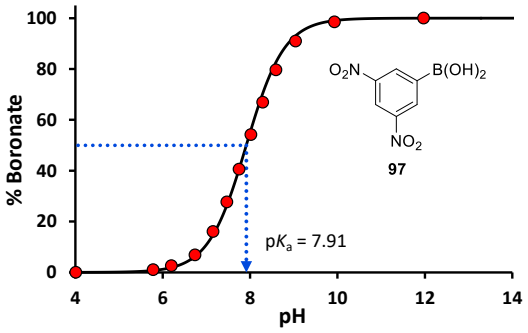
% Boronate
pH
O_2N
$B(OH)_2$
NO_2
97
pK_a = 7.91

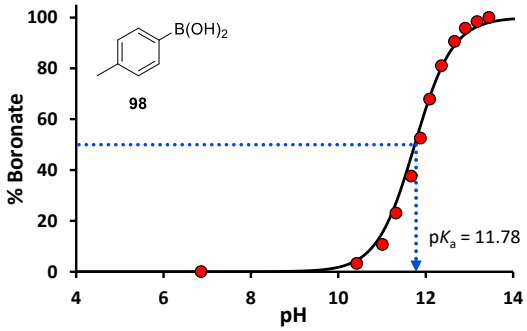
% Boronate
pH
$B(OH)_2$
98
pK_a = 11.78

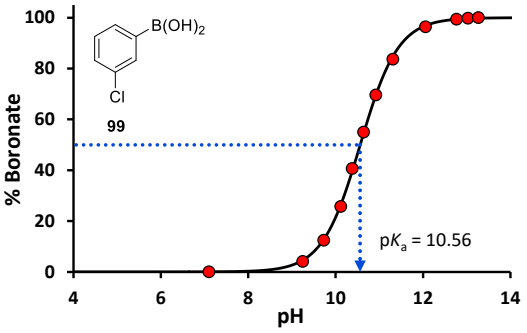
% Boronate
pH
$B(OH)_2$
Cl
99
pK_a = 10.56

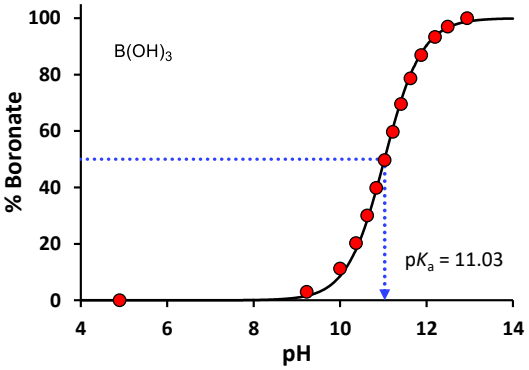
% Boronate
pH
$B(OH)_3$
pK_a = 11.03

8.2.3. pK_{aH} titrations in 1:1 H_2O/dioxane at 25 °C

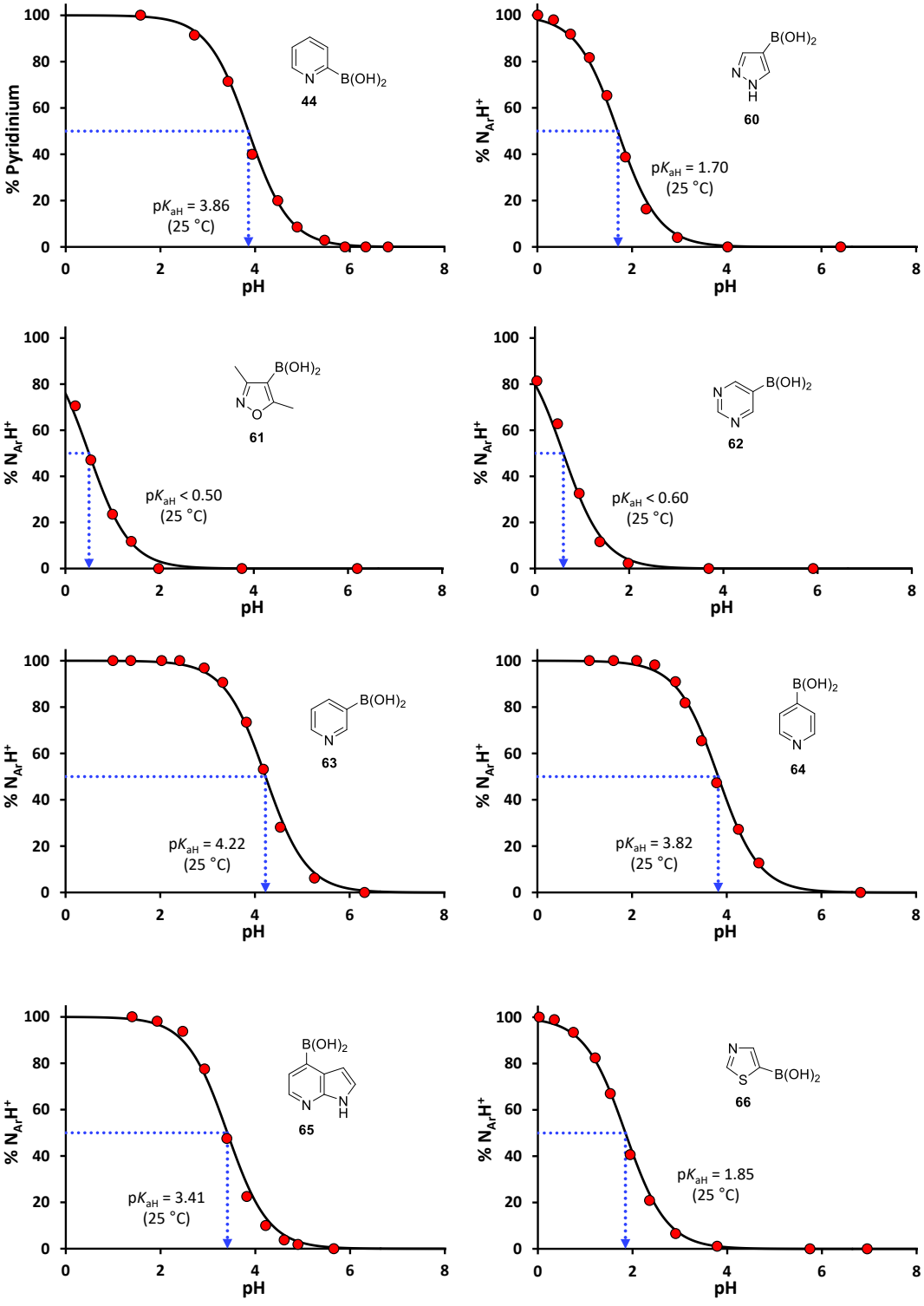

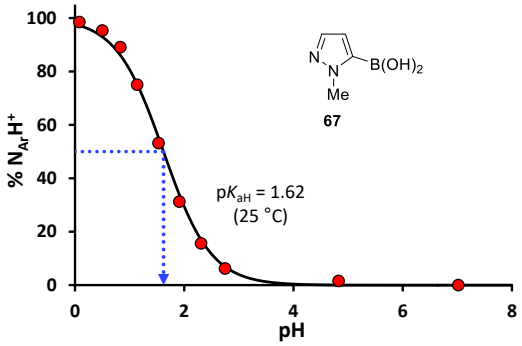
100
80
60
40
20
0
% $N_{Ar}H^+$
0
2
4
6
8
pH
pK_{aH} = 1.62
(25 °C)
N
N
Me
B(OH)$_2$
67

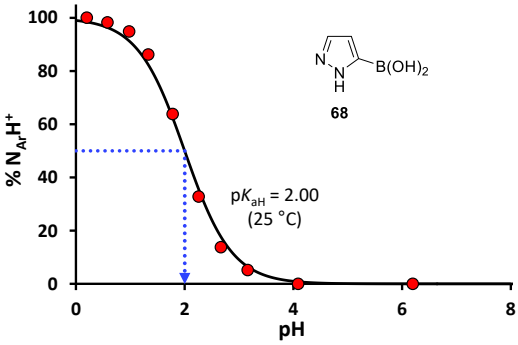
100
80
60
40
20
0
% $N_{Ar}H^+$
0
2
4
6
8
pH
pK_{aH} = 2.00
(25 °C)
N
N
H
B(OH)$_2$
68

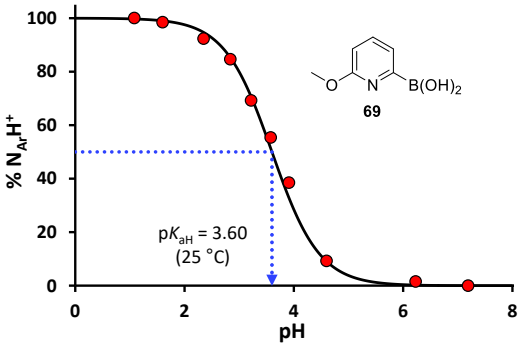
100
80
60
40
20
0
% $N_{Ar}H^+$
0
2
4
6
8
pH
pK_{aH} = 3.60
(25 °C)
O
N
B(OH)$_2$
69

8.3. General mechanistic model: Solving speciation terms

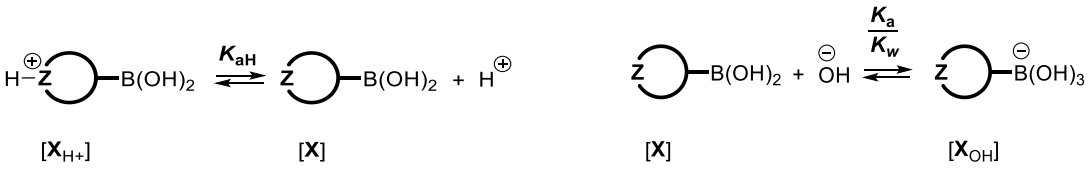

Scheme S1. Equilibria modelled in general model for the speciation of boronic acids.

$$\boldsymbol{K_{aH}} = \frac{[\mathbf{X}][H^+]}{[\mathbf{X}_{H+}]} \qquad \frac{\boldsymbol{K_a}}{\boldsymbol{K_w}} = \frac{[\mathbf{X}_{OH}]}{[\mathbf{X}][OH^-]} \qquad \boldsymbol{K_w} = [H^+][OH^-] \text{ (auto-ionisation of water)}$$

Solving mole fraction in terms of equilibrium constants ($\boldsymbol{K}$), $[H^+]$ and $[OH^-]$

$$\text{mole fraction of } \mathbf{X}_{H+} = x_{\mathbf{X}_{H+}} = \frac{[\mathbf{X}_{H+}]}{[\mathbf{X}_{H+}] + [\mathbf{X}] + [\mathbf{X}_{OH}]}$$

$$x_{\mathbf{X}_{H+}} = \frac{[\mathbf{X}_{H+}]}{[\mathbf{X}_{H+}]+ [\mathbf{X}]+[\mathbf{X}_{OH}]}$$

$$x_{\mathbf{X}_{H+}} = \frac{1}{\frac{[\mathbf{X}_{H+}]}{[\mathbf{X}_{H+}]}+\frac{[\mathbf{X}]}{[\mathbf{X}_{H+}]}+\frac{[\mathbf{X}_{OH}]}{[\mathbf{X}_{H+}]}}$$

$$x_{\mathbf{X}_{H+}} = \frac{1}{1+\frac{[\mathbf{X}]}{[\mathbf{X}_{H+}]}+\frac{[\mathbf{X}_{OH}]}{[\mathbf{X}_{H+}]}}$$

using $\boldsymbol{K_{aH}} = \frac{[\mathbf{X}][H^+]}{[\mathbf{X}_{H+}]}$; $\frac{\boldsymbol{K_a}}{\boldsymbol{K_w}} = \frac{[\mathbf{X}_{OH}]}{[\mathbf{X}][OH^-]}$

$$x_{\mathbf{X}_{H+}} = \frac{1}{1+\frac{\boldsymbol{K_{aH}}[\mathbf{X}_{H+}]}{[\mathbf{X}_{H+}][H^+]}+\frac{\boldsymbol{K_a}[\mathbf{X}][OH^-]}{\boldsymbol{K_w}[\mathbf{X}_{H+}]}}$$

$$x_{\mathbf{X}_{H+}} = \frac{1}{1+\frac{\boldsymbol{K_{aH}}}{[H^+]}+\frac{\boldsymbol{K_{aH}}\boldsymbol{K_a}[\mathbf{X}_{H+}][OH^-]}{\boldsymbol{K_w}[\mathbf{X}_{H+}][H^+]}}$$

$$x_{\mathbf{X}_{H+}} = \frac{1}{1+\frac{\boldsymbol{K_{aH}}}{[H^+]}+\frac{\boldsymbol{K_{aH}}\boldsymbol{K_a}[OH^-]}{\boldsymbol{K_w}[H^+]}}$$

using $\boldsymbol{K_w} = [H^+][OH^-]$

$$x_{\mathbf{X}_{H+}} = \frac{1}{1+\frac{\boldsymbol{K_{aH}}}{[H^+]}+\frac{\boldsymbol{K_{aH}}\boldsymbol{K_a}}{[H^+][H^+]}}$$

Converting into log terms;

$$= \frac{1}{1+\ 10^{pH-pK_{aH}} + 10^{2pH-pK_{aH}-pK_a}}$$

$$x_{\mathbf{X}} = \frac{[\mathbf{X}]}{[\mathbf{X}_{H+}]+ [\mathbf{X}]+[\mathbf{X}_{OH}]}$$

$$x_{\mathbf{X}} = \frac{1}{\frac{[\mathbf{X}_{H+}]}{[\mathbf{X}]}+\frac{[\mathbf{X}]}{[\mathbf{X}]}+\frac{[\mathbf{X}_{OH}]}{[\mathbf{X}]}}$$

$$x_{\mathbf{X}} = \frac{1}{\frac{[\mathbf{X}_{H+}]}{[\mathbf{X}]}+1+\frac{[\mathbf{X}_{OH}]}{[\mathbf{X}]}}$$

using $\boldsymbol{K_{aH}} = \frac{[\mathbf{X}][H^+]}{[\mathbf{X}_{H+}]}$; $\frac{\boldsymbol{K_a}}{\boldsymbol{K_w}} = \frac{[\mathbf{X}_{OH}]}{[\mathbf{X}][OH^-]}$

$$x_{\mathbf{X}} = \frac{1}{\frac{[\mathbf{X}][H^+]}{\boldsymbol{K_{aH}}[\mathbf{X}]}+1+\frac{\boldsymbol{K_a}[\mathbf{X}][OH^-]}{\boldsymbol{K_w}[\mathbf{X}]}}$$

$$x_{\mathbf{X}} = \frac{1}{\frac{[H^+]}{\boldsymbol{K_{aH}}}+1+\frac{\boldsymbol{K_a}[OH^-]}{\boldsymbol{K_w}}}$$

using $\boldsymbol{K_w} = [H^+][OH^-]$

$$x_{\mathbf{X}} = \frac{1}{\frac{[H^+]}{\boldsymbol{K_{aH}}}+1+\frac{\boldsymbol{K_a}}{[H^+]}}$$

Converting into log terms;

$$= \frac{1}{1+\ 10^{pK_{aH}-pH} + 10^{pH-pK_a}}$$

$$x_{\mathbf{X}_{OH}} = \frac{[\mathbf{X}_{OH}]}{[\mathbf{X}_{H+}]+ [\mathbf{X}]+[\mathbf{X}_{OH}]}$$

$$x_{\mathbf{X}_{OH}} = \frac{1}{\frac{[\mathbf{X}_{H+}]}{[\mathbf{X}_{OH}]}+\frac{[\mathbf{X}]}{[\mathbf{X}_{OH}]}+\frac{[\mathbf{X}_{OH}]}{[\mathbf{X}_{OH}]}}$$

$$x_{\mathbf{X}_{OH}} = \frac{1}{\frac{[\mathbf{X}_{H+}]}{[\mathbf{X}_{OH}]}+\frac{[\mathbf{X}]}{[\mathbf{X}_{OH}]}+1}$$

using $\boldsymbol{K_{aH}} = \frac{[\mathbf{X}][H^+]}{[\mathbf{X}_{H+}]}$; $\frac{\boldsymbol{K_a}}{\boldsymbol{K_w}} = \frac{[\mathbf{X}_{OH}]}{[\mathbf{X}][OH^-]}$

$$x_{\mathbf{X}_{OH}} = \frac{1}{\frac{[\mathbf{X}][H^+]}{\boldsymbol{K_{aH}}[\mathbf{X}_{OH}]}+\frac{\boldsymbol{K_w}[\mathbf{X}_{OH}]}{\boldsymbol{K_a}[\mathbf{X}_{OH}][OH^-]}+1}$$

$$x_{\mathbf{X}_{OH}} = \frac{1}{\frac{\boldsymbol{K_w}[\mathbf{X}_{OH}][H^+]}{\boldsymbol{K_{aH}}\boldsymbol{K_a}[\mathbf{X}_{OH}][OH^-]}+\frac{\boldsymbol{K_w}}{\boldsymbol{K_a}[OH^-]}+1}$$

$$x_{\mathbf{X}_{OH}} = \frac{1}{\frac{\boldsymbol{K_w}[H^+]}{\boldsymbol{K_{aH}}\boldsymbol{K_a}[OH^-]}+\frac{\boldsymbol{K_w}}{\boldsymbol{K_a}[OH^-]}+1}$$

using $\boldsymbol{K_w} = [H^+][OH^-]$

$$x_{\mathbf{X}_{OH}} = \frac{1}{\frac{[H^+][H^+]}{\boldsymbol{K_{aH}}\boldsymbol{K_a}}+\frac{[H^+]}{\boldsymbol{K_a}}+1}$$

Converting into log terms;

$$\frac{1}{1+\ 10^{pK_a-pH} + 10^{pK_{aH}+pK_a-2pH}}$$

8.4. 2-furyl boronic acid disproportionation NMR spectra

^{1}H and ^{11}B NMR spectra for the protodeboronation and disproportionation of 2-furyl boronic acid (**51**) into d_1-furan, boric acid, borinic acid and borane.

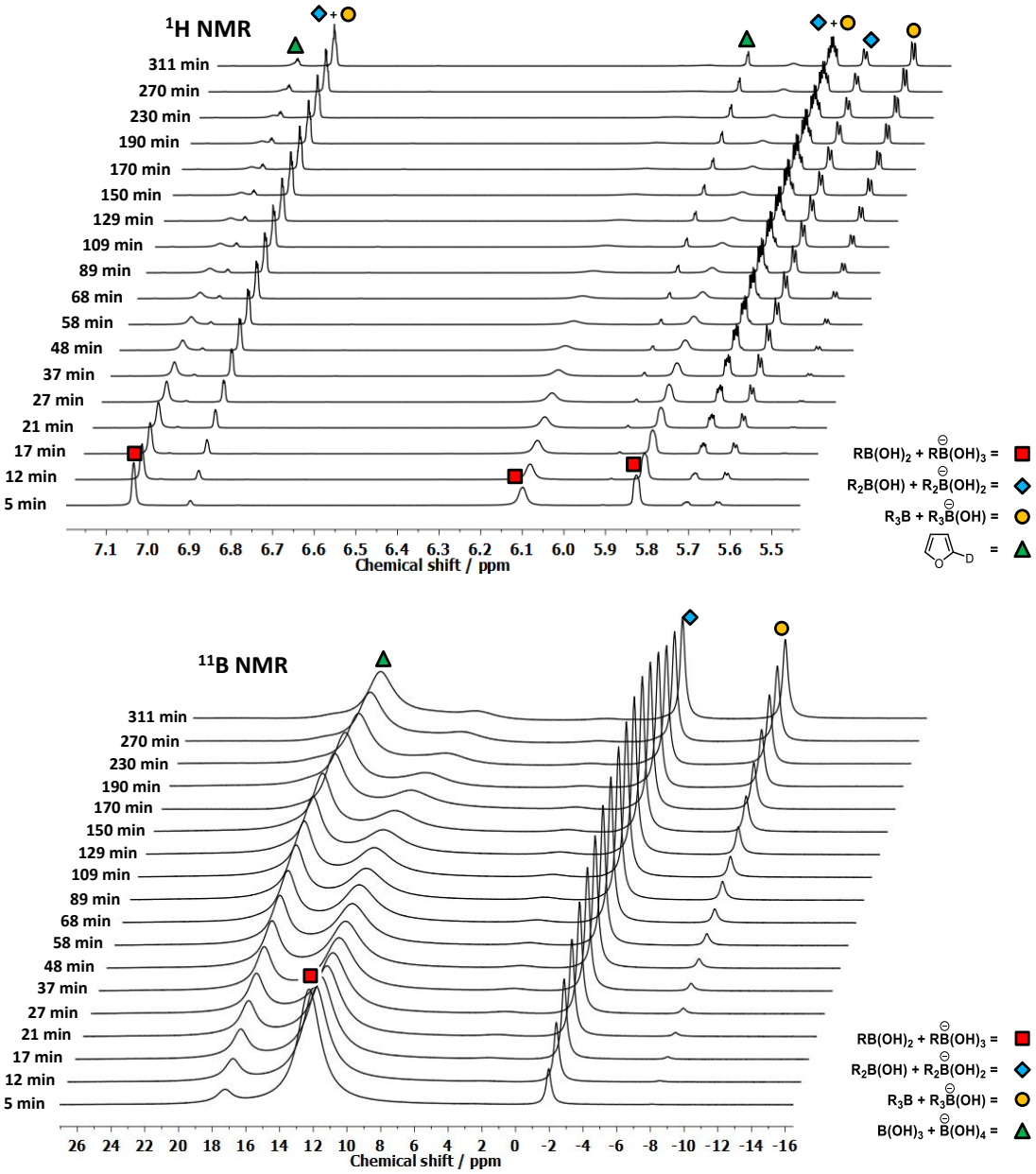

8.5. pH – log k_{obs} data and procedures

44		50		51		52	
pH	log k_{obs}	pH	log k_{obs}	pH	log k_{obs}	pH	log k_{obs}
0.95	-4.01[d]	0.62	-6.61[a]	1.08	-4.84[a]	0.98	-5.47[a]
1.09	-3.91[d]	1.08	-7.06[a]	1.46	-5.27[a]	1.42	-5.98[a]
1.30	-3.78[d]	1.38	-7.27[a]	1.97	-5.81[a]	1.92	-6.37[a]
1.71	-3.31[d]	5.11	-7.05[a]	2.46	-6.13[a]	2.43	-6.65[a]
1.95	-3.17[d]	5.54	-6.95[a]	2.86	-6.43[a]	6.85	-6.80[a]
2.35	-2.76[d]	5.95	-6.99[a]	3.34	-6.51[a]	7.27	-6.82[a]
3.28	-2.28[f],*	6.34	-7.10[a]	6.23	-7.08[a]	7.58	-6.92[a]
3.60	-2.12[f],*	6.75	-7.38[a]	6.92	-7.09[a]	8.32	-6.17[a]
4.40	-1.74[f],*	7.17	-7.43[a]	7.89	-6.76[a]	8.64	-5.90[a]
5.04	-1.68[f],*	7.66	-7.30[a]	8.34	-6.51[a]	8.91	-5.47[a]
6.48	-1.55[f],*	8.15	-7.09[a]	8.77	-6.07[a]	9.19	-5.19[a]
7.55	-1.52[f],*	8.71	-7.03[a]	9.26	-5.53[a]	9.50	-4.90[a]
8.22	-1.59[f],*	9.41	-6.79[a]	9.70	-5.12[a]	9.82	-4.53[a]
9.11	-1.60[f],*	9.59	-6.61[a]	10.14	-4.94[a]	10.12	-4.29[a]
9.82	-1.70[f],*	9.97	-6.42[a]	10.56	-4.91[a]	10.42	-4.12[a]
10.48	-1.79[f],*	10.42	-6.11[a]	11.02	-4.96[a]	10.75	-4.04[a]
11.50	-2.48[f],*	10.81	-5.94[a]	11.55	-5.02[a]	11.10	-3.98[a]
12.46	-3.20[d]	11.22	-5.94[a]	12.18	-5.00[a]	11.50	-3.95[a]
12.77	-3.49[c]	11.70	-5.95[a]	12.49	-5.01[a]	11.83	-3.94[a]
13.10	-3.84[c]	12.23	-5.99[a]	12.91	-4.88[a]	12.15	-3.94[a]
13.43	-4.18[c]	12.65	-5.98[a]			12.45	-3.94[a]
		12.94	-6.00[a]			12.74	-3.93[a]
						12.80	-3.83[g]

53		54		55		56	
pH	log k_{obs}	pH	log k_{obs}	pH	log k_{obs}	pH	log k_{obs}
1.21	-4.63[c]	1.03	-6.57[a]	0.65	-6.59[a]	0.96	-7.29[a]
2.26	-5.61[c]	1.42	-7.01[a]	1.10	-7.04[a]	1.33	-7.57[a]
3.21	-6.12[c]	2.00	-7.67[a]	1.80	-7.83[a]	1.83	-7.86[a]
4.13	-6.57[c]	2.70	-7.80[a]	2.76	-7.97[a]	2.27	-7.69[a]
5.07	-6.28[c]	3.42	-7.72[a]	3.15	-7.64[a]	2.88	-7.81[a]
6.08	-5.59[c]	4.25	-7.87[a]	5.63	-7.56[a]	3.34	-7.22[a]
6.57	-5.29[c]	5.14	-7.66[a]	6.35	-8.89[a]	3.83	-6.85[a]
7.25	-4.73[c]	5.92	-7.54[a]	7.14	-8.13[a]	4.25	-6.86[a]
8.18	-3.96[c]	7.05	-7.51[a]	7.99	-8.13[a]	5.84	-6.61[a]
8.72	-3.45[c]	7.77	-7.50[a]	8.79	-9.04[a]	5.90	-6.61[a]
9.20	-2.88[e],*	8.72	-7.04[a]	9.45	-8.53[a]	7.25	-6.64[a]
9.69	-2.69[e],*	9.35	-6.71[a]	10.04	-7.73[a]	8.03	-7.25[a]
10.28	-2.47[e],*	9.96	-6.28[a]	10.61	-7.48[a]	8.66	-7.71[a]
11.56	-2.29[e],*	10.51	-5.98[a]	11.22	-6.95[a]	9.21	-7.66[a]
13.15	-2.30[e],*	11.02	-5.83[a]	11.79	-6.61[a]	9.78	-7.50[a]
		12.66	-5.88[a]	13.17	-6.13[a]	10.84	-7.20[a]
		13.22	-5.98[a]			11.34	-6.95[a]
						11.77	-6.80[a]
						12.21	-6.76[a]
						12.60	-7.09[a]
						13.01	-7.27[a]

57		**58**		**60**		**61**	
pH	log k_{obs}	pH	log k_{obs}	pH	log k_{obs}	pH	log k_{obs}
0.63	-8.05[a]	1.07	-6.87[a]	0.57	-4.44[a]	0.59	-5.77[a]
1.06	-8.32[a]	1.65	-6.79[a]	0.89	-4.53[a]	1.03	-6.18[a]
1.52	-8.92[a]	2.20	-6.75[a]	1.21	-4.66[a]	2.04	-6.35[a]
2.02	-8.44[a]	2.75	-6.76[a]	1.63	-4.94[a]	2.54	-6.28[a]
2.50	-7.52[a]	3.35	-6.78[a]	2.09	-5.36[a]	5.00	-6.27[a]
2.62	-7.36[a]	3.94	-7.79[a]	2.56	-5.83[a]	5.63	-6.14[a]
3.07	-6.83[a]	4.64	-9.03[a]	3.02	-6.21[a]	6.38	-6.03[a]
3.12	-7.35[a]	5.31	-8.19[a]	3.44	-6.30[a]	6.99	-5.86[a]
3.63	-7.38[a]	6.00	-8.11[a]	3.83	-6.47[a]	7.47	-5.60[a]
6.79	-7.51[a]	6.18	-7.95[a]	4.23	-6.54[a]	8.12	-5.53[a]
7.35	-7.47[a]	6.88	-7.95[a]	4.65	-6.53[a]	8.53	-5.24[a]
7.83	-7.55[a]	7.68	-7.96[a]	4.80	-6.57[a]	9.06	-4.75[a]
8.30	-6.72[a]	8.55	-7.93[a]	5.38	-6.70[a]	9.54	-4.35[a]
8.81	-6.64[a]	9.17	-7.68[a]	6.30	-6.67[a]	10.01	-3.95[a]
9.31	-6.90[a]	9.77	-7.53[a]	7.32	-6.74[a]	10.52	-3.81[a]
9.87	-7.22[a]	10.42	-7.04[a]	8.30	-6.52[a]	11.09	-3.77[a]
10.32	-6.87[a]	10.99	-6.70[a]	8.76	-6.41[a]	11.66	-3.85[a]
10.84	-7.55[a]	11.72	-6.35[a]	9.15	-6.28[a]	12.04	-3.90[a]
11.35	-6.86[a]	12.18	-6.38[a]	9.58	-6.16[a]	12.59	-3.62[a]
11.85	-6.75[a]	12.74	-6.40[a]	10.09	-5.89[a]	13.00	-3.50[a]
12.58	-6.86[a]	13.13	-6.46[a]	10.45	-5.73[a]	13.36	-3.22[a]
				10.89	-5.52[a]		
				11.32	-5.23[a]		
				11.79	-5.22[a]		
				12.24	-5.19[a]		

62		**63**		**64**		**65**	
pH	log k_{obs}	pH	log k_{obs}	pH	log k_{obs}	pH	log k_{obs}
0.65	-5.44[a]	0.97	-7.89[a]	1.03	-5.90[a]	0.84	-7.14[a]
0.91	-5.39[a]	1.23	-7.26[a]	1.55	-5.81[a]	1.36	-7.02[a]
1.16	-5.35[a]	1.72	-7.95[a]	1.97	-5.68[a]	1.88	-7.13[a]
1.57	-5.35[a]	2.19	-6.75[a]	2.53	-5.87[a]	2.44	-7.06[a]
2.00	-5.37[a]	2.75	-6.75[a]	3.22	-5.66[a]	2.90	-6.98[a]
2.40	-5.46[a]	3.30	-6.28[a]	3.72	-5.73[a]	3.45	-7.01[a]
2.87	-5.54[a]	3.79	-6.03[a]	4.21	-5.55[a]	3.96	-6.91[a]
3.30	-5.49[a]	4.26	-5.87[a]	4.71	-5.64[a]	4.45	-6.97[a]
3.75	-5.51[a]	4.75	-5.77[a]	5.17	-5.76[a]	4.95	-6.90[a]
4.16	-5.47[a]	5.25	-5.77[a]	5.68	-5.79[a]	5.45	-6.93[a]
4.32	-5.48[a]	5.76	-5.78[a]	6.28	-5.79[a]	5.96	-6.92[a]
4.60	-5.54[a]	6.32	-5.78[a]	6.55	-5.69[a]	6.12	-6.84[a]
4.75	-5.46[a]	6.37	-5.67[a]	7.10	-5.71[a]	6.71	-6.85[a]
5.25	-5.48[a]	6.92	-5.66[a]	7.57	-5.65[a]	7.25	-6.86[a]
5.33	-5.41[a]	7.42	-5.66[a]	7.99	-5.47[a]	7.76	-6.80[a]
5.71	-5.47[a]	7.83	-5.46[a]	8.45	-5.65[a]	8.24	-6.55[a]
6.25	-5.43[a]	8.28	-5.54[a]	8.89	-5.53[a]	8.74	-6.43[a]
6.71	-5.35[a]	8.72	-5.48[a]	9.42	-5.47[a]	9.27	-5.88[a]
7.19	-5.29[a]	9.20	-5.45[a]	9.90	-5.60[a]	10.22	-5.82[a]
7.72	-4.99[a]	9.69	-5.41[a]	10.36	-5.69[a]	10.78	-5.87[a]
8.24	-5.01[a]	10.17	-5.52[a]	10.81	-5.88[a]	11.29	-6.16[a]
8.75	-4.95[a]	10.57	-5.61[a]	11.46	-5.91[a]	11.81	-6.21[a]
9.24	-4.99[a]	11.00	-5.78[a]	12.32	-6.03[a]	12.28	-6.16[a]
9.89	-5.03[a]	11.39	-5.64[a]	12.83	-5.99[a]	12.78	-6.26[a]
10.44	-5.04[a]	11.84	-5.87[a]			13.34	-6.26[a]
11.22	-5.06[a]	12.26	-6.27[a]				
11.86	-5.03[a]	12.62	-6.19[a]				
12.24	-5.05[a]	13.03	-5.99[a]				

66		**67**		**68**		**69**		**70**	
pH	log k_{obs}	pH	log k_{obs}	pH	log k_{obs}	pH	log k_{obs}	pH	log k_{obs}
0.85	-2.67[e]	0.61	-4.34[a]	0.91	-4.77[c]	1.31	-4.20[d]	1.19	-2.73[f]
2.59	-1.85[e]	0.93	-4.20[a]	1.38	-4.53[c]	1.71	-3.79[d]	2.36	-2.73[f]
3.01	-1.81[e],*	1.41	-3.99[a]	1.83	-4.38[c]	2.32	-3.36[d]	3.72	-2.75[f],*
5.20	-1.86[e],*	2.02	-3.81[a]	2.25	-4.32[c]	2.80	-3.02[d]	5.25	-2.76[f],*
6.23	-1.85[e],*	2.73	-3.76[a]	2.71	-4.30[c]	3.00	-2.85[f],*	6.28	-2.76[f],*
8.48	-1.92[e],*	3.44	-3.76[a]	3.20	-4.28[c]	3.30	-2.77[f],*	6.30	-2.74[f],*
9.79	-2.00[e],*	4.36	-3.77[a]	3.71	-4.29[c]	5.53	-2.41[f],*	8.51	-3.07[f],*
11.44	-2.03[e],*	5.30	-3.77[a]	4.15	-4.27[c]	6.86	-2.42[f],*	9.65	-3.95[f],*
13.09	-2.00[e]	6.02	-3.79[a]	4.58	-4.28[c]	8.76	-2.47[f],*	10.64	-4.88[d]
		6.71	-3.80[a]	4.64	-4.27[c]	10.00	-2.96[f],*	11.22	-5.35[d]
		6.73	-3.80[a]	5.01	-4.28[c]	10.53	-3.62[d],*	11.82	-6.18[d]
		7.17	-3.79[a]	5.05	-4.28[c]	10.97	-4.04[d],*	12.60	-6.49[d]
		7.76	-3.80[a]	5.56	-4.29[c]	11.50	-4.35[d],*		
		8.27	-3.80[a]	6.07	-4.27[c]	11.98	-4.75[d]		
		8.83	-3.80[a]	6.66	-4.29[c]	12.50	-5.26[c]		
		9.54	-3.84[a]	7.04	-4.26[c]	12.96	-5.72[c]		
		10.09	-3.85[a]	7.55	-4.29[c]	13.14	-6.11[c]		
		10.60	-3.86[a]	7.97	-4.29[c]				
		11.41	-3.88[a]	8.57	-4.24[c]				
		11.96	-3.88[a]	9.02	-4.26[c]				
		12.49	-3.87[a]	9.63	-4.29[c]				
				10.28	-4.35[c]				
				10.70	-4.35[c]				
				11.28	-4.37[c]				
				11.78	-4.37[c]				

[a] General procedure B (^{11}B NMR). [b] General procedure B (^{1}H NMR). [c] General procedure C (no quench solution required). [d] General procedure C (8 M KOH quench solution). [e] General procedure E (8 M HCl quench solution). [f] General procedure E (8 M KOH quench solution). [g] General procedure D (^{11}B NMR).

* Buffered solutions utilised. Refer to Experimental (section 6.3.2.) for further details.